UNIVERSITÀ DEGLI STUDI DI PALERMO

DOTTORATO DI RICERCA IN ENERGIA – INDIRIZZO ENERGETICA

DIPARTIMENTO DELL'ENERGIA

SSD ING IND 11

NUMERICAL ANALYSIS OF AN ALTERNATIVE VENTILATION SYSTEM AND COMPARISON WITH TRADITIONAL ONE FOR BOTH FULL AND REDUCED-SCALE ROAD TUNNEL

IL DOTTORE
ING. LORENZO BARBATO
IL TUTOR
PROF.SSA MARILENA MUSTO

IL COORDINATORE
PROF. ALDO ORIOLI

XXVI CICLO

A.A. 2016/2017

SUMMARY

Introduction 1

Symbols 3

1. Generalities on ventilation systems for road tunnels 4

1.1. Overview about investigation of ventilation systems for road tunnel 7

1.2. Main factors and configurations of a ventilation system and their influence on performances 8

1.3. The effects of fire in tunnel 11

1.4. Numerical methods for road tunnel analysis 17

2. Critical velocity formulations 19

3. Numerical analysis of different turbulent models and comparison with experimental data 32

3.1. Introduction 32

3.2. Domain for experimental testing and measurements 32

3.3. System description 33

3.4. Geometrical model 36

3.5. Mesh analysis 37

3.6. Numerical simulation and turbulence model comparison 39

3.7. Results 40

4. Numerical comparison between alternative and traditional jet fans in a longitudinal tunnel ventilation system – free tunnel vs traffic jam condition 42

4.1. Introduction 42

4.2. CFD model 42

4.3. Performances of ventilation models 45

4.4. Optimal pitch angle in free tunnel configuration 50

4.5. Optimal pitch angle in traffic jam condition 52

4.6. Results 54

5. Numerical comparison between alternative and traditional jet fans in a longitudinal tunnel ventilation system in traffic jam condition – with vs without fire case 55
6. Numerical comparison of performances between traditional and alternative jet-fan in emergency condition – tiled tunnel case 63
6.1. Introduction 63
6.2. CFD model 64
6.3. Results 66
7. Numerical analyses of scale factor for laboratory tunnel design 72
7.1. Scale factor evaluation 72
7.1.1. Sensitivity analysis 73
7.1.1.1. Results 83
7.1.2. Materials optimization for reduced scale model 100
7.1.3. Preliminary tunnel geometry configuration 108
7.1.4. Fire case 110
7.1.5. Case 1 – Mesh and boundary conditions 111
7.1.6. Case 1 – Results 112
7.1.7. Case 2 – Mesh and boundary conditions 140
7.1.8. Case 2 – Results 141
7.2. Results 153
7.3. 1:20 reduced scale model 153
8. Numerical analyses and comparison with experimental data of laboratory reduced scale model 158
8.1. Validation of experimental apparatus as tunnel subsystem 158
8.1.1. Models description 158
8.1.1.1. Full scale tunnel 158
8.1.1.2. Reduced scale tunnel 159
8.2. Numerical analysis for different traffic conditions and comparison with experimental data 165
8.2.1. Boundary conditions 166
8.2.2. Pressure drop evaluation 166
8.2.3. Reduced scale parameters 169

8.2.4. The influence of vehicles 171
8.2.5. CFD parameters 173
8.2.6. Results 173
Conclusions 181
Appendix 185
References 189

Introduction

The fire safety in road tunnel is a worldwide problem. After several accidents, occurred for example in Mont Blanc tunnel (39 victims) or San Gottardo one (899 accidents and 31 victims)[1], in 1995 the European Union has started a specific program to increase tunnel safety. In recent years, an increasing of initiatives occurred as support to this program until the issue of a Directive in 2004 that uniforms safety level in the whole EU by mean of observatory and defining the minimum safety requirements.

Together with legislative activities, the research received a relevant impulse especially concerning the role of ventilation systems in road tunnels, which shall provide a suitable level of air quality during operating conditions by means of pushing-out of exhaust gases while, when a fire accident occurs, they shall confine fire gases in order to allow a fast and safety tunnel evacuation.

In this scenario, research activities summarized in this work take place. In particular, the main aim is the optimization of the ventilation system in order to increase general performances, for both operating and emergency conditions, by means of a new generation of jet fans with an innovative and optimized geometry.

The first step concerned a deep investigation in scientific literature about the main and mature technologies for ventilation systems. The analysis allowed to highlight, at first, the relationship between several parameters needed for system design for both ordinary and emergency conditions: tunnel geometry, jet fans location, fire conditions (e.g. thermal power source, fire location in tunnel), etc. represent main parameters with high impact on the so called *critical ventilation velocity*, that defines the limit condition in order to avoid the smoke back-layering in case of fire. As result, the investigation showed several articles concerning experimental and/or numerical studies about the evaluation of this critical velocity for different case studies by means of numerical, empirical and semi-empirical formulations.

This investigation represents also a preparatory phase to a second one where numerical analyses are performed to investigate a new generation of jet fan for road tunnel ventilation systems. By means of commercial software, several computational fluid dynamics (CFD) simulations are carried out to check an efficiency increasing for ventilation systems applying an alternative configuration for suction and exhaust fan

[1] A wide list of fire accidents in world's tunnel fire is provided in Appendix 1.

nozzles: a more efficient tunnel flow field can lead to the critical velocity by means of minor energy waste. Numerical analyses concerned at first a comparison between alternative and traditional configuration of jet fans in road tunnel; several case studies are carried out by changing main parameters such as tunnel slope, traffic jam condition, fire case, etc. in order to analyze main features, strength and weakness in different conditions.

Relevant results obtained from these analyses justified the interest to set up an experimental apparatus in order to validate results from CFD analyses. Considering main technical and economical aspects, several numerical analysis are carried out to define a reduced scale tunnel equipped with jet fan in terms of dimensions (e.g. the optimal scaling factor to preserve similitude and technical feasibility), materials (surfaces roughness has a relevant impact on velocity profiles), facilities (e.g. instrumentation and logical controls of fan). As result, a plexiglass tunnel is realized in Metrology Lab of the University "Federico II" of Naples.

Symbols

A	Cross-sectional area
a	Saccardo area
b_{fo}	Fire source radius
c_P	Specific heat at constant pressure
C_R	Drag coefficient
D	Tunnel diameter
F	Force, trust
Fr	Froude number
g	Gravity acceleration
H	Tunnel height or generic vertical distance with a subscript
$\bar{H}$	Hydraulic diameter of tunnel
I	Laser intensity
k	Kempf coefficient
L	Generic length
l	Back-layering length
$\dot{m}$	Mass flow rate
p	Pressure
Q	Heat Release Rate (HRR)
R	Tunnel radius
Ri	Richardson number
r	Density ratio
S	Tunnel slope
T	Temperature
u	Generic velocity
$\dot{V}$	Volumetric flow rate
W	Tunnel Width
Z	Fan distance from ceiling

Greek symbols

α	Pitch angle for jet fan silencer
β	Correction factor for critical velocity by Tetzner [55]
δ, ε	Empiric constants by L.H. Hu et al. [56][57]
γ	Ratio of specific heats
η	Efficiency
ρ	Density
Ω	Temperatures ratio by Wu et al. [53]

Subscripts

amb	Ambient
avg	Average
cr	Critical
ef	Fire source bottom/floor – tunnel ceiling
fc	Fire source surface – tunnel ceiling
H	Hydraulic dimension

Apex

*	Dimensionless quantity

1. Generalities on ventilation systems for road tunnels

The primary task of a ventilation system in road tunnel is to reduce under fixed limits, by means of air dilution, the concentration of pollutants, mainly due to vehicle emissions. Together with this aim, these systems attend in case of emergency such as fire in order to restore, where possible, safety condition for people and goods by reducing the impacts of smoke and fire.

The ventilation system represents one of several facilities installed in road tunnel to guarantee health and safety. Its use concerns mainly long road tunnel where fire extinguishers, escape routes, SOS phones and other facilities may be not enough for the purpose. According to this, several national regulations impose to equip with ventilation systems all tunnels with length major than 500 m also in consideration of most stringent concentration rate for main pollutant substances such as CO and particulate (as reference, see Table 1 for Italian regulation).

Table 1 – Max concentration of air pollutant – D.Lgs. 155/2010

Pollutant	**Reference value**	**Concentration [μg/m³]**
CO	Limit for medium consecutive 8h	10000
CO_2	Hourly medium limit < 18 times/year	200
	Alarm limit consecutive 3h for all regions	400
	Annual medium limit	40
PM10	Daily medium limit < 35 times/year	50
	Annual medium limit	40
PM2.5	Annual medium limit	25

In case of lack of laws/regulations for the specific case of road tunnel, it can be taken as reference for system design the World Road Association that consider limit values for CO, visibility, altitude, etc.

Table 2 – CO limits for road tunnel by World Road Association

Tunnel type	CO limit [ppm]
Urban Tunnel	
Daily congested	100-150
Less congested	150
Highway tunnel	250

Table 3 – Visibility limits by World Road Association

Tunnel type	Visibility limit (m^{-1})
Urban tunnel – normal traffic	0.005
Congested traffic	0.009
Gallery to be closed	0.012

Results can be drawn in two diagrams referring to 1 km length, 1 lane, filled by 100 vehicles at 10 km/h at sea level for different tunnel slope.

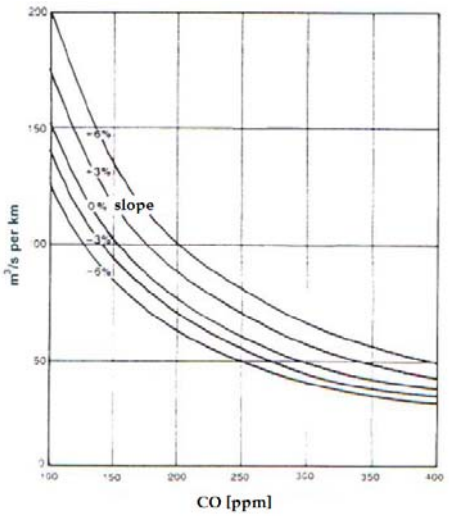

Figure 1 – Air flow vs CO (sea level)

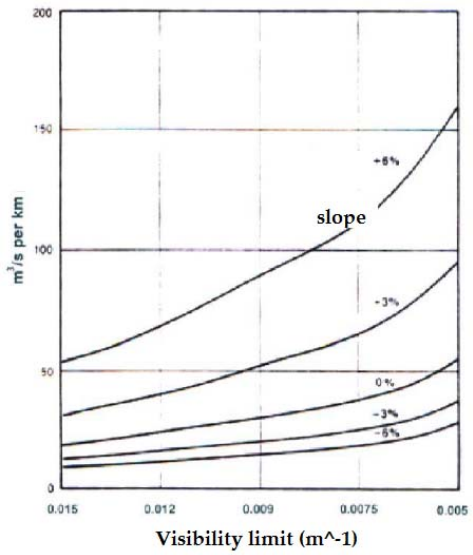

Figure 2 – Air flow vs Visibility limit (sea level)

The effect of the altitude has impacts on several physical parameters as temperature, pressure and density. By increasing the reference altitude from sea level (0 m) to highest ones (> 0 m) the effects of pressure, temperature and density decreasing lead to move to highest values the curves showed in previous Figure 1 and Figure 2.

Results show that, in both ordinary and emergency conditions, several parameters occur for ventilation system design and operation: vehicle intensity and typology (heavy good vehicles vs cars), tunnel geometry, traffic direction(s), slope, etc. shall be considered as input data whereas pollutant concentration, smoke shape and direction, temperature shall be considered as variables to be controlled. According to the high number of parameters involved, each case should be considered as stand-alone with a customized ventilation system. These can be classified as shown in Table 4.

Longitudinal ventilation system

The longitudinal ventilation realize a longitudinal airflow through the tunnel in order to wash its capacity in ordinary condition and confine smoke in case of fire (Figure 3).

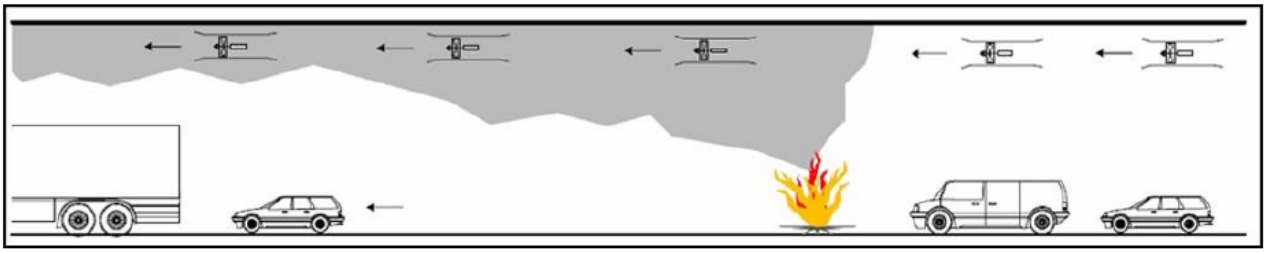

Figure 3 – Longitudinal ventilation system (fire case)

Transverse ventilation system

This kind of system takes advances from the buoyancy forces that occur in case of fire: the worm fraction of air (hot and polluted) tends to rise up to the tunnel ceiling where it is mechanically extracted. Thus, the fresh air became stratified in the lower part of tunnel section allowing a safe evacuation by occupants and operation of emergency task force (Figure 4).

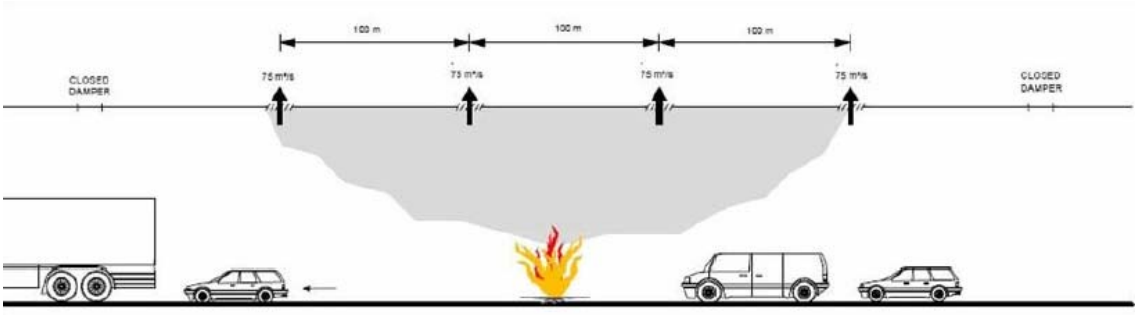

Figure 4 – Transverse ventilation system (fire case)

As shown, the application of this kind of system appears quite difficult and expensive for both design/construction and operation although applicable in any tunnel.

1.1. Overview about investigation of ventilation systems for road tunnel

After the diffusion and implementation of CFD software, several research activities have concerned the set up of numerical methods able to schematize:

- combustion mechanisms of a vehicle in fire in a tunnel;
- description of the fire-induced smoke (e.g. its properties, shape, motion, interaction with ceiling, etc.);
- relationship between the main factors influencing the ventilation system (e.g. heat release rate, reference length, etc.).

One of the most important parameter controlled through a ventilation system is the longitudinal velocity of the air especially when a fire occur. Here, in case of a not well-designed system, the fire-induced smoke can reach the ceiling, form two gas streams and rise the tunnel (backlayering phenomenon). Hence the necessity of a formulation about a "critical ventilation velocity" just able to prevent the formation of the backlayering, widely discussed in Chapter 2. Numerical results provided by CFD codes are compared with experimental ones in order to validate the proposed models and/or schemes. Since the majority of these data are obtained from scale-reduced tunnel, scaling techniques (e.g. Froude scaling) are considered by several authors, highlighting strength and weakness.

1.2. Main factors and configurations of a ventilation system and their influence on performances

The complexity in the study of tunnel ventilation systems is mainly due to the great variety of factors that can influence performances and so the safety conditions they have to provide. In this section, an overview about the influence of fan configurations on the whole system is given and the piston effect, due to moving vehicles, is described although this one is often not taken into account because the majority of cases analyzed consider a traffic-stop due to a vehicle fire in the tunnel.

As said before, the different locations of fans in a tunnel may give different performances. The presence of a fan close to a wall or a ceiling of the tunnel causes pressure drops that influence the energy transfer from the fan itself to the induced airflow. Moreover, other factors may influence the flow motion in the tunnel: one of these is represented by the shape of the blades in the impeller that gives a rotational component to the air flow creating an helical motion; besides, the shape of the air jet depends also by the presence of silencers or nozzles on fan delivery. Martegani and Pavesi [1] have conducted an experimental study in order to investigate the influence of these factors on the air flow in a tunnel.

Considering a single fan on the tunnel ceiling, they have shown how the jet remains close at least for 40 diameters. The induction is guaranteed from both the dynamic exchange on

the jet boundaries and the air mixing. Increasing the ratio between the distance of the fan from the tunnel ceiling and the hydraulic diameter $Z/\overline{H}$, the induction is essentially produced by this exchange with an increase of the mixing length and a reduction of the Coanda effect.

Defining the Kempf coefficient (k) as follow, authors have shown how 1/k increases against ($Z/\overline{H}\cdot d/\overline{H}$).

$$F_{tunnel} = F_{fan}\left(1 - \frac{u_{tunnel}}{u_{fan}}\right)\frac{1}{k} \quad (1)$$

Since it is shown that the Reynolds number variations seems to not influence the Kempf coefficient, this trend can be considered for the generality of cases. When a vortex is generated, this influence the divergence of the jet encouraging the mixing with the air in the tunnel. Downstream the nozzle the air jet is divided in two parts and the vortex close to wall migrate to the road and then to the central region of tunnel. When these phenomena occur, the energy exchange prevalent is due to a mixing process and so the portion of energy for the thrust is heavily reduced. The increasing of the rotational component causes a reduction of the jet effectiveness. Armstrong et al. [2] have proposed an installation efficiency equation for a round section tunnel for a jet velocity between 23 and 38 m/s, an area ratio of 0.0076÷0.0268, a separation ratio Z/R=0.029÷0.465.

$$\eta = 97 + \left(6.2 + \frac{0.093A}{a}\right) log_{10}\frac{Z}{R} + 2.2(u_{fan} - 33) \quad (2)$$

where a is the Saccardo area, D and R are the tunnel diameter and radius respectively. By the definition of the Jet Fan Fluid Power as $1/2\rho a(u^2_{fan} - u^2)$, Armstrong has given an approximated expression of the Power Efficiency defined as follow:

$$Power\ efficiency = \frac{Useful\ Work\ Done}{Jet\ Fan\ Fluid\ Power} = 2\eta/100(1 + u_{fan}/u_{tunnel}) \quad (3)$$

The air flow motion in a tunnel when normal conditions of traffic occur, can be modified by the motion of vehicles because it is generated an induced effect on air flow motion called ‘‘piston effect’’. This one has an influence on the tunnel ventilation. The impact of location of jet fan on airflow structure in tunnel fire has been also studied by Se et al. [3]. Results show that the airflow structure for pool fire is not altered by changes in dimensions or orientations of the fire source, provided that the fire does not occupy a significant cross-sectional area in the tunnel. Nonetheless, authors have shown that the presence of solid fire imposes adverse effect on the airflow. It creates a sudden contraction

to the air passageway that should enhance the airflow velocity. Finally, the correlation between distance of active fan group from the fire source and the upstream velocity shows a leveling-off feature when active fan group is located 200 m or more. Performances of several configurations of the ventilation system have been discussed by Li and Chow [4]. They have highlighted the advantages and disadvantages for each them, as reported in the following Table 4 (Li and Chow, 2003).

Table 4 [4]

Tunnel ventilation system	Advantages	Disadvantages
Longitudinal	Less space required for ventilation building and ductwork Less initial capital cost Simple installation Effective for one-directional traffic Good smoke control for entire range of fire size Simple system control	Greater height or width of tunnel envelope Application is limited by tunnel length Not desirable for bi-directional traffic operation Smoke is not removed from tunnel Careful consideration required for detection of fire High portal emission
Semi-transverse	Smoke is removed from tunnel Clear zones on both sides of fire site for evacuation Simple system control Low maintenance costs Applicable for bi-directional traffic Uniform vehicle emission concentration	No directional smoke control Ventilation building and ductwork required High investment costs Careful consideration required for detection of fire Ineffective in smoke management
Transverse	Suitable for long tunnels Applicable for bi-directional traffic Effective in temperature management Adequate fresh air supply Uniform vehicle emission concentration	Large ventilation building and ductwork High investment cost Careful consideration required for detection fire Ineffective in smoke management
Partial (pseudo) transverse	Intermediate characteristics between transverse and semi-transverse systems	
Combination of longitudinal	Smoke is removed from tunnel Good smoke control	Relatively complex system control Higher investment costs

and semi-transverse system	Clear zones on both sides of fire site for evacuation Applicable for bi- and one-directional traffic operation Smaller critical velocity required Good control for firefighting access Either one of the system can be used in normal condition	Higher operating and maintenance costs Careful consideration required for detection of fire

In order to increase the energy efficiency and improve the performances of a longitudinal ventilation system, Betta et al. [5][6] have compared numerically both traditional and alternative jet fans for a road tunnel. These ones consist in longitudinal fans with inclined silencers toward the tunnel floor of a pitch angle. The technical solution provides for a better longitudinal velocity distribution decreasing the thrust needed and reducing the interaction of the accelerated air flow with tunnel ceiling. Two scenarios are investigated: with and without traffic. Results show that, in the first case, the alternative system guarantees for a pitch angle equal to 2°, a lower temperature value near the ceil. In the second case, the same result is obtained with an angle of 4°.

Chen et al. [7] have shown how the distribution of velocity due to the presence of vehicles in movement weakly depends upon their speed, spacing and size. The results also show that the so called *piston effect* in a tunnel is not confined to the vicinity of vehicles, in fact this effect in the upper region of the tunnel is 40% of that around the vehicle. The authors have shown the ratio of the mean flow velocity to the vehicle speed for different traffic conditions; this ratio varies from a minimum of 2.7% (two-way traffic, alternate small and large vehicles, 2 m vehicle spacing) to 33% (one-way traffic small vehicles, 1 m vehicle spacing).

1.3. The effects of fire in tunnel

Several authors have tried to understand the mechanisms of fire processes in tunnels, its effects as the induced smoke, the distribution of temperatures and its connection with the ventilation system. Wang [8] have carried out a study on the characteristics of a tunnel fire in three aspects: the length of backlayering, the flame length and the effect of an object within the tunnel. Ingason and Lönnermark [9] have investigated the heat release rate (HRR) for four large-scale tests for HGV in a road tunnel with longitudinal ventilation. In Table 5 (Ingason and Lönnermark, 2005) are presented the results: peak HRRs in the range

of 66–202 MW were measured and the time to obtain each peak was found to be in the range of 7–18.5 min from ignition. As results, for all tests the fire growth rate in the range 5–100 MW was found by authors to be nearly linear. Note that the method used to estimate the HRR includes many uncertainties: calculations show that the combined expanded relative standard uncertainty with a 95% confidence interval was 14.9%.

Table 5 [9]

Test	Time from ignition to peak HRR (min)	Linear fire growth rate from 5MW up to 100MW - Linear regression coefficient (MW/min) -	Peak HRR (MW)
T1	*18.5*	*20.1 (0.996)*	*201.9*
T2	*14.1*	*26.3 (0.992)*	*156.6*
T3	*10.0*	*16.4 (0.998)*	*118.6*
T4	*7.4*	*16.9 (0.996)*	*66.4*

As mentioned before, the fire induced smoke has a direct influence on safety in road tunnels and thus on the ventilation system design. Hence, several authors have tried to understand this influence and schematize it by a numerical approach in order to describe the phenomenon strictly linked to the safety of people in a fire tunnel. Modic [10] have carried out a numerical fire simulation, starting before the ventilation system is activated, involving air velocity, air temperature and wall temperature in case of fire. Vauquelin [11], through the set up of a scale model, has used a mixture of air and helium at ambient temperature to simulate the smoke fire plume. The duality between inertial and buoyant forces is considered by the author one of the most important factor for smoke control applications, so the aim is to reproduce with accuracy the mixed convection process. Radiation and heat losses to the walls are not taken into account. The approach wants to be a simplified method to understand phenomenological aspects and get the orders of magnitude of the main factors. Moreover, Vauquelin has tried to understand the main factors involved in the ventilation mechanisms. As results, tunnel height and width, cross-section, slope, HRR, fire source geometry and location have an important role on the minimum velocity able to prevent the rising of the fire-induced smoke (critical velocity) as presented widely in the Chapter 2. With a reduced-scale tunnel model provided by adjustable angle varying up to 30° to the horizontal, Chow et al. [12] have carried out experiments in order to observe the movement of smoke. This patterns indicates that the shape of the buoyant plume inside the tunnel depends on the tilted angle and the bending angle of the plume depends on the tunnel angle. Another study on the smoke spread in a tilted tunnel has been carried out by Junmei et al. [13]. In particular, they have studied the

spread for tunnels with different tilted gradients under different longitudinal velocity by a reduced-scale model. The results show that, because of the stack effect in a tilted tunnel, hot smoke spreads much faster to the top exit than in the level one, and a thick smoke layer is formed when smoke moved to the upward part of the tunnel and filled it up. Moreover, the ventilation speed is found to have a great influence on temperature distribution along the tunnel: maximum temperature in tunnel due to the fire would be reduced and the smoke stratification would be distributed when the longitudinal ventilation speed becomes large. Authors have highlighted how a lower ventilation speed should be adopted at the beginning to ensure the smoke downstream of the fire keep stratified to give the tunnel users more time to escape. On the other hand, the effects of pool size and fuel type on the characteristics of pool fire have been examined by Apte [14] who in particular has studied the correlations between the smoke extinction area (SEA) and the yields of CO_2 and CO, as presented in Eqs. (4) and (5).

$$SEA = \frac{\dot{V}_{exhaust}(1/L_{laser})\ln(I_{laser,0}/I_{laser})}{\dot{m}_{fuel,loss}} \quad (4)$$

$$\begin{cases} SEA \sim (CO\ yield)^{1.3} \\ SEA \sim (CO_2\ yield)^{6.5} \end{cases} \quad (5)$$

Here $\dot{m}_{fuel,loss}$ is the fuel mass loss rate (kg/s), L_{laser} is the laser beam path length through smoke (m), $I_{laser,0}$ and I_{laser} are the laser intensity before and after attenuation due to smoke respectively. Apte has shown that these correlations indicate that the SEA and the CO_2 and CO yields vary mainly with the type of fuel and not so much with the pool size. Relevant studies about the carbon monoxide behavior due to a fire in a tunnel and validation of numerical models, have been performed by Hu et al. [15][16][17]. Through a theoretical analysis with comparison of experimental data from a full-scale model, authors have studied the longitudinal decay profiles of CO concentration and smoke temperature with their difference, for a fire-induced smoke in a road tunnel. With numerical CFD simulations by Fire Dynamic Simulator (FDS), Hu et al. have shown how the smoke temperature decays much faster than the CO concentration along the tunnel, highlighting that, by increasing the longitudinal ventilation velocity, their longitudinal profiles difference decreases. Moreover, the role of the fresh air mass entrainment for the CO concentration and both this and heat loss from the smoke to the ambient for temperature profile are highlighted. In particular, the longitudinal profile difference increases along with the distance away from the fire source asymptotically to a quasi-steady value. The velocity of CO concentration decay is shown to be less affected by the longitudinal ventilation velocity for a relative larger fire because of higher buoyancy forces which

counteracts the inertial forces of longitudinal ventilation air flow. Also the vertical distribution of CO concentration has been investigated through FDS simulations. Results have shown that this one would linearly increase with the height above the floor.

The possibility of using an *air curtain* for smoke and CO confinement is investigated by Hu et al. [18]. They have shown that gasses are mainly confined to remain in the near fire region at one side of the air curtain. In particular, the curtain realizes a sort of accumulating effect when the discharging velocity is no more than 3 m/s and a diluting effect for that up to 4 m/s. Thus the CO concentration in the near fire confinement zone reached a maximum level at discharging velocity of about 3 m/s.

Another factor linked to the fire-induced smoke is defined and evaluated by Vauquelin and Telle [19]. In their work, in order to extract the whole smoke, the extraction rate has been adjusted for several values of HRR and for each steady state, the longitudinal velocity induced by extraction has been measured. This velocity is called the ''total confinement velocity''. Authors have noticed that total confinement requires a large extraction capability and the associated induced velocity appears to be greater than the corresponding critical velocity. For a smoke layer length lower than 4 times the tunnel height, the induced longitudinal velocity is significantly reduced. For this reason, they have decided to define a *confinement velocity* for a backlayering length equal to 4H. Note that this velocity is only related to the specific ventilation configuration tested: only two vents are activated, one on each side of the fire source.

Deutrieue and Jacques [20], through numerical simulations, have confirmed the existence of a local additional pressure drop due to the presence of a fire in the tunnel and have provided an empirical formula to evaluate its value. Putting together the three equations previously found where the pressure drop Δp_{fire} is sub-sequentially expressed as a function of HRR (Q), the upstream velocity (u) and the hydraulic diameter ($\bar{H}$), they have estimated a mathematical formula able to estimate the pressure drop due to a fire, when a 1D model is considered in a unidirectional tunnel without slope and with a constant square section. Moreover, the Eq. (6) assumes that there is not heat transfer at the walls, smoke is considered to be heated air and the fire has a constant HRR produced by a car-like object.

$$\Delta p_{fire} = \frac{Q^{0.8} u^{1.5}}{\bar{H}^{1.5}} c_1 \text{ where } c_1 \approx 41.5\ 10^{-6} s^{1.9} kg^{0.2}/m^{2.6} \qquad (6)$$

The calculated value of c_1 has been obtained for the three considered parameters within realistic ranges of values chosen for each of them (HRR=2.5÷30MW; u=1.5÷4.5m/s,

$\bar{H}$=4÷7.5m). The value of this parameter may vary if other ranges for these parameters are taken, thus the formula has a limited application range.
Another aspect linked to the presence of fire in a tunnel is the temperature profile generated by the source term. Several authors, as Li et al. [21], Li and Ingason [22], Nyman and Ingason [23], have investigated the effects induced on temperature when a fire occur in a tunnel. In particular, these ones have analyzed the effects of different ventilation systems, ventilation velocities, HRRs, tunnel geometries and fire source on the maximum excess gas temperature beneath the ceiling in large tunnel fires. The proposed equation reads:

$$\begin{cases} DTR1, & DTR1 < 1350 \\ 1350, & DTR1 \geq 1350 \end{cases} \text{when } u^* \leq 0.19$$
$$\begin{cases} DTR2, & DTR2 < 1350 \\ 1350, & DTR2 \geq 1350 \end{cases} \text{when } u^* \geq 0.19 \quad (7)$$

where

$$\begin{cases} DTR1 = 17.5 \dfrac{Q^{2/3}}{H_{ef}^{5/3}} \\ DTR2 = \dfrac{Q}{u b_{fo}^{1/3} H_{ef}^{5/3}} \end{cases} \quad (8)$$

Here, H_{ef} is the vertical distance between the fire source bottom and tunnel ceiling (m) and b_{fo} the radius of the fire source (m). As one can see, this correlation is valid up to a given maximum excess gas temperature of 1350 °C, considered the upper limit for temperature obtained from large scale tunnel tests depending mainly on the HRR then others parameters. Hu et al. [24] have done experimental studies on fire-induced smoke temperature distribution along tunnel ceiling. Results show that to a fire size increasing, the smoke temperature below the ceiling is higher, but it decays faster while traveling down the tunnel. Authors sustain that longitudinal ventilation velocity seems to take much influence on the smoke temperature decay speed downstream. A ''barrier effect'' was shown for the smoke temperature distribution of the upstream backlayering. The temperature measured were higher upstream than downstream before the ''barrier'', and were much lower and decreased faster along the tunnel ceiling after the ''barrier''. Hu et al. also have shown how the temperature and traveling velocity of the upstream smoke flow decrease largely when the longitudinal ventilation velocity increases a bit. According to them, the results show that Delichatsisos' model over estimates the decay speed of ceiling jet temperature for the downstream flow, in disagreement with what sustained by Kunsch [25]. Another study on the fire-induced buoyancy flow stratification behavior has

been done by Yang et al. [26], considering the effect of the velocity shear between the hot buoyant flow and the cool air flow. They have shown that the thermal stratification and the consequent flow patterns are well correlated with the Richardson number (Ri). In particular, authors have shown that the stratification pattern found in three regimes:

- $Ri > 0.9 \rightarrow$ stable buoyant stratification
- $0.3 < Ri < 0.9 \rightarrow$ stable buoyant stratification but with interfacial instability
- $Ri < 0.3 \rightarrow$ unstable stratification

Kurioka et al. [27] have studied in deep the phenomena in the near field of a fire source in a tunnel having a rectangular and horseshoe cross-section. The fire sources have been modeled as square ones and the aspect ratio of the tunnel cross-section, HRR and longitudinal forced ventilation were varied. Empirical formulae are extrapolated for flame tilt, apparent flame height, maximum temperature of smoke layer and its position. Here authors have found that the length defined by $H^{3/2}/W^{1/2}$ became a representative length for investigating fire phenomena in tunnels.

The interaction between the ventilation system on fires has been investigated by Carvel et al. [28][29] and Colella et al. [30]. In particular they have investigated the influence of forced longitudinal ventilation on car fires, pool fires and HGV fires in tunnels. Results show that each of them responds in a different way to the forced ventilation: it is predicted that size of HGV fires is greatly increased by ventilation (until ten times larger than if natural ventilation is used), large pool fires growths with HRR (also up to 50%) while an opposite trend is for smaller pool fires and a forced ventilation velocity does not affect the HRR of a car fire in a tunnel, compared to natural ventilation.

Similar results, as the ones shown by Li et al. [31], have been obtained by Roh et al. [32] studying an n-heptane pool fires in a reduced-scale tunnel with HRR ranging from 3.71 kW to 15.6 kW. The mass loss rate of burning fuel and the temperature distribution have been measured. As results, there is an inverse proportionality between the burning rate and the ventilation velocity: when this one increases, it is highlighted that the supply oxygen effect is larger than the cooling effect. The HRRs in experiment are larger than constant HRRs by 4.45 ÷ 11.3 times in the n-heptane pool fires. Thus authors have highlighted how a ventilation system designed with the critical ventilation velocity based on the constant HRR can make the fire grow further, so that it may give rise to conflagration in tunnel. Another study on the influence of ventilation on HRR and fire growth rate (for solid fuels) has been provided by Ingason and Li [33]. They have found that the fuel mass loss rate per unit fuel surface area in a tunnel fire test is in a range of 1.4 ÷ 1.55 times the value measured in a free burning test. This is much lower than studies by

Carvel et al. [28]. According to Ingason and Li [33], one possible explanation of this, is the way the fuel was compared. If a fuel has a low porosity factor, an increase of the order can be easily obtained, as presented by Carvel et al. [28]. However Ingason and Li [33] are agree about their result: the increasing longitudinal ventilation rate increases the fire growth rate.

A description of the manner the cross-flow affects the burning rate (mass consumption rate per unit area) of gasoline pool fires is presented by Hu et al. [34]. They have found that, in opposition to a quiescent air condition, the burning rates decrease with the increasing of pool size under certain cross air flow speed. Moreover, the temperature of the trailing, parallel rim walls are increased greatly due to extensive heating by the deflected flame.

1.4. Numerical methods for road tunnel analysis

A numerical approach for tunnel analysis, not only in case of fire, can be very useful to understand the thermo-fluid dynamics mechanisms and design a ventilation system. Several authors have tried to schematize numerically a domain as complete as possible and, at the same time, to set up models able to predict the own experimental data. Jain et al. [35] have carried out a comparative study between two types of deterministic models to study fire growth and smoke movement: the zone model (through CFAST) and the field model (through the ''generic'' CFD code CFX). They have shown that CFAST is very sensible to the location of fire source and it is not able to provide temperature profiles at selected locations, so the zone model can give only global views. On the other hand, CFX provides detailed information regarding smoke movement inside tunnel: it not only provides temperatures at various locations but it also predicts the movement of smoke. A same potential about a CFD commercial code is found by Vega et al. [36] who, through a detailed analysis of several factors as temperature and CO distribution of a smoke generated during a fire inside a road tunnel, have tried to schematize numerically a longitudinal ventilation system. Authors have opted for a volumetric heat source vehicle-size parallelepiped where the lateral surfaces suck air and the upper one exhausts a gas mass flow rate according the following equations where a typical hydrocarbons stoichiometric combustion is considered.

$$\begin{cases} \dot{m}_{gas} = \dfrac{\dot{Q}}{c_p\left(T_{gas} - T_{amb}\right)} \\ \dot{m}_{air} = \dot{m}_{gas} - \dfrac{1}{3}\dot{m}_{CO_2} \end{cases} \qquad (9)$$

On the other hand, Migoya et al. [37] have mixed both field and zone models (FLUENT and PHOENICS) in a single and simplified one (UPMTUNNEL) for steady-state conditions. They have divided the domain into two zones: the first one includes the region upstream from the contact point of the smoke on the ceiling and it is treated by a one-dimensional model, the second zone is the diffusion region that spreads downstream from the plume. The proposed model is able, in the aims of authors, to provide results for all the flow quantities at every point of the calculation field, while maintaining the one-dimensional character of the calculations for the plume. Results of UPMTUNNEL model are found to be in good agreement with both 3D models and measurements. The most important limitation is the need of a minimum air ventilation speed that should be greater than the critical one needed to prevent backlayering. In case of lower air speeds, the backward movement of smoke upstream from fire cannot be predicted with this model. Moreover, they have found discrepancy with FLUENT results in terms of curvature of plume, temperature field and shape of flames.

The smoke development, in case of tunnel fire, has been also simulated using the only commercial CFD software PHOENICS 3.5 by Yang et al. [38] with field modeling method. They have studied the spreading rules and characteristics of concentration field and temperature field of smoke flow with different longitudinal ventilation speeds. In particular they have highlighted that the distance upstream the fire source and the temperature of winds are linked with an inverse proportionality. Moreover, the decreasing temperature is reduced to a constant when the distance is large enough, so the influences scope of the high temperature are limited. The highest temperature firstly appears in side wall and then it spreads to the middle of the tunnel with time, so it is better for passengers to evacuate along the midline of the tunnel.

One of the approximations occurring in numerical studies of tunnels regards the evaluation of boundary conditions and solver settings. Among these, are relevant the coefficients useful to define them. Jang and Chen [39] have provided in their work an optimization approach that can simultaneously determine the four major aerodynamic coefficients: friction coefficient of tunnel wall, averaged drag coefficients of small-size and large-size vehicles and the pressure-rise coefficient of jet fans. Two approaches for the turbulence model are considered by Maele and Merci [40] to predict the critical ventilation velocity on a computational tunnel of reduced length: Reynolds-Averaged Navier–Stokes (RANS) and Large Eddy Simulations (LES). It has been illustrated that the LES results can strongly depend on the mesh, particularly in case of not sufficiently fine mesh. As this becomes too coarse, the unsteadiness is no longer resolved to a sufficient extent and the

predicted critical ventilation velocity differs strongly from the value obtained on a sufficient fine grid. Authors have demonstrated that there is much more turbulent thermal diffusion in the LES calculations than in the RANS simulations. The major reason is that the unsteady motions are captured by LES and this strongly increased the amount of large-scale turbulent mixing, which is not present in the RANS simulations. They also have shown that the predicted critical velocity with LES is only slightly dependent on the value of the constant applied in the *Smagorinsky subgrid model* for eddy viscosity.

A similar work has been carried out by Gao et al. [41] who have applied large eddy simulation to study pool fire in a ventilated tunnel with a field model. Their results show that the model can well predict the flame shape and the smoke backflow. According to author's opinion, both approaches using large eddy simulation and RANS methods can get good results for simple problems. Although higher-level computer configuration and more computing time are required for carrying out LES, more complex structures can be simulated.

A set up of a numerical model for the study of flow in tunnel at ambient temperature able, at the same time, to require a low computational cost is provided by Colella et al. [42]. They have proposed two different multi-scale techniques validated by experimental data. The first one, using a *direct coupling* between a mono-dimensional model and a CFD one, can lead to very accurate results with a significant reduction of the computational requirements. On the other hand, the second multi-scale model, with an *indirect coupling* between a mono-dimensional model and a CFD one, has been used to reconstruct the behavior of a pair of jet fans in order to obtain a better estimation of the thrust and its dependence on the bulk flow velocity. The model shows that the niches where the fans are installed produce a significant reduction of the ventilation system performance due to a decrease of the thrust of the jet fans. Moreover, the models have been demonstrated to be a valid tool for the simulation of the complex behavior of the tunnel ventilation systems.

2. *Critical velocity formulations*

In case of fire tunnel, one of the most important phenomenon to take into account for guarantee the safety is the backlayering, i.e., the fire-induced smoke reaches the ceiling, forms two gas streams rising the tunnel. To avoid this event it is necessary the presence of a well-designed ventilation system in order to realize a *critical ventilation velocity*, defined as the minimum one just able to prevent the smoke rising. In several years, researches have proposed analytical formulations able to calculate the value of the critical velocity as a function of the main parameters occurring in road tunnel problems.

Several theories for the critical velocity calculation are based on Froude number preservation. This number is defined as follow:

$$Fr = \frac{u^2}{gL} = \frac{inertial\ forces}{gravity\ forces} \tag{1}$$

where g is the gravitational acceleration, u and L are the characteristic velocity and length respectively. The Froude number is often used as a scaling techniques in fire situations especially where the Reynolds number is sufficiently large. It is sometimes combined with the density ratio of the smoke ($\Delta\rho/\rho$) in order to include the effects of stratification. In these cases it is called *Richardson number* or *Modified Froude number* (Eq. (2)).

$$Ri = \frac{\Delta p g L}{\rho_0 v^2} = \frac{1}{Fr} \cdot \frac{\Delta\rho}{\rho} \tag{2}$$

Using a simple theory based on the conservation of Richardson number, Thomas [43] has found a simple relationship for the critical velocity (Eq. (12)). To this aim he suggested that, at critical condition, Richardson number is close to unity (i.e., buoyant forces equal inertial ones).

$$u_{cr} = \left(\frac{gQH}{\rho_0 T_0 c_p A}\right)^{1/3} \tag{3}$$

In the previous Eq. (3) Q is the rate of convective heat release, H is the tunnel height, ρ_0 is the density of the inflow, T_0 is the inlet temperature, c_p is the heat capacity of the inflow at constant pressure and A is the cross-sectional area of the tunnel. Lee et al. [45] also defined a modified Froude number which was similar to the Thomas one in order to estimate a critical velocity formulation but they consider the density difference instead of temperature.

A similar approach is followed by Hinkley [46] and Heselden [47] for the calculation of hot gases velocity along the roof of a shopping mall. Their relationship reads:

$$u_{cr} = 0.8\left(\frac{gQT}{c_p\rho_0 T_0^2 W}\right)^{1/3} \quad (4)$$

Based on Thomas' suggestion, Danziger and Kennedy [48] have proposed a model able to represent the asymptotic behavior of the critical velocity. They show that a fire of heat release rate Q, only modifies the mean temperature of the air between upstream and downstream, according to the energy balance. Expressing the heat release rate (HRR) as a function of the Richardson number (see Eq. (2)) and assuming that critical conditions are obtained for a critical Richardson number (Ri_{cr}), the critical velocity reads:

$$u_c = \left(\frac{gHQ}{\rho_0 c_p T_b A R i_{cr}}\right)^{1/3} \quad (5)$$

where T_b is the buoyant release temperature (K). To define the Ri_{cr} parameter, Danziger and Kennedy use the value of 4.5 obtained by Lee et al. [45] for experimental tests on a scale model.

As predict by the Thomas [43] empirical relationship (Eq. (3)), Oka and Atkinson [49] have shown that the critical velocity varies with the heat release rate. They provide to simple formulae testing the method of scaling model results by a comparison with large-scale test data. This technique is known as the ''Froude scaling'', conveniently described in the following steps and able to scale the values of heat release and velocity in order to produce a similar flow in both model and full-scale tunnel.

Scaling of heat release rate

The model and full-scale heat release rate Q_{model} and Q_{full} scale are related by Eq. (6)

$$\frac{Q_{model}}{Q_{full\ scale}} = \left(\frac{L_{model}}{L_{full\ scale}}\right)^{5/2} \quad (6)$$

where L_{model} and $L_{full\ scale}$ are the length scales of the model and full-scale tunnels respectively.

Scaling of velocity

The model and full-scale inlet velocities v_{model} and v_{full} scale are related by Eq. (7)

$$\frac{v_{model}}{v_{full\ scale}} = \left(\frac{L_{model}}{L_{full\ scale}}\right)^{1/2} \tag{7}$$

Since the critical velocity changes with the burner's size, shape, location or when a blockage is introduced into the tunnel near the fire, Oka and Atkinson [49] have suggested a ''general'' expression of the critical velocity (Eq. (8)). This formula, limited for tunnels with the arched colliery shape, can be applied to small and large fires.

$$\begin{gathered} u_{cr}^{*} = u_{max}^{*}(0.12)^{-1/3}(Q^{*})^{1/3}\ for\ Q^{*} < 0.12 \\ u_{cr}^{*} = u_{max}^{*}\ for\ Q^{*} > 0.12 \end{gathered} \tag{8}$$

At least they have shown that the fire geometry has a relatively minor effect on the critical velocity; the critical velocities are reduced when the fire occupies a large proportion of the width of the tunnel. The problem with the dimensionless analysis proposed by the authors is that the tunnel height is used as the characteristic length. Experimental results show clearly that, at constant tunnel height, the critical velocity varies with its width.

The effect of the tunnel slope on critical velocity is studied by Atkinson and Wu [50]. They have estimated a correction factor for 0–16% slope range to calculate the critical velocity value (Eq. (9)) that is in a perfect agreement with experiments carried out subsequently by Vauquelin [51], Vauquelin and Wu [52], with a ± 10% channel slope.

$$u_{cr}(S_{\%}) = u_{cr}(0)[1 - 0.014\tan^{-1} S/100] \tag{9}$$

According to Oka and Atkinson [49] experience about the choice of the reference length, Wu and Bakar [53] have proposed to use the tunnel mean hydraulic diameter ($\overline{H}$) in substitution of the tunnel height as the characteristic length in the dimensional analysis. Of the same opinion is Kang [54] that has highlighted how this choice may provide a better characterization of critical ventilation velocity. Note that a different representative length is proposed by Kunsch [25], as presented before. According to authors, this choice allows

to derive a universal formulation able to predict the critical velocity for tunnels with various cross-sectional shapes. The one-directional suggested equations are:

$$u_{cr}^{*} = 0.40(0.20)^{-1/3}(Q^{*})^{1/3} \text{ for } Q^{*} \leq 0.20$$
$$u_{cr}^{*} = 0.40 \text{ for } Q^{*} > 0.20 \quad (10)$$

Tetzner et al. [55] suggest a variation of Eq. (5) to account for the deviation from uniform mixing at the fire site due to large or wide tunnel cross sections. A correction factor ($0 < \beta < 1$) was introduced, as presented in Eq. (11).

$$u_{cr} = \left(\frac{gHQ}{\beta Fr_c \rho_0 c_p A T}\right)^{1/3} \quad (11)$$

The intent was to take into account the situation when only a percentage of the airflow mixes with the fire plume, whereas the rest will bypass the fire and remain in the lower layer. From the fire tests in a reduced scale tunnel, the correction factor was found to be between 0.25 and 0.30 for fires up to 20 MW.

Kunsch [25] has provided an alternative formulation of the critical velocity. He has assumed a rectangular cross section for the tunnel, a constant static pressure during the plume rise and he has neglected the heat losses in the turning region. Here, the maximum temperature of the plume before deflection at ceiling is given by a semi-empirical dimensionless formula provided by Heskestand and Delichatios:

$$\frac{\Delta T_{max}}{T_a} = \frac{T_{max} - T_a}{T_a} = \Delta T^{*} Q^{*2/3} \text{ with } Q_0^{*} = \frac{Q}{\gamma/(\gamma-1) p \sqrt{g} H^{5/2}} \quad (12)$$

where Q^{*} is a dimensionless heat-release rate, ΔT^{*} a dimensionless constant equal to 6.13, p the ambient pressure in, γ the ratio of specific heats of the fire gases. Since the model assumes a vertical axisymmetric fire plume, in case of a tunnel fire ventilated from one side the fire plume will be tilted to the downside. Thus the model with a vertical fire plume over-predict the critical velocity and so it can be considered as a conservative one. The temperature increase can also be expressed as a function of a buoyancy factor $B=(QgH/c_p T_a \rho_a A)^{1/3}$, so Eq. (12)(12) became

$$\frac{\Delta T_{max}}{T_a} = \frac{C_4}{gH} B^2 \text{ with } C_4 = \Delta T_0^* \left(\frac{W}{H}\right)^{2/3} \tag{13}$$

where $A = WH$ is the cross sectional area of the tunnel with W and H the width and height respectively. Defining the sequent coefficients as reported:

$$C_1 \cong 1 - 0.10\left(\frac{H}{W}\right)$$

$$C_2 = \frac{1 - 0.10\left(\frac{H}{W}\right)}{1 + 0.10\left(\frac{H}{W}\right)} 0.574\left(1 - 0.20\frac{H}{W}\right)$$

$$C_3 = 0.613$$

The critical velocity reads

$$u_{cr} = C_3\sqrt{C_1 C_4}\frac{\sqrt{1 + (1 - C_2/C_1)C_4 B^2/gH}}{1 + C_4 B^2/gH} B \tag{14}$$

Kunsch [25] has shown that in case of *small* heat release rate Q, the buoyancy factor becomes small and Eq. (14) became

$$u_{cr} \cong C_3\sqrt{C_1 C_4} B \tag{15}$$

Consequently, when the heat release rate is *large*, the critical velocity becomes independent of the factor B, i.e.

$$u_{cr} \cong C_3\sqrt{C_1 - C_2}\sqrt{gH} \tag{16}$$

A dimensionless formulation allows to consider the influence of the aspect ratio (height/width) of the tunnel cross section on the critical velocity negligible. Note that if on the one hand, during the growing phase of the fire, the heat release rate increases, on the other one the buoyancy of the hot smoke gases decreases because of the heat transfer with the colder rock layers of the ceiling. Thus, the formula for the critical velocity is valid after

the initial transients following the start of the fire, when the regime is steady or quasi-steady.

Hu et al. [56][57] have carried out studies on temperature and velocity distribution along a corridor showing how these properties can be fairly fitted by an exponential equation. Moreover, other studies analyze the backlayering length (l^*) when the longitudinal ventilation velocity is lower than the critical one through e semi-empirical model:

$$l^* = ln\left[g\delta\frac{Q^{2/3}}{Fr^{1/3}}\cdot\frac{C_k H}{u^2}\right]/0.019 \tag{17}$$

where Q is the dimensionless HRR defined for correlation of maximum temperature by Kurioka et al. [27], C_k is an empirical constant founded to fall in 0.19 ÷ 0.37 range, δ depends from $Q^{2/3}/Fr^{1/3}$, as showed below. In particular, authors have shown how this length increases with increase of fire size and decreases with increase of tunnel height and longitudinal ventilation velocity. Considering in the previous Eq. (17) l^* equal to zero, Hu et al. have found the following equation for the critical ventilation velocity:

$$u^* = \left[C_k gH\cdot\delta\cdot Q^{2\varepsilon/3}\left(g\cdot H_{fc}\right)^{\varepsilon/3}\right]^{1/(2+2\varepsilon)} \tag{18}$$

Where H_{fc} is the height from the surface of fire source to the ceiling in the tunnel and ε is given as a function of $Q^{2/3}/Fr^{1/3}$:

$$\begin{cases}\varepsilon = 6/5;\ \delta = 1.77\ for\ \ Q^{2/3}/Fr^{1/3} < 1.35\\ \varepsilon = 0;\ \delta = 2.54\ for\ \ Q^{2/3}/Fr^{1/3} \geq 1.35\end{cases}$$

Therefore, authors have compared the critical ventilation velocity in Eq. (18) with FDS predictions and models provided by Wu and Bakar [53], Danziger and Kennedy [48], Kunsch [25], Thomas [43][44], model scale experimental results of Vauquelin [51].

Hwang and Edwards [58] have used a CFD program (Fire Dynamics Simulator, FDS) to model floor-level fires in a ventilated tunnel, through a comparison between ventilation velocity numerical data and experimental ones. Tunnels of different sizes and fire source geometries have been selected for simulations. The CFD results show the leveling-off of the critical ventilation velocity when the heat release rate surpasses a certain value. At this

critical ventilation, the ceiling temperature above the fire reaches a maximum. Furthermore, they have highlighted how the critical ventilation velocity is roughly proportional to the 1/5 power of the fire heat generation rate. In particular, according to Quintiere, the reference velocity for a fire plume is:

$$u = \sqrt{g}\left(\frac{Q}{\rho_0\sqrt{g}c_pT_0}\right)^{1/5} \tag{19}$$

Hwang and Edwards [58] have shown that the fire-plume velocity is the base velocity of the backlayer's one when the plume reaches the ceiling region. This velocity eventually becomes zero (or turns around) for critical ventilation and thus the maximum value of the critical velocity (at leveling-off) may be considered proportional to u (Eq. (19)) and so to $Q^{1/5}$. CFD results also show that the fuel type and the ambient temperature have a negligible effect on the value of the critical velocity. On the other hand, the tunnel configuration (size and fire-source configuration) appears to have effects on the $u_{cr}^* - Q^*$ relationship. Note that the Froude modeling used in the correlation requires geometric similarity. With the FDS code, authors have tried to predict the critical ventilation velocity in case of tunnel inclination highlighting that the change of this velocity is not a linear function of the inclined angle of the tunnel whereas others, as Atkinson and Wu [50], propose two formulas where u_{cr} varies linearly with that angle. Theoretical considerations have led to evaluate the following expression about the dimensionless velocity applicable also for the critical one:

$$u^* = 1.42\Omega(Q^*)^{1/3} \text{ where } \Omega = \left(\frac{T_{inlet}}{T_{avg}}\right)\left(\frac{\Delta T_{avg}}{\Delta T_{ef}}\right)^{1/3} \tag{20}$$

where ΔT_{ef} is the difference between the gas temperature near the ceiling and near the floor, ΔT_{avg} is the average temperature rise relative to ambient. According to numerical results, Hwang and Edwards show that the Froude modeling is an approximation for tunnel fires. The Froude-scaling law does not apply to two geometrically similar fire tunnels.

Differently by other authors, Palazzi et al. [59] have analyzed the worst scenario of hydrocarbon pool fire extended to the whole tunnel section considering an uniform distribution of chemico-physical properties of fire and smoke along the considered

transverse section of the tunnel. By solving mass, momentum and energy balances obtained considering possible dynamics interactions among the different fluxes, they have evaluated the critical velocity. In particular they have determinated, through experimental data, the inertial action exerted by fresh air on backlayering.

$$u = \alpha \frac{(r-1)^{1/2}}{r} \frac{1-b^2}{(1+3b)^{3/2}} (gH)^{1/2} \text{ where } r = \frac{\rho_a}{\rho_f}, \alpha = \frac{\dot{m}_a}{\dot{m}_f}, b = \frac{\dot{m}_{b2}}{\dot{m}_f} \quad (21)$$

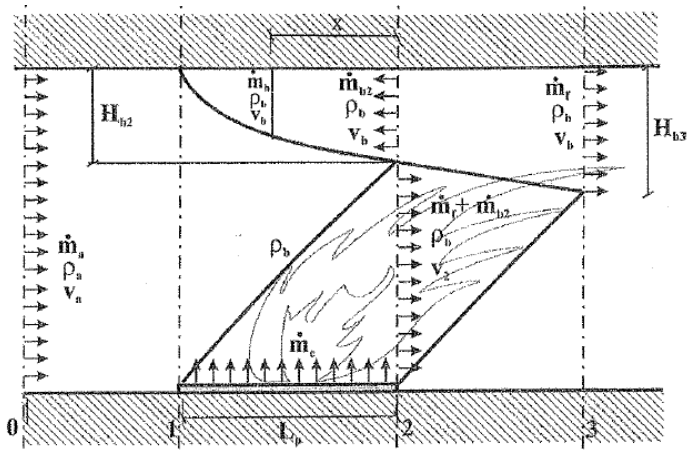

Figure 5 – Model representation of the smoke flow under forced longitudinal ventilation conditions (Kunsch [25]).

$$u_{cr,max} = \frac{\alpha}{2} (gH)^{1/2} \quad (22)$$

According to authors, their model is adaptable to the evaluation of u_{cr} when dealing with geometrical conditions different from the ones studied (e.g., different tunnel geometry, sloping tunnels, etc.) (see Figure 5).

Vauquelin [51] has highlighted that the great number of theoretical and semi-empirical formulations about the critical velocity, not correctly take into account the influence of geometrical parameters. Hence, he has shown through a parametrical approach and a laboratory model, the influence of different (rectangular) channel dimensions and buoyant source characteristics on the critical velocity. In particular, a set of tests have been realized to evaluate the critical velocity as a function of the source size, the source buoyant flux, the channel slope, the channel height and width. It is highlighted that the source nozzle diameter variations (for a given buoyant flux) significantly modify the value of the critical velocity. Its experimental trend against the HHR is in good agreement with the

formulation of Kunsch [25]. While the model of Danziger and Kennedy [48] underestimate the critical velocity in the range of dimensionless HRR investigated (0 ÷ 0.2), the Thomas' one [43] appears to be in good agreement only for small buoyant fluxes but it is not able to represent the asymptotic behavior of critical velocity for higher values of HRR. Finally it is highlighted how the model of Oka and Atkinson [49] predict smaller values of $u_{c,max}$. At least, authors' results have shown that the critical velocity is roughly independent with the channel height, expect for small values of H while it does not vary monotonically with the tunnel width. For small W/H ratios (less than unity) it appears that the critical velocity increases with the tunnel width but for aspect ratios (W/H) greater than unity, the critical velocity decreases when W increases. This last case does not appear to be in accordance with Thomas theory which, according to Vauquelin and Wu [52], overestimates the decrease of u_c by considering this velocity proportional to $W^{-1/3}$. In order to extract the whole smoke, Vauquelin and Telle [19] have been adjusted the extraction rate for several values of HRR and for each steady state, the longitudinal velocity induced by extraction has been measured. This velocity is called the ''total confinement velocity''. Authors have noticed that total confinement requires a large extraction capability and the associated induced velocity appears to be greater than the corresponding critical velocity. For a smoke layer length lower than 4 times the tunnel height, the induced longitudinal velocity is significantly reduced. For this reason, they have decided to define a *confinement velocity* for a backlayering length equal to $4H$. Note that this velocity is only related to the specific ventilation configuration tested: only two vents are activated, one on each side of the fire source.

Roh et al. [60] have investigated the difference of upstream smoke layer (e.g., backlayering) between natural and forced ventilated heat release rate by comparing numerical results (by using FDS) with experimental ones. This difference calculated in backlayering is a remarkable contrast, especially as fire size increases. They also have highlighted how the un-dimensional velocity is proportional to 1/3 power of the un-dimensional heat release rate according to Wu and Bakar [53]. In particular, the ventilation system design with the critical velocity based the constant HRR obtained by empirical relationship, can make the fire grow further.

According to Hui et al. [61], the influence of combustion process and the fire source area on the critical ventilation velocity are not included in models based on Froude number preservation theory. Thus, authors have supposed that the large differences in the models in the literature may be due to their different fire source conditions, especially the combustion process and the fire source area. However they are agree on the proportionality of the critical velocity to the one-third power of the HRR but only when

the location where the thermal plume impinges on the tunnel roof does not vary with HRR for the critical ventilation velocity i.e., the thermal plume inclination angle is constant. This angle, as highlighted by authors, reflects the equilibrium between the natural convection induced by buoyancy and the forced convection caused by ventilation. As result, when the fire source length increases (and so proportionally the source area) the critical velocity levels off to a certain level. Here, when the heat source surface is quite long, several thermal plume ascend from the heat source instead of just one, which might result in a maximum critical velocity for the high HRR. By the analysis of these phenomena, Hui et al. [61] show that the effect of the combustion process on the critical velocity is much more important than the effect of the fire length. Moreover, Tsai et al. [62] have highlighted the influence of the distance of fire from the tunnel exits on the critical ventilation velocity. In particular, they have shown how u_{cr} decreases when the fire source is near the exits.

The effects of a blockage and its locations in the tunnel on the flame length have been analyzed in deep through experimental studies in case of gaseous fuels. Results show that a blockage creates complex turbulent flow conditions. In particular, a difference occurs if the blockage is located upstream or downstream from the fire source. For the first case, a lower critical ventilation velocity seems sufficient to arrest the backlayering flow. On the other hand, with a blockage downstream from the fire source, it appears that the impact of the blockage on the flow dynamics is similar to the one of the buoyancy forces within a smooth tunnel, and thus, both the cases have practically the same relationship between the critical velocity and the HRR.

Li et al. [63], through experimental model-scale tests and theoretical analysis, have investigated the critical velocity together with the backlayering length in fire ventilated tunnels. Both the theoretical and experimental data show that the backlayering length can be related to the ratio of longitudinal ventilation velocity to critical one. They show that the equations proposed by Oka and Atkinson [49] and those proposed by Wu and Bakar [53] underestimate the experimental data, especially where the critical velocity varies with the HRR (Q^* < 1.5) and when there are no vehicle obstruction. Thus, the equation proposed by Li et al. are Eqs. (23) and (24) for tunnel with and without the 20% of vehicle obstruction respectively.

$$u_{cr}^* = \begin{cases} 0.81\, Q^{*1/3} & Q^* \leq 0.15 \\ 0.43 & Q^* > 0.15 \end{cases} \tag{23}$$

$$u^*_{cr,ob} = \begin{cases} 0.63\, Q^{*1/3} & Q^* \leq 0.15 \\ 0.33 & Q^* > 0.15 \end{cases} \quad (24)$$

Authors also propose an expression in order to estimate the reduction ratio of the critical velocity due to vehicle obstruction:

$$\frac{u_{cr} - u_{cr,ob}}{u_{cr}} = \frac{u^*_{cr} - u^*_{cr,ob}}{u^*_{cr}} \quad (25)$$

They have found that the reduction of the critical velocity due to obstruction is slightly larger than the ratio of cross-sectional area of vehicles to tunnel cross-sectional area; similar results are obtained by Oka and Atkinson [49]. The critical Froude and Richardson number are investigated. The first one is almost constant with a value of 1.15 when the dimensionless HRR is below than 0.15 and increases linearly with it at higher HRR values, the second one, instead, is found to increase with the dimensionless release rate (Eqs. (26) and (27)).

$$Fr_{cr} = \begin{cases} 1.15 & Q^* \leq 0.15 \\ 1.15 + 3.7(Q^* - 0.15) & Q^* > 0.15 \end{cases} \quad (26)$$

$$Ri_{cr} = \begin{cases} 1.15 + 2.35Q^* & Q^* \leq 0.15 \\ 1.15 + 8.5(Q^* - 0.15) & Q^* > 0.15 \end{cases} \quad (27)$$

Finally, a correlation based on experimental data to predict the backlayering length is proposed (Eq. (28)):

$$l^* = \begin{cases} 18.5 \ln(0.81 Q^{*1/3}/u^*) & Q^* \leq 0.15 \\ 18.5 \ln(0.43/u^*) & Q^* > 0.15 \end{cases} \quad (28)$$

For information purposes, Mao et al. [64] have studied the back drought phenomenon in subway tunnels fire for both mechanical and natural ventilation. They indicate that the key parameter determining the occurrence of back drought in these tunnels is the mass fraction of the volatilized unburned fuel in the tunnel. The critical values of this parameter

in natural and mechanical ventilation are found equal to 8.78% and 11.71% respectively, with a humidity of 15% in fresh air.

Zhang et al. [65][66] show that the critical velocity is controlled by three factors: fire size, ventilation flow and tunnel height. Hence, according to authors, the Thomas' correlation is inadequate to predict the behavior of the critical ventilation velocity because it take into account only two of the three parameters presented above (i.e. fire and ventilation). They also have highlighted how the critical Froude number is limited by the Archimedes' principle regardless of fire size; in experimental scaling, a lowering tunnel height has the same effect as the increasing fire size. As long as the phenomenon is convection dominated, the relation between tunnel height and the flame height of fire is strictly linear. Authors suggest that flame height (Eq. (29)) is the most important design parameter in fan sizing, in particular the condition $L=H$ gives the maximum requirement for fan power.

$$H_{flame} = \frac{Q}{\rho_a u_a h_a W} \tag{29}$$

3. *Numerical analysis of different turbulent models and comparison with experimental data*

3.1. Introduction

The aim of this chapter is to investigate strength and weakness of three different turbulent models by means of CFD analysis through a comparison with experimental data. These ones, related to a jet fan placed near a surface in a large enclosure, are compared with both CFD simulation and Regenscheit semi-empirical formula, suitable to assess jet characteristics, such as the maximum velocity reduction and the volume flow rate of induced air [71][72][73][74][75].

The semi-empirical formulas, provided by Regenscheit [74] and Awbi [75], are obtained for undisturbed jets with no obstructions in the throw. Actually, obstructions are present disturbing the jet profile of course. This means that semi-empirical formulas are of limited use for jet fans.

Moreover, this paper presents a preliminary experimental and Computational Fluid-Dynamic (CFD) investigation in order to simulate the velocity field induced by an axial jet fan. Since temperature fields by mathematical models can be affected by uncertainty, experimental test has carried out in order to measure the axial air velocity accelerated by the jet fan placed in an open environment (considering the floor influence). The air velocity, accelerated by jet fan, is measured experimentally by a hot wire anemometer device. In view of that, this chapter presents results of an investigation that compares numerical, analytical and experimental data of a velocity field induced by an axial jet fan in open environmental [73][74][75][76][77].

3.2. Domain for experimental testing and measurements

The technical data of the jet fan under investigation (Figure 6) are shown in following Table 6. The jet fan is positioned and fixed on a rigid structure to maintain its axis parallel to the floor, at h=1.78 m from the floor (Figure 7).

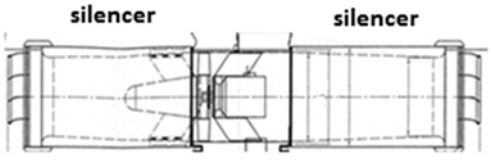

Figure 6 – Jet fan

Table 6 – Main features of jet fan (Figure 6)

Theoretical thrust	F_t	941 N
Area, jet fan outlet	A	0.40 m^2
Moment source section	A_m	0.50 m^2
Average axial velocity at jet fan out flow	v_{jet}	44.0 m/s

The axial air velocity is measured by means of hot wire anemometers placed at fixed measurement points, equally spaced from the jet fan outlet section (4, 8, 12 m), for different y-coordinate values, along the vertical symmetry xy-plane passing through the center of the jet fan engine (Figure 7).

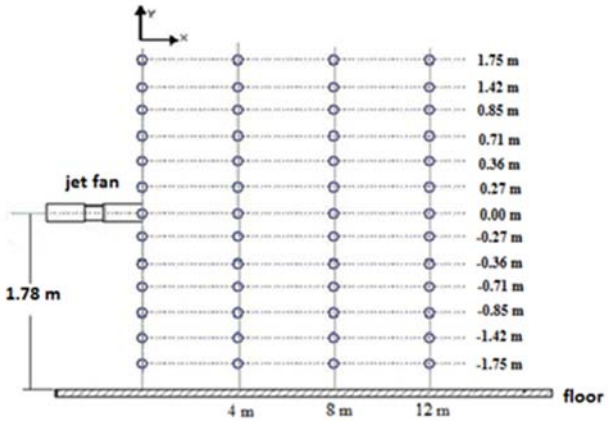

Figure 7 – Measurement points

The hot wire anemometer used for the experimental velocity assessment has a velocity range of 0-40 m/s with a uncertainty equal to ±2% and a resolution equal to ±0.01 m/s. For each grid point shown in Figure 7, the velocity measurements are repeated three times.

3.3. System description

The air flow can be classified into different types, or a combination of these ones. The *free jet* considers the walls, the ceiling or obstacles not influencing the airflow while, if air flowing parallel to a wall and the entrance located near the wall, one speaks of a *wall jet*.

Free jet

A free jet is a jet that flows into an infinitely large space. The effect of the channel diameter and the flow speed on the average speed loss of the jet is examined by Awbi [75] that divides the development of a jet in four zones, based on the speed loss respect of the axis. Figure 8 shows the development of isothermal free jet.

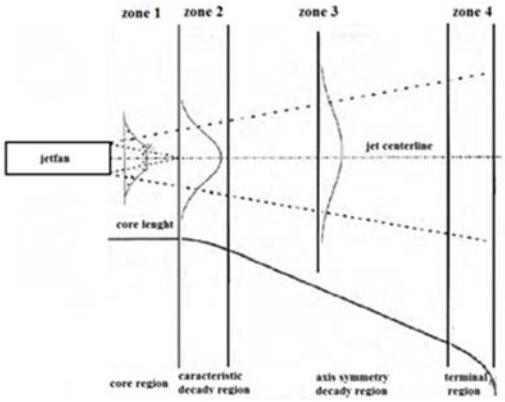

Figure 8 – Isothermal free jet development

Thus, the development of the jet can be distinguished into four zones:

- a conical core zone 1, where the speed on the axis is the same size as the feed speed;
- a transitional zone 2, where the speed begins to take off: the speed is accessed as x^(-n), where x is the distance to the axis;
- zone 3, where transversal speed profiles are equal at different distances of x and the speed loss approached on x^(-1);
- zone 4, the area where the speed on the axle rapidly declining.

The first two zones are strongly influenced by the shape and size of the injection opening, while the third one is the developed jet and the fourth is the end of the jet. In the first three zones, the air in that region is induced in the radius and mixed with the supply air.

For the first zone, the following equation applies for velocity in the axis of the exhaust at a distance x, $v(x)$:

$$v(x) = v_{out} \qquad (10)$$

where v_{out} is the air velocity at the outlet section of jet fan (m/s).

The second zone is the characteristic decay region; the following equation applies where n is a characteristic index depending on the nature of air in 1/3 ÷ 1 range.

$$v(x) \propto v_{out} \frac{1}{x^n} \qquad (11)$$

The length of this field and the value of n depend on the shape and character of the exhaust. For square or round openings this area is negligible (n = 1), for openings with a large rectangular aspect ratio this area became more relevant (n = 1/3).

The third zone is referred to as the "axis-symmetric decay region". This area displays the jet dominated by an extremely turbulent flow, which is produced by the viscous friction. This is usually meant for three-dimensional jets as a fully developed flow, where the angle of divergence of the jet is constant. This angle of divergence causes a gradual decrease of the jet. The speed reduces to ashes here reversed with the distance to the exhaust:

$$v(x) \propto v_{out} \frac{1}{x} \qquad (12)$$

The fourth zone is the "terminal region". It is a zone of rapid spread and the jet is not more distinguishable from the surrounding air. The speed on the axis decreases with the distance with an exponential law as per Eq. (11).

In technical literature, are available a certain number of semi-empirical formulas in order to calculate the axial velocity performed by an axial jet fan. One of formulas to calculate axial velocity are the following Regenscheit formulas (13) and (14):

$$v_{x_i} = \frac{v_{out} \cdot D}{x \cdot m} \qquad (13)$$

that allows to calculate the centerline axial velocity and it is inversely proportional to axial distance x;

$$v_{x_j} = e^{\left(-2\frac{y}{x \cdot m}\right)} \cdot v_{x_i} \qquad (14)$$

that allows to calculate the correspondent axial velocity values at different y-distance from centerline and this velocity decreases with an exponential law with y-distance. The velocity field expressed by above formulas has been compared with experimental and numerical data. In the Table 7, measurement velocities of the jet on a symmetry plane evaluated by means Regenscheit formulas are reported.

Table 7 – Velocity field on symmetry plane

	acc. to Regenscheid (theory)			meassurement		
	4m	8m	12m	4m	8m	12m
-11.36	0.00	0.00	0.00			
-5.68						
-4.25			0.01			
-3.40			0.09			
-2.84		0.01	0.43			
-2.55		0.04	0.85		floor	
-1.70		1.27	4.18	0.00	1.00	3.00
-1.42		3.03	6.14			
-0.85	2.55	10.94	10.86	2.00	10.00	6.00
-0.71	6.06	13.59	11.96			
-0.36	27.17	19.77	14.13			
-0.27	33.76	20.87	14.47	17.00	20.00	14.00
0.00	44.80	22.40	14.93	33.00	21.00	16.00
0.27	33.76	20.87	14.47	33.00	21.00	16.00
0.36	27.17	19.77	14.13			
0.71	6.06	13.59	11.96			
0.85	2.55	10.94	10.86	3.00	11.00	10.00
1.42	0.02	3.03	6.14	0.00		
1.70	0.00	1.27	4.18		2.00	4.00
2.55		0.04	0.85		0.00	1.00
2.84		0.01	0.43			0.00
3.40		0.00	0.09			
4.25			0.01			
5.68			0.00			
11.36						

3.4. Geometrical model

The jet fan under investigation consists of a cylindrical central part and of two cylindrical silencers at the ends (Table 6 and Figure 6).

The domain under investigation (Figure 9), in which the jet fan is placed, is constituted by a parallelepiped computational volume: Vc = L x W x H = (25 x 10 x 6) m^3. This geometry is the real one used.

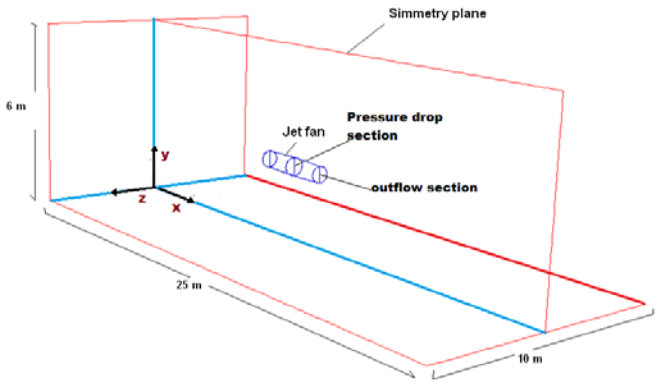

Figure 9 – computational volume

The moment source is applied where the pressure (Δp) condition occurs. This geometry is accomplished using the Gambit software.

The overall computational domain is discretized by using non-uniform grids: the system (jet fan and ambient) is divided in two types of blocks, it is necessary to create the blocks-grid (V_{fan} and V_{amb}) to obtain different discrete zones. The V_{fan} block (as presented in Figure 10) represents the jet fan and the V_{amb} block represents the ambient zone around the jet fan. The unstructured mesh is made by means of prismatic cells with triangular base. The tetrahedral grid choice is needed to obtain a good discretization of the different geometrical blocks shape.

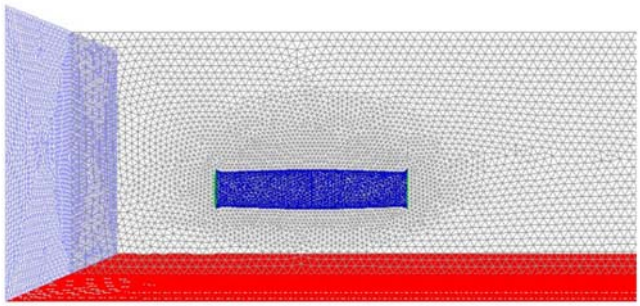

Figure 10 – Discretization of the computational domain (jet fan and ambient)

3.5. Mesh analysis

The analysis of mesh was been conducted for all k-ε turbulence models, obtaining the same results in term of mesh size. Figure 11 to Figure 13 show the mesh analysis, using the RNG k–ε turbulent model. The computational volume of the ambient (V_{amb}) mesh sizes, chosen for comparison, were 0.16 m (type A), 0.18 m (type B) and 0.20 m (type C), fixing the computational volume of the jet fan (V_{fan}) mesh size at 0.08 m.

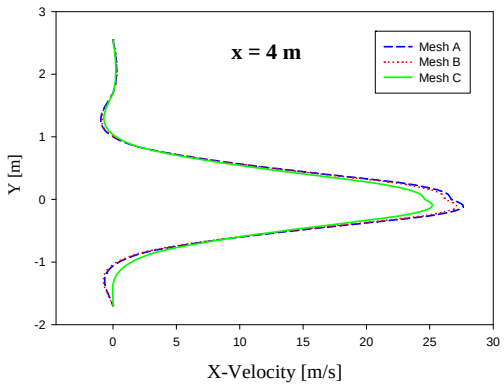

Figure 11 – Mesh analysis; comparison for x=4m

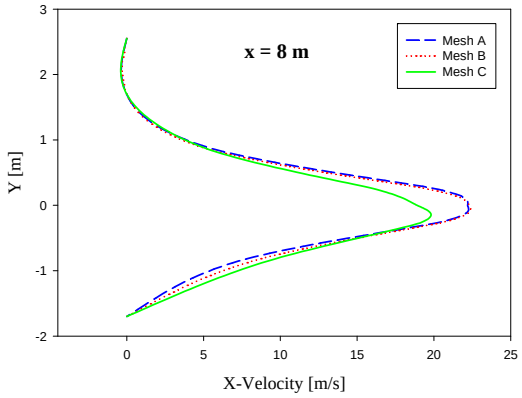

Figure 12 – Mesh analysis; comparison for x=8m

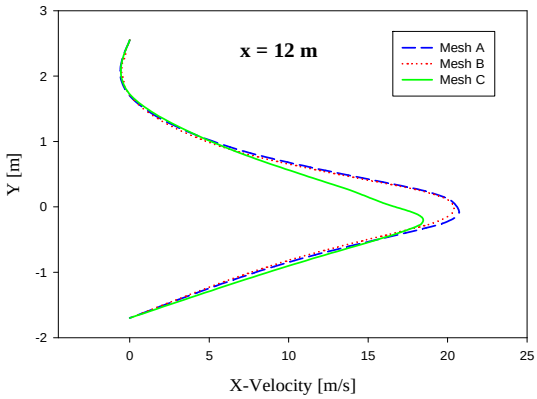

Figure 13 – Mesh analysis; comparison for x=12m

It is chosen a tetrahedral grid shape, needed to fit the cylindrical fan shape. The mesh analysis is carried out for both volumes in terms of air velocity profiles, in the axial section at distance equal to 4 m, 8 m, 12 m from the jet fan out flow, on the symmetric plane of the computational volume. In all cases (x = 4 m, 8 m and 12 m), it possible observe the quite overlapping of air velocity profiles of mesh types A and B. It is chosen the B-type mesh because it represents an acceptable compromise between the accuracy of numerical results and the computational time.

3.6. Numerical simulation and turbulence model comparison

A CFD analysis is carried out to reproduce the axial jet fan tests, solving the differential equations for the conservation of mass, momentum and closing the equation set with turbulence modeling. It is decided to proceed with simulations using three different k-ε turbulence models, standard k-ε model; RNG k-ε and Realizable k-ε, in order to choose the one that simulates better axial velocity profile obtained from experimental measurements.

Standard k-ε model is the simplest complete model of turbulence; it is performed by two-equation models in which the solution of two separate transport equations allows the turbulent velocity and length scales to be independently determined [1][78]. This model is characterized by economy and reasonable accuracy for a wide range of turbulent flows. It is used despite the known limitations of the model: its performances become poor for complex flows involving severe pressure gradient, separation and strong streamline curvature.

RNG k-ε is a suitable model for complex shear flows involving rapid strain, moderate swirl, vortices, and locally transitional flows. RNG k-ε model is similar in form to the standard k-ε model, but includes the following refinement: the RNG model has an additional term in list ε equation that significantly improves its accuracy for rapidly strained flows; the effect of swirl on turbulence is included in the RNG model, enhancing accuracy for swirling flows; the RNG theory provides an analytical formula for turbulent Prandtl numbers, while the standard k-ε model uses user-specified, constant values. While the standard k-ε model is a high-Reynolds-number model, the RNG theory provides an analytically-derived differential formula for effective viscosity that accounts for low-Reynolds-number effects.

Realizable k-ε model is a relatively recent development and differs from the standard k-ε model in two important ways: the realizable k-ε model contains a new formulation for the turbulent viscosity. A new transport equation for the dissipation rate ε has been derived from an exact equation for the transport of the mean-square vorticity fluctuation. One limitation of the realizable k-ε model is that it produces non-physical turbulent viscosities in situations when the computational domain contains both rotating and stationary fluid zones.

The result is that (on equal terms to the boundary conditions) the profile of the jet fan velocity that best follows the evolution of the experimental ones, fixing the position x

equal to 4, 8 and 12 meters and varying y, is obtained using the realizable k-ε turbulence model.

3.7. Results

Figure 14 ÷ Figure 16 show the comparison of experimental, semi empirical and numerical axial air velocity profiles, at fixed y equal to 0 m, along variable x-axes from 4 m to 12 m, in open space. The Figure 14 shows the comparison of the axial velocity profiles, for fixed distance from jet fan outflow section, x=4 m. Moreover, the figure shows that the experimental and numerical results are in good accordance, while the semi-empirical model overestimates the axial velocity value and the standard k-ε model underestimates the velocity value. In particular, it could be seen that the numerical results of RNG k-ε model provided the best good agreement with the experimental data, but also the realizable k-ε is quite close to the experimental results. The Figure 15 shows the comparison of the axial velocity profiles, for fixed distance from jet fan outflow section, x=8 m. The Figure 15 shows that the experimental, semi-empirical and realizable k-ε numerical axial velocity profiles are in overlapping.

The standard k-ε model continues to underestimate, also in this case. Away from the jet fan outflow section to the x=12 m (Figure 16), once again, the realizable k-ε numerical model better fits the experimental and semi-empirical data.

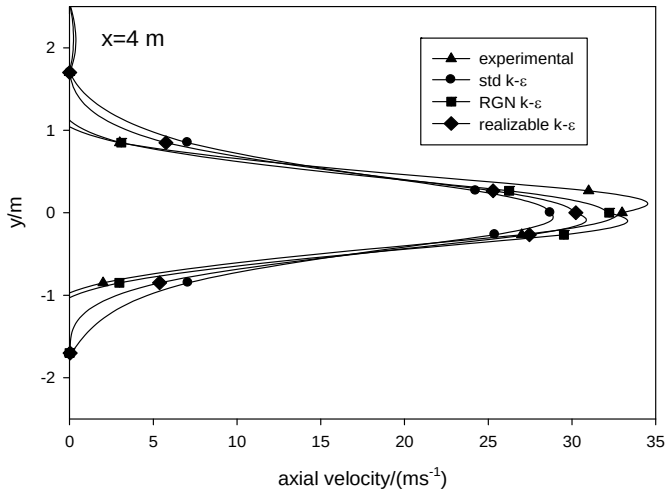

Figure 14 – Comparison between experimental, semi-empirical and numerical axial air velocity profiles, at different y values, along x-axes equal to 4 m

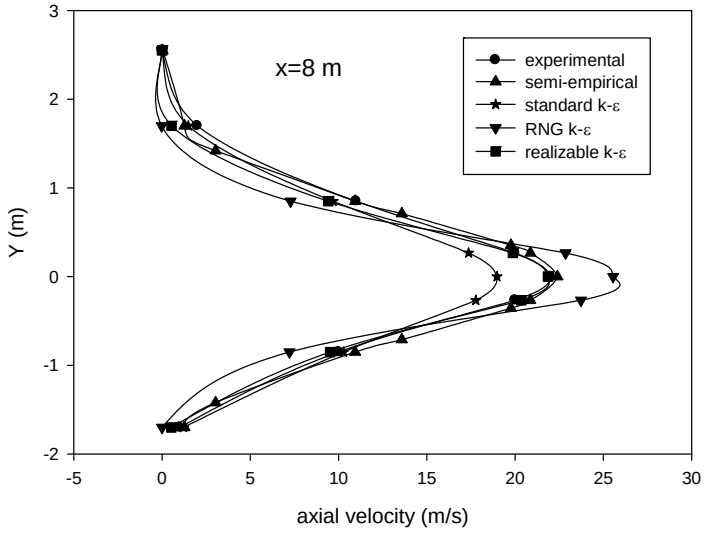

Figure 15 – Comparison between experimental, semi-empirical and numerical axial air velocity profiles, at different y values, along x-axes equal to 8 m

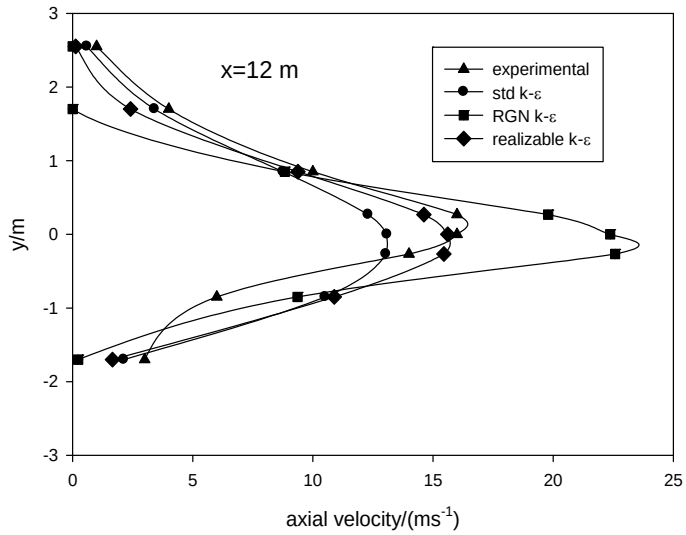

Figure 16 – Comparison between experimental, semi-empirical and numerical axial air velocity profiles, at different y values, along x-axes equal to 12 m

As conclusion, numerical analysis, carried out in order to choose the best turbulent model that simulates the axial velocity profile obtained from experimental data, shows that:

- the numerical model realizable k-ε fits better the experimental results at each investigated distance;
- the RNG k-ε turbulence model is the most explicative only at short distance,

- the k-ε turbulent model falls, even if there are no severe pressure conditions and strong streamline curvature;
- the Regenscheit semi-empirical formula tends to overestimate the axial velocity value close to the jet fan outflow section.

4. *Numerical comparison between alternative and traditional jet fans in a longitudinal tunnel ventilation system – free tunnel vs traffic jam condition*

4.1. Introduction

As shown in previous chapters, jet-fan alternative configurations (LAVS, Longitudinal Alternative Ventilation System) are available in order to increase ventilation performances in tunnels. Several technical solutions are provided to this aim such as a different pitch angle (*banana jet fan* [69]) or variable section for silencers (*mojo jet fan*).

The banana jet fan, analyzed in this work, presents the inlet and outlet silencers inclined toward the tunnel floor and forms a pitch angle (α) away from the ceiling. Obviously, traditional jet fan considers a pitch angle $\alpha = 0°$ [6].

The numerical simulations, considered in this chapter, are carried out for two different configurations: with (traffic jam condition) and without vehicles.

4.2. CFD model

Physical domain

The physical domain under investigation, is shown in Figure 17 (tunnel sketched not in scale). The tunnel length is 800 m ($109D_H$, with D_H = 7.3 m) and the vehicle flux is considered unidirectional together with longitudinal ventilation.

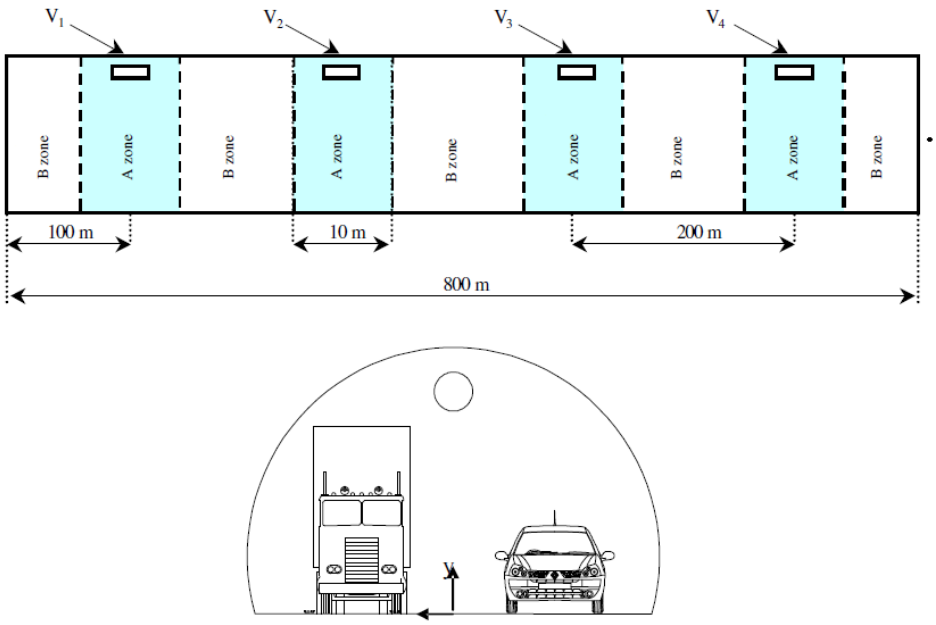

Figure 17 – Numerical model of CFD analysis

The ventilation system is made by four jet fans, all positioned at 5.60 m above tunnel floor (Figure 18). The fans V1 and V4 are installed at a distance of 100 m (13.7 D_H) from inlet and outlet tunnel sections respectively; the distance between the two successive fans is 200 m (27.4 D_H).

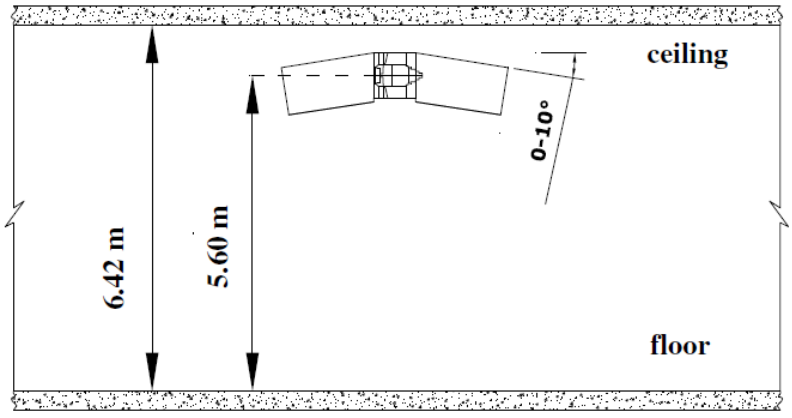

Figure 18 – Jet fan sketch

According to Mantegani et al. [1] results, distance between two adjacent fans is chosen equal to 200 m in order to guarantee the complete discharge of jet momentum (primary air flow) in the tunnel air flow (secondary). As result, Figure 19 shows that local axial velocity, evaluated on a line passing through engine center, tends to design value near the following fan inlet section (as shown in deep in following paragraphs).

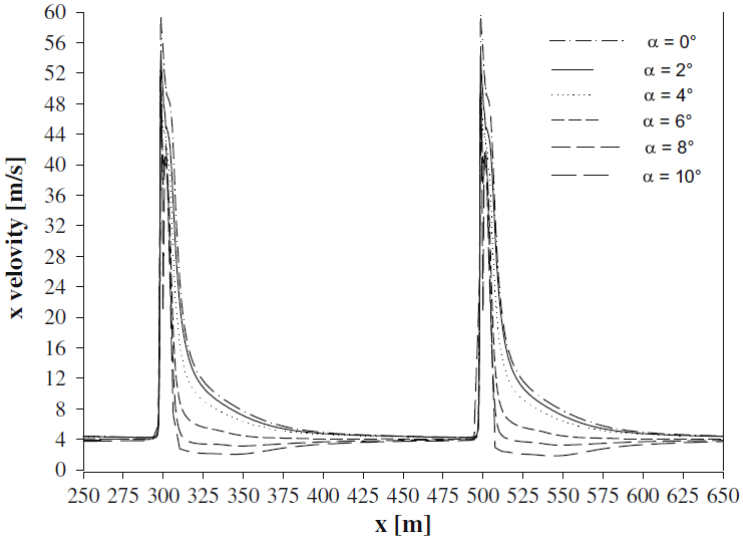

Figure 19 – Local velocity on longitudinal line passing through engine center

The 0°÷10° range is considered in order to analyze the performances of both alternative and traditional fan: for the first case, five models are considered with 2° step for pitch angle (2°, 4°, 6°, 8°, 10°) while the second case (traditional) refers to 0° angle.

Simulation are carried out for both scenarios with and without traffic in order to have a more complete overview about different performance for both jet fan typologies. The same flowrate is imposed in tunnel in order to obtain the total thrust necessary to guarantee the longitudinal air flux.

Mathematical model

Unsteady, turbulent and 3D flux is considered for the domain. The averaged mass Navier-Stokes equations are combined with k-ε standard model.

Mesh definition

In order to optimize computational time, the domain is divided in two different zones for mesh sizing (Figure 17): for the A zone, where high velocities occur, a 0.1 m grid is considered while for B zone a sensitivity analysis is carried out. In consideration of the need to adapt the mesh to the analyzed system geometry (tunnel + fans + vehicles), several tetrahedral meshes are considered: 0.3 m, 0.4 m and 0.5 m.

Figure 20 shows several air velocity profiles at different distances from the fan ($3D_H$ and $4D_H$) for the three mesh sizes considered. In consideration of distribution of velocity values vs distance from floor (h[m]), the 0.4 m grid is considered for the analysis.

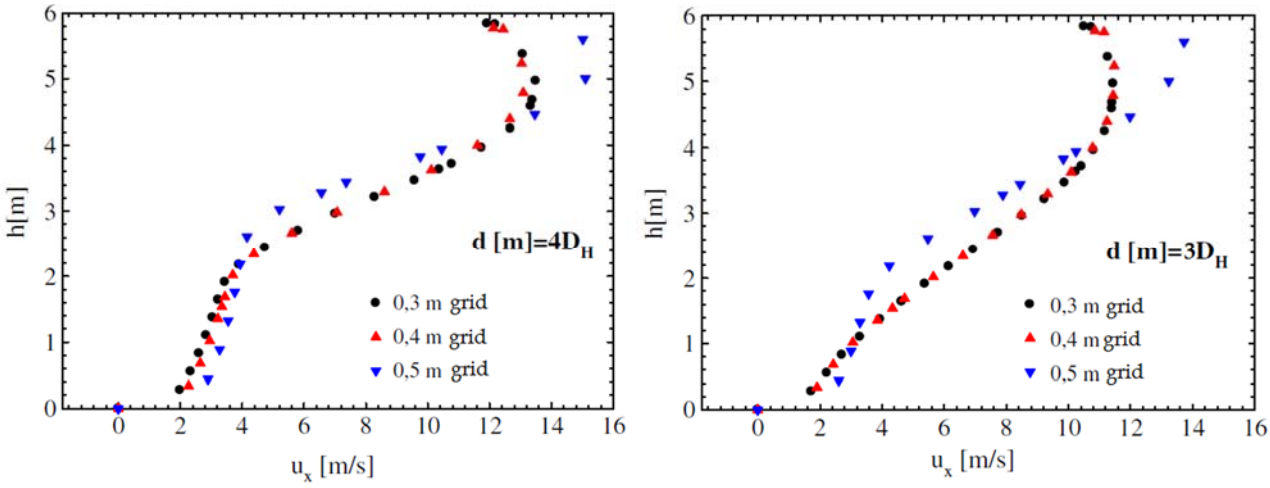

Figure 20 – Air velocity profiles @ $3D_H$ and $4D_H$

Boundary conditions

The fan is modeled by means of momentum source by imposing the pressure drop in order to obtain an average air velocity in tunnel equal to 4 m/s.

Air properties are considered constant with temperature and evaluated at 300K and air swirl component through the fan is considered negligible.

In the traffic jam configuration, vehicles are considered as parallelepiped blocks able to obstacle the air flow in tunnel, set in two-lanes dual carriageway arrangement; the 12% of vehicles is considered as heavy good vehicle (HGV).The distance between two adjacent vehicles is considered 2 m. Ceiling and floor roughness is considered equal to 0.03 and 0.01 meters respectively.

The simulation is isothermal.

4.3. Performances of ventilation models

The interaction of air flow with the tunnel walls lead to reduce the theoretical jet force considered in a free and static field. This phenomenon can be considered by means of the

Kempf reduction coefficient as mentioned in previous par. 1.2. This coefficient, evaluated experimentally, let to estimate the air velocity reduction according following equation:

$$\frac{1}{k_{2\alpha}} = \cos\alpha - \frac{v_t}{v_{jet}} \qquad (15)$$

where $1/k_{2\alpha}$ is the second reduction coefficient and α is the pitch angle of silencer (zero for traditional jet fan). Thus, the real longitudinal force is:

$$F_r = F_t \frac{1}{k_{2\alpha}} \frac{1}{k_1} \qquad (16)$$

k_1 parameter results constant since all parameters used for its calculation are considered constant.

Equation (15) gives approximate results since it is assumed that, in the outlet zone of the jet fan, the air velocity value in tunnel is equal to the average one in the section. The analysis of velocity profiles appear complex, in particular for the calculation of the local velocity variation with the air jet pitch.

In order to compare performances between both traditional and alternative jet fan and, in particular, to investigate the optimum configuration for the alternative case, different thrust values with different jet fan pitch angle values are evaluated.

Local velocities profiles on tunnel centerline are shown in following Figure 21, Figure 22 and Figure 23 for a 0°, 6°, 10° pitch angle respectively. Here, the longitudinal component of air average velocity is shown for several distances.

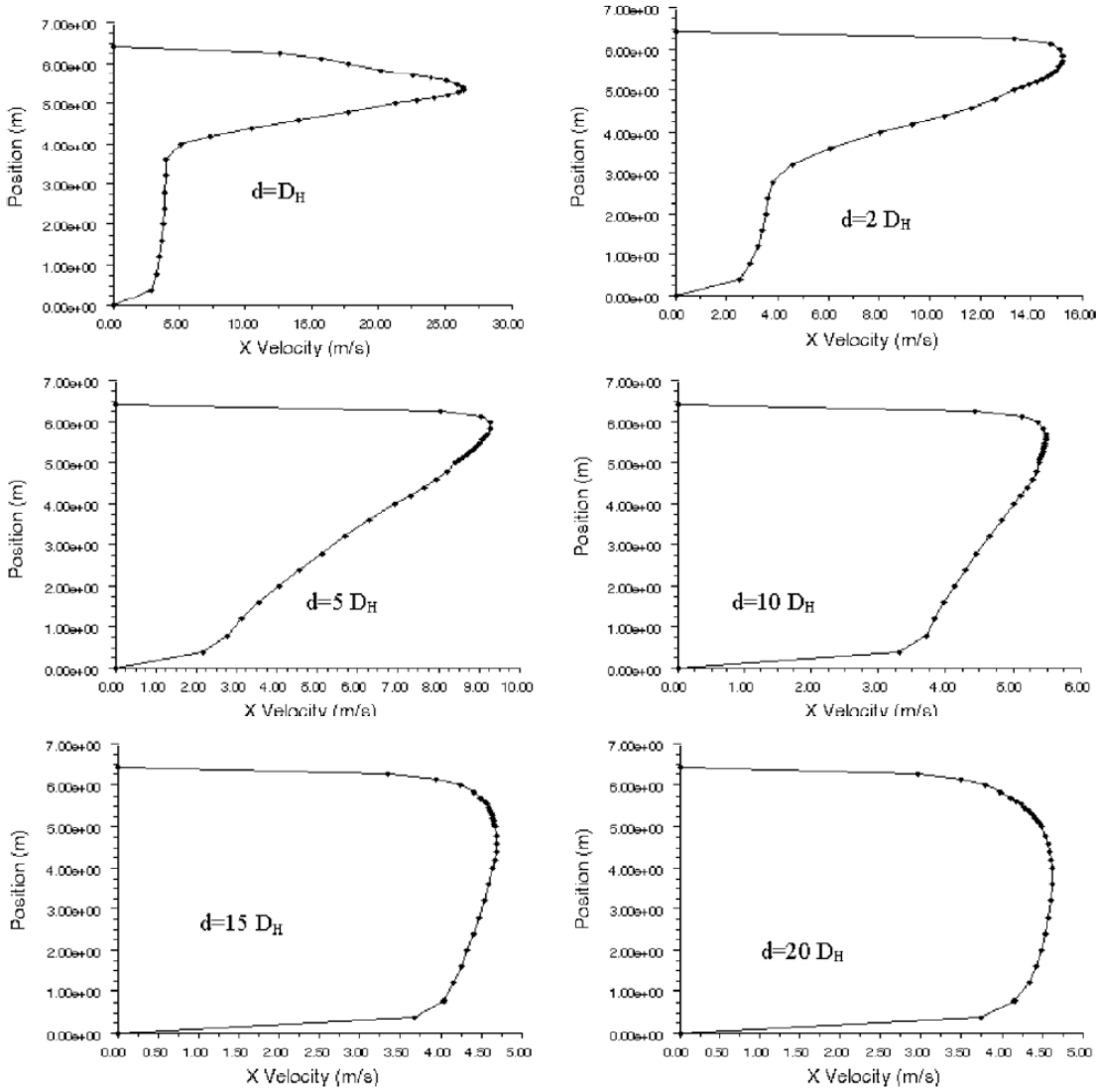

Figure 21 – Local velocity values at difference distances for pitch angle α=0°

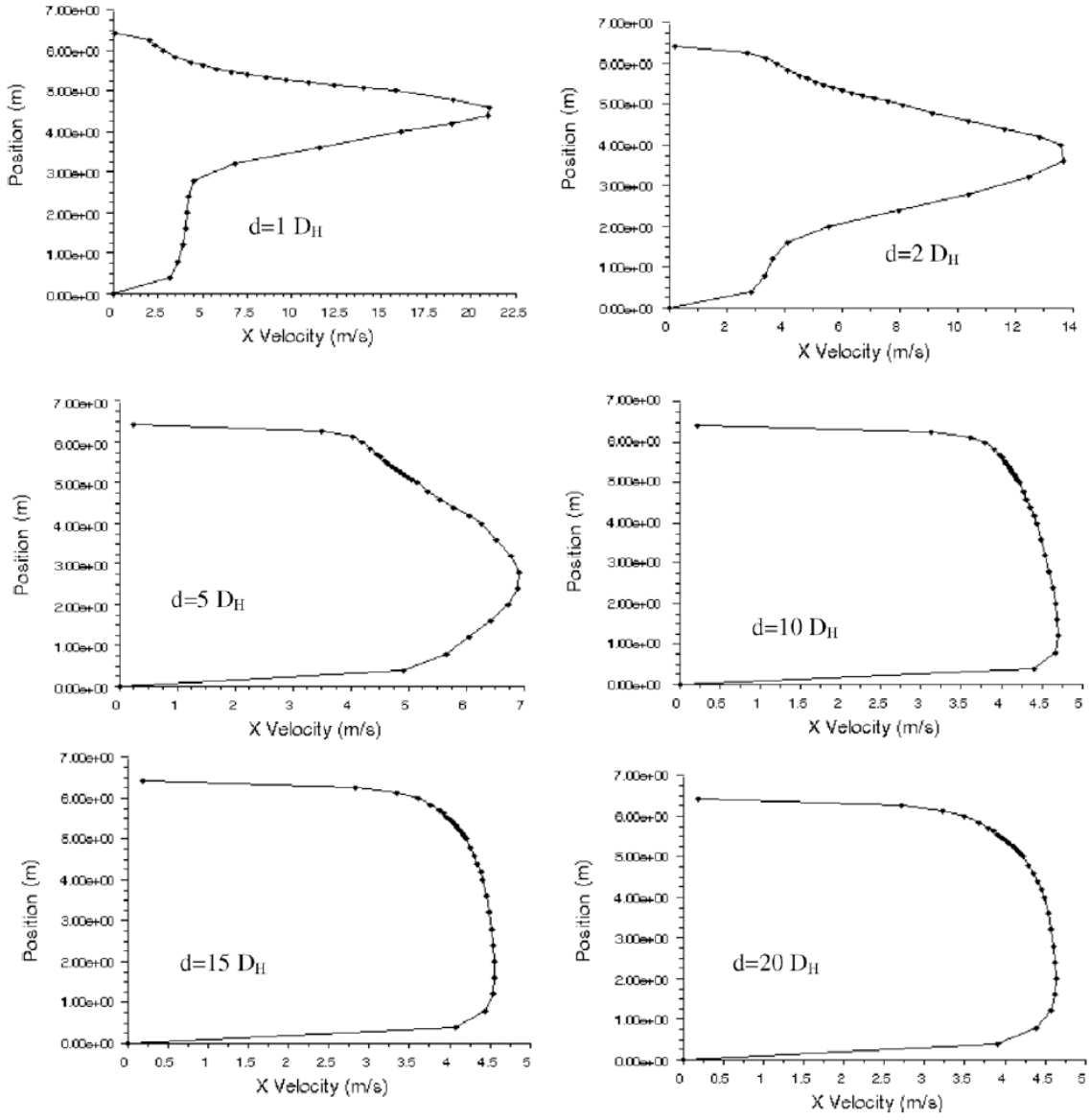

Figure 22 – Local velocity values at difference distances for pitch angle α=6°

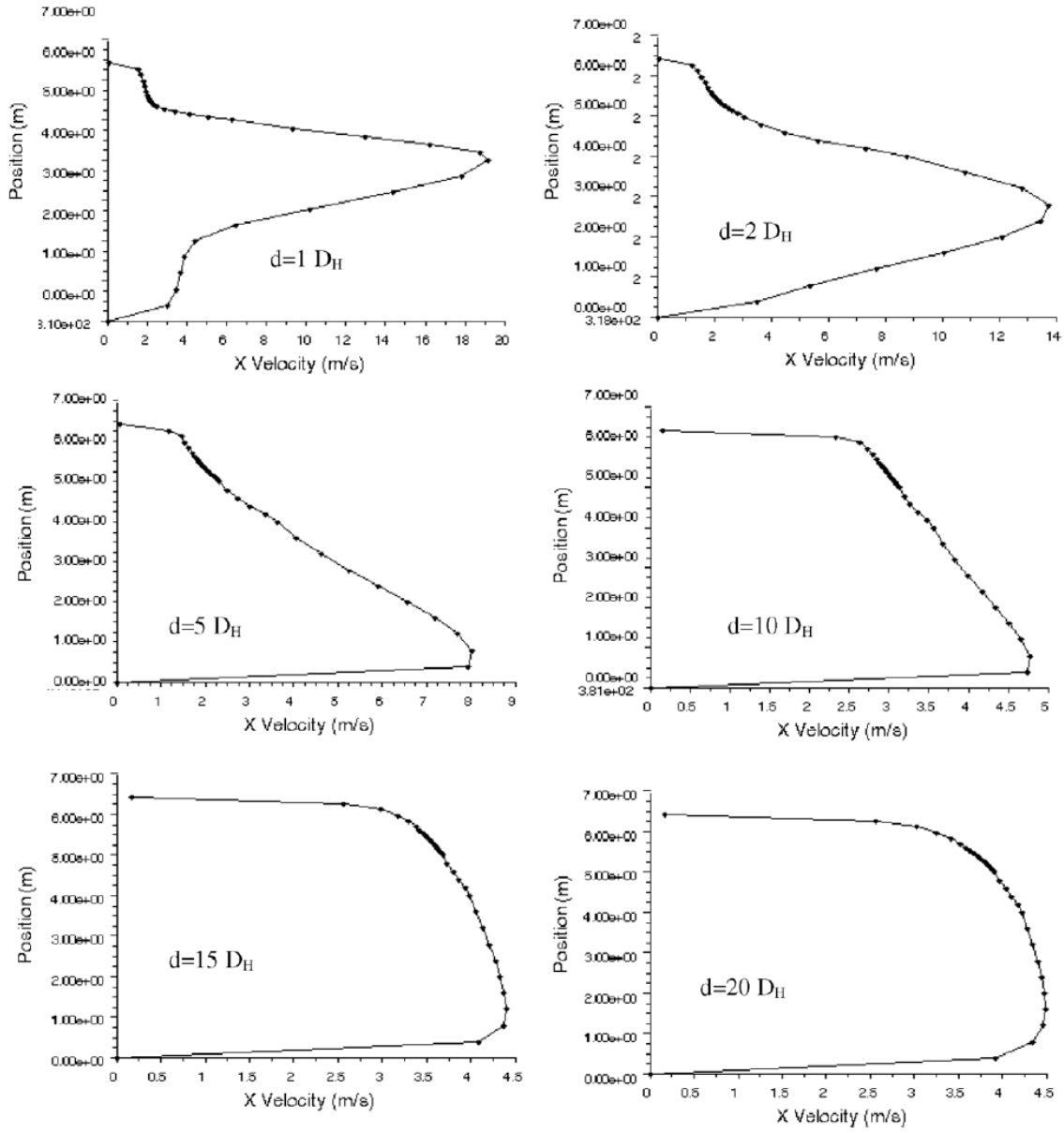

Figure 23 – Local velocity values at difference distances for pitch angle α=10°

At $d=2D_H$ from the outlet jet fan, the height of the maximum axial velocity and the axial velocity value (along x component) decrease with increasing pitch angle.

For the traditional jet fan ($\alpha=0°$), at a distance of $5D_H$, the velocity profile becomes more uniform with respect to other pitch angle values (Figure 22 and Figure 23). This is due to the ceiling/floor symmetrical effect.

4.4. Optimal pitch angle in free tunnel configuration

Defining a Performance Ratio (PR) as the ratio between thrusts (at α=0° and α>0°) able to guarantee a defined longitudinal flux in tunnel, it is possible to evaluate the optimal pitch angle for an alternative jet fan.

$$PR = \frac{F_{\alpha=0°}}{F_{\alpha>0°}} \qquad (17)$$

The velocity fields and the shear stress fields, for different pitch angle values, are shown in Figure 24 and Figure 25, respectively.

At the outlet zone of the jet fan, the air stream that blows along the ceiling is glued to the ceiling due to the Coanda effect for the traditional jet fan (α=0°), while alternative pitch angles do not go along the ceiling, thereby decreasing its shear stress (Figure 24 and Figure 25a). As the angle increases, the air stream tends toward the tunnel floor and, consequently, increasing its shear stress (Figure 24 and Figure 25b).

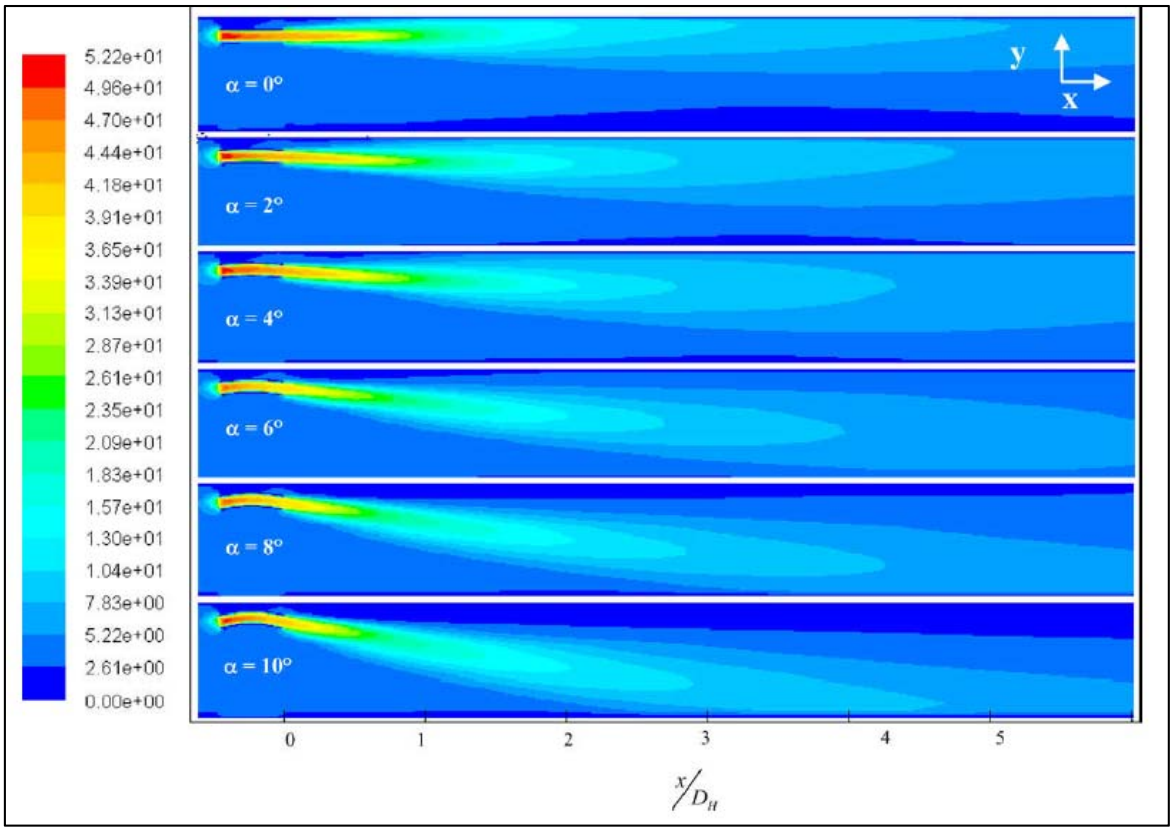

Figure 24 – Velocity field on symmetrical plane tunnel for different pitch angles (free tunnel)

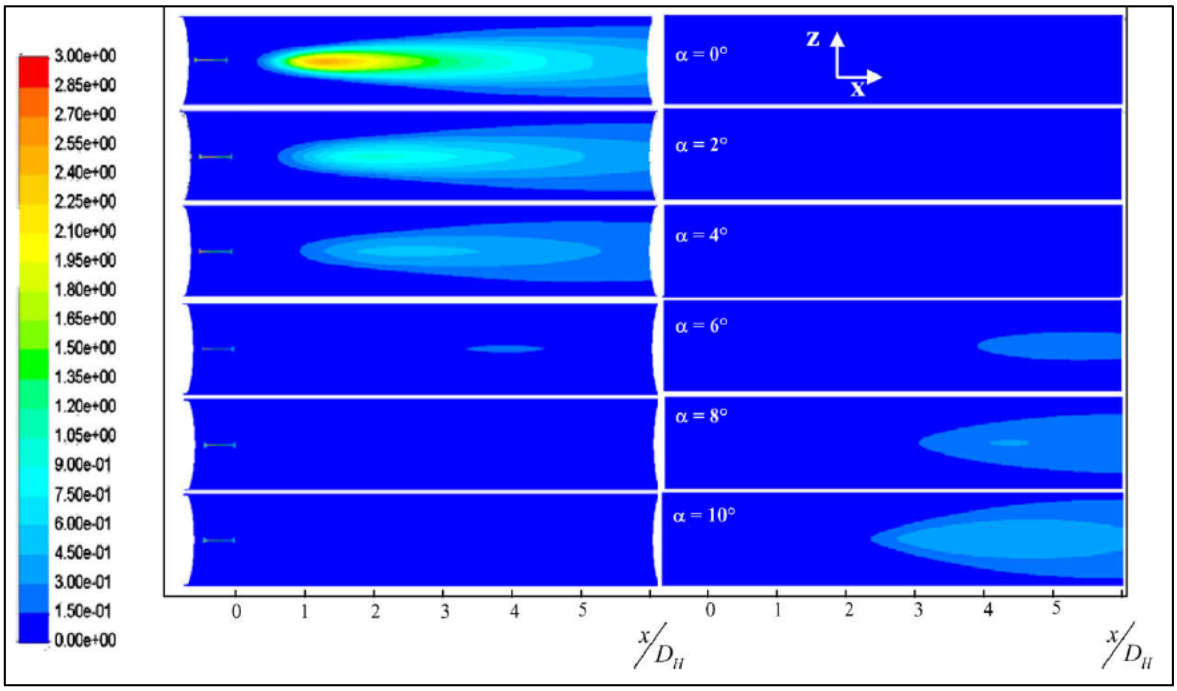

Figure 25 – Shear stress fields for different pitch angle values; (a) ceiling shear stress; (b) floor shear stress

According to CFD results shown in following Table 8, the optimal pitch angle results 6° since the corresponding total thrust reaches the minimum value while PR the maximum one.

Table 8 – Shear stress on ceiling and floor, thrust and PR for different pitch angles (free tunnel case)

α (°)	$F_{a,ceiling}$ (N)	$F_{a,floor}$ (N)	$F_{a,tot}$ (N)	F_{α} (N)	PR
0	2066	402	2468	885	1.00
2	1637	416	2053	754	1.17
4	1377	488	1825	673	1.31
6	1114	546	1660	623	1.42
8	1054	676	1730	650	1.36
10	1070	884	1954	712	1.24

By comparison of viscous stress values at tunnel ceiling and floor (Figure 26 and Figure 27) it appears that the stress field for the inclined jet fan is characterized by a maximum peak five times less than traditional jet fan. On the other hand, viscous stress values on the tunnel floor show a reverse condition in a less prominent manner, with respect to the viscous stress values on the ceiling.

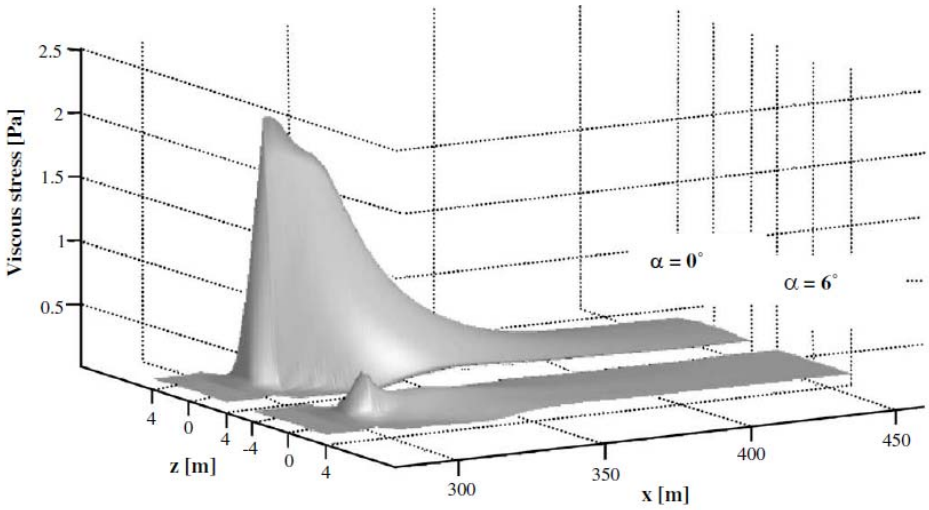

Figure 26 – Three-dimensional viscous stress at tunnel ceiling @ α=0° and α=6° (free tunnel case)

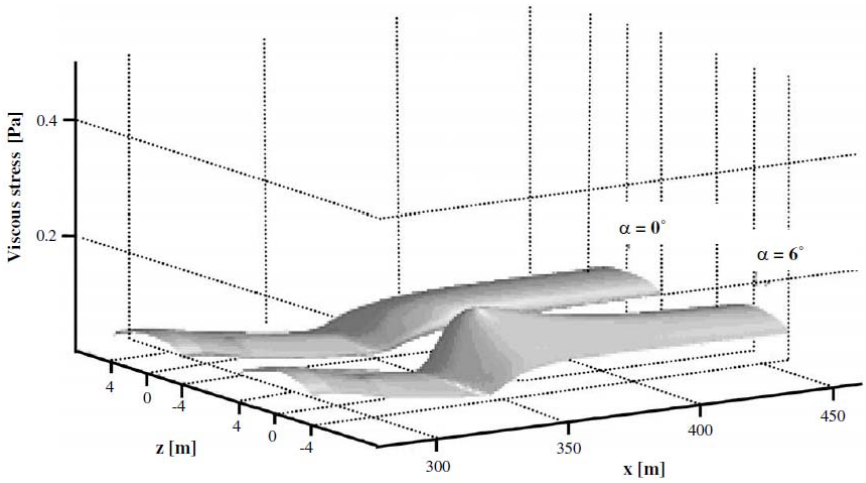

Figure 27 – Three-dimensional viscous stress at the tunnel floor @ α=0° and α=6° (free tunnel case)

4.5. Optimal pitch angle in traffic jam condition

CFD analysis shows that inclined jet fan configuration is able to guarantee the same average air velocity in tunnel for traffic jam conditions by means of lower thrust with respect to traditional jet fan. Moreover, the performances in traffic jam conditions decrease with respect to the condition without vehicles.

The shear stress fields, for different pitch angle values, are shown in Figure 28: the presence of vehicles in tunnel increases the shear stress and the total force value with respect to the case without vehicles (free tunnel).

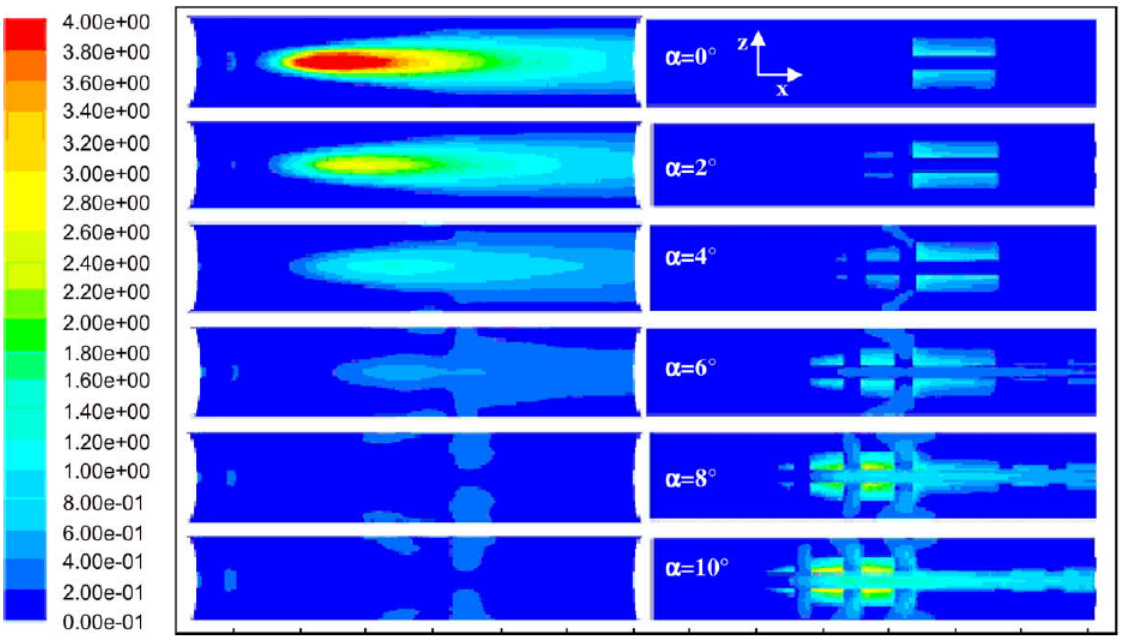

Figure 28 – Shear stress filed for different pitch values; (a) ceiling; (b) floor (traffic jam case)

At last, results show that the optimal configuration for pitch angle in traffic jam case is obtained for 2° and 4° for which the total thrust assumed the minimum value and the PR attained the maximum value.

Table 9 – Shear stress on ceiling and floor, thrust and PR (traffic jam case)

α (°)	$F_{\alpha,\ ceiling}$ (N)	$F_{\alpha,\ floor} + F_{\alpha,\ vehicle}$ (N)	$F_{\alpha,\ tot}$ (N)	F_{α} (N)	PR
0	3350	3384	6734	1900	1.00
2	2640	3654	6294	1786	1.06
4	2126	4154	6280	1786	1.06
6	1638	5978	7616	2128	0.89
8	1350	8776	10126	2812	0.68
10	1206	11062	12268	3420	0.56

4.6. Results

The CFD numerical analysis shows that there exists an optimal pitch angle, which minimizes the pressure losses due to the flow attachment and maximizes the PR. It gives the following results, in terms of energetic operating costs reductions:

Case	Optimal pitch angle
Free tunnel	6°
Traffic jam	2°÷4°

Results show also that the advantage obtained in the traffic jam conditions are minimal with respect to the free tunnel case. This can let to consider the possibility of an automatic system able to varying the value of the pitch angle for each operational condition.

5. *Numerical comparison between alternative and traditional jet fans in a longitudinal tunnel ventilation system in traffic jam condition – with vs without fire case*

In this chapter, results showed in previous par. 3 are considered as starting point in order to analyze the effects of the presence of fire in a road tunnel for traffic jam conditions.

The same geometry and configuration showed in Figure 17 and Figure 18 are considered. In addition to what already stated, an HGV (parallelepiped shape) is positioned as "burning vehicle" on the tunnel centerline at 50 m distance from the outlet of the second jet fan, as shown in Figure 29. Thus, results of the previous sensitivity analysis for mesh grid definition can be also considered.

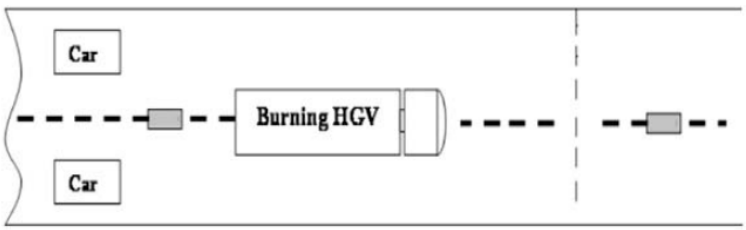

Figure 29 – Burning HGV position

As difference with respect to par. 3 analysis, where the jet fans are simulated by means of fluid region with an imposed constant positive pressure gain, here the pressure gain (Δp_{jet}) induced by jet fan is imposed for each pitch angle. This, in order to obtain an axial velocity greater than critical one considering that the vehicle fire is simulated with an Heat Rate Released (HRR) equal to 20 MW. In particular, it is set a heat flux on HGV surface, comprehensive of radiative heat flux.

The ventilation system is considered running in steady state condition before fire starting, and the fire scenario is simulated for 60 seconds.

Table 10 shows main results in terms of velocity and flowrate for different pitch angles with and without fire.

Table 10 – Main parameters for several pitch angles in traffic jam condition – fire vs no fire case

		$v_{average,in}$ (m/s)	$v_{average,tunnel}$ (m/s)	$v_{average,section1}$ (m/s)	$v_{average,section2}$ (m/s)	v_{ceil1} (m/s)	v_{ceil2} (m/s)
α=0°	**Fire**	1.9	2.67	2.04	3.07	4.8	-0.1
	No fire	2.1	2.44	2.43	2.34	6	4.5
		$\dot{m}_{in}$ (kg/s)	$\dot{m}_{out}$ (kg/s)	$\dot{m}_{fan1,out}$ (kg/s)	$\dot{m}_{fan2,out}$ (kg/s)	$\dot{m}_{fan3,out}$ (kg/s)	$\dot{m}_{fan4,out}$ (kg/s)
	Fire	64.4	97.0	9.88	9.89	8	9.93
	No fire	73.5	73.5	9.89	9.88	9.77	9.75
α=2°		$v_{average,in}$ (m/s)	$v_{average,tunnel}$ (m/s)	$v_{average,section1}$ (m/s)	$v_{average,section2}$ (m/s)	v_{ceil1} (m/s)	v_{ceil2} (m/s)
	Fire	1.6	2.39	1.74	2.73	5.01	2.35
	No fire	1.95	2.27	2.17	2.17	6.18	4.69
		$\dot{m}_{in}$ (kg/s)	$\dot{m}_{out}$ (kg/s)	$\dot{m}_{fan1,out}$ (kg/s)	$\dot{m}_{fan2,out}$ (kg/s)	$\dot{m}_{fan3,out}$ (kg/s)	$\dot{m}_{fan4,out}$ (kg/s)
	Fire	54.6	86.2	9.16	9.13	6.95	9.16
	No fire	71.5	71.5	9.41	9.4	9.28	9.27
α=4°		$v_{average,in}$ (m/s)	$v_{average,tunnel}$ (m/s)	$v_{average,section1}$ (m/s)	$v_{average,section2}$ (m/s)	v_{ceil1} (m/s)	v_{ceil2} (m/s)
	Fire	2.30	2.97	2.34	3.35	3.84	2.21
	No fire	2.41	2.27	2.65	2.66	4.81	4.23
		$\dot{m}_{in}$ (kg/s)	$\dot{m}_{out}$ (kg/s)	$\dot{m}_{fan1,out}$ (kg/s)	$\dot{m}_{fan2,out}$ (kg/s)	$\dot{m}_{fan3,out}$ (kg/s)	$\dot{m}_{fan4,out}$ (kg/s)
	Fire	73.8	105.4	8.74	8.77	6.9	8.71
	No fire	87.2	87.2	8.93	8.96	8.79	8.76
α=6°		$v_{average,in}$ (m/s)	$v_{average,tunnel}$ (m/s)	$v_{average,section1}$ (m/s)	$v_{average,section2}$ (m/s)	v_{ceil1} (m/s)	v_{ceil2} (m/s)
	Fire	2.0	2.94	2.22	3.23	3.56	2.76
	No fire	2.5	2.55	2.77	2.78	5.2	4.7
		$\dot{m}_{in}$ (kg/s)	$\dot{m}_{out}$ (kg/s)	$\dot{m}_{fan1,out}$ (kg/s)	$\dot{m}_{fan2,out}$ (kg/s)	$\dot{m}_{fan3,out}$ (kg/s)	$\dot{m}_{fan4,out}$ (kg/s)
	Fire	70.1	101.8	8.41	8.43	6.58	8.39
	No fire	87.4	87.4	8.5	8.55	8.36	8.33
α=8°		$v_{average,in}$ (m/s)	$v_{average,tunnel}$ (m/s)	$v_{average,section1}$ (m/s)	$v_{average,section2}$ (m/s)	v_{ceil1} (m/s)	v_{ceil2} (m/s)
	Fire	1.8	2.75	2.02	3.02	-0.42	2.04
	No fire	2.2	2.24	2.45	2.45	2.6	2.96
		$\dot{m}_{in}$ (kg/s)	$\dot{m}_{out}$ (kg/s)	$\dot{m}_{fan1,out}$ (kg/s)	$\dot{m}_{fan2,out}$ (kg/s)	$\dot{m}_{fan3,out}$ (kg/s)	$\dot{m}_{fan4,out}$ (kg/s)
	Fire	64.0	95.7	8.52	8.54	6.5	8.45
	No fire	80.8	80.8	8.73	8.76	8.59	8.57
α=10°		$v_{average,in}$ (m/s)	$v_{average,tunnel}$ (m/s)	$v_{average,section1}$ (m/s)	$v_{average,section2}$ (m/s)	v_{ceil1} (m/s)	v_{ceil2} (m/s)
	Fire	1.84	2.74	2.01	3.02	-0.55	2.06
	No fire	2.2	2.2	2.42	2.42	2.24	2.72

		$\dot{m}_{in}$ (kg/s)	$\dot{m}_{out}$ (kg/s)	$\dot{m}_{fan1,out}$ (kg/s)	$\dot{m}_{fan2,out}$ (kg/s)	$\dot{m}_{fan3,out}$ (kg/s)	$\dot{m}_{fan4,out}$ (kg/s)
	Fire	63.7	95.4	8.85	8.89	6.78	8.89
	No fire	79.7	79.7	9.07	9.11	8.94	8.91

As results, following Figure 30 and Figure 31 show respectively the temperature fields (K) in the longitudinal sections on the symmetric plane for different pitch angle values.

In particular, the Figure 30 shows that minimum imposed pressure gain values Δp_{jet} (see Table 10) assures the absence or containment of the smoke spread against longitudinal ventilation (back-layering phenomena) near the truck, for every pitch angle values, at fixed truck position.

In Figure 31, it is possible to note that where the pitch angle value increases from 2° to 10°, the efficiency ceil sweep decreases and the stratification of hot gases increases. However, it seems that the alternative system with α=2° guarantees the lowest temperature value, in particular near the tunnel ceiling.

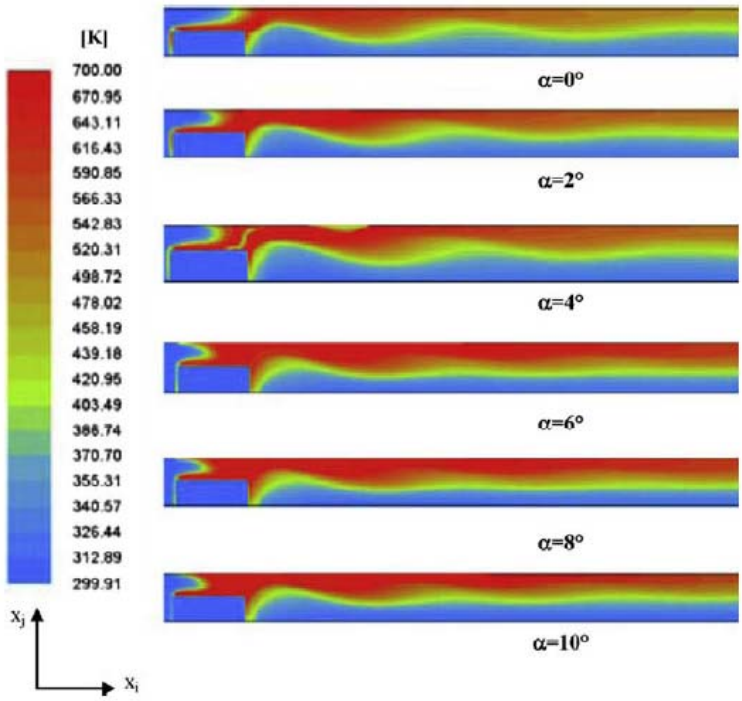

Figure 30 – Temperature fields (K) in the longitudinal sections on the symmetric plane for different pitch angle values, in the fire with traffic scenario.

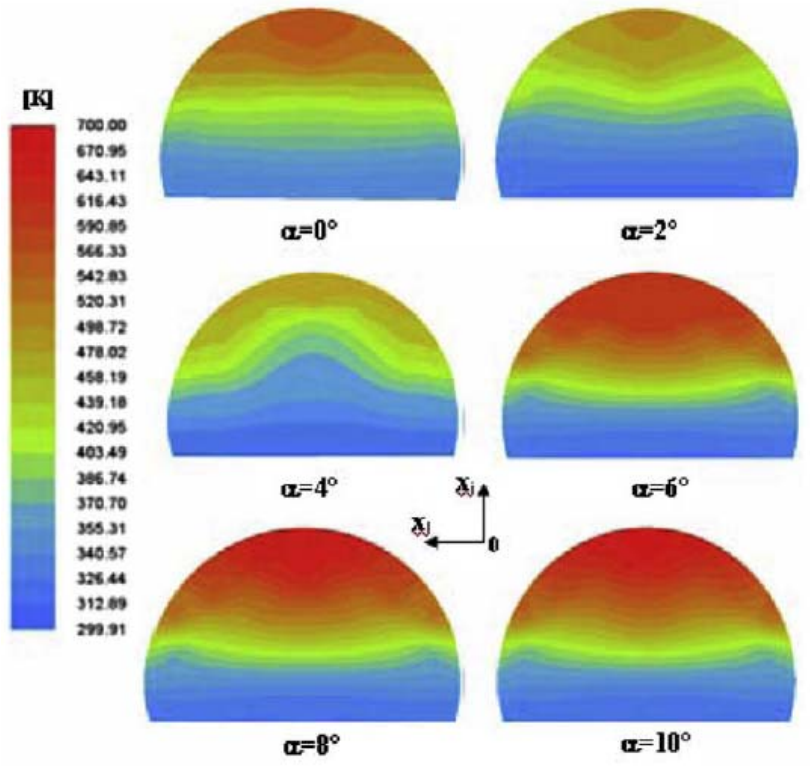

Figure 31 – Temperature fields (K) on the transversal sections at 50 m from burning HGV, for different pitch angle values, in the fire with traffic scenario.

From the analysis of the temperature and velocity fields (see Table 10), it is possible state that the tunnel average velocity ($v_{average,tunnel}$) and the average velocity ($v_{average,section1}$) at the tunnel section upstream fire source, are not significant to predict the presence of back-layering. In particular, the comparison between the $v_{average,section1}$ values for α=2° and α=8° and 10°, even if $v_{average,section1}$ (α=2°) is less than $v_{average,section1}$ (α=8°) (see Table 10 and Figure 32 ÷ Figure 40), shows the presence of back-layering only for α=8° and 10°.

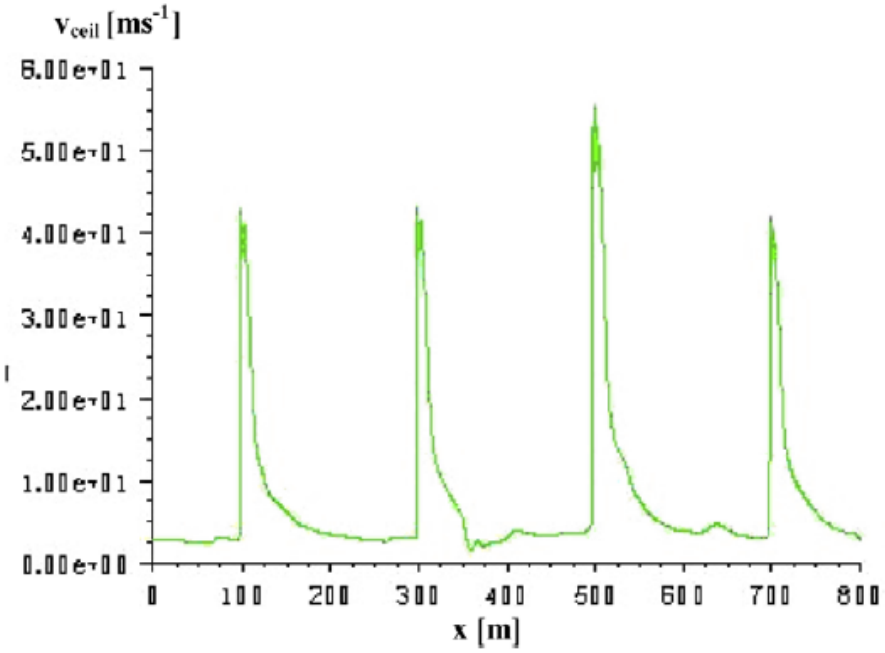

Figure 32 – Axial velocity v_{ceil} at y = 5.60 m and z = 0 m, for α=2°.

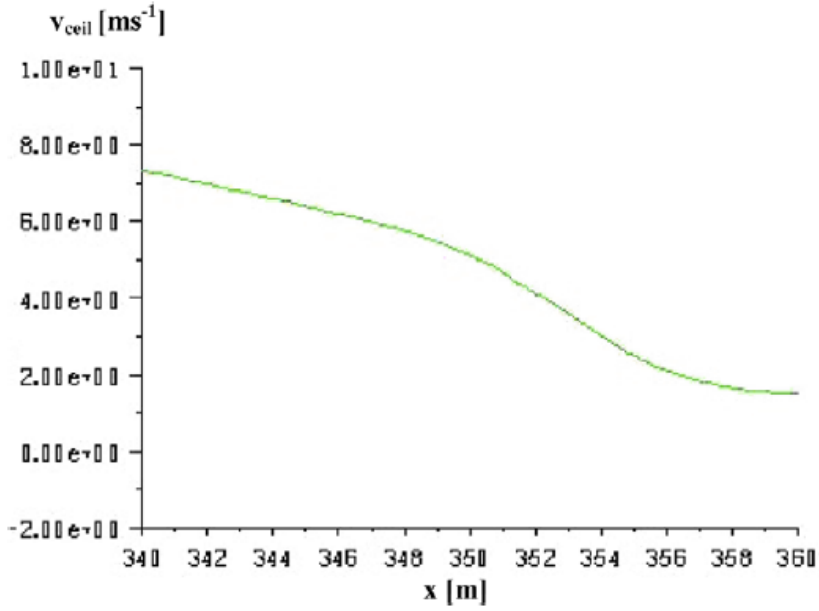

Figure 33 – Axial velocity v_{ceil} at y = 5.60 m and z = 0 m, for α=2°.

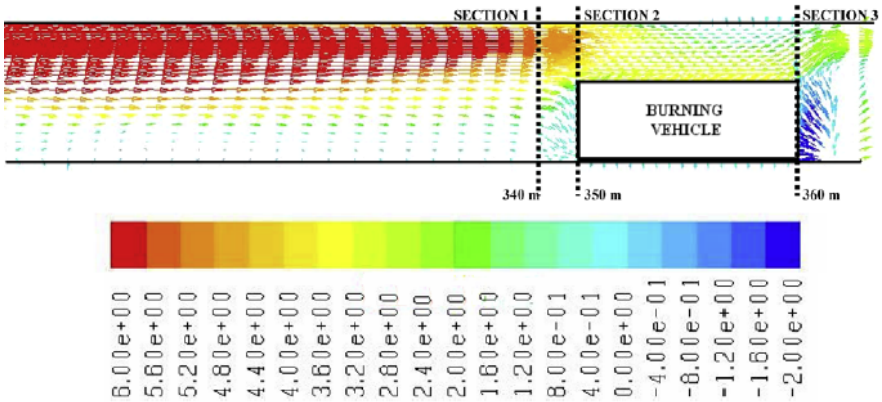

Figure 34 – Axial velocity field close to the ceil, α=2°

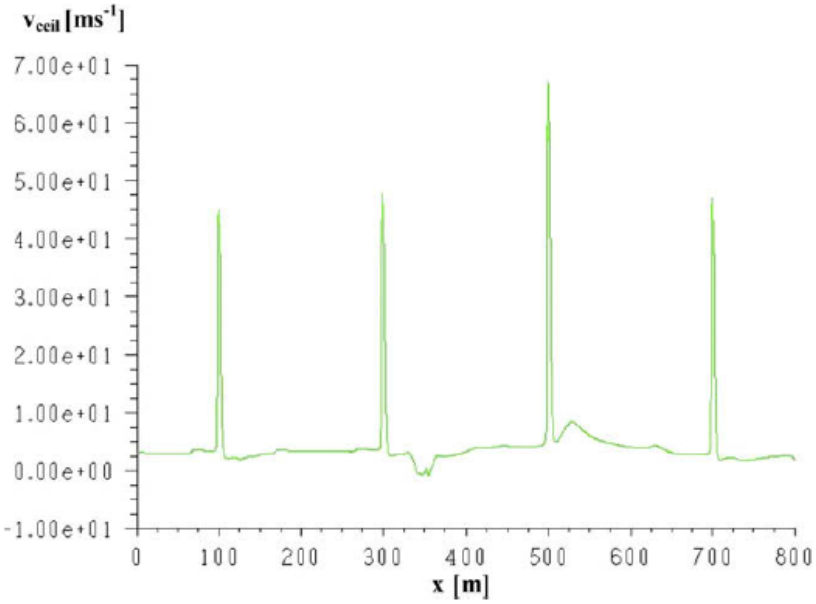

Figure 35 – Axial velocity v_{ceil} at y = 5.60 m and z = 0 m, for α=8°.

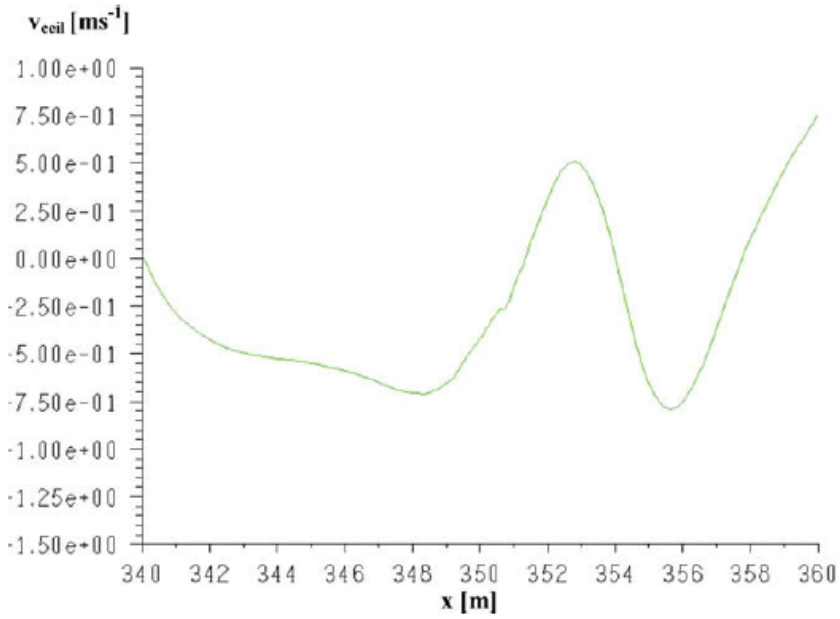

Figure 36 - Axial velocity v_{ceil} at y = 5.60 m and z = 0 m, for α=8°.

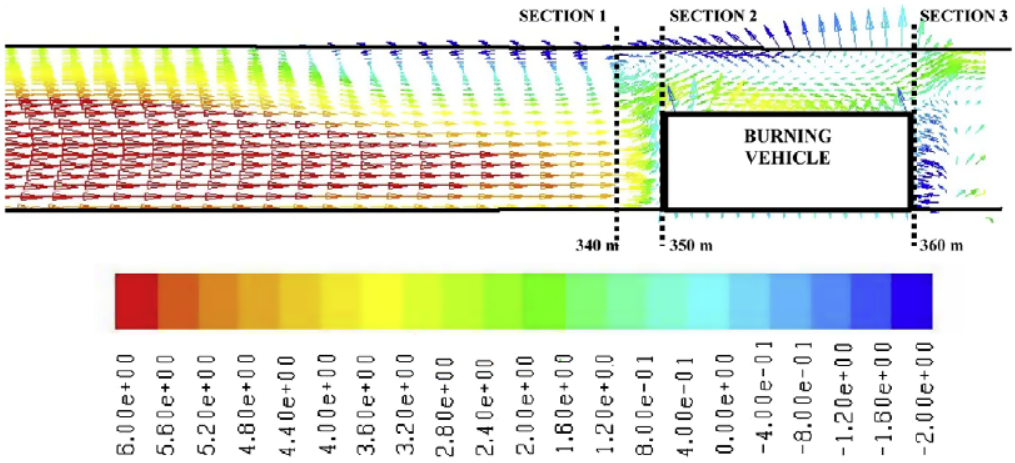

Figure 37 – Axial velocity field close to ceil, α=8°.

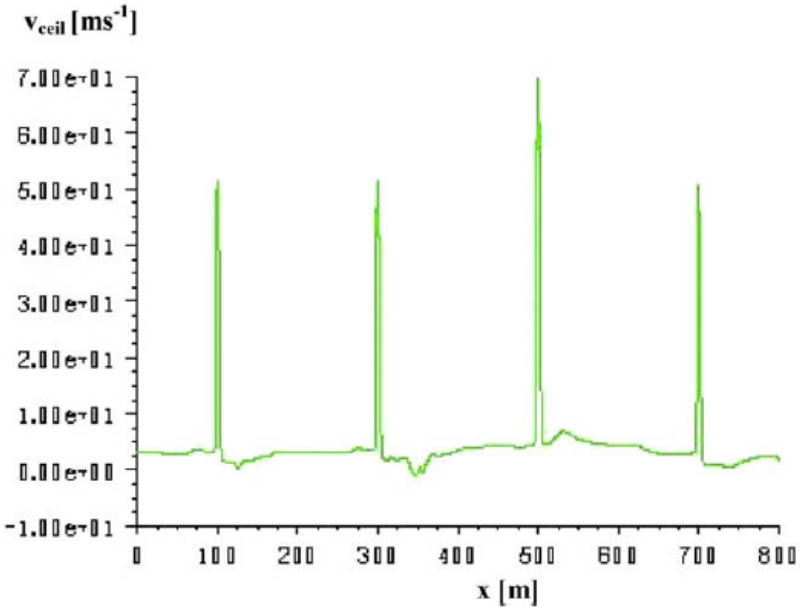

Figure 38 – Axial velocity v_{ceil} at y = 5.60 m and z = 0 m, for α=10°.

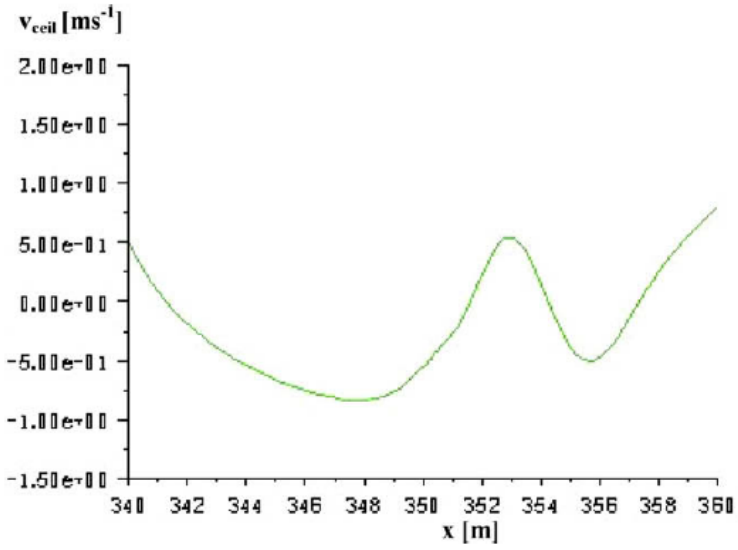

Figure 39 – Axial velocity v_{ceil} at y = 5.60 m and z = 0 m, for α=10°.

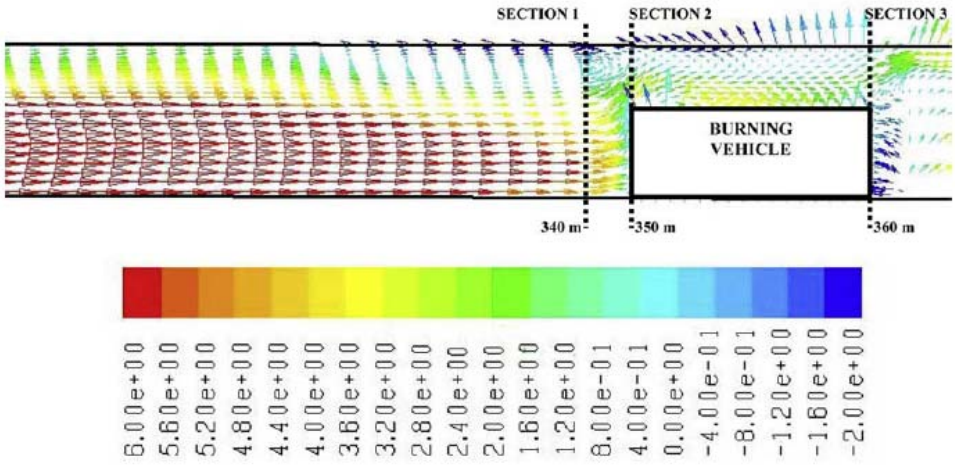

Figure 40 – Axial velocity field close to ceil, α=10°

The significant parameter able to predict the absence of back-layering is axial component of the velocity ($v_{x,jetfan}$). Hence, comparing the results obtained in the fire configuration with those obtained in the precedent CFD simulations in the ordinary tunnel ventilation, it is possible to note that, maintaining the same Δp_{jet} for every pitch angle values, the mass flow rate elaborated by the jet fan subsequent burning vehicle diminishes and, consequently, the jet fan performance is reduced about 15–25%. On the other hand, the thermal expansion of the gases due to the fire, increases the air x-velocity downstream fire source: the average air velocity values ($v_{average,section2}$), at the transversal section x = 363,6 m (downstream the burning HGV), is greater than the value ones ($v_{average,section1}$) at the transversal section x = 350 m (upstream the burning HGV).

6. *Numerical comparison of performances between traditional and alternative jet-fan in emergency condition – tiled tunnel case*

6.1. Introduction

Following results shown in previous chapters, here below are shown the numerical analyses carried out to investigate the performances of alternative and traditional configuration jet fan in a tiled tunnel for emergency conditions.

The comparison is made in terms of total thrust required to prevent back-layering phenomena and numerical results are provided in terms of thrust of jet fan values, average velocity values and temperature profiles, for different tunnel slope values.

6.2. CFD model

The analyzed model is those considered in previous chapter 3 that consists in an 800 m one directional road tunnel equipped with four longitudinal jet fan positioned at 5.60 meters from ground (Figure 18). The distance between the two a fans is fixed in 200 m while the jet fans J_{f1} and J_{f4} (Figure 41) are installed at a distance of 100 m from inlet and outlet sections of the tunnel, respectively. The pitch angle is fixed to 6°.

This configuration and the thrust of jet fans are chosen to guarantee a local velocity value close to designed one in the proximity of the subsequent inlet jet fan section for an optimized system ventilation without fire [6].

Optimizing the computational time, also in this case the physical domain is divided into three different zones (A, B and C) with different grid sizes as shown in Figure 42. The domain takes into account the high gradients of the air velocity and temperature that along the tunnel: the B type zone is meshed by tetrahedral grid with step equal to 0.1 m while the A and C type zones were meshed with hexahedral grid with step equal 0.4 m obtained by previous mesh analysis [6]. The tetrahedral grid and the very fine grid step choices are necessary, respectively, to adapt the different geometrical blocks shape, to simulate very high velocity gradients.

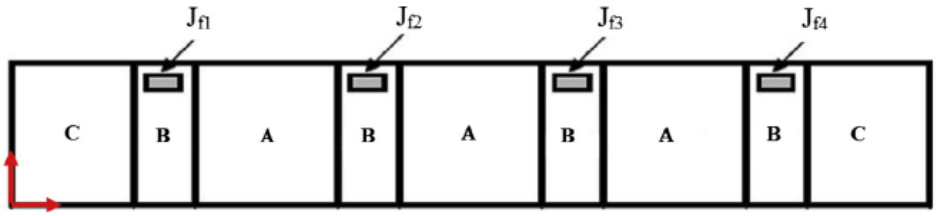

Figure 41 – Tunnel scheme

Each jet fan is simulated as momentum source divided into tetrahedral grids with step equal to 0.1 m [6], as shown in Figure 42.

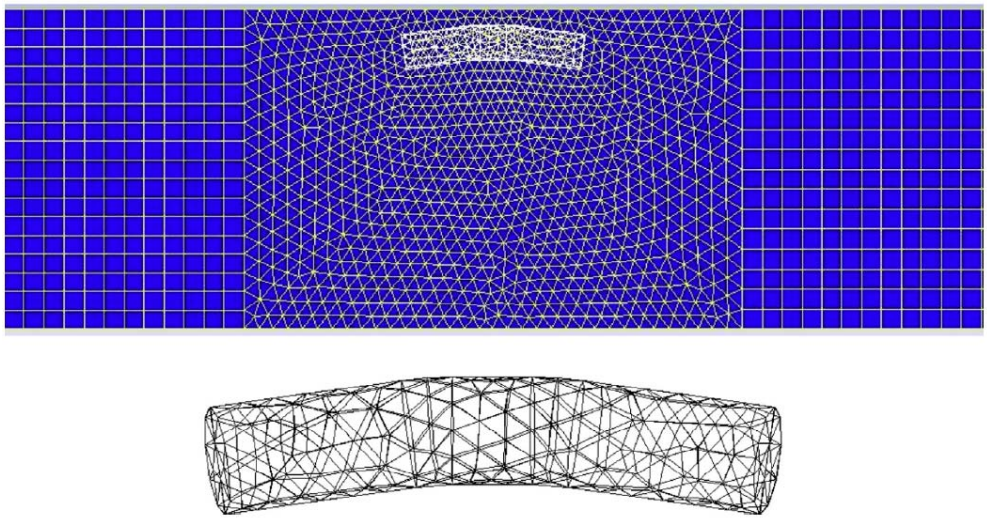

Figure 42 – Mesh for tunnel and jet fan

Turbulent model

The governing equations of the fluid region in unsteady and turbulent states and three-dimensional flux are time Averaged mass Navier Stokes [67] combined with k–ε realizable model. The k–ε turbulence model proposed by Launder and Spalding [68] is largely validated by the scientific community.

Boundary Conditions

Following hypotheses are considered in CFD analysis:

- Air properties, considered as an ideal gas, are assumed constant with the temperature and evaluated at the ambient temperature equal to 300 K.
- The swirl component due to the air flux passage through the fan wheel is neglected.
- The pitch angle of the jet fan in the simulation represents the real baffle plates.
- Different tunnel slopes: 0%, 2.5%, 5% and 10%.

The following boundary conditions are imposed:

- The representation of the fan is a simple momentum source with the jet fan pressure drop imposed to avoid back-layering phenomena.
- The values of tunnel ceiling and floor roughness are equal to 0.03–0.01 m respectively.
- The value of truck roughness is equal to 0.01 m.
- Heat flux of source surface is equal to 180 kW/m2.

- No sleep condition.
- The fire is located 150 m downstream the second jet fan.
- The pitch angle of jet fan is fixed equal to 0 and 6°.
- Computational time is equal to 300 s.[2]

6.3. Results

The comparison of numerical results between traditional and alternative jet fan are shown in Figure 43 and Table 11 where values of pressure drop and thrust are indicated for different tunnel slope values in order to avoid back layering phenomena.

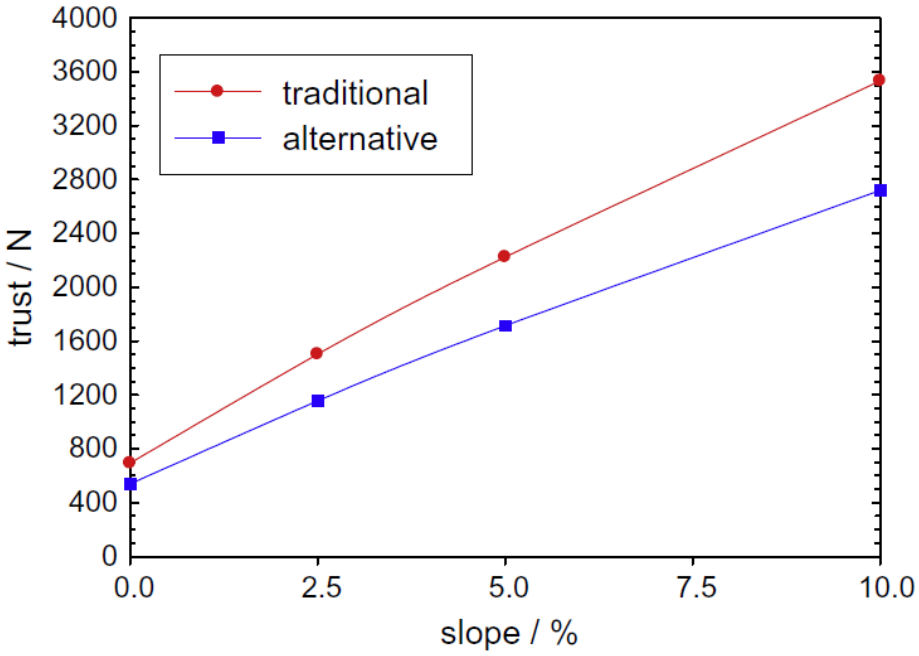

Figure 43 – Trust vs tunnel slope for both traditional and alternative jet fan

[2] Previous analysis have showed that 300 s is a enough time to evaluate the back layering phenomena.

Table 11

	Slope (%)			
	0.0	**2.5**	**5.0**	**10.0**
Δp (Pa) - traditional	1800	3900	5775	9175
Δp (Pa) - alternative	1400	3000	4450	7063
Thrust (N) - traditional	648	1404	2079	3303
Thrust (N) - alternative	504	1080	1602	2543
Thrust reduction for alternative jet fan with respect to traditional one (%)	22	23	23	23

It is possible to note that the thrust of a jet fan increases as tunnel slope value increases, for both type jet fans; in particular for traditional jet fan the thrust value increases from 693 to 3532 N, and for alternative jet fan the thrust value increases from 539 to 2719 N. As shown in Table 11, for all slope values, the thrust required by traditional jet fan to guarantee the absence of back-layering is greater than alternative jet fan.

The numerical critical velocity u_{cr} is obtained as average velocity on the cross-section surface placed at 2 m upstream fire source (Figure 44).

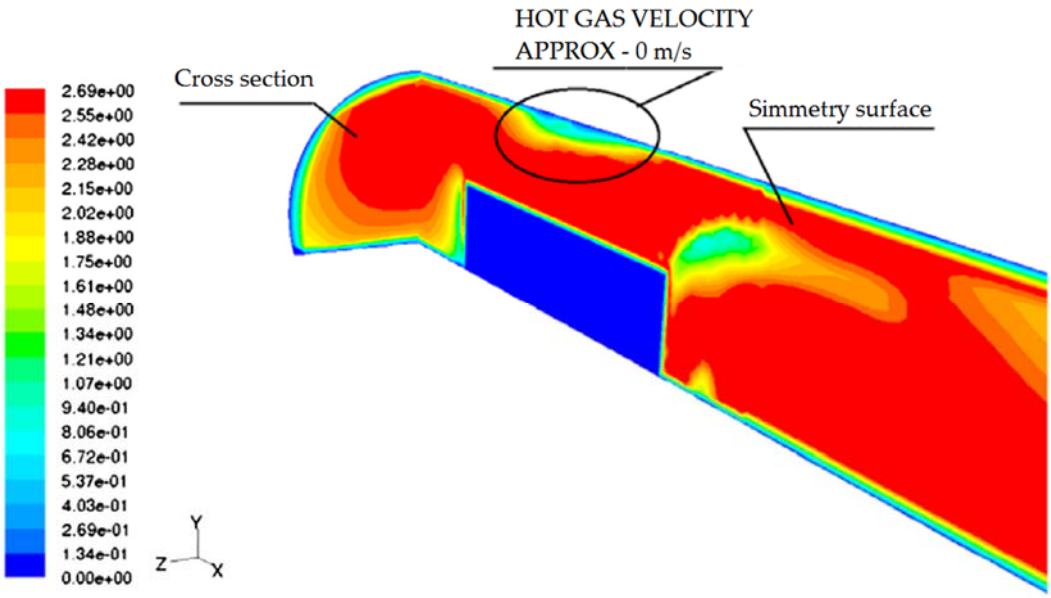

Figure 44 – u_{cr} in mid cross section

The numerical critical velocity, the average volume axial velocity in the tunnel and axial critical velocity values obtained from analytical formula, are reported in Table 12. The analytical value of critical velocity is calculated by modified Thomas' relationship [43]:

$$u_{cr} = k_g \left(\frac{gQH}{\rho \ T_{\mathrm{hg}} c_p A} \right)^{1/3} \tag{18}$$

where k_g is the parameter that considers the dependence of the analytical critical velocity on the tunnel inclination:

$$k_g = (1 + 0.0374|\min(grade, 0)|^{0.8}) \tag{19}$$

Table 12 shows that numerical and analytical critical velocity values for both jet fans are very close. This is due to the critical velocity that mainly depends on the thermal power released from fire source, for fixed tunnel geometry. As expected, the critical velocity increases as tiled angle increases. Numerical and analytical critical velocity values are in good agreement.

Table 12

Slope (%)	**k_g**	**u_{ax} (m/s)**			
		average	**numerical (traditional)**	**numerical (alternative)**	**analytical**
0	1	2.73	2.27	2.28	2.38
2.5	1.0778	2.94	2.50	2.48	2.56
5	1.1355	3.10	2.66	2.67	2.70
10.0	1.2360	3.37	2.93	2.93	2.94

Figure 45 shows the axial velocity fields for different slope values for both configurations. It can be observed that, for all tunnel slope values analyzed, the velocity fields are very similar. The presence of small areas with almost zero axial velocity above HGV, indicates that the thrust provided by the jet fan is the minimum required to prevent the backlayering phenomena.

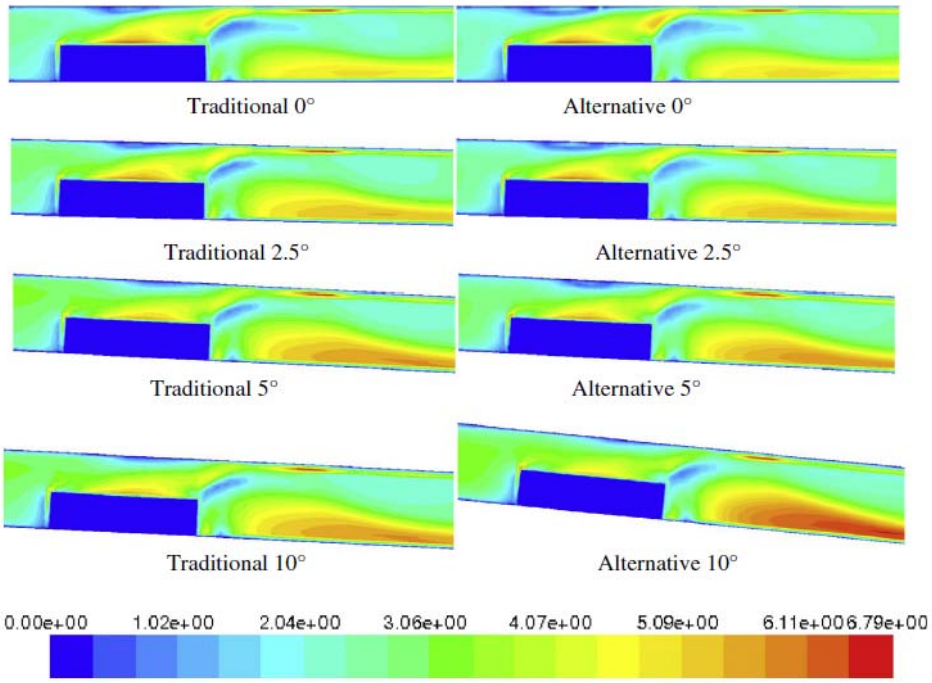

Figure 45 – Comparison of ventilation velocity for different tunnel slopes for alternative and traditional jet fan @ 150 m after second jet fan

Figure 46 shows the temperature fields at different tunnel slope values (0% and 10%, respectively) for both LTVS and LAVS. In both cases, the ceiling temperature is always lower when alternative jet fan is installed.

Figure 47 shows the ceiling (z = 6.42 m) and floor (z = 0 m) temperature profiles, respectively, downstream of the fire (x = 450 m). Starting from the third fan inlet (x = 500 m) and for the next 50 m, the temperature profiles are always lower in the case of alternative jet fan because it directs part of the jet of hot gases toward the tunnel floor (Figure 47 right side). Temperature profiles overlaps again for every slope values for the whole tunnel.

Moreover, results show that as the tiled angle increases the temperature value at the ceiling decreases for both jet fans. On the other hand, as the slope increases, differences in temperature between alternative and traditional jet fan, decrease. The same considerations can be repeated for the temperature profiles shown in (Figure 47 left side). In this case, as the tiled angle increases the temperature value at the floor increases for both jet fans.

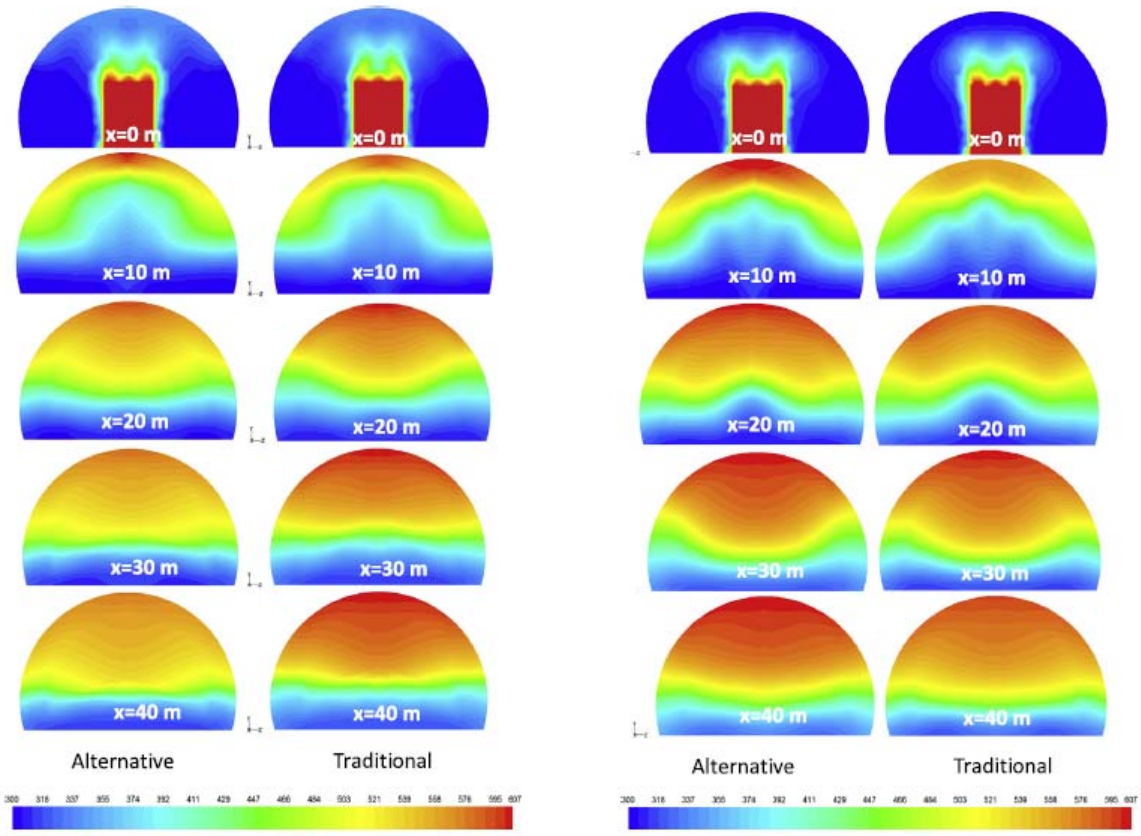

Figure 46 – Temperature field for 0% tunnel slope (left) and 10% tunnel slope (right)

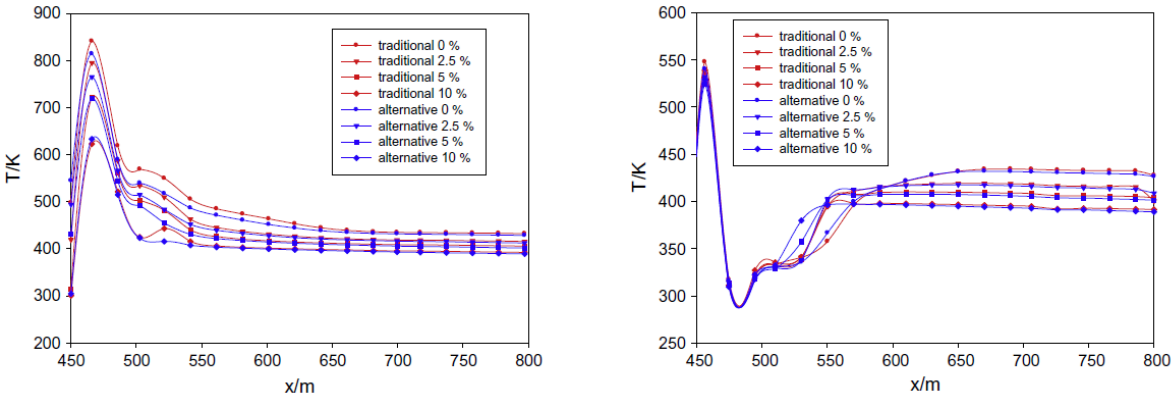

Figure 47 - Temperature profiles evaluated on the ceiling (left) and floor (right) centerline along the longitudinal axis of the tunnel at different slope values.

Figure 48 shows the temperature profile at centerline passing through the jet fan for both traditional and alternative configurations for all investigated tunnel slopes: the temperature profiles are always higher in the case of traditional jet fan with respect to the alternative one (from 10 up to 35 °C).

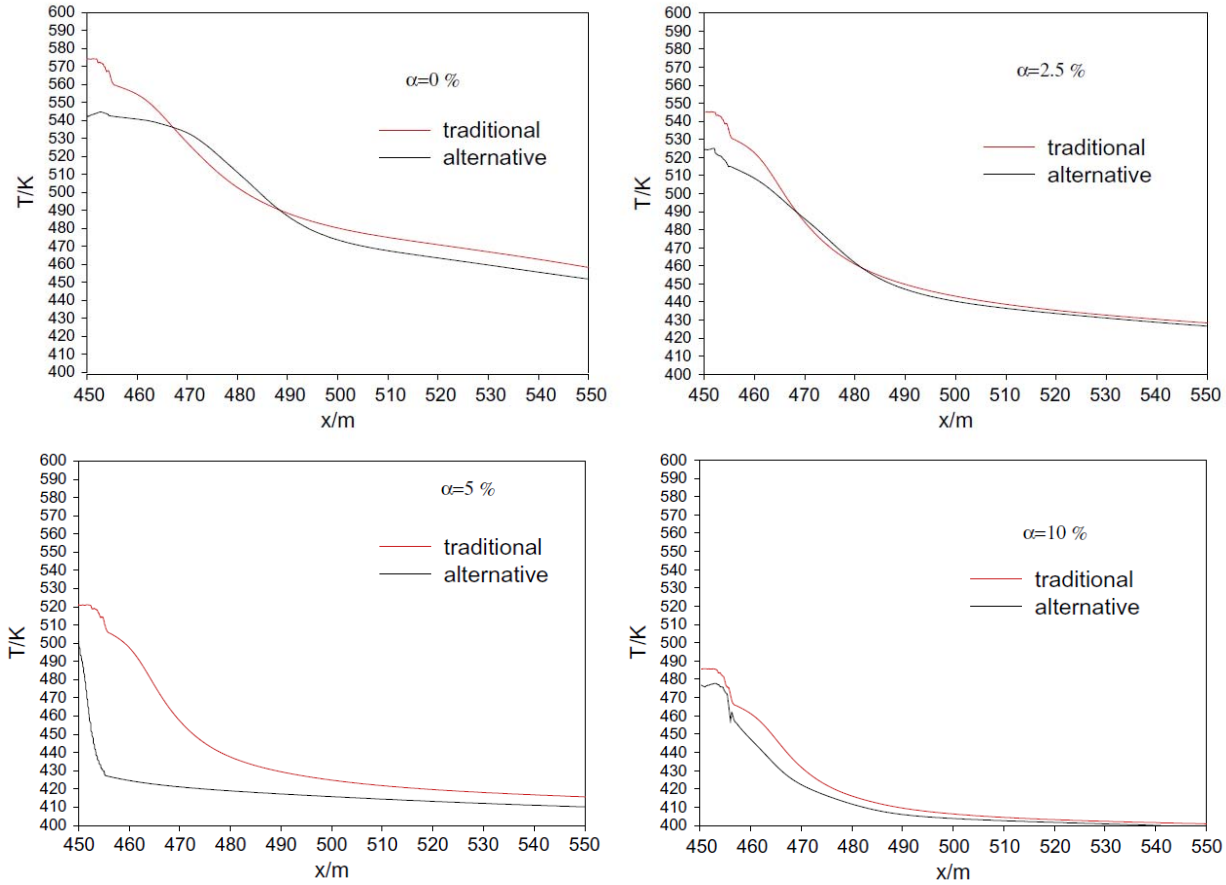

Figure 48 – Air temperature profiles evaluated at the centerline of jet fan downstream fire source, for both jet fans and for all investigated tunnel slopes

As conclusion, for all investigated tunnel slopes, the advantages for the alternative jet fan with respect to the traditional one in emergency condition for tiled tunnel, are:

- Alternative jet fan requires lower total thrust with respect to LTVS to prevent back-layering; in particular the ratio between the total thrust required for both the fans is equal to 0.77 for all tunnel slope considered.
- Lower ceiling temperature values obtained for LAVS could guarantees the integrity of the tunnel ceiling for more time with respect to the traditional one.
- The lower temperature values at centerline passing through the jet fan obtained for LAVS could ensure a more lasting operation, but this advantage is reduced as slope increase.

Moreover, the agreement between numerical and analytical critical velocity values, for both traditional and LAVS, indicates the goodness of CFD analysis.

7. *Numerical analyses of scale factor for laboratory tunnel design*

Aim of this chapter is to show result of activities done to define the size of a laboratory scale model for a tunnel in order to validate, through experimental analysis, numerical results. Similitude analysis is made in order to preserve geometry, kinematic and dynamic aspects by means of Froude's scaling procedure.

7.1. Scale factor evaluation

As first step in the analysis, it is assumed a geometric scaling factor (λ) equal to 50 considered as the ration between the characteristic lengths of two systems. Dynamic similitude is considered preserving the Froude number, defined as the ration between gravity forces and inertia ones (Equation (1)).

In order to reach a full similitude, other no-dimensional numbers (as Reynolds number) should be preserved. In most of cases, high Reynolds numbers can let to consider the sole Froude number preserving to ensure both dynamic and kinematic similitude. Thus, when a turbulent flow occurs, a not-so-high scaling factor let to consider Froude's number preserving as a reasonable approach to define a similitude between two models (full and reduced scale) as shown by Carvel and Karaaslan [79].

$$Fr = \frac{\rho v_{av,m}^2}{g L_m} = \frac{\rho v_{av,f}^2}{g L_f} \qquad (20)$$

from which

$$v_{av,m} = v_{av,f} \sqrt{\frac{L_m}{L_f}} \qquad (21)$$

Thus, since the volume average velocity for the full scale tunnel is about 3.7 m/s, considering the defined λ value, the flow motion for the reduced model results turbulent ($v_{av,m}$=0.52 m/s → Re=5000).

7.1.1. Sensitivity analysis

The comparison analysis of traditional and alternative solution for jet fan has considered following boundary condition shown in Table 13. Here, the full scale simulations consider an average velocity equal to 3.7 m/s and 3.8 m/s for traditional and alternative jet fan respectively.

Table 13

Full scale model	
Solver	Pressure based
Regime	Steady state
Fluid	Air
Pressure drop (traditional fan)	2300 Pa
Pressure drop (alternative fan)	1700 Pa
Fluid temperature	300 K
Gouge pressure (inlet/outlet section)	0 Pa
Floor roughness	0,01 m
Roof roughness	0,03 m
Turbulent model	k-ε realizable

By means of CFD analyses, where both kinematic and dynamic similitude are preserved, boundary conditions for reduced model are defined. At first, different roughness for roof and floor are considered in order to reach same values of average velocity for both traditional and alternative jet fans (see equation (22) known as continuity condition). In addition, pressure drop values for reduced model are calculated in consideration of Froude scaling procedure; in particular, traditional and alternative fan consider respectively 46 Pa and 36 Pa of pressure drop. Considering a constant ratio between ceiling and roof roughness from full scale to reduced model, simulations lead to results shown in following tables for traditional and alternative jet fan.

$$\frac{\partial \rho}{\partial t} + \frac{\partial}{\partial x_j}(\rho v_i) = S_m \qquad (22)$$

Table 14

Traditional fans						
	Δp (Pa)	v (m/s)	Roof rough (m)	Floor rough (m)	Re	Fr_{av}
Full scale tunnel	2300	3.7	0.03	0.01	$1.7 \cdot 10^{6}$	0.23
Reduced tunnel	100	0.53	0.03	0.01	5400	0.24
	92	0.51	0.01	0.0033	4800	0.21
	85	0.50	0.005	0.0017	4700	0.20
	64	0.51	0.0015	0.0005	4800	0.21
	55	0.51	$1.5 \cdot 10^{-6}$	$1.5 \cdot 10^{-6}$	4700	0.20
	50	0.50	$1.0 \cdot 10^{-8}$	$1.0 \cdot 10^{-8}$	4700	0.20

Table 15

Alternative fans						
	Δp (Pa)	v (m/s)	Roof rough (m)	Floor rough (m)	Re	Fr_{av}
Full scale tunnel	1800	3.80	0.03	0.01	$1.8 \cdot 10^{6}$	0.25
Reduced tunnel	70	0.53	0.01	0.0033	5400	0.24
	55	0.56	0.005	0.0017	5700	0.27
	46	0.51	0.0015	0.0005	4800	0.21
	44	0.50	$1.5 \cdot 10^{-8}$	$1.5 \cdot 10^{-8}$	4700	0.20
	42	0.49	$1.0 \cdot 10^{-8}$	$1.0 \cdot 10^{-8}$	4600	0.20

Velocity profiles are shown in following Figure 49 to Figure 54 for traditional jet fan.

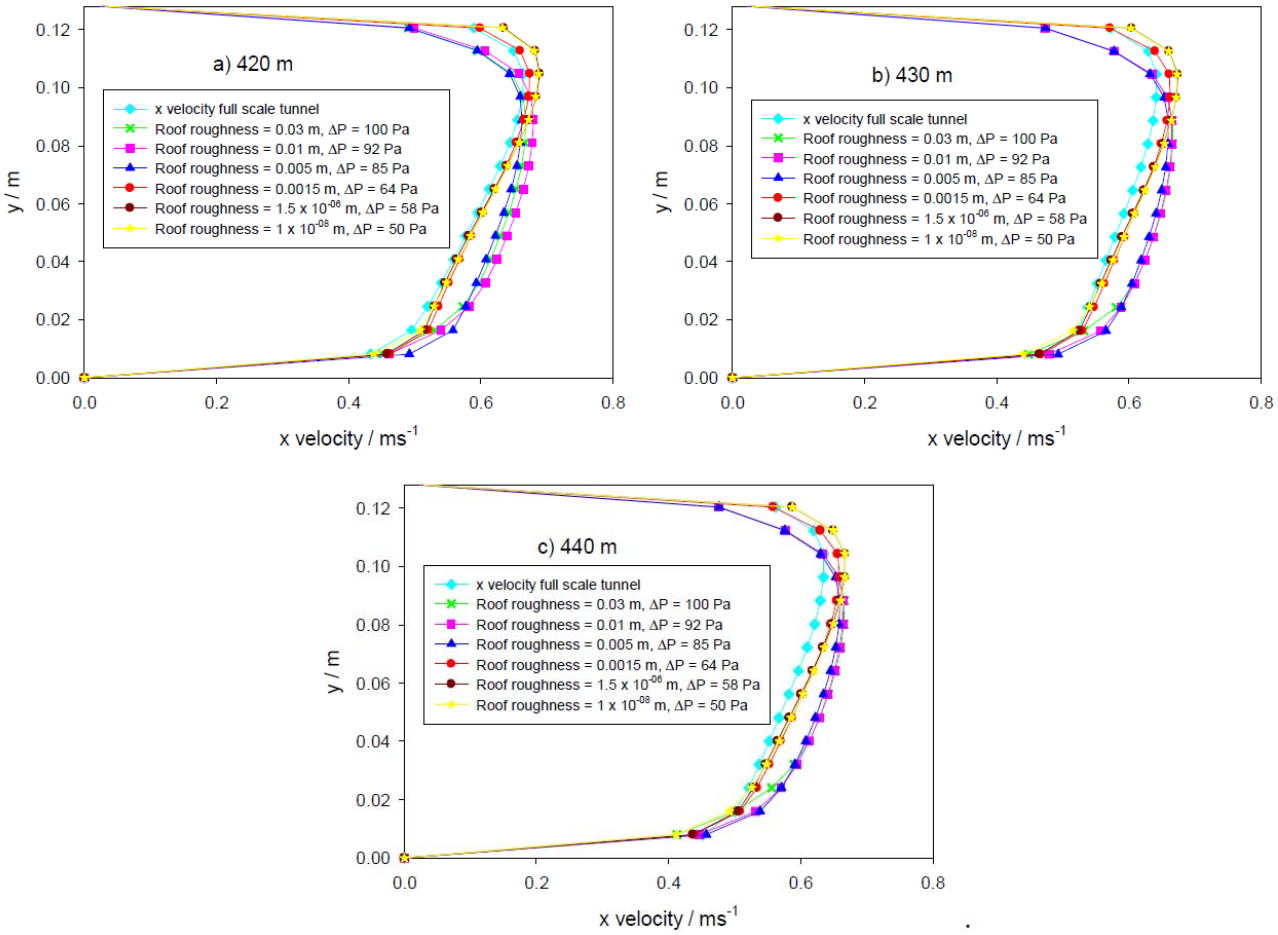

Figure 49 – Axial velocity on symmetry plane, comparison between full and reduced model at (a) 10 m, (b) 20 m and (c) 30 m before the HGV by changing roughness and pressure drop for traditional jet fans (Table 14)

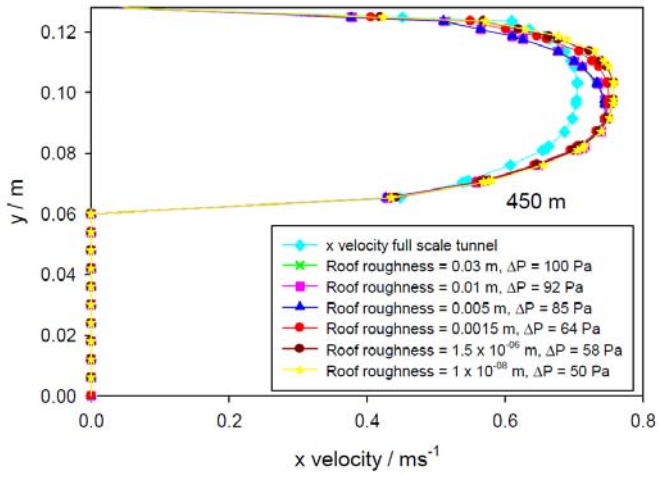

Figure 50 – Axial velocity on symmetry plane, comparison between full and reduced model in correspondence to HGV by changing roughness and pressure drop for traditional jet fans (Table 14)

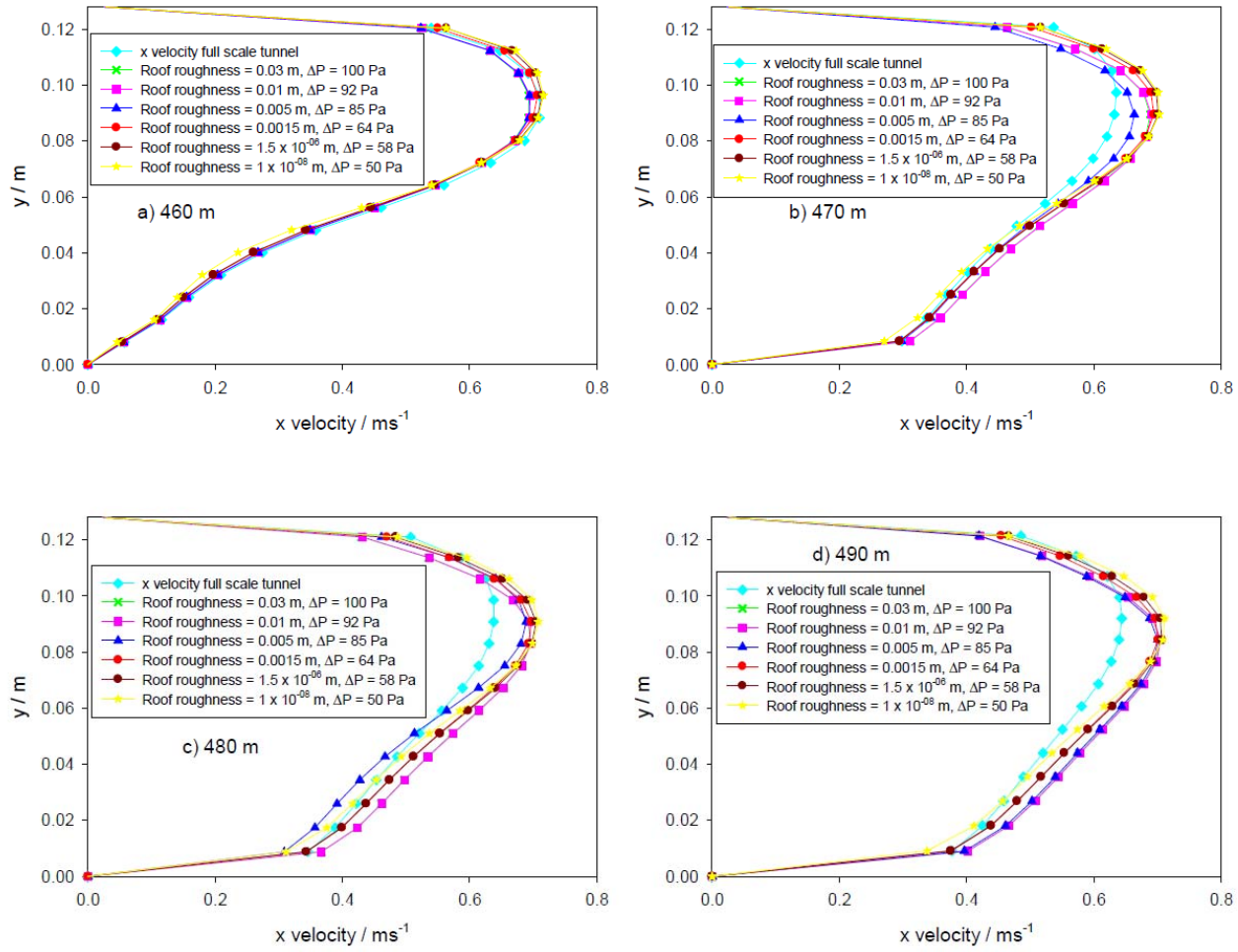

Figure 51 – Axial velocity on symmetry plane, comparison between full and reduced model at (a) 10 m, (b) 20 m, (c) 30 m and (d) 40 m after the HGV by changing roughness and pressure drop for traditional jet fans (Table 14)

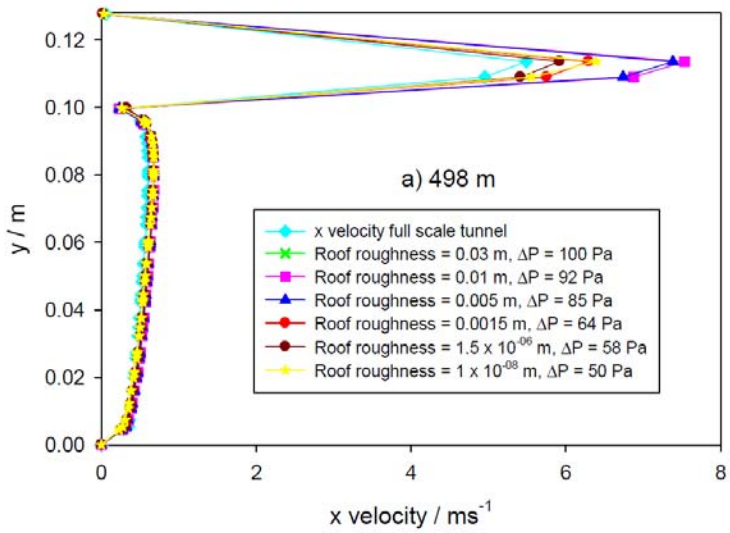

Figure 52 – Axial velocity on symmetry plane, comparison between full and reduced model at 3rd jet fan inlet by changing roughness and pressure drop for traditional jet fans (Table 14)

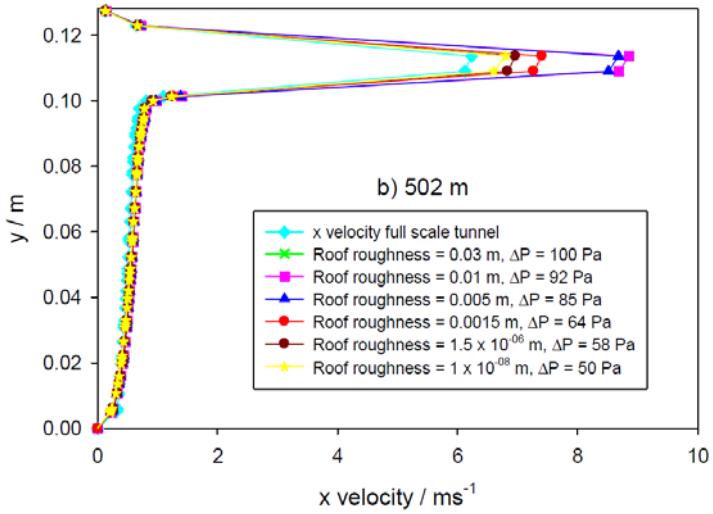

Figure 53 – Axial velocity on symmetry plane, comparison between full and reduced model at 3rd jet fan outlet by changing roughness and pressure drop for traditional jet fans (Table 14)

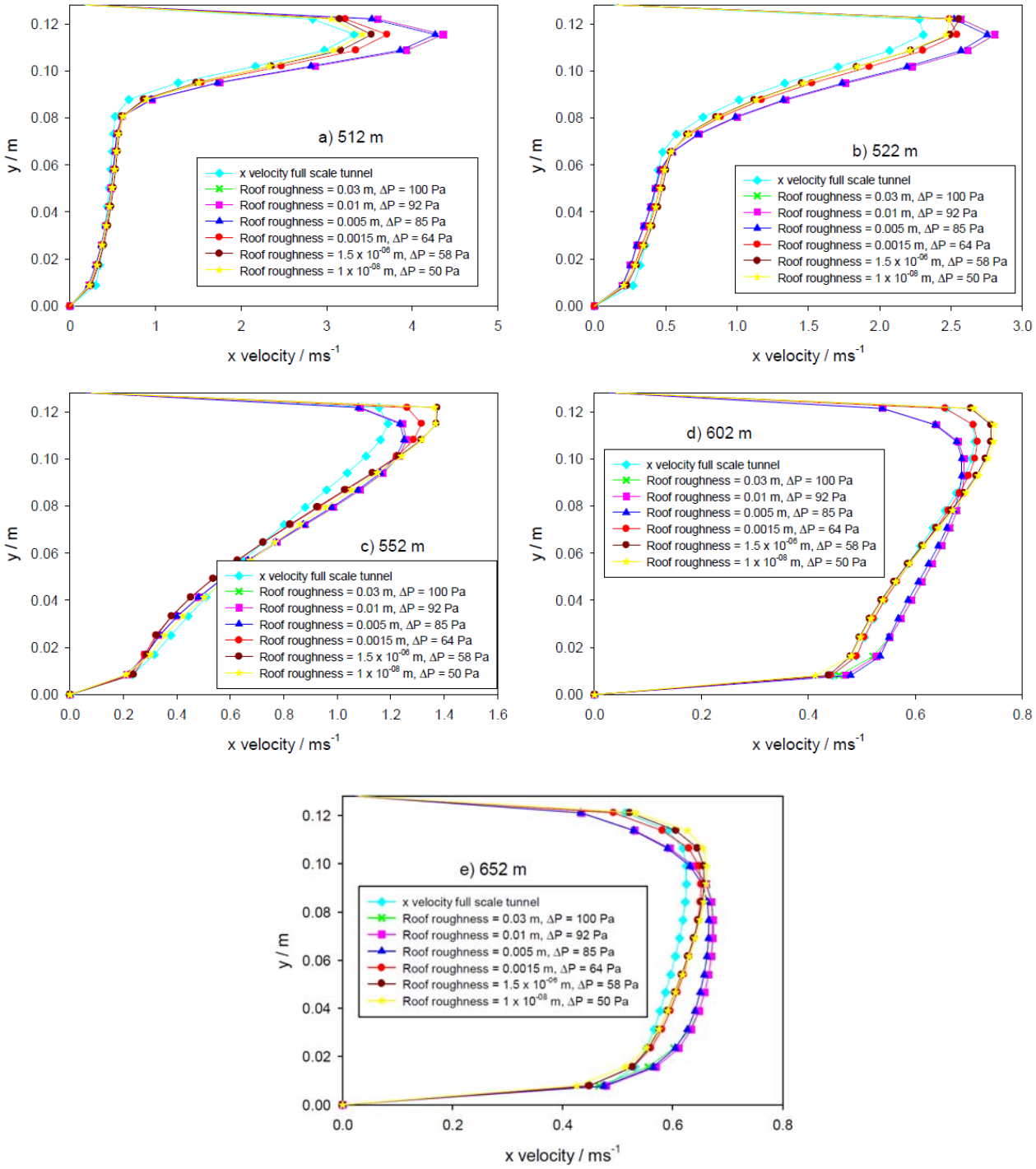

Figure 54 – Axial velocity on symmetry plane, comparison between full and reduced model at (a) 10 m, (b) 20 m, (c) 50 m, (d) 100 m and (e) 150 m after the HGV by changing roughness and pressure drop for traditional jet fans (Table 14)

Results for alternative jet fans are shown in following figures.

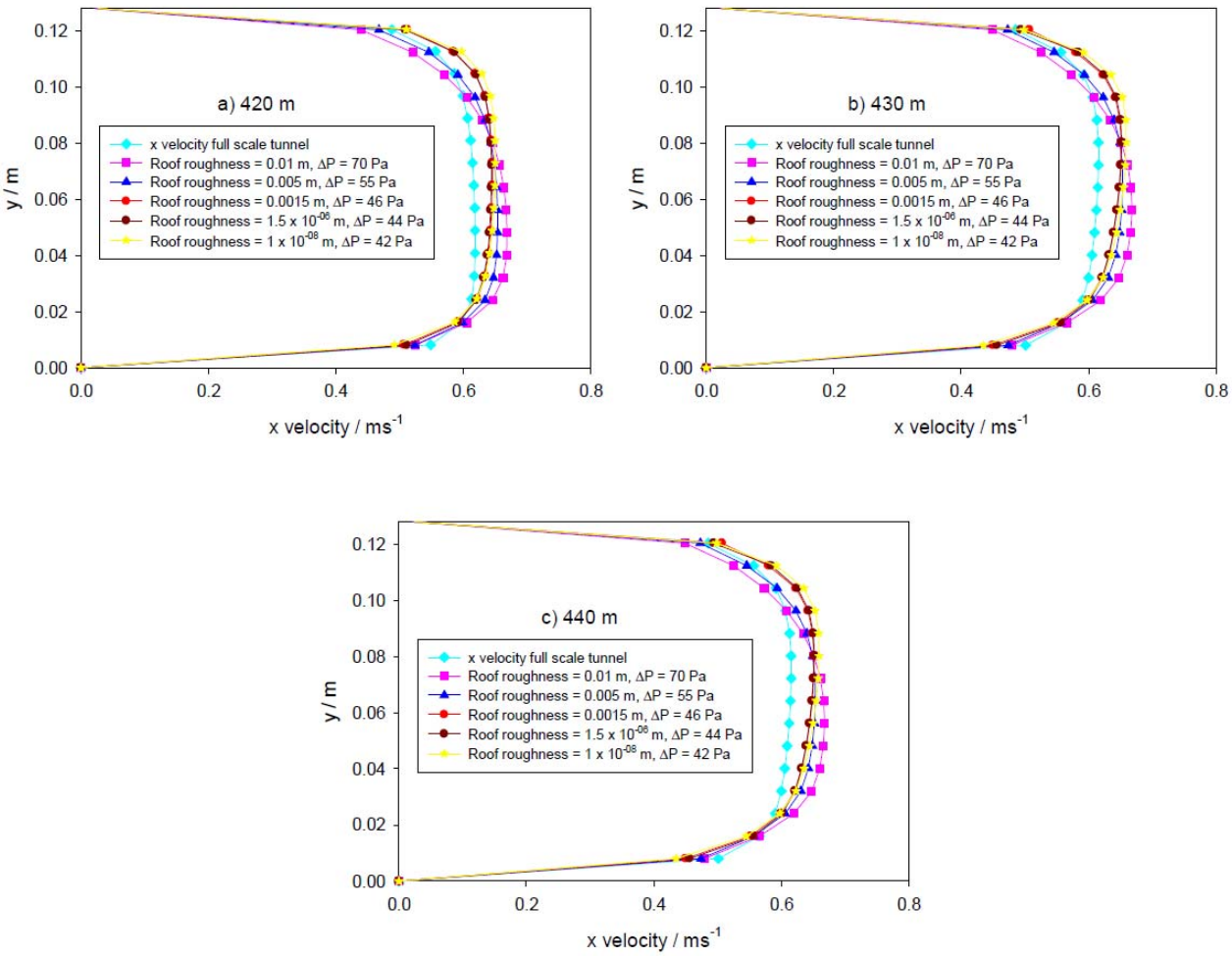

Figure 55 – Axial velocity on symmetry plane, comparison between full and reduced model at (a) 10 m, (b) 20 m and (c) 30 m before the HGV by changing roughness and pressure drop for alternative jet fans (Table 15)

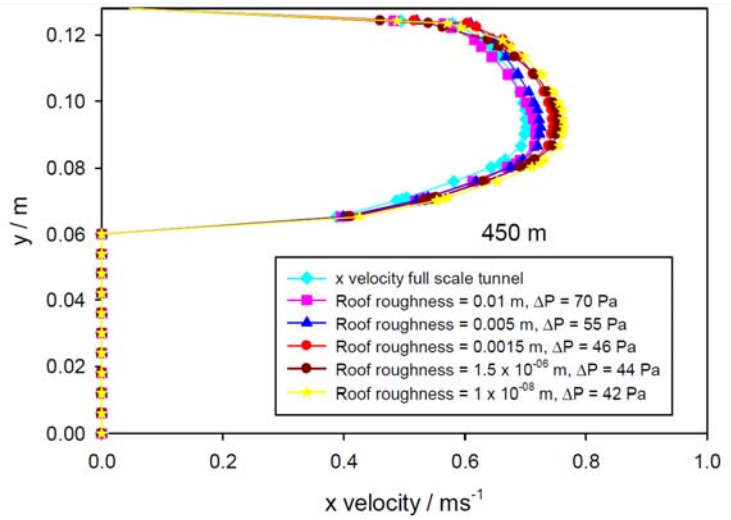

Figure 56 – Axial velocity on symmetry plane, comparison between full and reduced model in correspondence to HGV by changing roughness and pressure drop for alternative jet fan (Table 15)

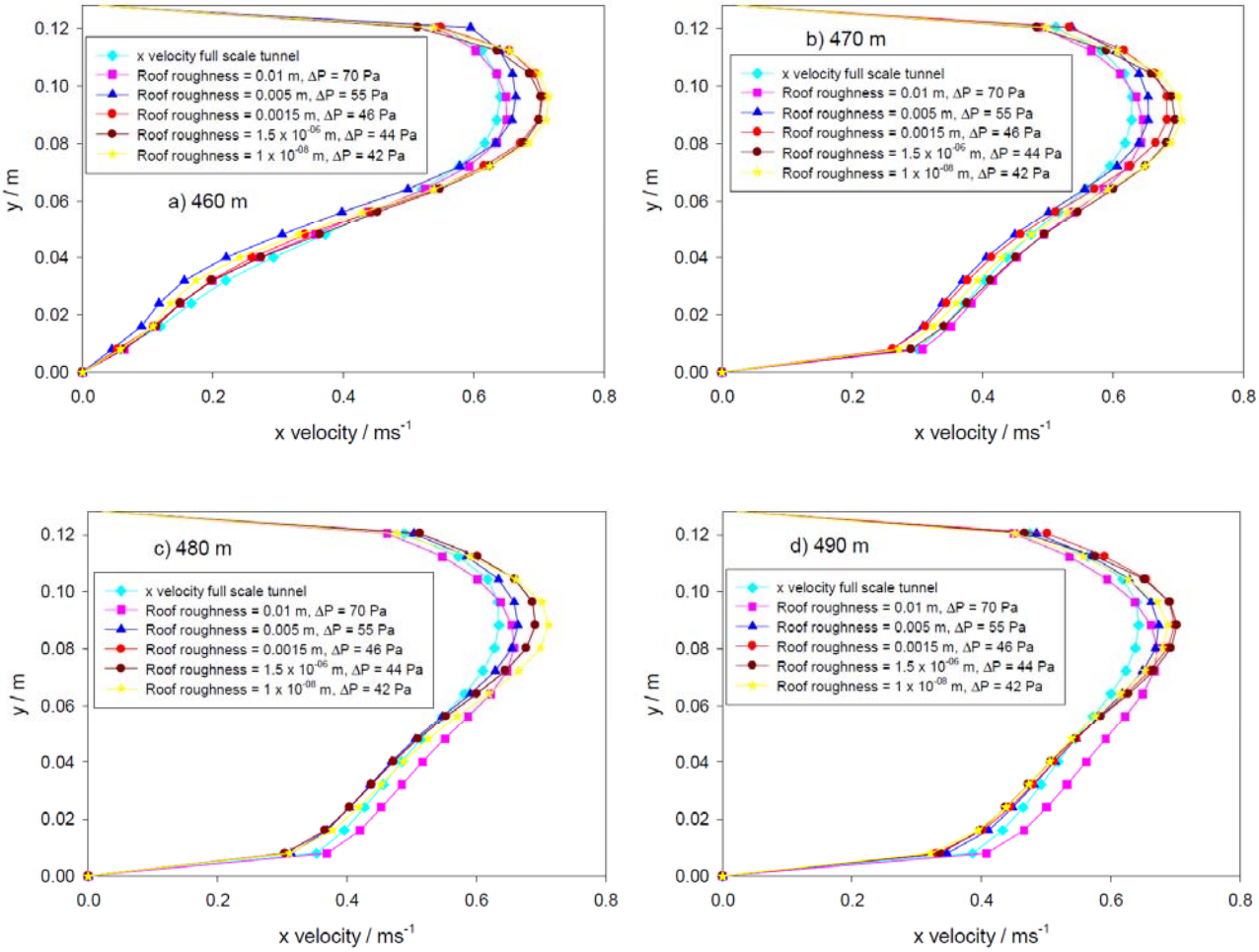

Figure 57 – Axial velocity on symmetry plane, comparison between full and reduced model at (a) 10 m, (b) 20 m, (c) 30 m and (d) 40 m after the HGV by changing roughness and pressure drop for alternative jet fan (Table 15)

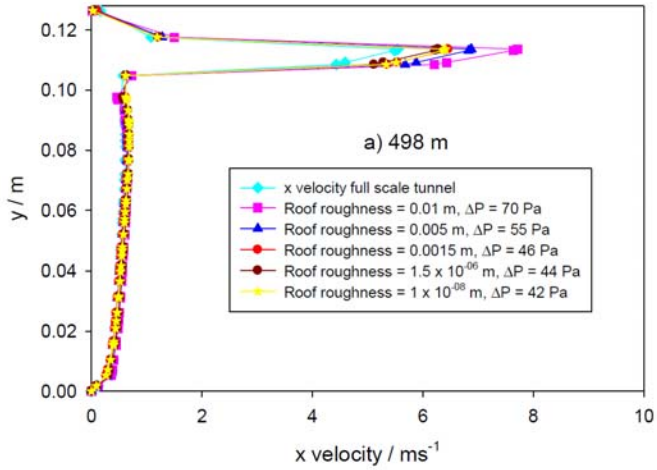

Figure 58 – Axial velocity on symmetry plane, comparison between full and reduced model at 3rd jet fan inlet by changing roughness and pressure drop for alternative jet fans (Table 15)

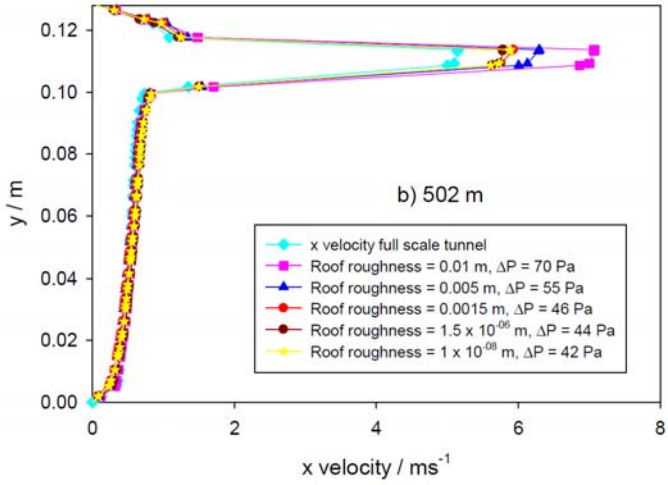

Figure 59 – Axial velocity on symmetry plane, comparison between full and reduced model at 3rd jet fan outlet by changing roughness and pressure drop for alternative jet fans (Table 15)

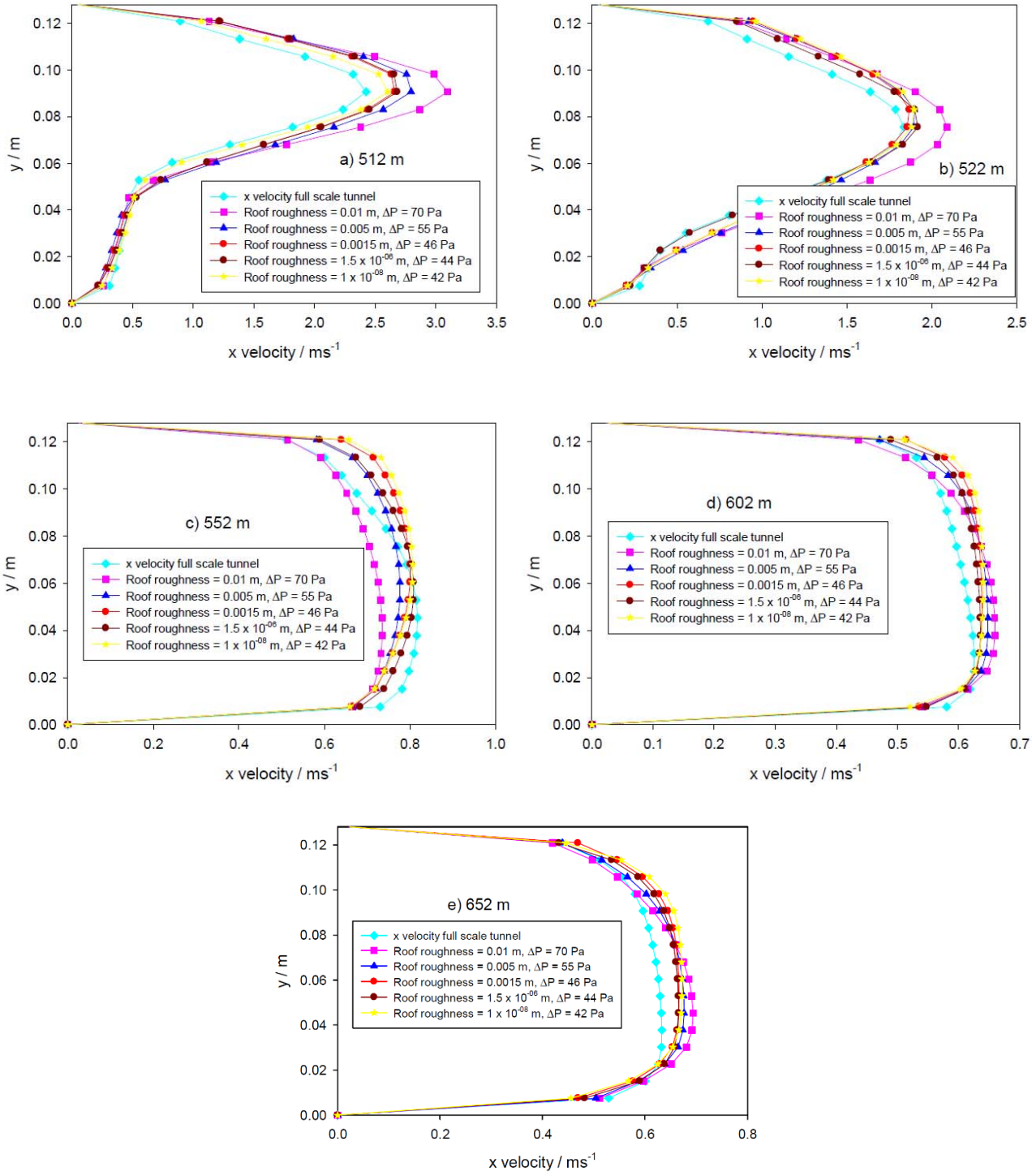

Figure 60 – Axial velocity on symmetry plane, comparison between full and reduced model at (a) 10 m, (b) 20 m, (c) 50 m, (d) 100 m and (e) 150 m after the HGV by changing roughness and pressure drop for alternative jet fans (Table 15)

As results, pressure drop values defined before require very low values for wall roughness to preserve kinematic similitude. In consideration of technical limits to reach a reasonable value of roughness, plexiglass ($1.5 \cdot 10^{-6}$ m) can be considered suitable to realize tunnel

walls for a scaled model. Thus, values of pressure drop are increased till to 50 Pa and 40 Pa for traditional and alternative jet fan respectively. Moreover, results show that velocity profiles related to 10^{-8} m of roughness for a scaled model are close to those of full scale tunnel with both traditional and alternative jet fan.

7.1.1.1. Results

Several x-velocity profiles and turbulent intensity fields on tunnel symmetry plane for both full and reduced scale models are shown. Full scale velocity profiles are scaled according to equation (21) to highlight differences with numerical results for scaled model (Figure 61 to Figure 70).

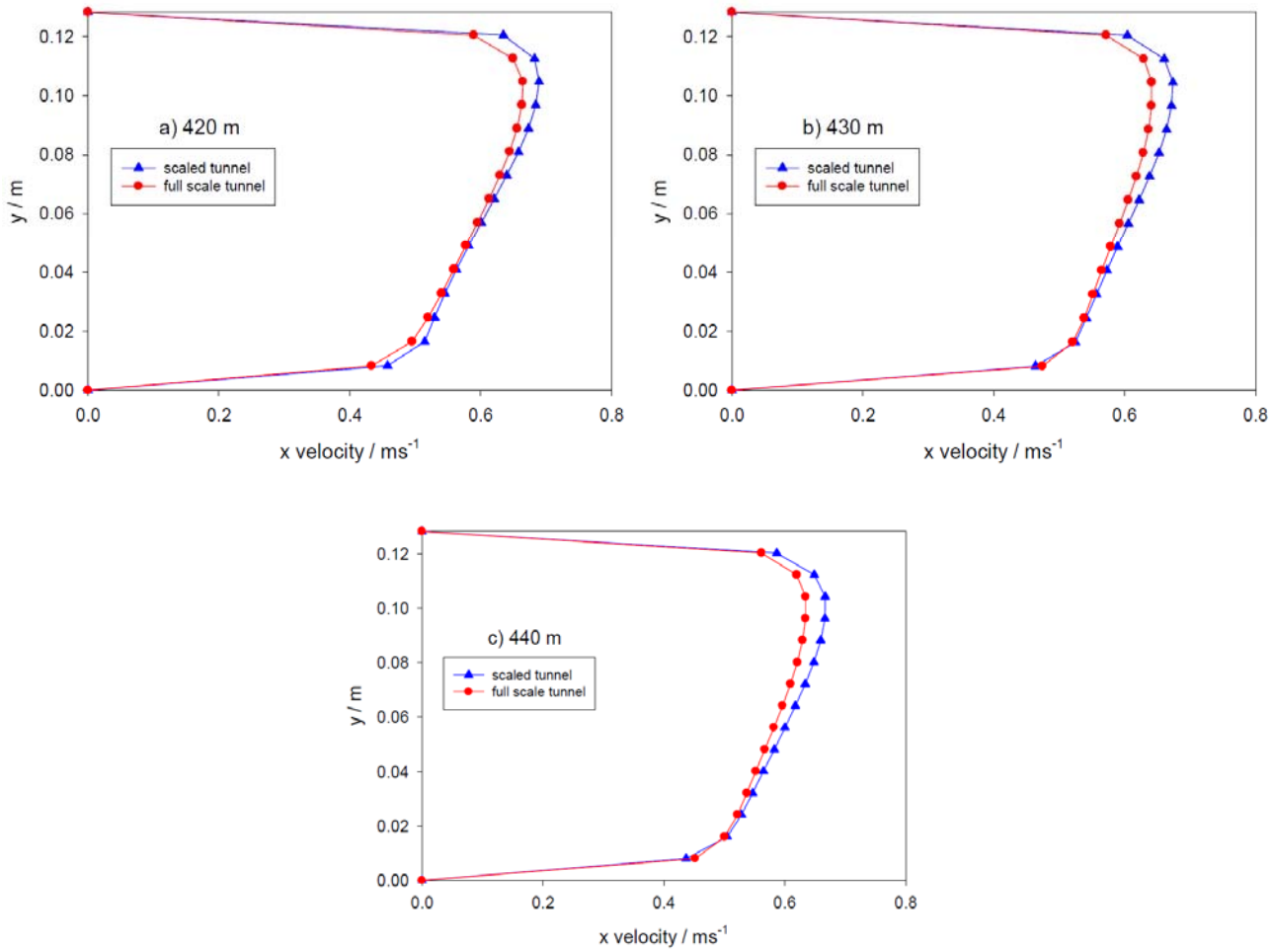

Figure 61 – Axial velocity on symmetry plane, comparison between full and reduced model at (a) 10 m, (b) 20 m and (c) 30 m before the HGV for traditional jet fans

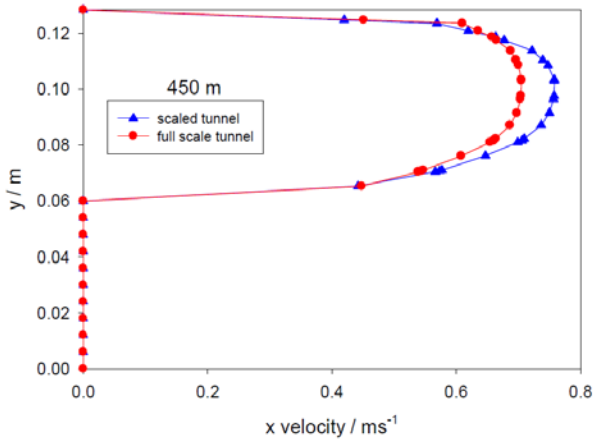

Figure 62 – Axial velocity on symmetry plane, comparison between full and reduced model in correspondence of HGV for traditional jet fans

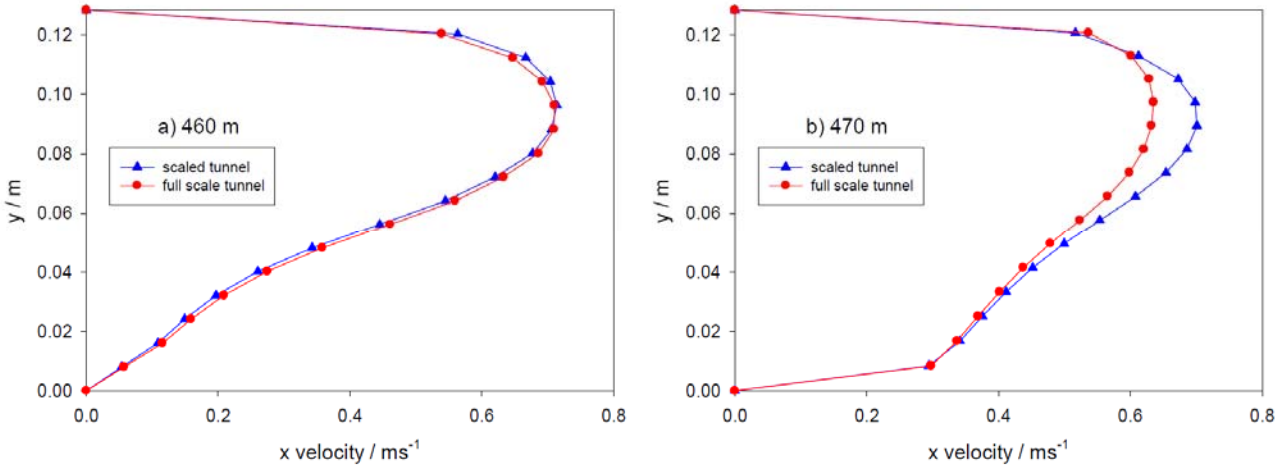

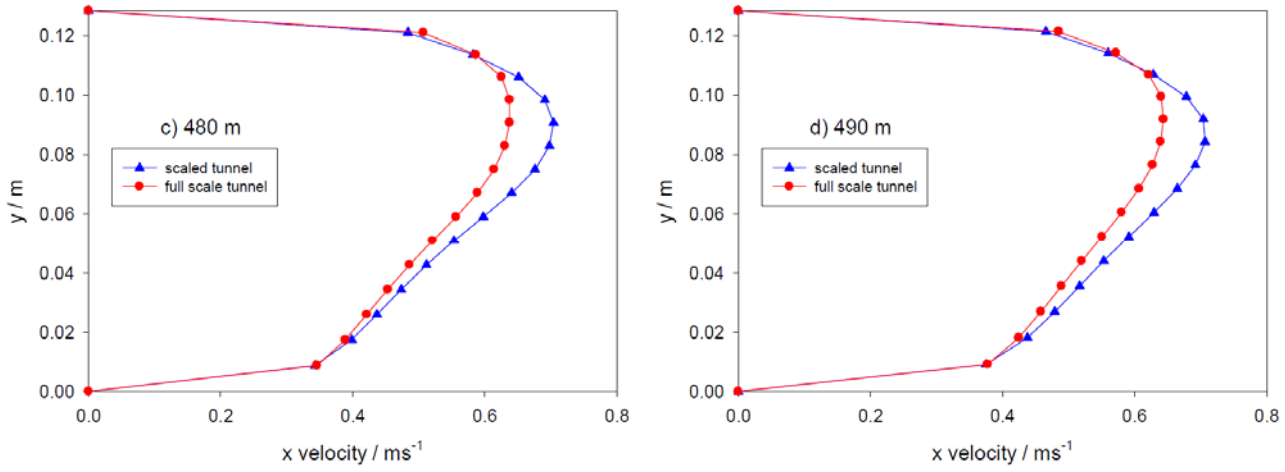

Figure 63 – Axial velocity on symmetry plane, comparison between full and reduced model at (a) 10 m, (b) 20 m, (c) 30 m and (d) 40 m after the HGV for traditional jet fans

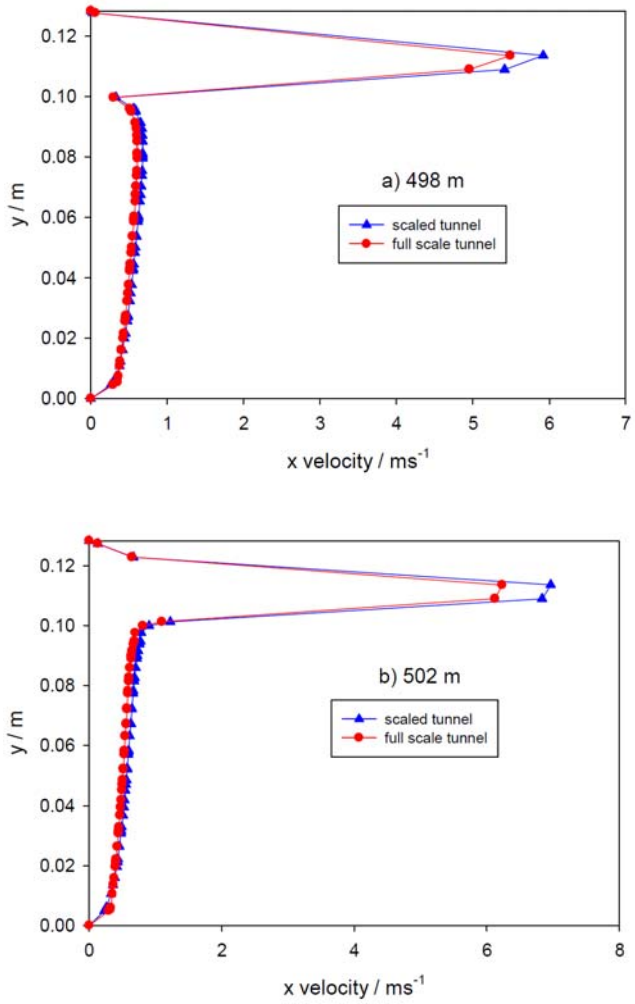

Figure 64 – Axial velocity on symmetry plane, comparison between full and reduced model at 3rd jet fan inlet (a) and outlet (b) for traditional jet fans

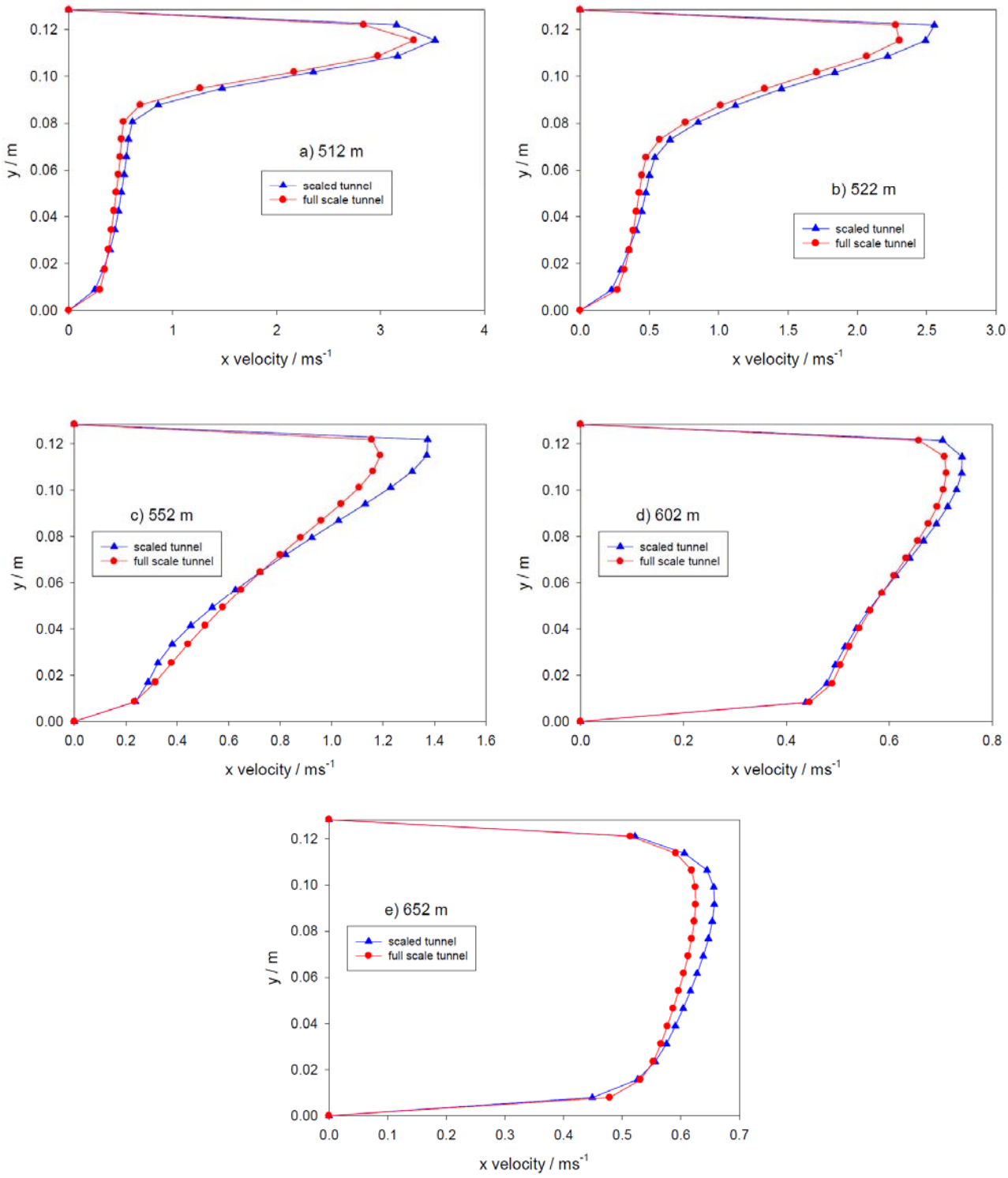

Figure 65 – Axial velocity on symmetry plane, comparison between full and reduced model at (a) 10 m, (b) 20 m, (c) 50 m, (d) 100 m and (e) 150 m after the HGV for traditional jet fans

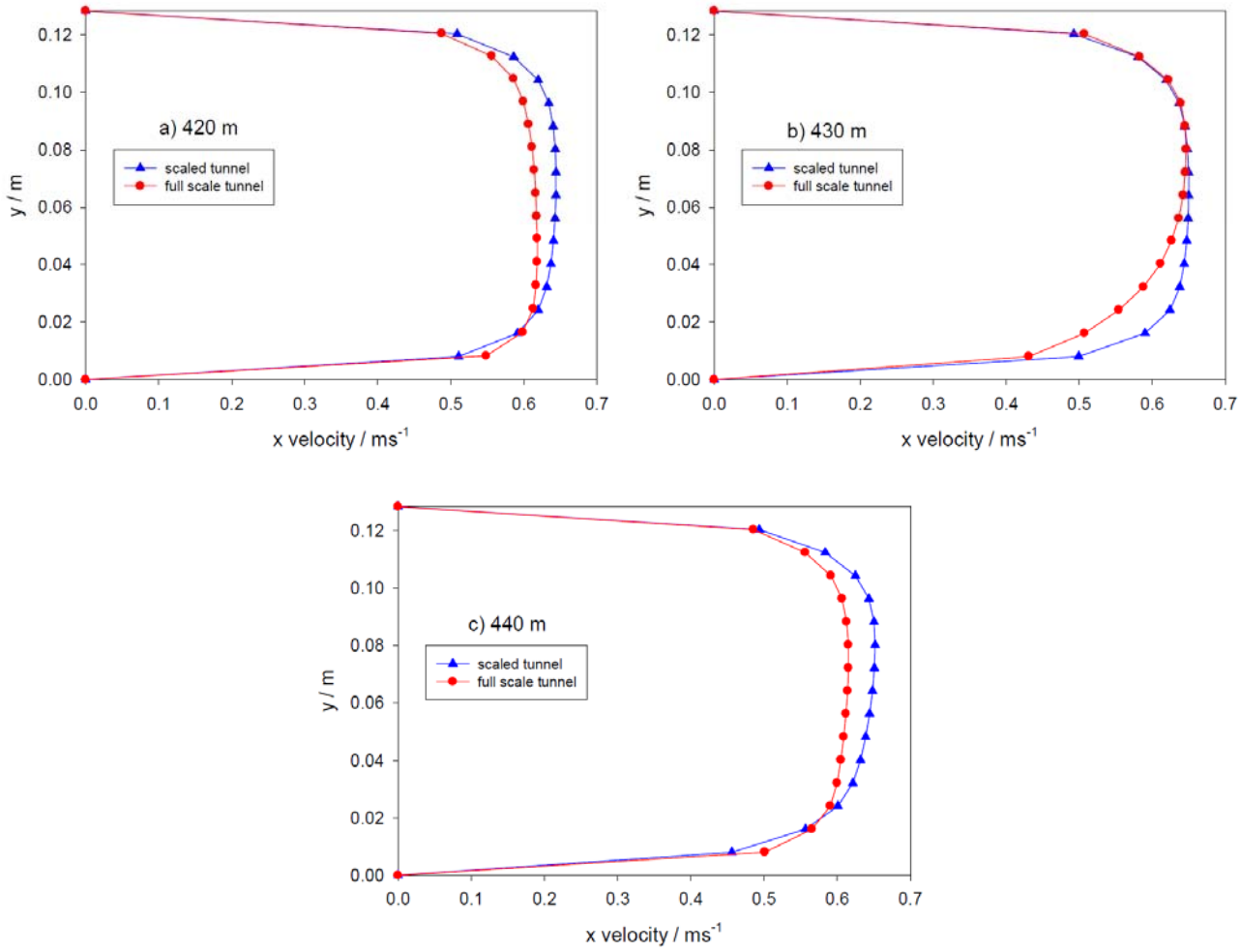

Figure 66 – Axial velocity on symmetry plane, comparison between full and reduced model at (a) 10 m, (b) 20 m and (c) 30 m before the HGV for alternative jet fans

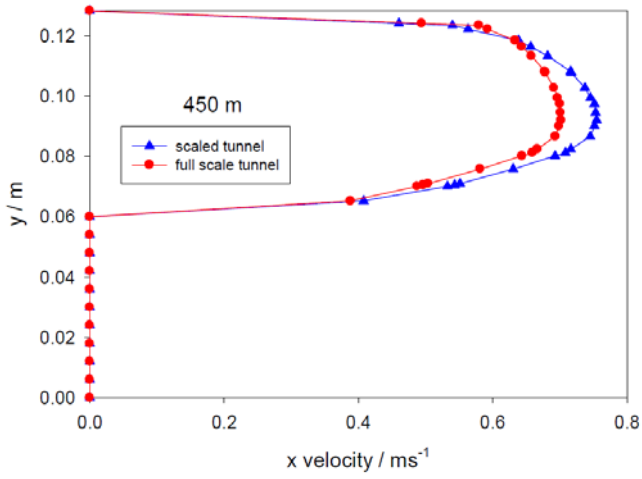

Figure 67 – Axial velocity on symmetry plane, comparison between full and reduced model in correspondence of HGV for alternative jet fans

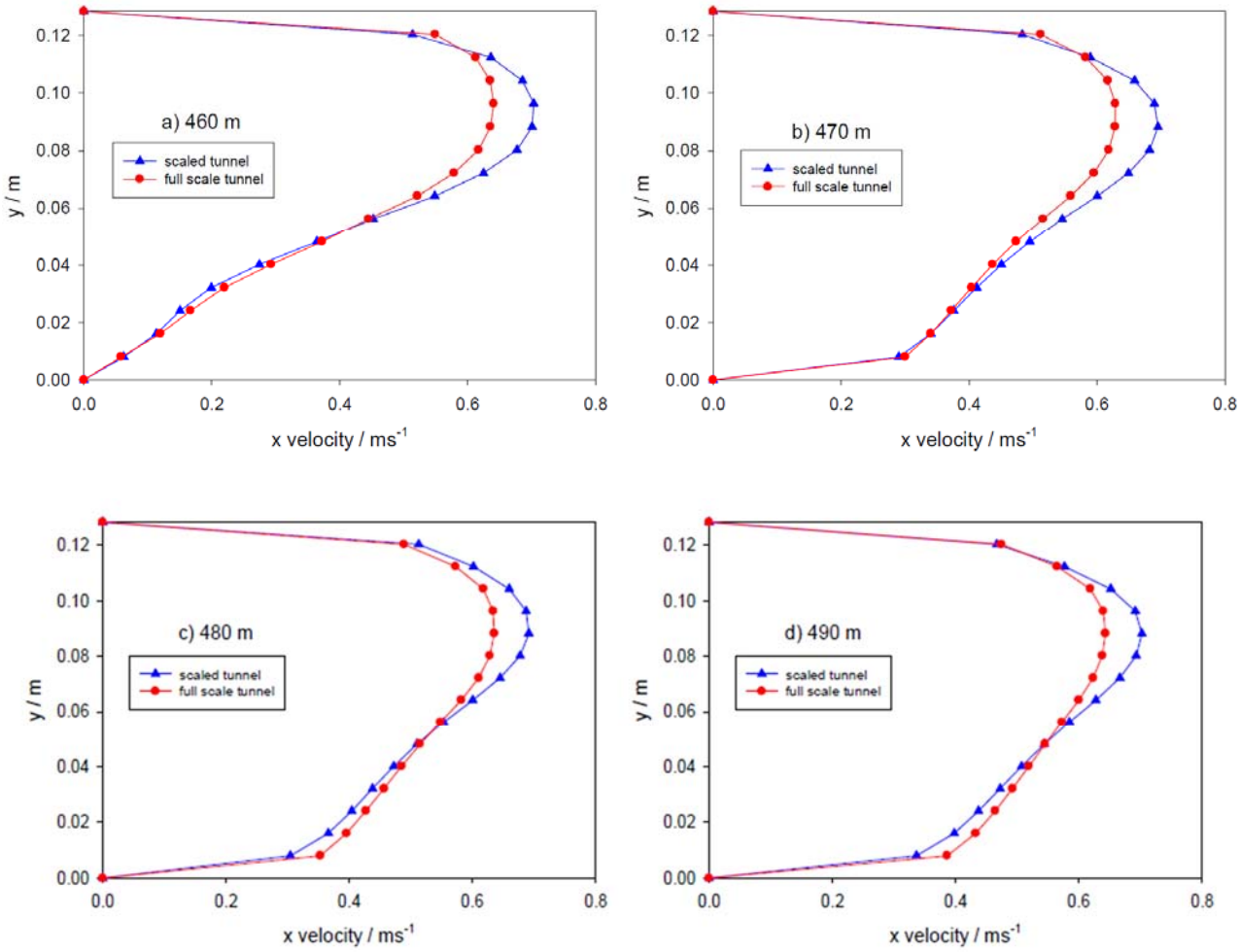

Figure 68 – Axial velocity on symmetry plane, comparison between full and reduced model at (a) 10 m, (b) 20 m, (c) 30 m and (d) 40 m after the HGV for alternative jet fans

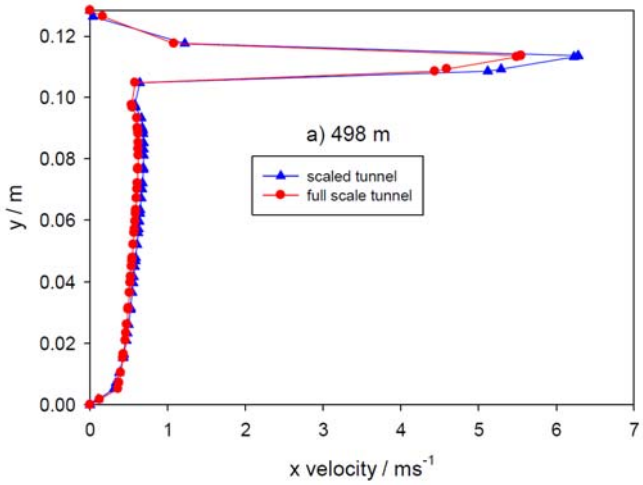

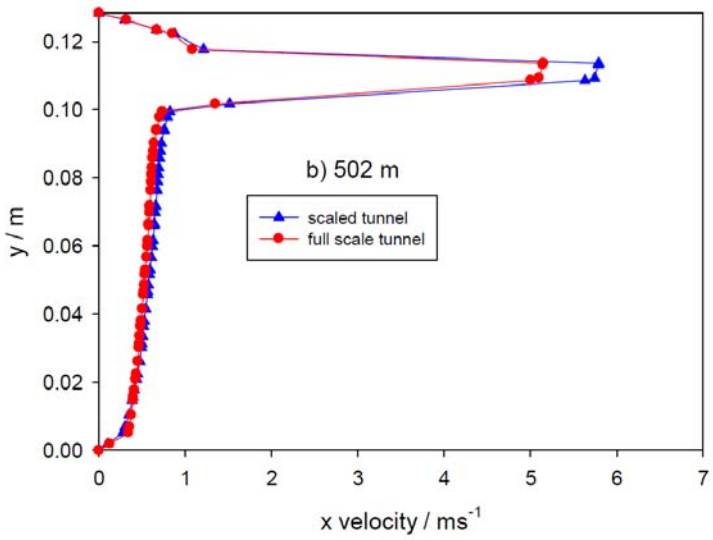

Figure 69 – Axial velocity on symmetry plane, comparison between full and reduced model at 3rd jet fan inlet (a) and outlet (b) for alternative jet fans

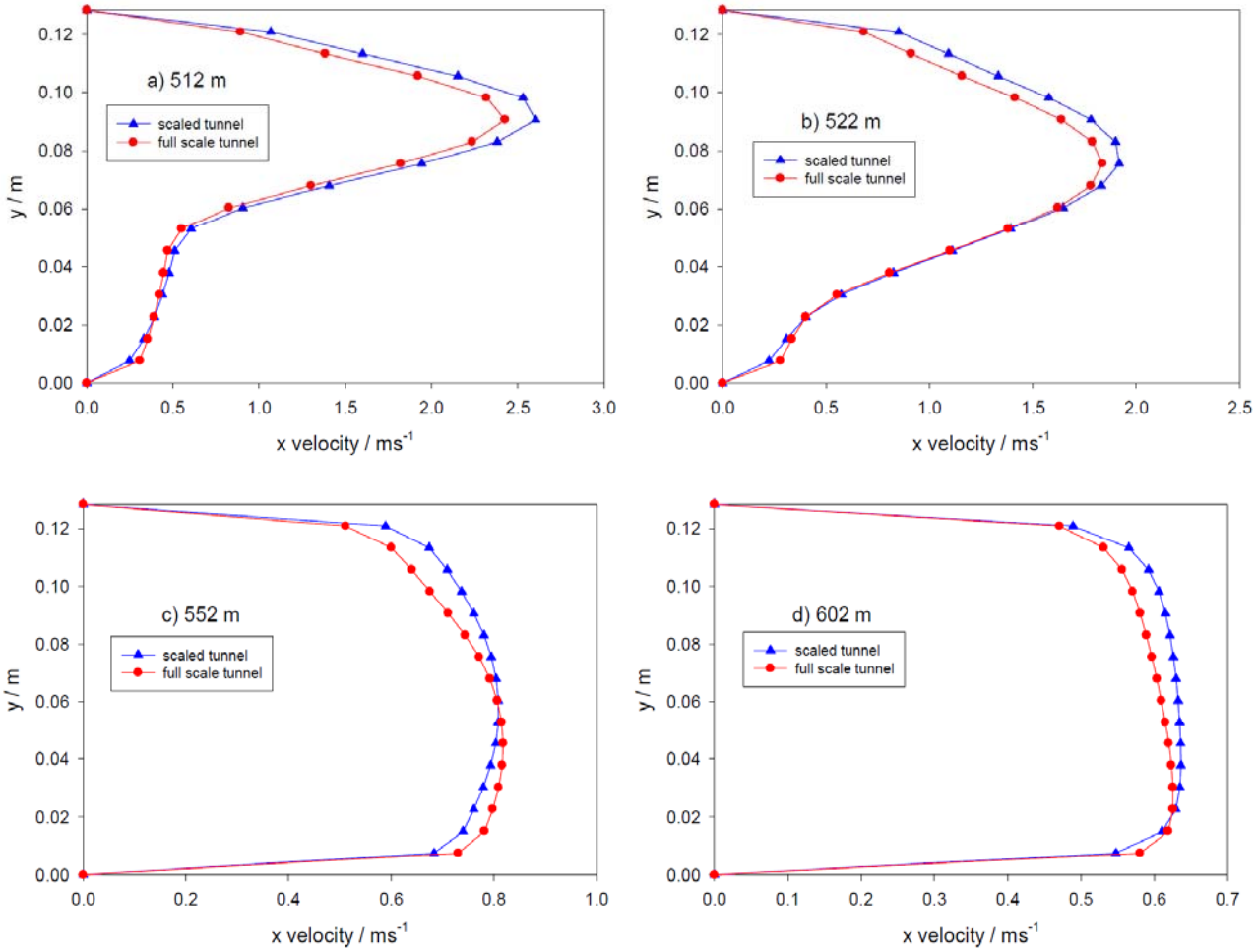

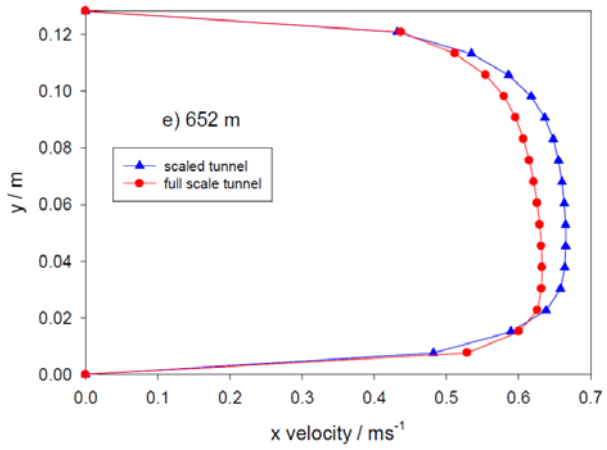

Figure 70 – Axial velocity on symmetry plane, comparison between full and reduced model at (a) 10 m, (b) 20 m, (c) 50 m, (d) 100 m and (e) 150 m after the HGV for alternative jet fans

Although high velocity gradients occur due to HVG presence, Figure 61a shows that velocity profiles are similar between full and reduced scale model for both traditional and alternative jet fans. In particular, Figure 61 (upstream the HVG) show how the gradient impacts on velocity profile. On the other hand, results shown relevant differences for x-velocity profile in correspondence of HGV in scaled model between alternative and traditional jet fan configuration.

Close to outlet section of jet fan, x-velocity for scaled model appears greater than full model one because of the pressure drop greater than Froude's one. Averages errors increase up to 10.8% and 8.8% for traditional and alternatives configuration respectively. Far from these sections, these decrease up to 0.4% and 4.8% respectively.

Following table shows errors (e%) between full and reduced scale model for x-velocity: far to disturbances error range results 1.9 ÷ 5.1 % for traditional jet fan configuration and 3.9 ÷ 5.6 % for alternative one.

$$e\% = \frac{1}{N}\sum \left| \frac{v_{x-scaled,N} - v_{x-full,N}}{v_{x-full,N}} \right|$$

where N in the number of cells on y-axis.

Axial distance (m)	Average axial vekocity error (%)	
	Traditional ventilation system	Alternative ventilation system
420	2.5	3.8
430	2.6	4.1
440	3.2	3.9
450	5.7	6.0
460	3.1	6.0
470	4.8	4.7
480	5.2	5.0
490	5.2	4.8
498	9.8	9.8
502	10.8	9.3
512	10.0	8.4
522	8.7	7.3
552	7.9	7.5
602	2.1	5.0
652	3.0	7.8

Differences in velocity profiles between full and reduced model are mainly due to different turbulent intensity fields (lower in reduced scale model); this is related to impossibility in Reynolds number preservation (see figures).

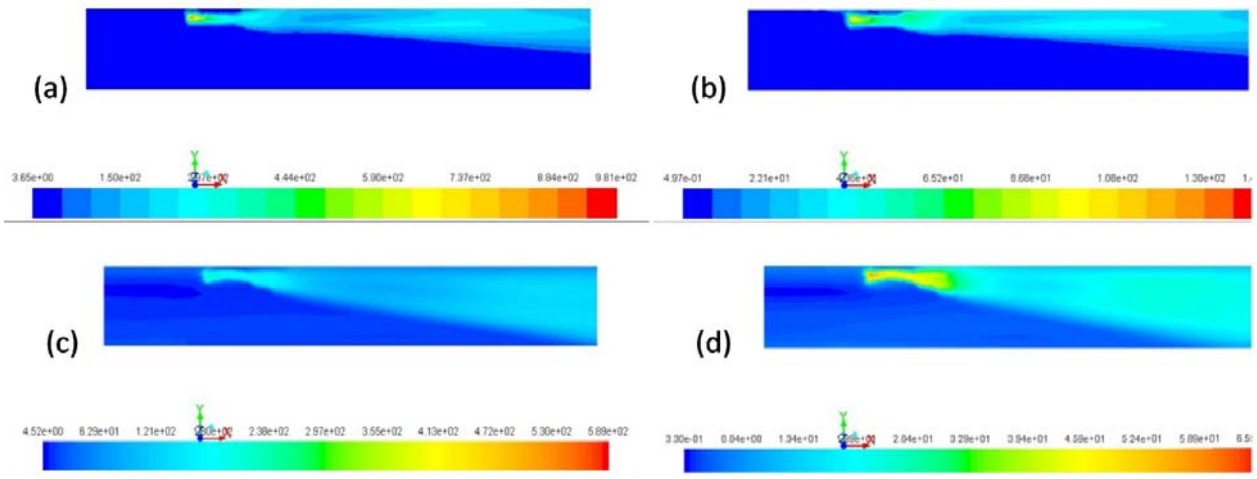

Figure 71 - Turbulent intensity profile on symmetry plane (z=0) for different x-position downstream jet fan: comparison between full and scaled model for fixed roughness value for traditional (a, and b) and alternative (c and d) jet fan.

Turbulent intensity field is lower in the reduced scale with respect to the full-scale model (one order of magnitude), but they present similar behaviors.

In order to verify that the similitude is preserved in the whole domain, the velocity fields along several tunnel cross sections at different axial distance values are analyzed (Figure

72 to Figure 83) both in the tunnel equipped with traditional fans and in the tunnel with alternative fans (Figure 84 to Figure 93).

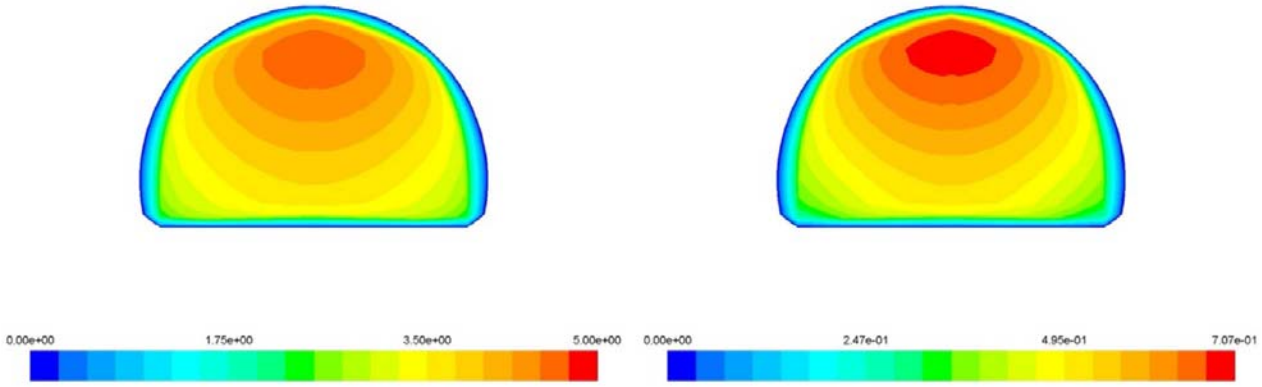

Figure 72 – Axial velocity profile on tunnel cross section @ 420 m: comparison between full (left) and scaled tunnel (right) – traditional jet fans

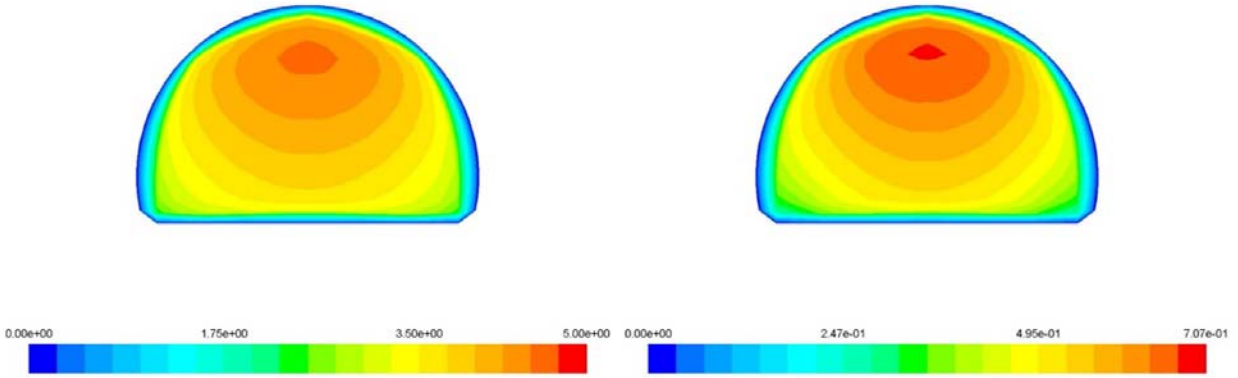

Figure 73 – Axial velocity profile on tunnel cross section @ 430 m: comparison between full (left) and scaled tunnel (right) – traditional jet fans

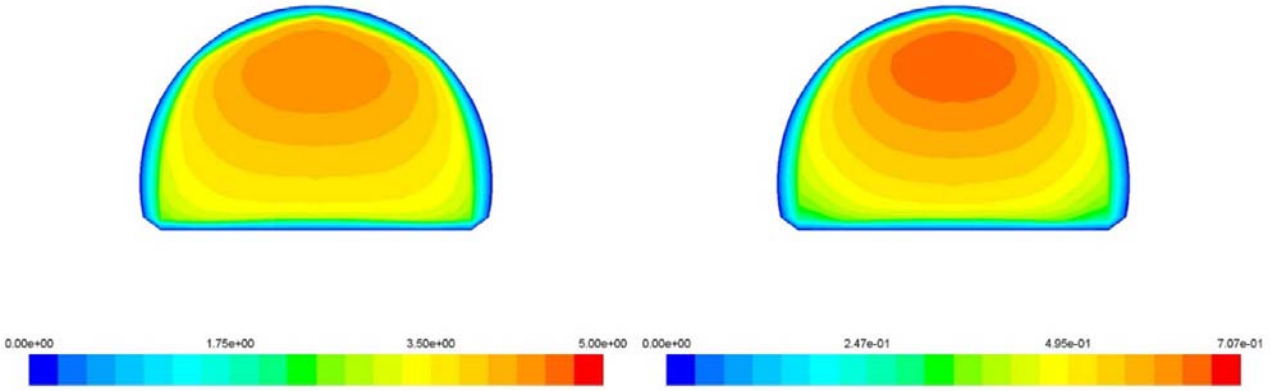

Figure 74 – Axial velocity profile on tunnel cross section @ 440 m: comparison between full (left) and scaled tunnel (right) – traditional jet fans

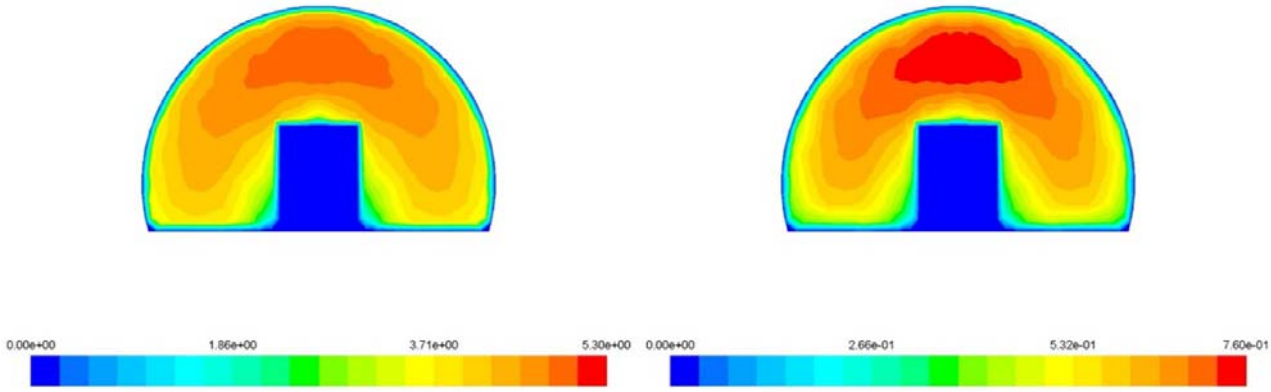

Figure 75 – Axial velocity profile on tunnel cross section @ 450 m: comparison between full (left) and scaled tunnel (right) – traditional jet fans

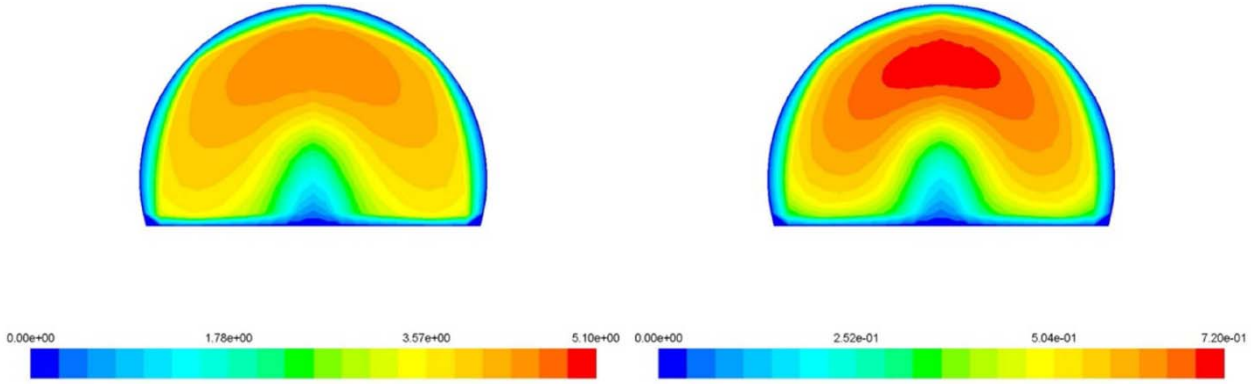

Figure 76 – Axial velocity profile on tunnel cross section @ 460 m: comparison between full (left) and scaled tunnel (right) – traditional jet fans

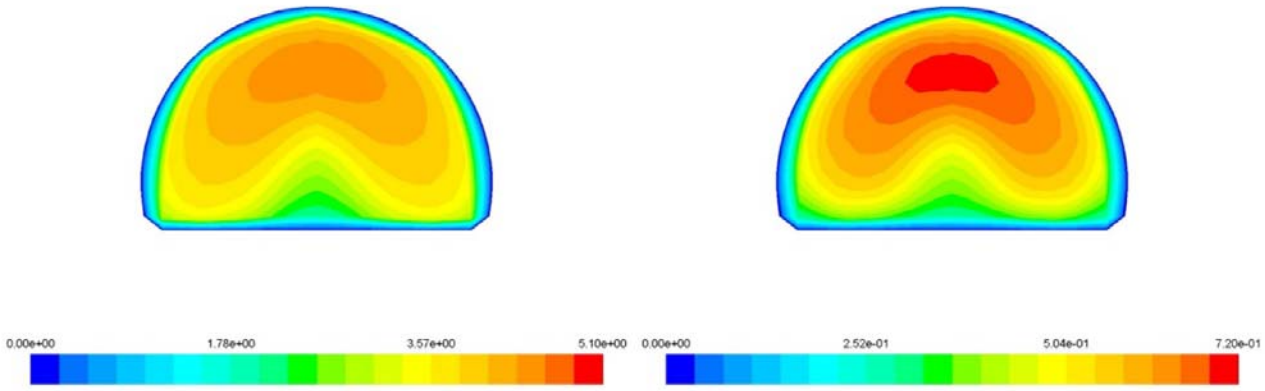

Figure 77 – Axial velocity profile on tunnel cross section @ 470 m: comparison between full (left) and scaled tunnel (right) – traditional jet fans

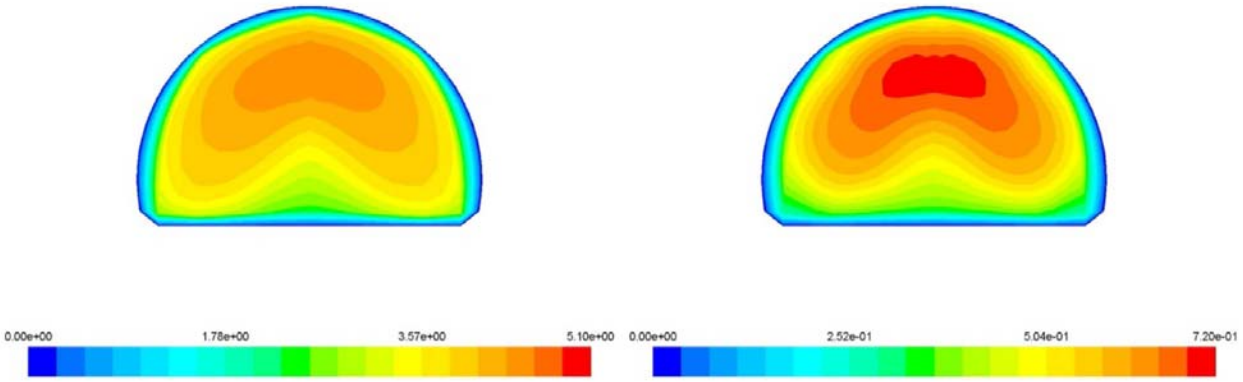

Figure 78 – Axial velocity profile on tunnel cross section @ 480 m: comparison between full (left) and scaled tunnel (right) – traditional jet fans

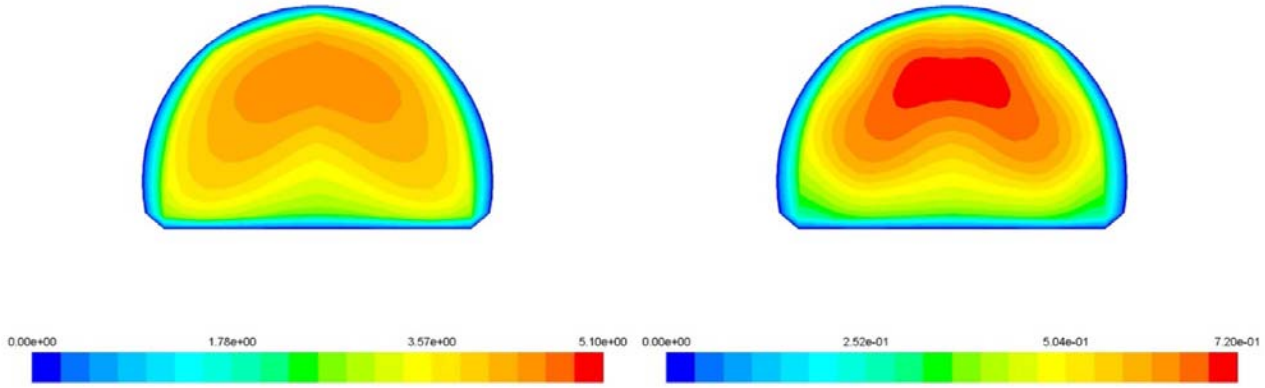

Figure 79 – Axial velocity profile on tunnel cross section @ 490 m: comparison between full (left) and scaled tunnel (right) – traditional jet fans

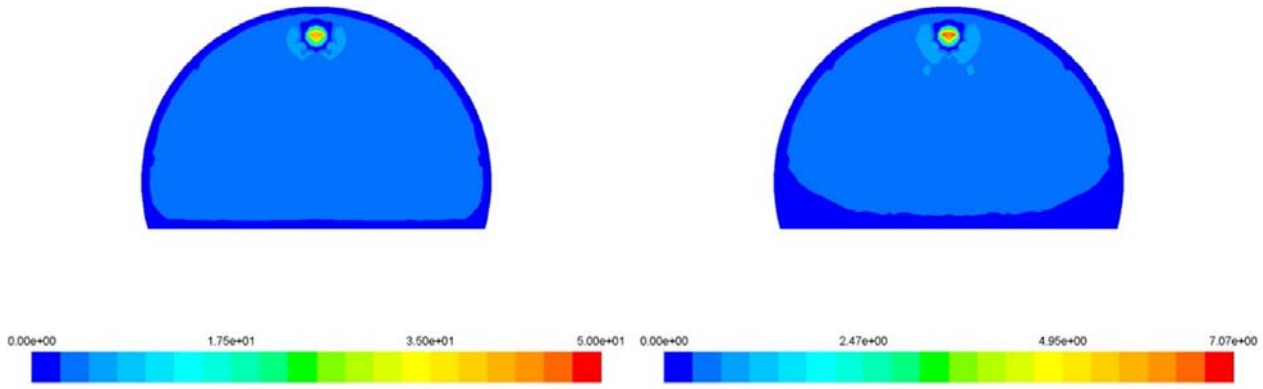

Figure 80 – Axial velocity profile on tunnel cross section @ 498 m: comparison between full (left) and scaled tunnel (right) – traditional jet fans

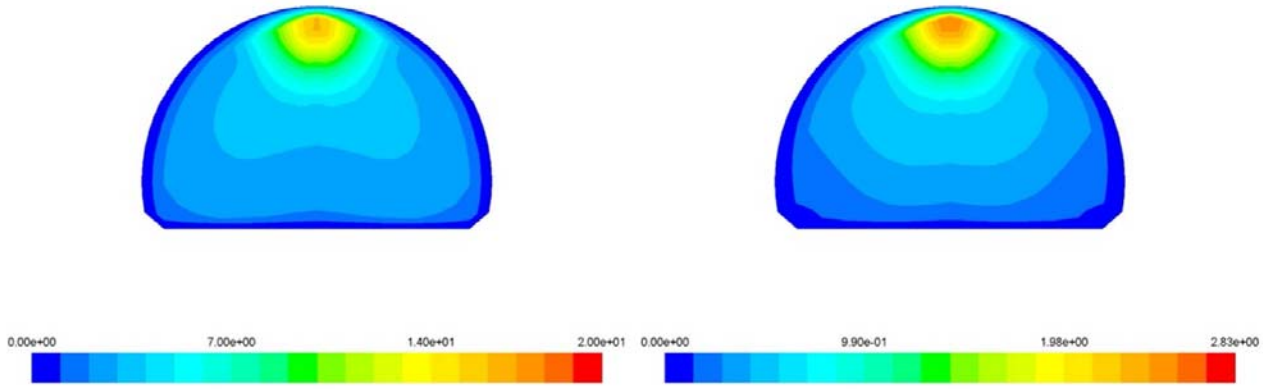

Figure 81 – Axial velocity profile on tunnel cross section @ 522 m: comparison between full (left) and scaled tunnel (right) – traditional jet fans

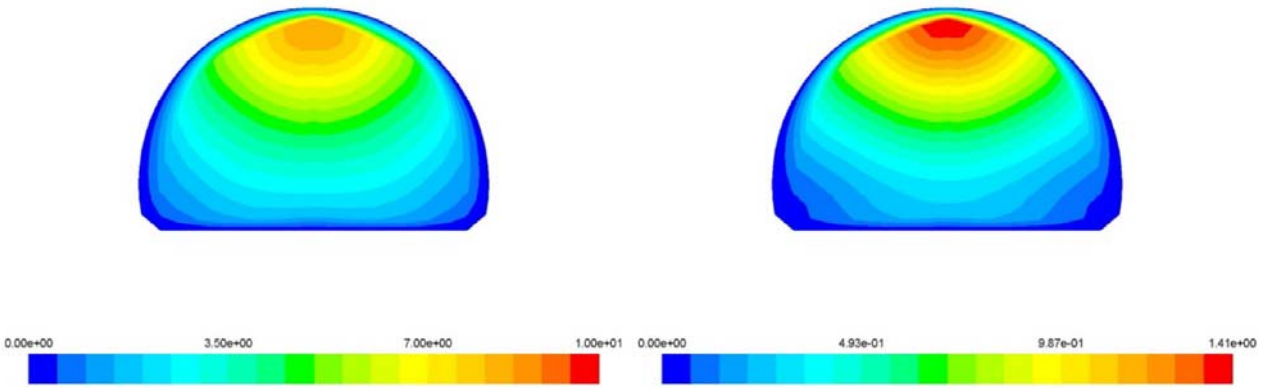

Figure 82 – Axial velocity profile on tunnel cross section @ 552 m: comparison between full (left) and scaled tunnel (right) – traditional jet fans

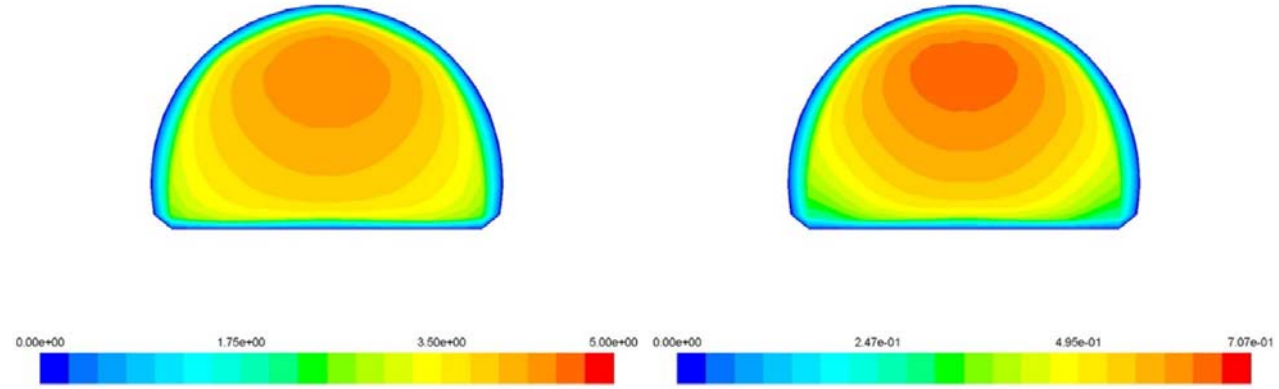

Figure 83 – Axial velocity profile on tunnel cross section @ 652 m: comparison between full (left) and scaled tunnel (right) – traditional jet fans

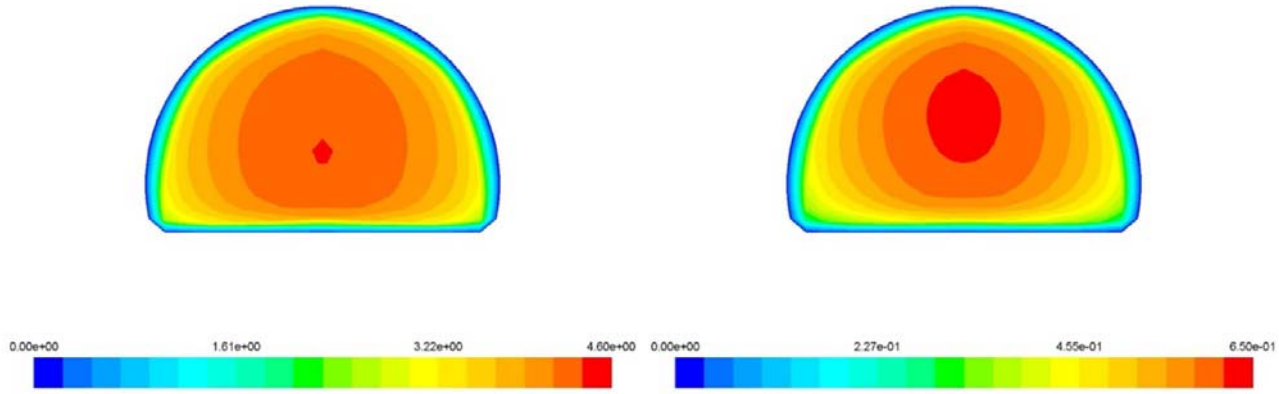

Figure 84 – Axial velocity profile on tunnel cross section @ 420 m: comparison between full (left) and scaled tunnel (right) – alternative jet fans

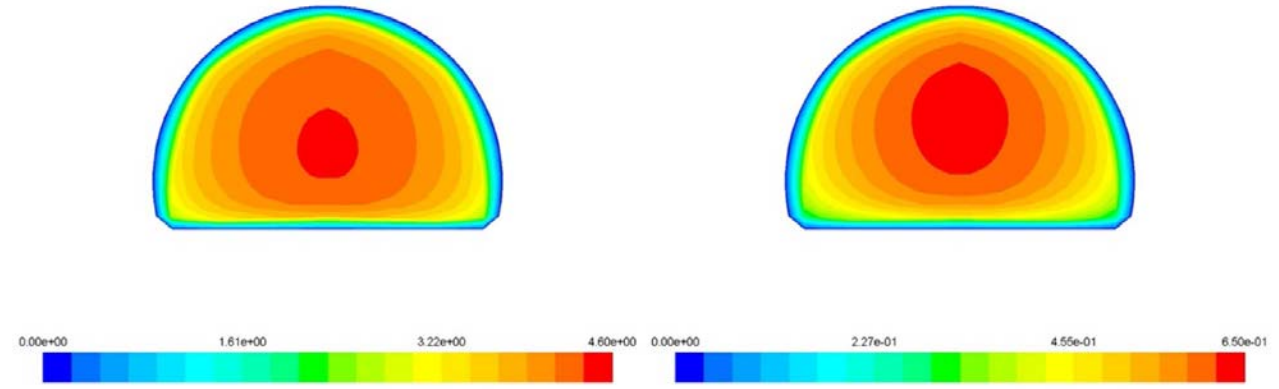

Figure 85 – Axial velocity profile on tunnel cross section @ 430 m: comparison between full (left) and scaled tunnel (right) – alternative jet fans

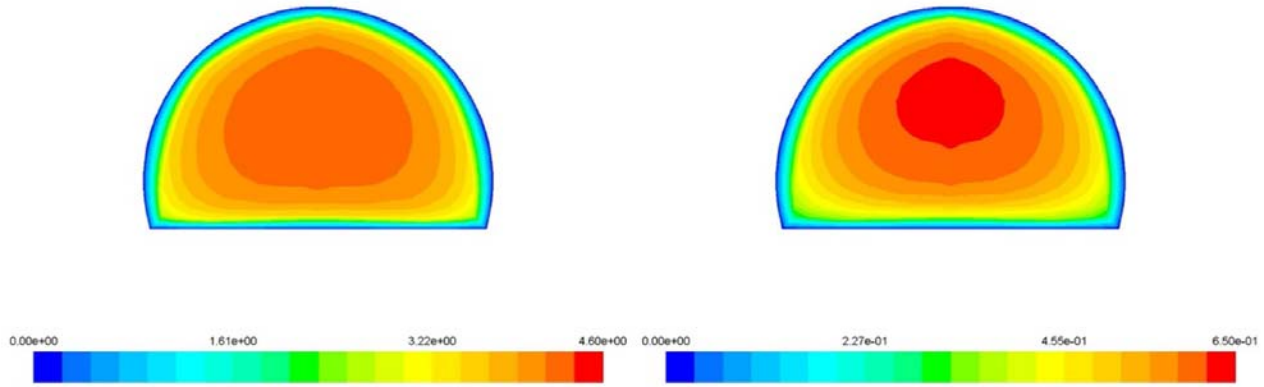

Figure 86 – Axial velocity profile on tunnel cross section @ 440 m: comparison between full (left) and scaled tunnel (right) – alternative jet fans

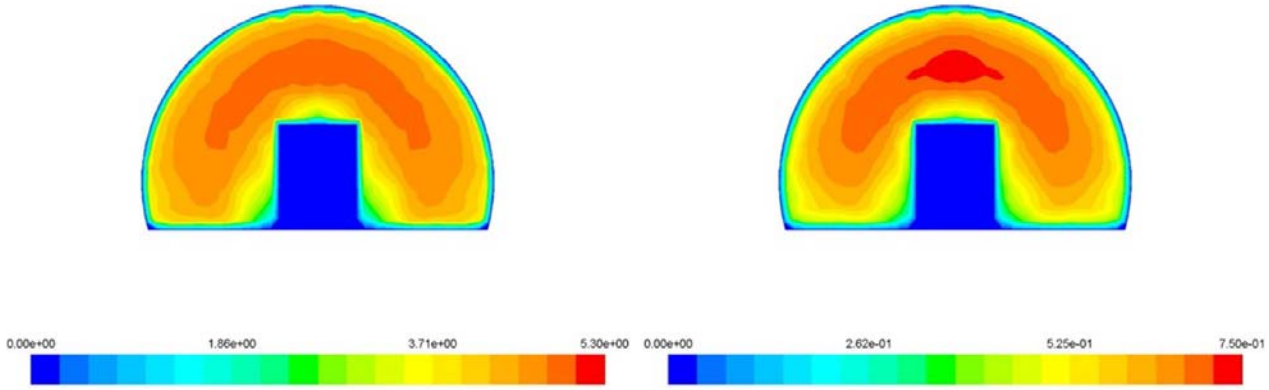

Figure 87 – Axial velocity profile on tunnel cross section @ 450 m: comparison between full (left) and scaled tunnel (right) – alternative jet fans

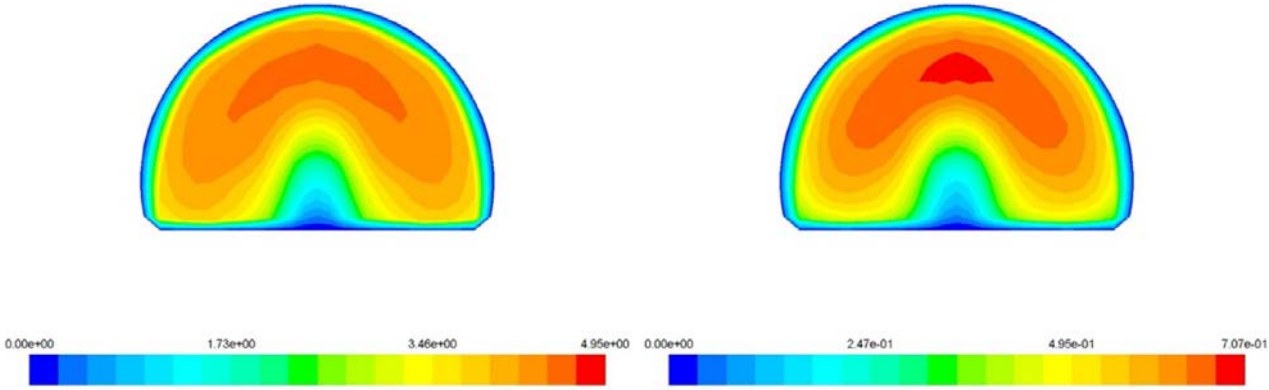

Figure 88 – Axial velocity profile on tunnel cross section @ 460 m: comparison between full (left) and scaled tunnel (right) – alternative jet fans

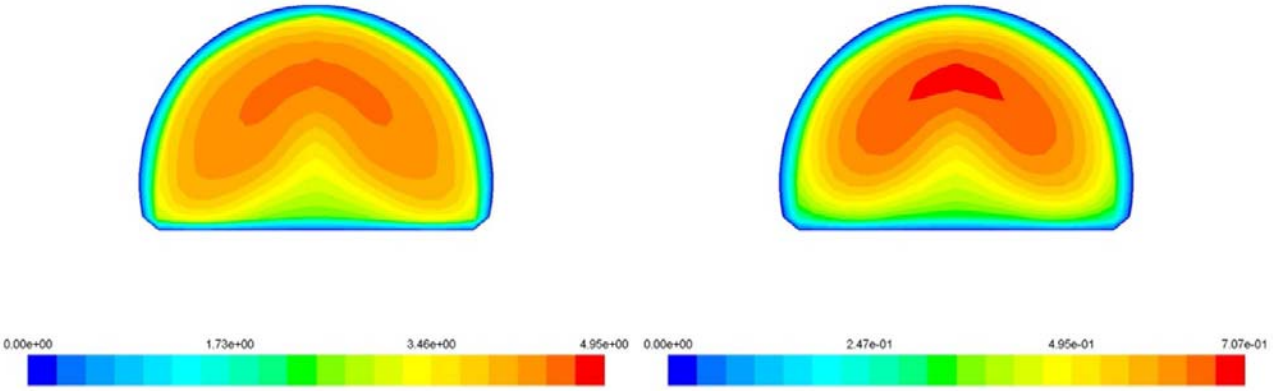

Figure 89 – Axial velocity profile on tunnel cross section @ 480 m: comparison between full (left) and scaled tunnel (right) – alternative jet fans

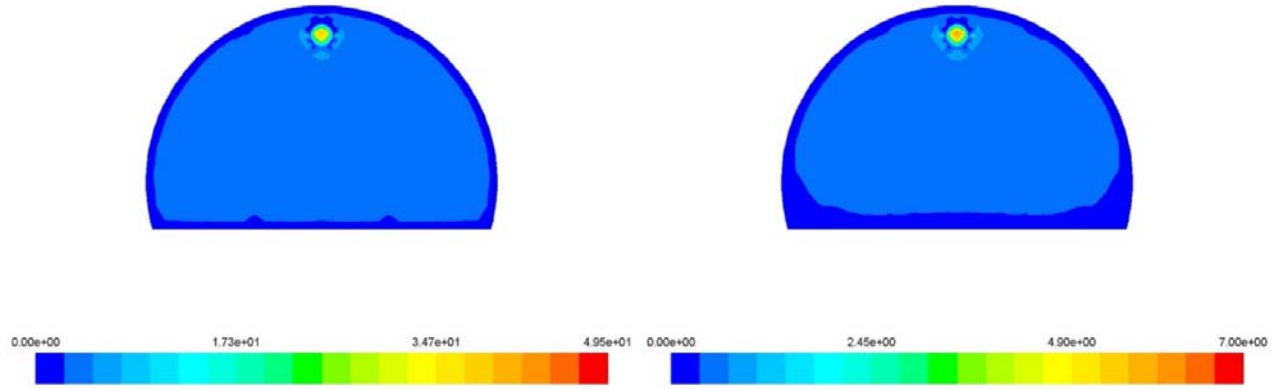

Figure 90 – Axial velocity profile on tunnel cross section @ 498 m: comparison between full (left) and scaled tunnel (right) – alternative jet fans

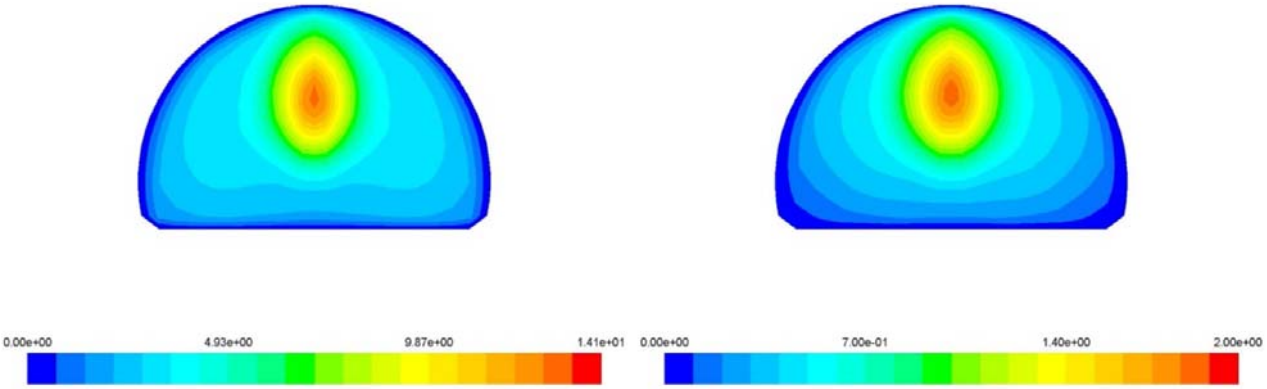

Figure 91 – Axial velocity profile on tunnel cross section @ 522 m: comparison between full (left) and scaled tunnel (right) – alternative jet fans

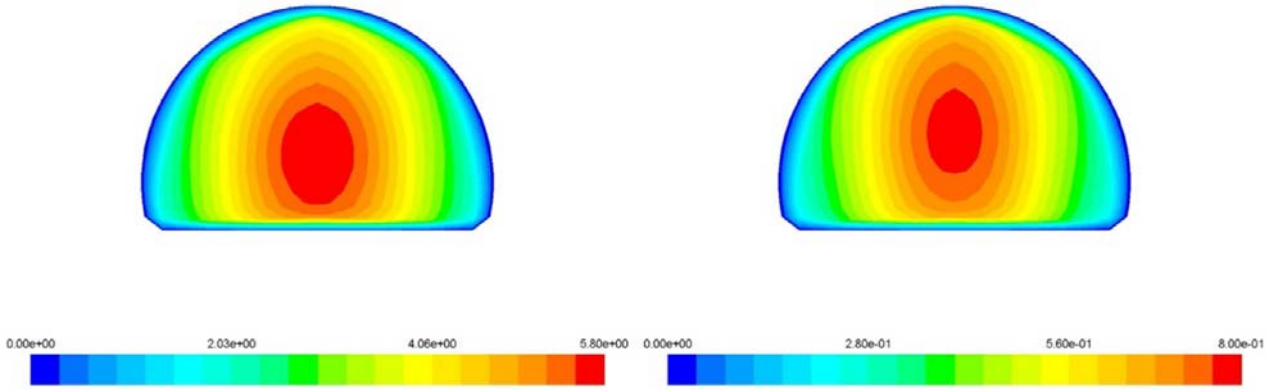

Figure 92 – Axial velocity profile on tunnel cross section @ 552 m: comparison between full (left) and scaled tunnel (right) – alternative jet fans

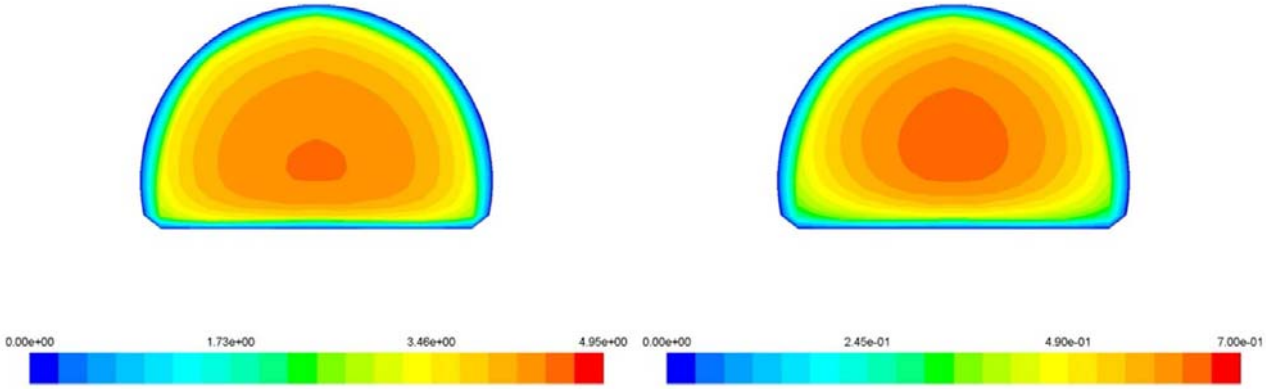

Figure 93 – Axial velocity profile on tunnel cross section @ 652 m: comparison between full (left) and scaled tunnel (right) – alternative jet fans

7.1.2. Materials optimization for reduced scale model

As shown in previous paragraphs, numerical analyses consider different values for wall and floor roughness in order to comply with scaling methods (see Table 14 and Table 15).

As a practical task, in order to simply the construction of the experimental apparatus (reduced scale model) by realizing the whole scaled model by means of the same material, several simulations are carried out in order to check the effects of floor roughness on flow field. In the following Table 16 and Table 17, are shown the main parameters considered in the analyses with a fixed roof roughness (0.0015 m) and three different floor one for traditional and alternative fan respectively.

Table 16

Traditional fans					
Δp (Pa)	v (m/s)	Roof rough. (m)	Floor rough. (m)	Re	Fr_{av}
65	0,51	0,0015	0,01	4800	0,21
64	0,53	0,0015	0,0015	5400	0,24
64	0,51	0,0015	0,0005	4800	0,21

Table 17

Alternative fans					
Δp (Pa)	v (m/s)	Roof rough. (m)	Floor rough. (m)	Re	Fr_{av}
54	0,53	0,0015	0,01	5400	0,24
46	0,53	0,0015	0,0015	5400	0,24
46	0,51	0,0015	0,0005	4800	0,21

In following figures, axial velocity profiles are shown by changing the floor roughness and pressure drop in the scale model for both traditional and alternative jet fan cases according to previous Table 16 and Table 17.

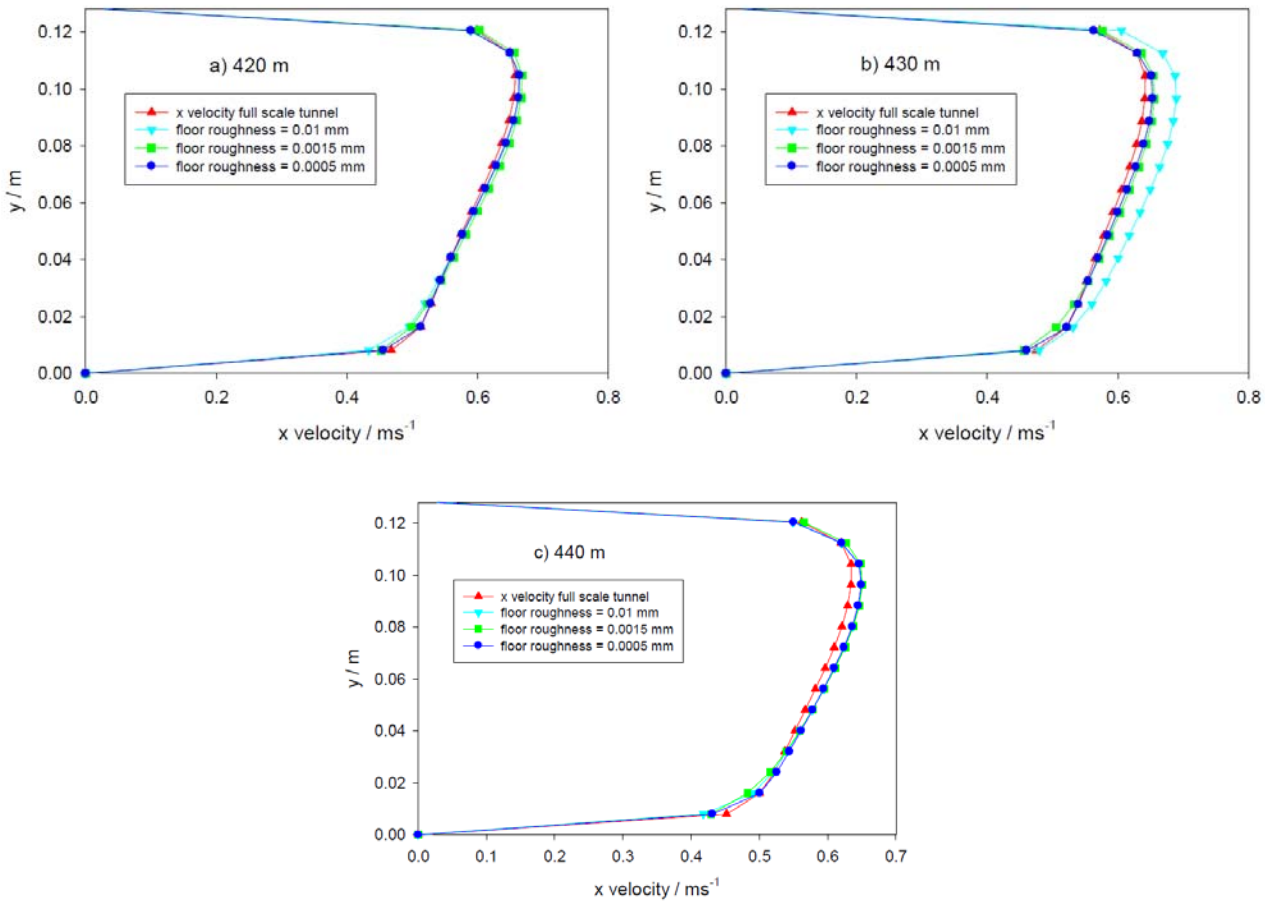

Figure 94 – Axial velocity profile on symmetry plane @ (a) 10 m, (b) 20 m, (c) 30 m before the HGV for different floor roughness and pressure drops in reduced scale model and comparison with full scale one – traditional jet fan case

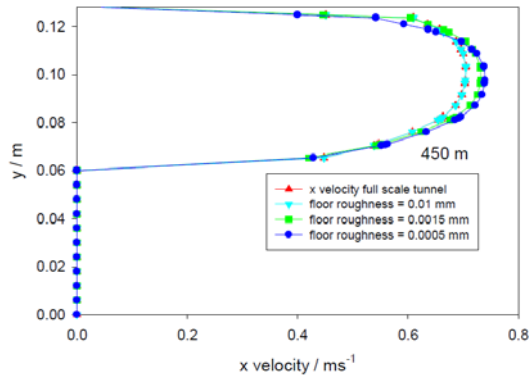

Figure 95 – Axial velocity profile on symmetry plane in correspondence to the HGV for different floor roughness and pressure drops in reduced scale model and comparison with full scale one – traditional jet fan case

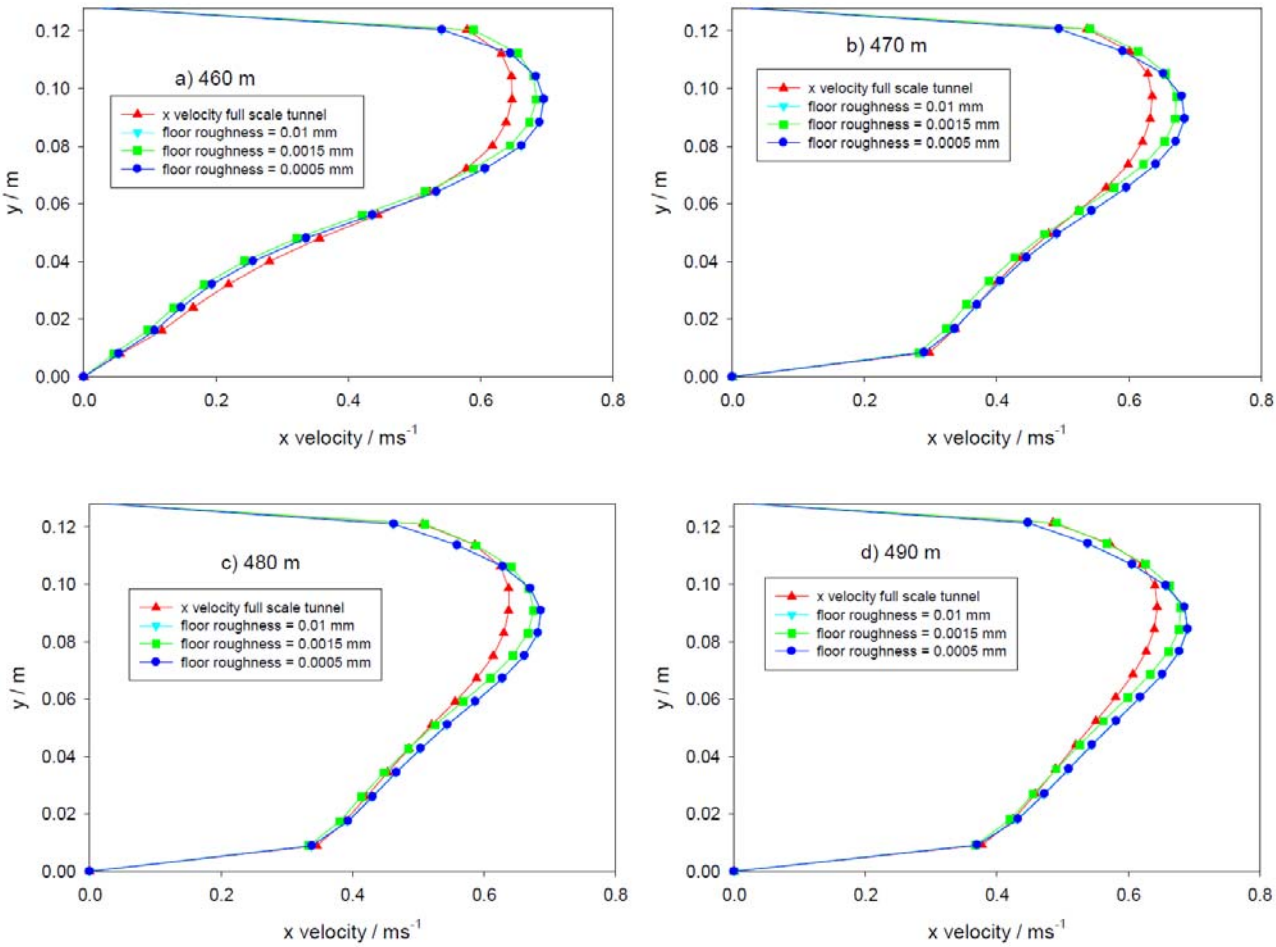

Figure 96 – Axial velocity profile on symmetry plane @ (a) 10 m, (b) 20 m, (c) 30m, (d) 40 m after the HGV for different floor roughness and pressure drops in reduced scale model and comparison with full scale one – traditional jet fan case

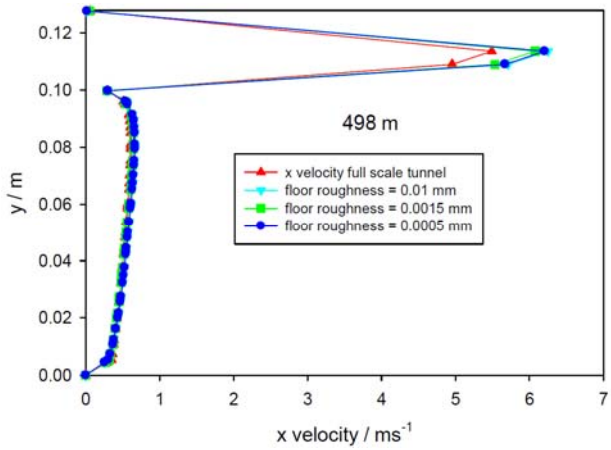

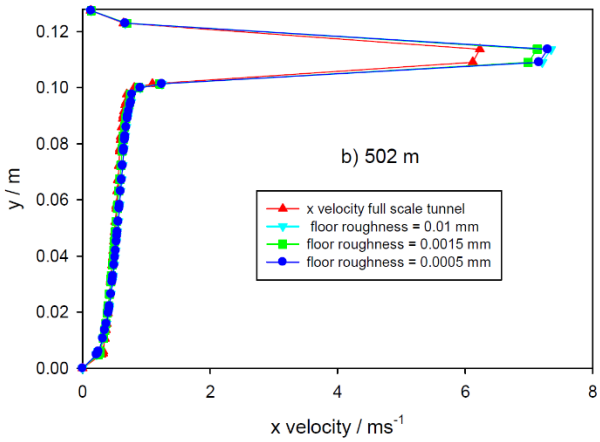

Figure 97 – Axial velocity profile on symmetry plane in correspondence to (a) inlet and (b) outlet section of the 3rd fan for different floor roughness and pressure drops in reduced scale model and comparison with full scale one – traditional jet fan case

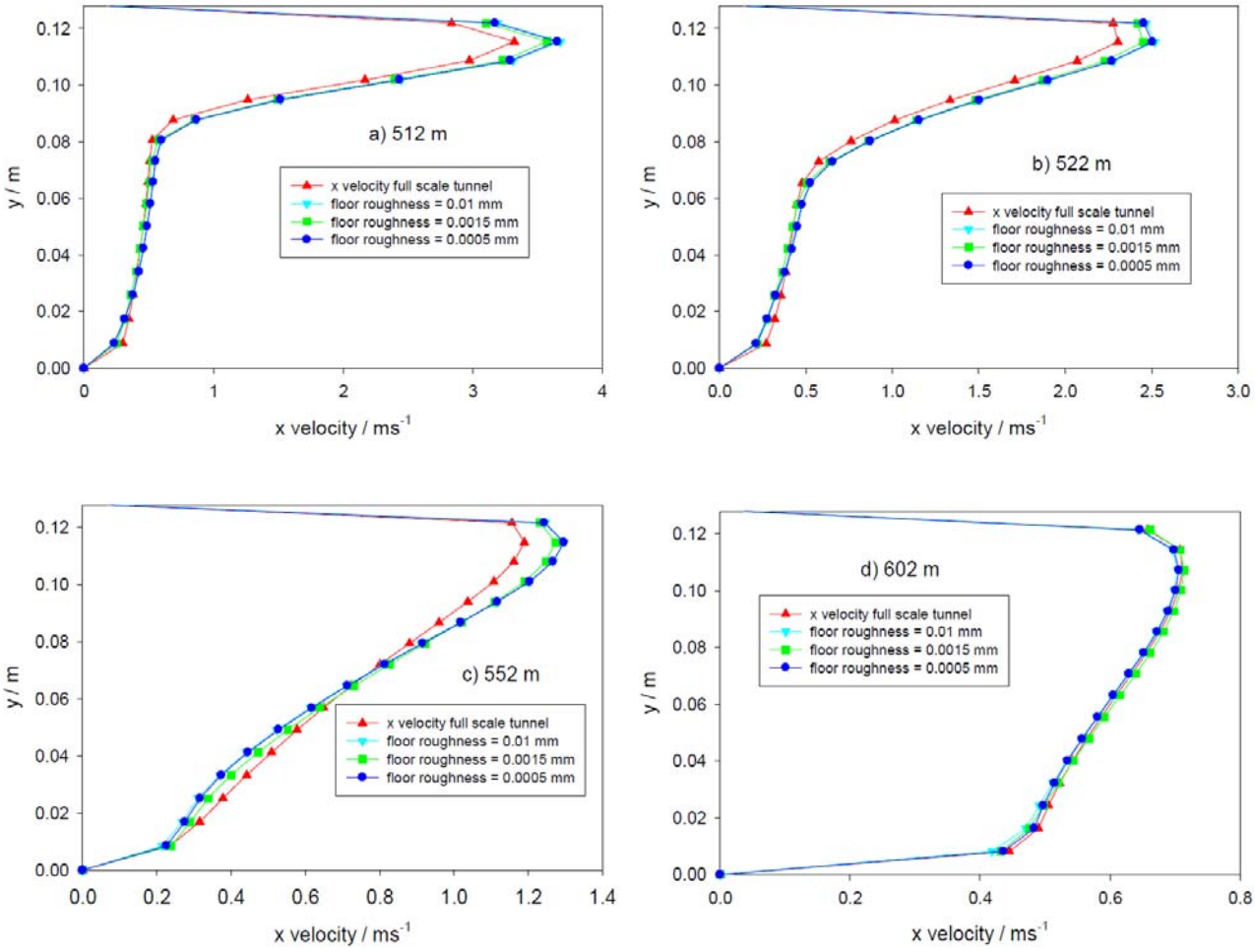

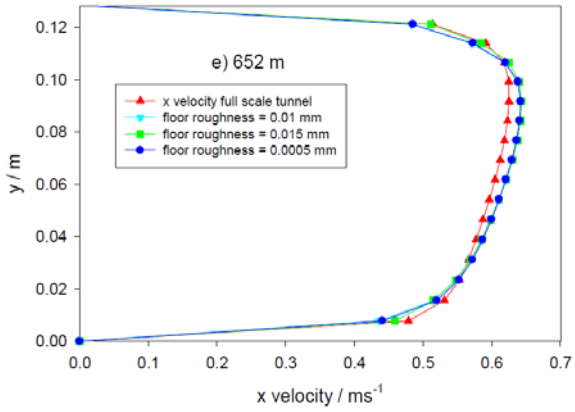

Figure 98 – Axial velocity profile on symmetry plane @ (a) 10 m, (b) 20 m, (c) 50m, (d) 100 m, (e) 150 m after the HGV for different floor roughness and pressure drops in reduced scale model and comparison with full scale one – traditional jet fan case

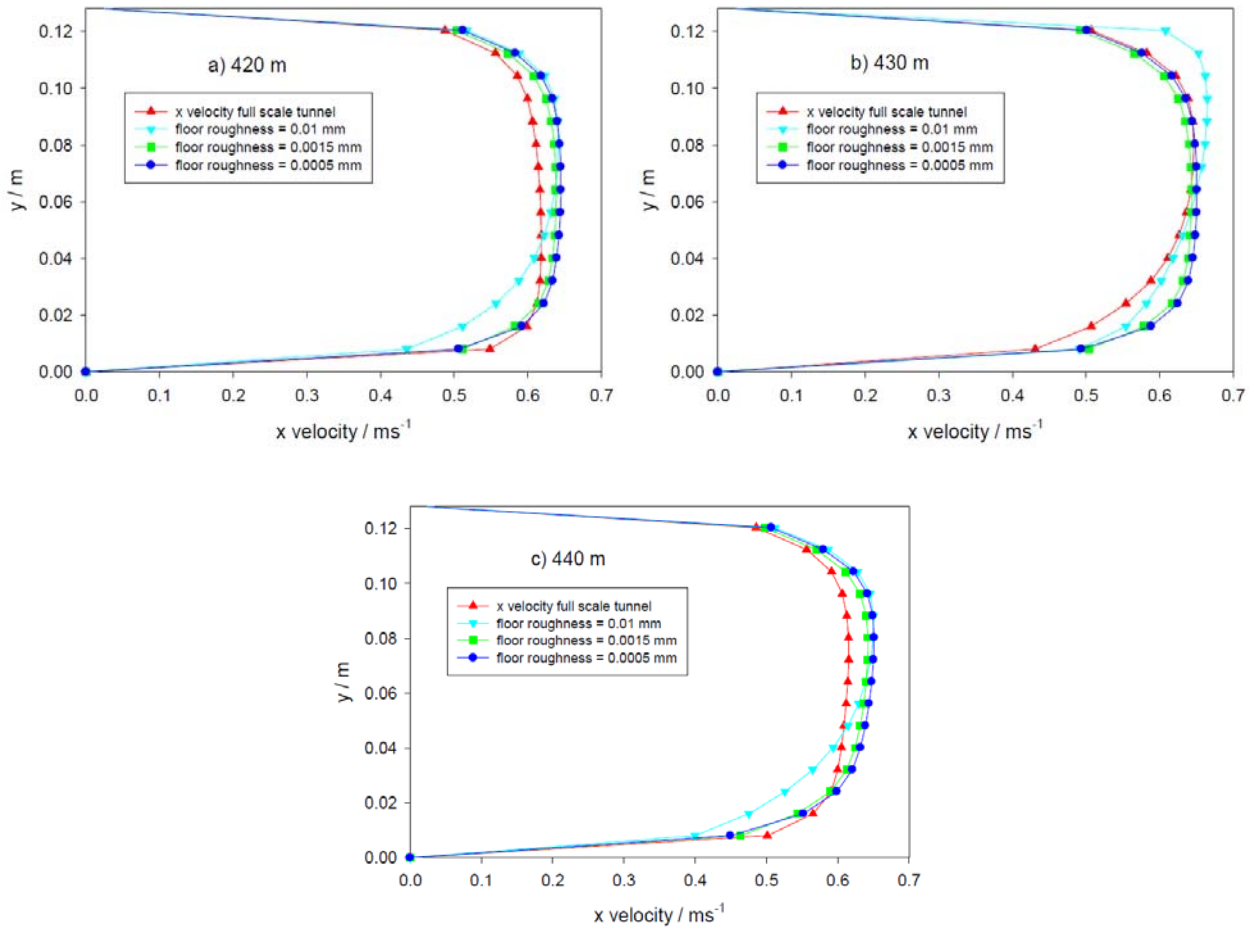

Figure 99 – Axial velocity profile on symmetry plane @ (a) 10 m, (b) 20 m, (c) 30 m before the HGV for different floor roughness and pressure drops in reduced scale model and comparison with full scale one – alternative jet fan case

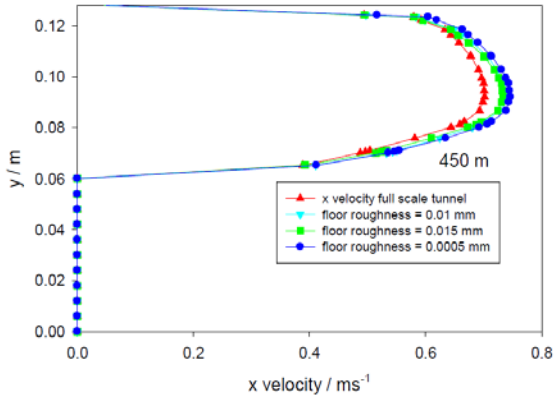

Figure 100 – Axial velocity profile on symmetry plane in correspondence to the HGV for different floor roughness and pressure drops in reduced scale model and comparison with full scale one – alternative jet fan

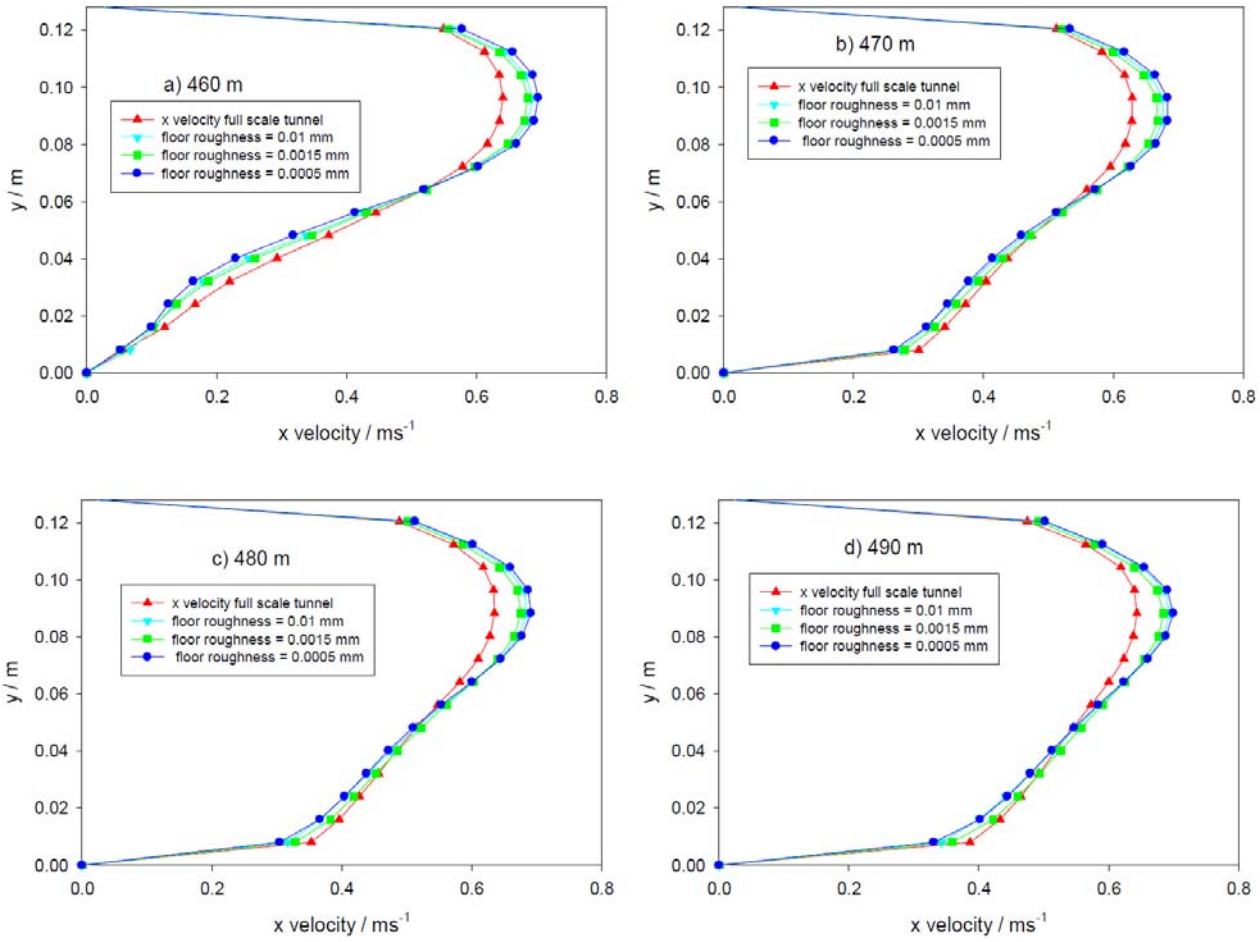

Figure 101 – Axial velocity profile on symmetry plane @ (a) 10 m, (b) 20 m, (c) 30m, (d) 40 m after the HGV for different floor roughness and pressure drops in reduced scale model and comparison with full scale one – alternative jet fan case

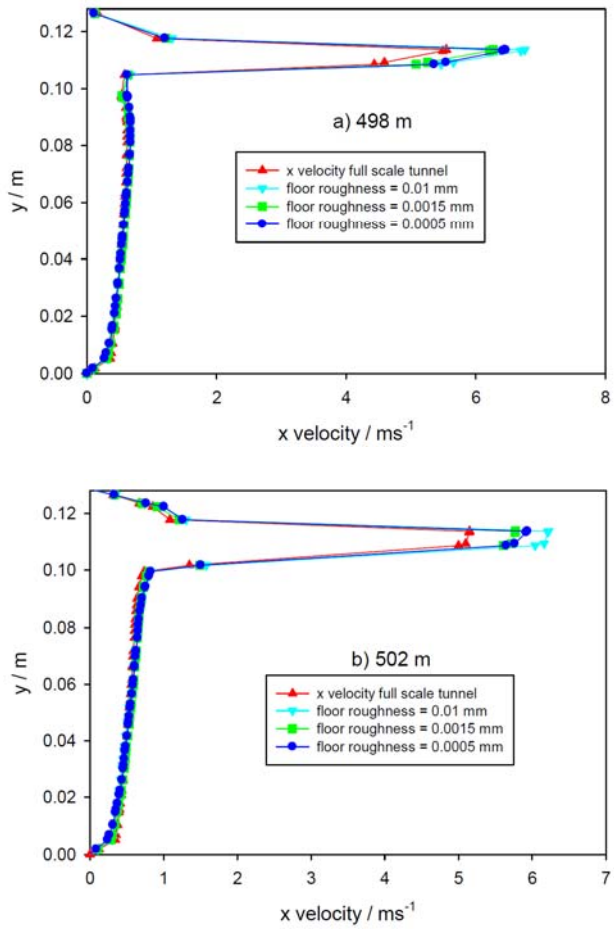

Figure 102 – Axial velocity profile on symmetry plane in correspondence to (a) inlet and (b) outlet section of the 3rd fan for different floor roughness and pressure drops in reduced scale model and comparison with full scale one – alternative jet fan case

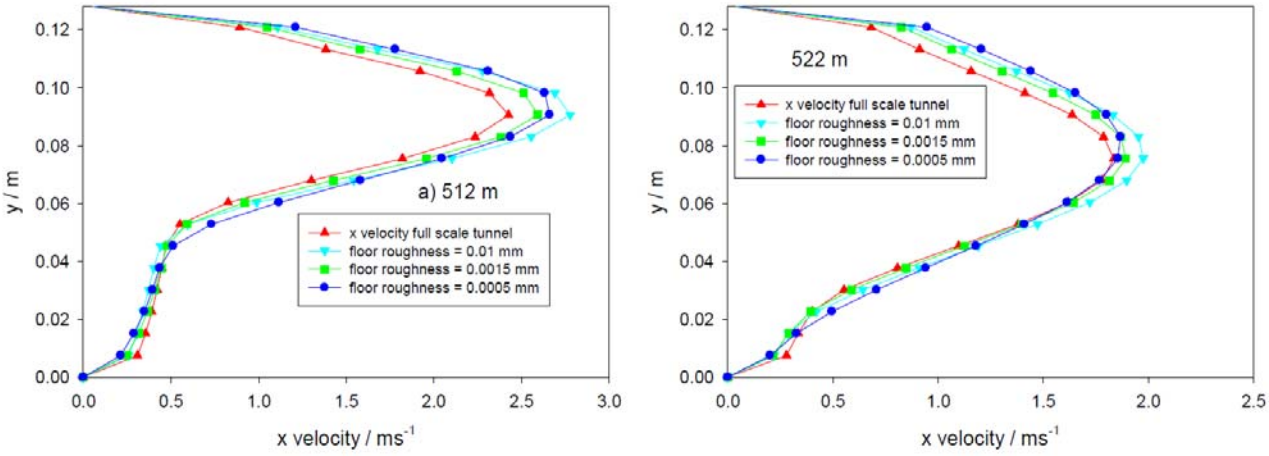

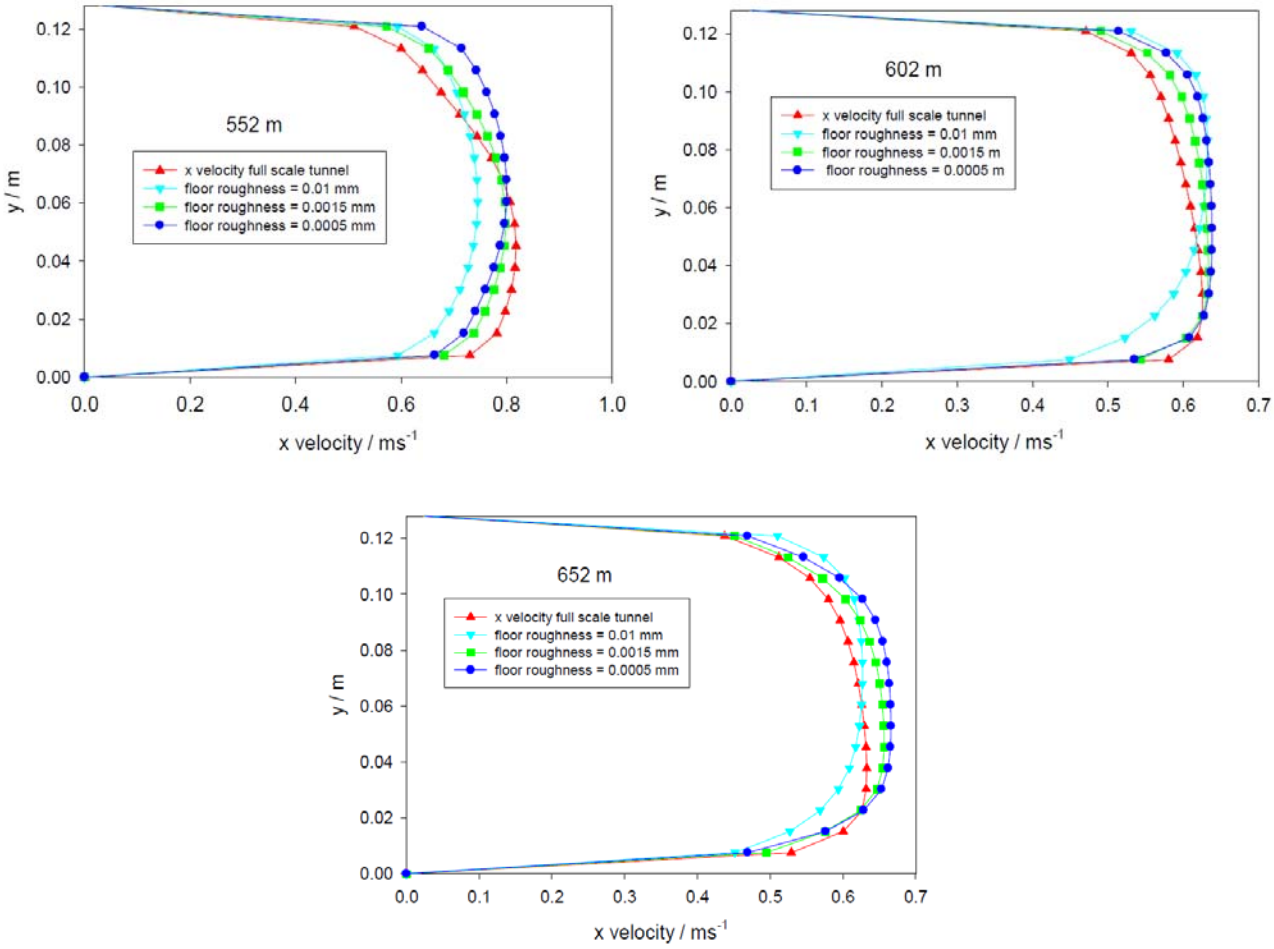

Figure 103 – Axial velocity profile on symmetry plane @ (a) 10 m, (b) 20 m, (c) 50m, (d) 100 m, (e) 150 m after the HGV for different floor roughness and pressure drops in reduced scale model and comparison with full scale one – alternative jet fan case

Figures show that velocity profile appears quite similar for both 0,0015 m and 0,0005 m values of roughness; thus the Plexiglas (rough. 0,0015 m) can be considered as the optimal choice for both technical and economical aspect of course. Moreover, results show a higher impact of floor roughness on flow field in alternative jet fan case instead of traditional one.

7.1.3. Preliminary tunnel geometry configuration

A preliminary definition of main geometrical features of the 1/50 scale model is supposed and summarized below.

Main tunnel geometrical features	
Tunnel length	16 m
Tunnel hydraulic diameter	0,146 m
HGV length	0,240 m
HGV height	0,060 m
HGV width	0,230 m
FAN diameter	0,015 m

Since the aim of scaled tunnel is to compare experimental data with numerical ones for traditional vs alternative jet fan, an external fan (usually adopted) can't be considered. Considering the scale ratio (1/50), the fan diameter became 1.5 cm and its realization appears very challenging: the use of an external compressor pushing air in an internal pipe system is thus considered. Thanks to pipe flexibility, it is possible to simulate nozzle inclination of alternative jet fans.

A preliminary study is carried out in order to check the availability of this solution: pressure drop of pipe circuit related to both distributed and concentrated losses is compared with those due to fan. Applying the Froude scaling method, a preliminary evaluation of head losses is calculated for both alternative and traditional jet fan.

	Traditional jet fan	Alternative jet fan
Volume flow rate – full scale model	18 m^3/s	15 m^3/s
Volume flow rate – scaled model	3.6 m^3/h	3.0 m^3/h

Traditional jet fan										
Element		Diameter (m)	D1 (m)	D2 (m)	Length (m)	Degrees (°)	Vol. flow rate (m3/s)	Material	Fluid	Head loss (mmH2O)
Pipe	2	0.015			0.01		3.6	Steel	Air (20°C)	0.1
Pipe	2	0.015			0.05		3.6	Steel	Air (20°C)	0.5
Pipe	2	0.015			0.01		3.6	Steel	Air (20°C)	0.1
Pipe	2	0.015			0.01		3.6	Steel	Air (20°C)	0.1
Pipe	2	0.031			0.02		3.6	Steel	Air (20°C)	0
Pipe	1	0.055			0.10		3.6	Steel	Air (20°C)	0
Bend	6	0.015				90	3.6	Steel	Air (20°C)	2.0
Bend	2	0.031				90	3.6	Steel	Air (20°C)	0.1
Gradual enlargement	1		0.015	0.031		10	3.6	Steel	Air (20°C)	0.5
Gradual enlargement	1		0.031	0.055			3.6	Steel	Air (20°C)	0
Gradual enlargement	1	0.013	0.031	0.015		10	3.6	Steel	Air (20°C)	0.1
Gradual enlargement	1		0.031	0.055			3.6	Steel	Air (20°C)	0

Alternative jet fan										
Element		Diameter (m)	D1 (m)	D2 (m)	Length (m)	Degrees (°)	Vol. flow rate (m3/s)	Material	Fluid	Head loss (mmH2O)
Pipe	2	0.015			0.01		3.0	Steel	Air (20°C)	0.1
Pipe	2	0.015			0.05		3.0	Steel	Air (20°C)	0.4
Pipe	2	0.015			0.01		3.0	Steel	Air (20°C)	0.1
Flexible pipe	2	0.015			0.04		3.0	Steel	Air (20°C)	0.9
Pipe	2	0.031			0.02		3.0	Steel	Air (20°C)	0
Pipe	2	0.055			0.10		3.0	Steel	Air (20°C)	0

Bend	4	0.015				90	3.0	Steel	Air (20°C)	1.3
Bend	2	0.031				90	3.0	Steel	Air (20°C)	0.1
Gradual enlargement	1		0.015	0.031		10	3.0	Steel	Air (20°C)	0.3
Gradual enlargement	1		0.031	0.055			3.0	Steel	Air (20°C)	0
Gradual enlargement	1	0.013	0.031	0.015		10	3.0	Steel	Air (20°C)	0.1
Gradual enlargement	1		0.031	0.055			3.0	Steel	Air (20°C)	0

After a preliminary market analysis, it is considered as a suitable solution for the fan of experimental scale apparatus the AD3812UB-B51GP fan (characteristic curve in following picture).

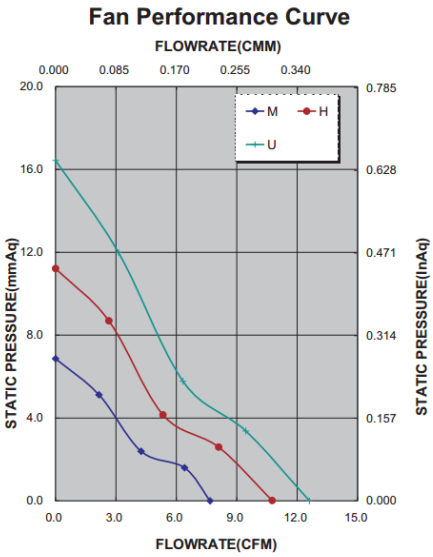

Figure 104 – Fan characteristic curve

7.1.4. Fire case

Starting from results shown in this paragraph, the presence of fire is analyzed in order to verify the suitability of the 1/50 reduced model also for this scenario. Both temperature and velocity fields, influenced by fire, are analyzed. In order to guarantee the dynamic similitude, the temperature field shall be quite similar for both models since the presence of fire lead to increase buoyancy forces.

Two different models are tested to simulate fire:

- Case 1: heat source (20 MW) imposed on HGV walls;
- Case 2: (simplified) combustion model EDC with Discrete Phase Model.

Case 1 results not suitable since a 1:50 scaling factor for geometry lead to not-realistic temperature values reached locally. Thus, other scaling factors are analyzed. About the Case 2 model, following equations are considered to integrate the mathematical model used in the "unfired case".

$$\frac{\partial}{\partial x_i}(\rho C_7H_{16} v_i) = \frac{\partial}{\partial x_i}\left(\rho D_{C_7H_{16}} \frac{\partial C_7H_{16}}{\partial x_i}\right) + R_i + S_i \quad (23)$$

$$m_p(t+\Delta t) = m_p(t) - k_i([C_7H_{16}]_{i,S} - [C_7H_{16}]_{i,\infty}) A_p M_{w,i} \Delta t \quad (24)$$

$$m_p c_p \frac{dT_p}{dt} = hA_p(T_\infty - T_p) + \frac{dm_p}{dt} h_{fg} \quad (25)$$

7.1.5. Case 1 – Mesh and boundary conditions

The mesh used in this case is the same for previous analysis (λ=50 model). Boundary condition are summarized in following table (full scale).

Traditional jet fan		
	Full scale	Reduced scale (λ=50)
Solver	Pressure based	Pressure based
Fluid	Air	Air
Pressure drop	2300 Pa	64 Pa
Fluid temperature	300 K	300 K
Gauge pressure inlet/outlet tunnel section	0 Pa	0 Pa
Floor roughness	0,01 m	0,0015 m
Roof roughness	0,03 m	0,0005 m
Heat flux at truck walls	180 kW/m^2	25 kW/m^2

7.1.6. Case 1 – Results

In following figures, results are shown: full scale and reduced (λ=50) model are compared in terms of axial velocity; profiles on symmetry plane for different x-coordinate are compared.

Differences became relevant between the third fan and HGV, especially in comparison with the "unfired" case due to buoyancy forces related to heat flux.

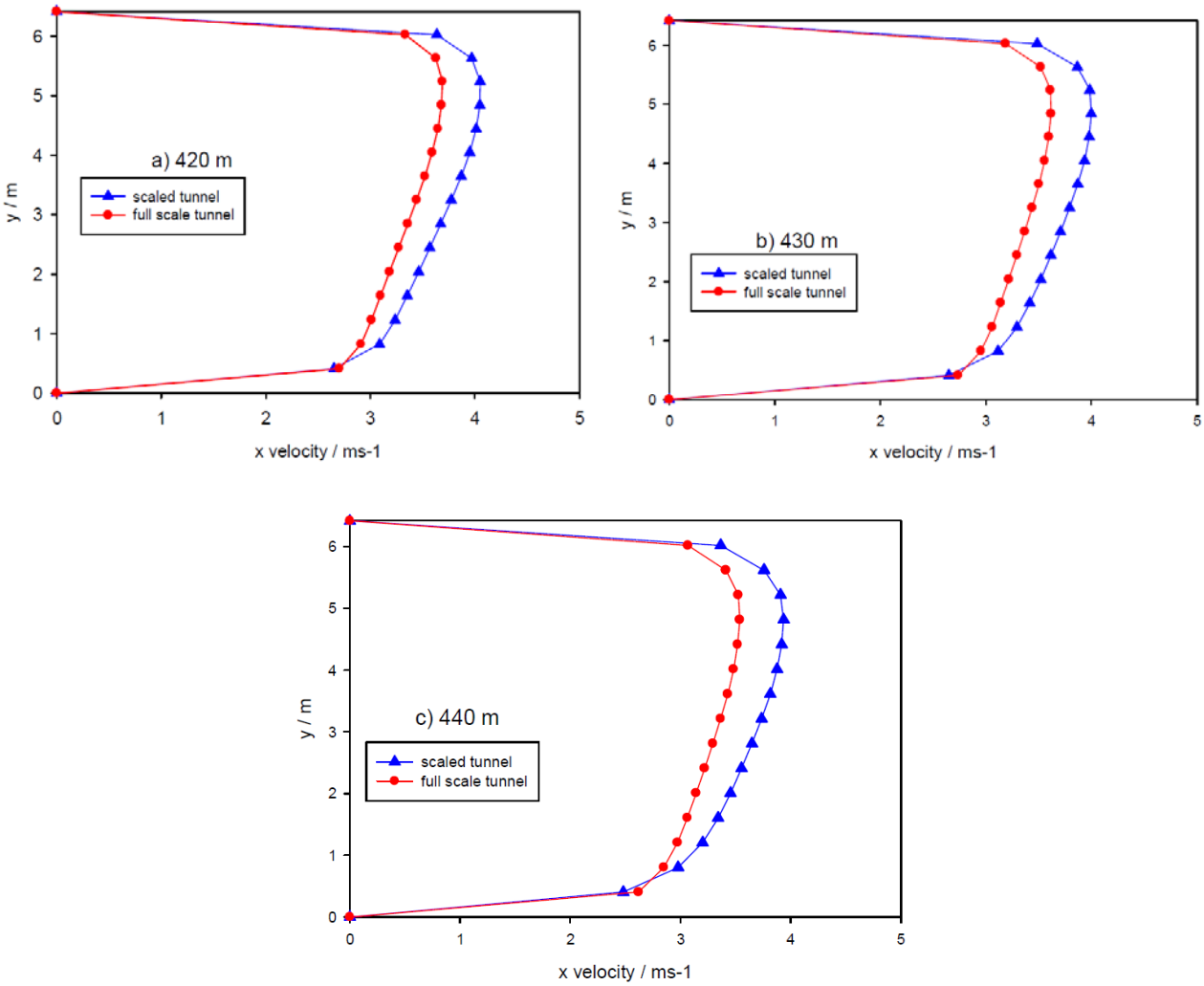

Figure 105 – Axial velocity profile on symmetry plane @ (a) 10m, (b) 20m, (c) 30 m before HGV, comparison between full and reduced scale model (1:50) – traditional jet fans

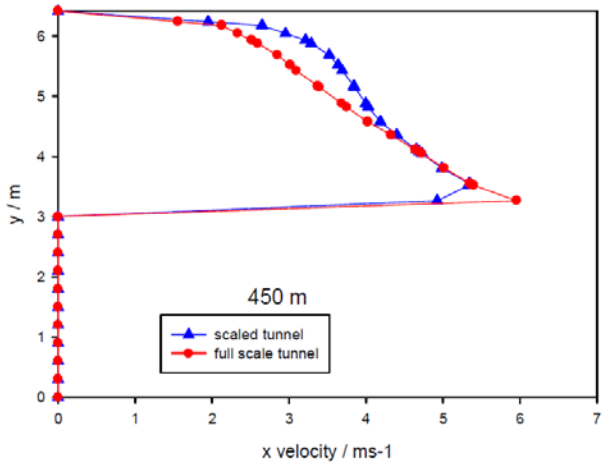

Figure 106 – Axial velocity profile on symmetry plane in correspondence of the HGV, comparison between full and reduced scale model (1:50) – traditional jet fans

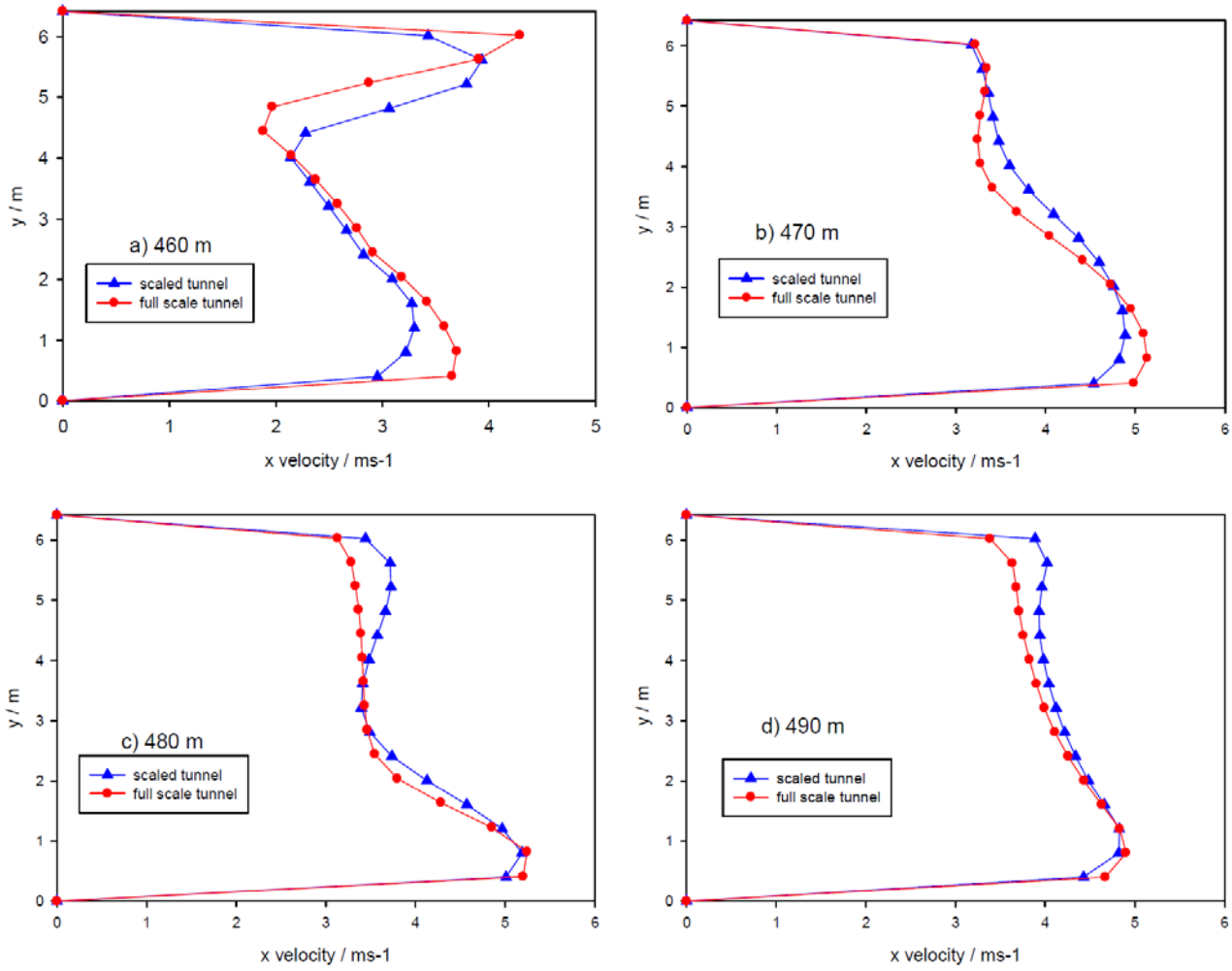

Figure 107 – Axial velocity profile on symmetry plane @ (a) 10m, (b) 20m, (c) 30 m, (d) 40 m after HGV, comparison between full and reduced scale model (1:50) – traditional jet fans

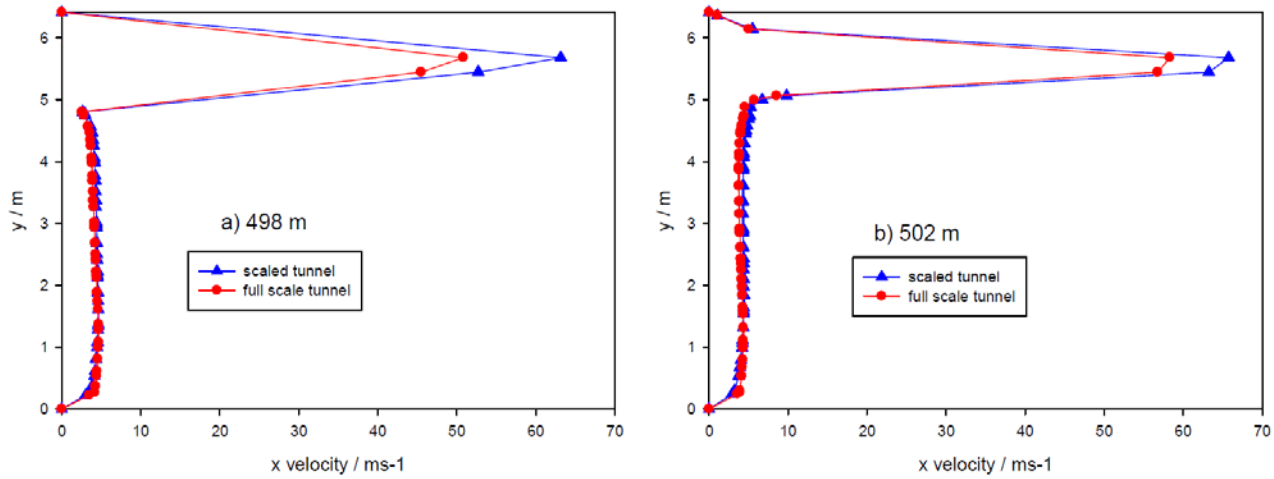

Figure 108 – Axial velocity profile on symmetry plane @ (a) inlet and (b) outlet section of 3rd jet fan, comparison between full and reduced scale model (1:50) – traditional jet fans

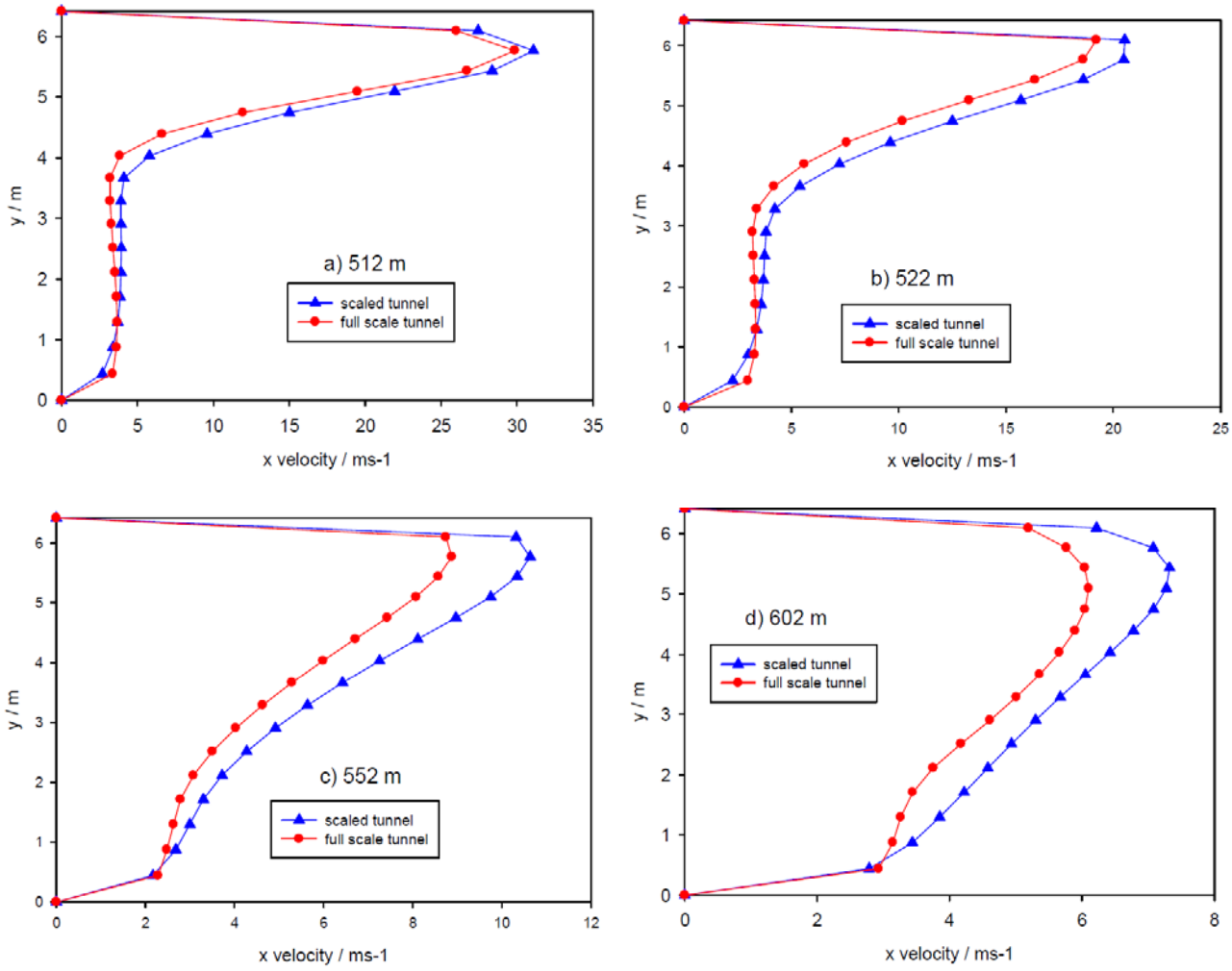

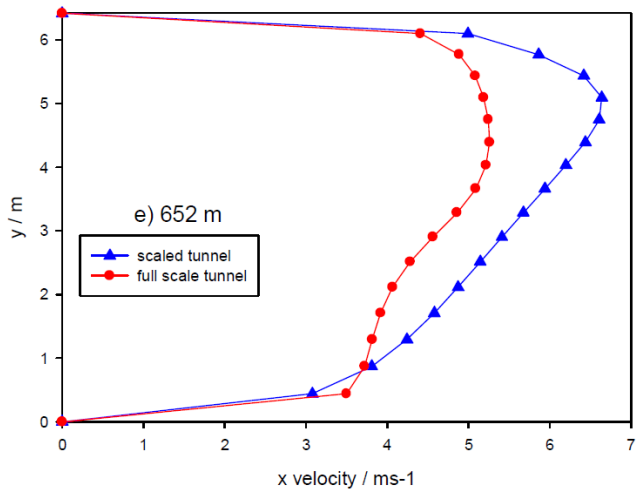

Figure 109 – Axial velocity profile on symmetry plane @ (a) 10m, (b) 20m, (c) 50 m, (d) 100 m, (e) 150 m after HGV, comparison between full and reduced scale model (1:50) – traditional jet fans

Figures show that the scaling factor 50 is not suitable to guarantee the similitude between full and reduced scale: temperature fields are not constant (Figure 110 to Figure 113).

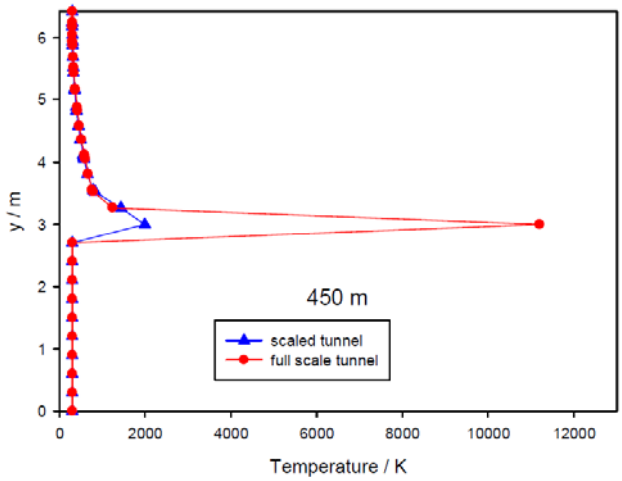

Figure 110 – Temperature profile on tunnel symmetry plane in correspondence of HGV vehicle, comparison between full and reduced (1:50) model – traditional jet fan case

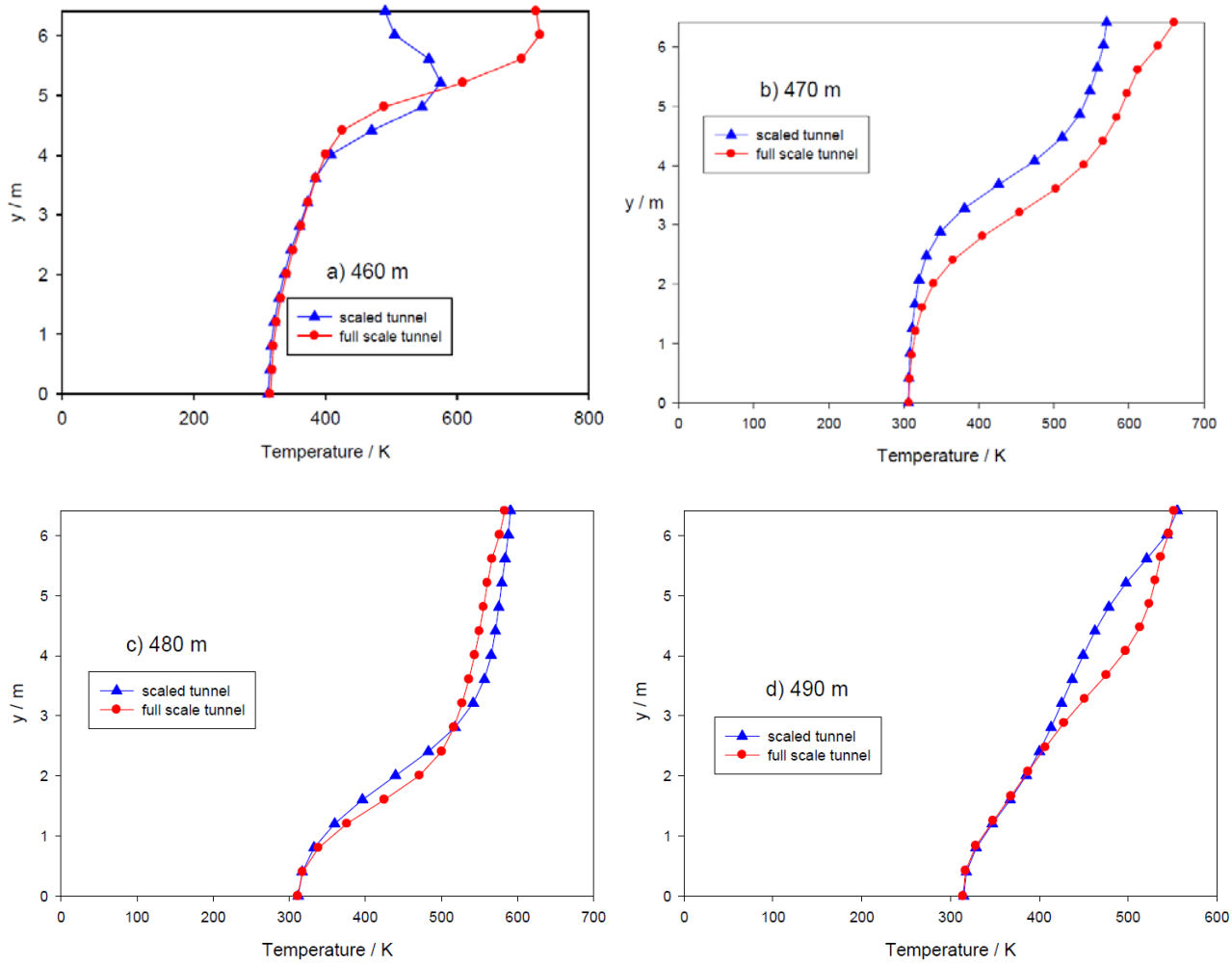

Figure 111 – Temperature profile on tunnel symmetry plane @ (a) 10m, (b) 20m, (c) 30 m after HGV, comparison between full and reduced scale model (1:50) – traditional jet fans

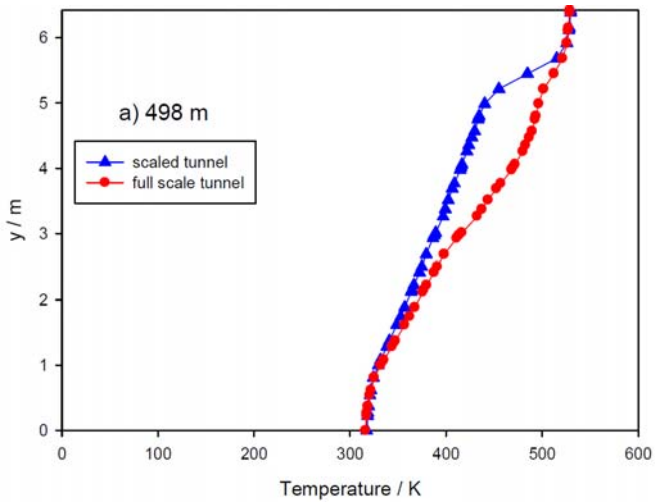

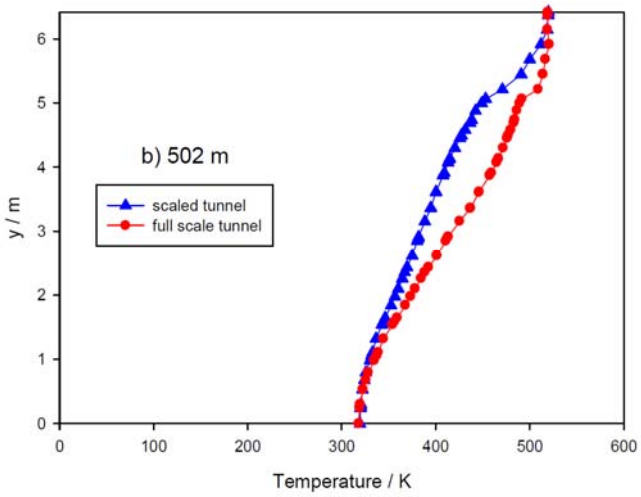

Figure 112 – Temperature profile on symmetry plane @ (a) inlet and (b) outlet section of 3rd jet fan, comparison between full and reduced scale model (1:50) – traditional jet fans

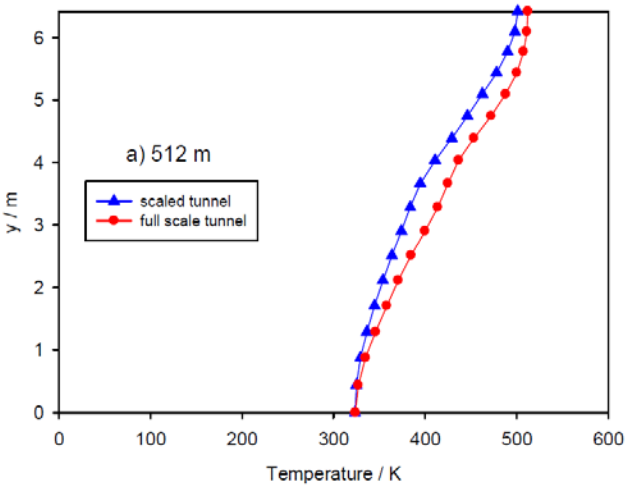

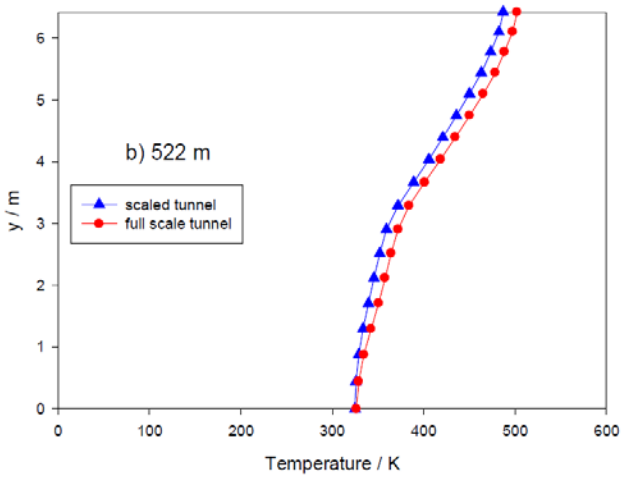

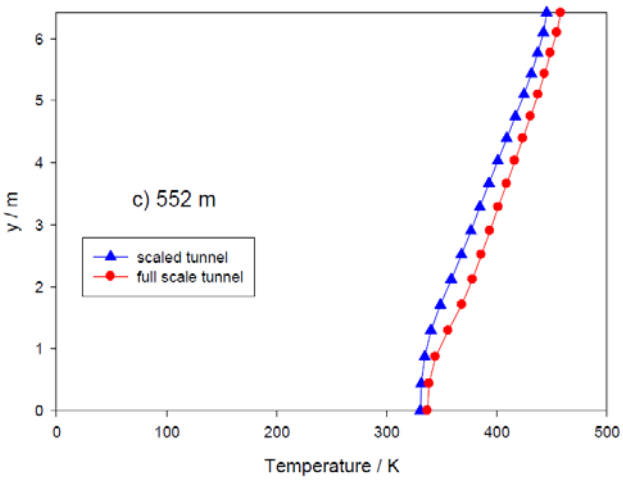

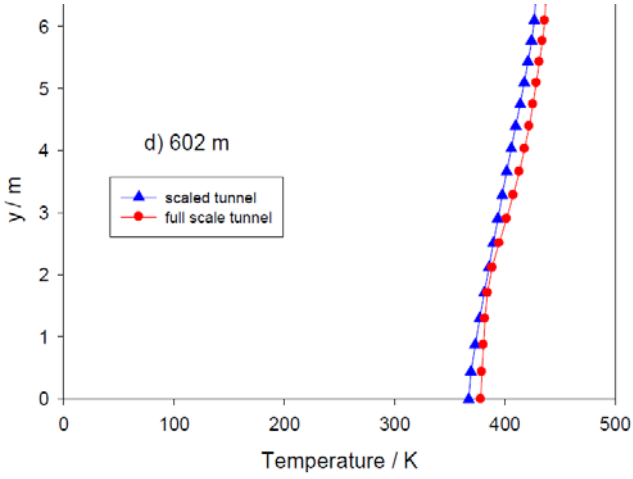

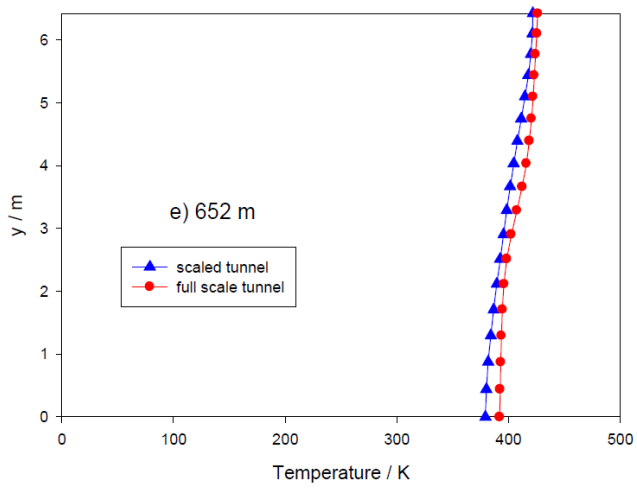

Figure 113 – Temperature profile on symmetry plane @ (a) 10m, (b) 20m, (c) 50 m, (d) 100 m, (e) 150 m after HGV, comparison between full and reduced scale model (1:50) – traditional jet fans

Results show limits of λ=50 model in terms of kinematic similitude and temperature field. For this reason, several simulations are carried out decreasing λ value in order to reach the optimum scale factor for maintain similitude.

Scaling factor – roughness and heat flux imposed			
	λ=20	**λ=20**	**λ=2**
Pressure drop (Pa)	115	230	1150
Floor roughness (m)	5E-4	1E-3	5E-3
Roof roughness (m)	1.5E-3	3E-3	1.5E-2
Heat flux on HGV walls (kW/m^2)	40	57	127

In order to obtain a pressure drop value according to Froude scaling method, roughness value is chosen accordingly. In particular, for each case the average error on x-velocity is considered in order to evaluate the optimum λ value. Results show that a scaling factor equal to 20 gives the minimum error (less than 10%).

Velocity average errors in comparison between full and several scaled models				
Axial distance (m)	Average axial velocity error (%)			
	Scale 1:2	Scale 1:10	Scale 1:20	Scale 1:50
420	0.88	2.73	3.79	7.58
430	0.87	2.81	5.33	8.03
440	0.93	2.83	5.78	8.27
450	1.22	4.99	7.42	9.50
460	0.47	1.75	2.55	11.1
470	0.67	2.06	3.28	4.84
480	0.59	1.27	1.79	4.79
490	0.43	0.90	1.23	4.01
498	1.74	6.50	9.08	22.59
502	0.85	1.80	2.30	10.58
512	1.16	5.45	9.77	15.65
522	0.81	2.02	3.92	15.13
552	0.66	1.73	2.71	16.60
602	0.91	3.06	4.18	14.73
652	1.25	3.71	4.86	16.06

Velocity average errors in comparison between full and several scaled models				
Axial distance (m)	Average axial velocity error (%)			
	Scale 1:2	Scale 1:10	Scale 1:20	Scale 1:50
420	0	0	0	0
430	0	0	0	0
440	0	0	0	0
450	50	175	283	377
460	2	10	18	45
470	5	20	29	42
480	1	5	9	15
490	1	5	7	17
498	3	10	28	25
502	3	10	19	25
512	1	5	7	18
522	1	3	6	12
552	1	2	4	14
602	1	2	4	17
652	1	3	5	8

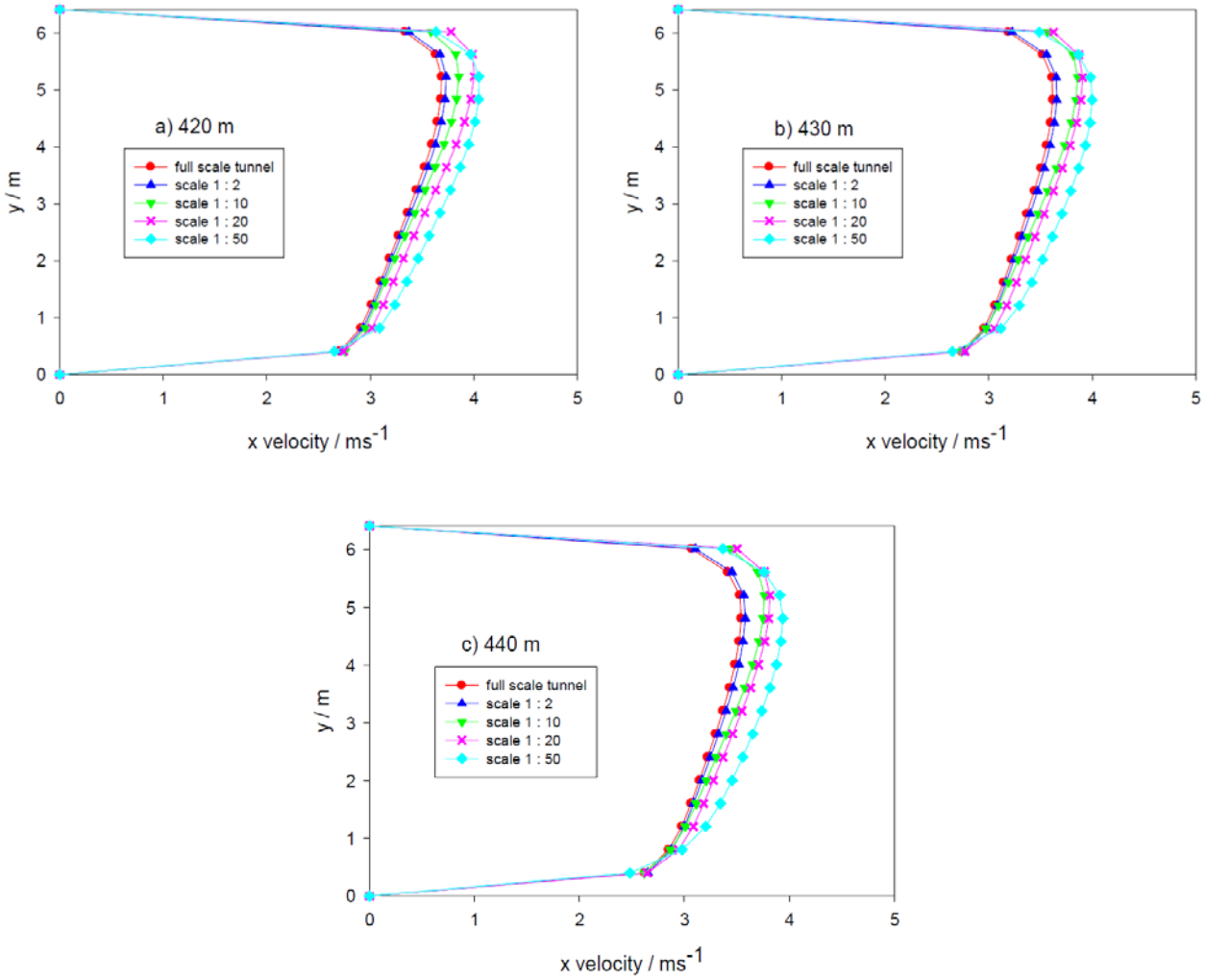

Figure 114 – Axial velocity on tunnel symmetry plane @ (a) 10m, (b) 20 m, (c) 30 m before the HGV: comparison between different scaling factors – traditional jet fan case

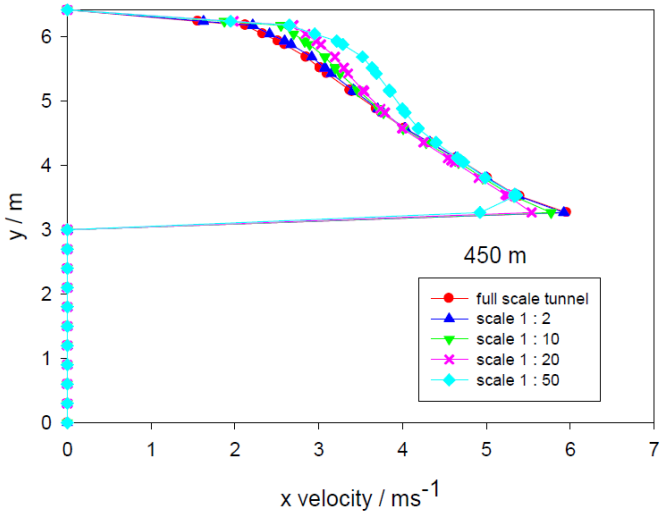

Figure 115 – Axial velocity on tunnel symmetry plane in correspondence to the HGV: comparison between different scaling factors – traditional jet fan case

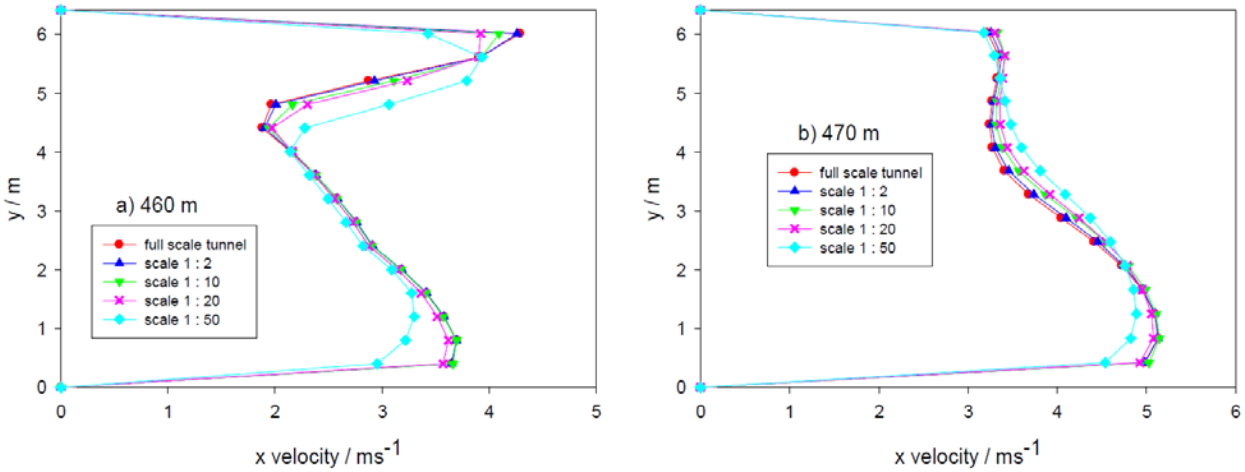

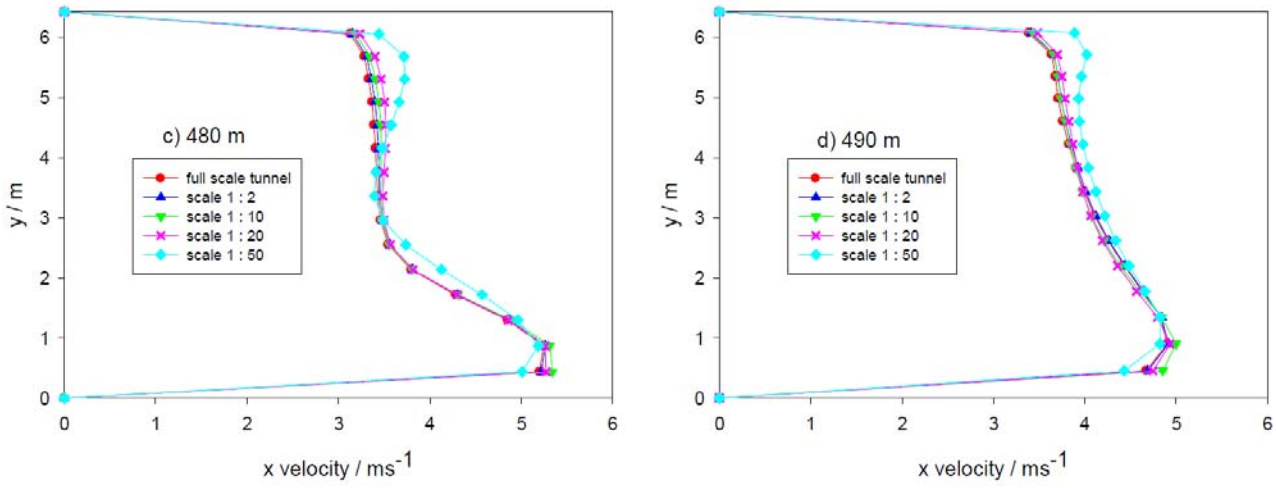

Figure 116 – Axial velocity on tunnel symmetry plane @ (a) 10m, (b) 20 m, (c) 30 m, (d) 40 m after the HGV: comparison between different scaling factors – traditional jet fan case

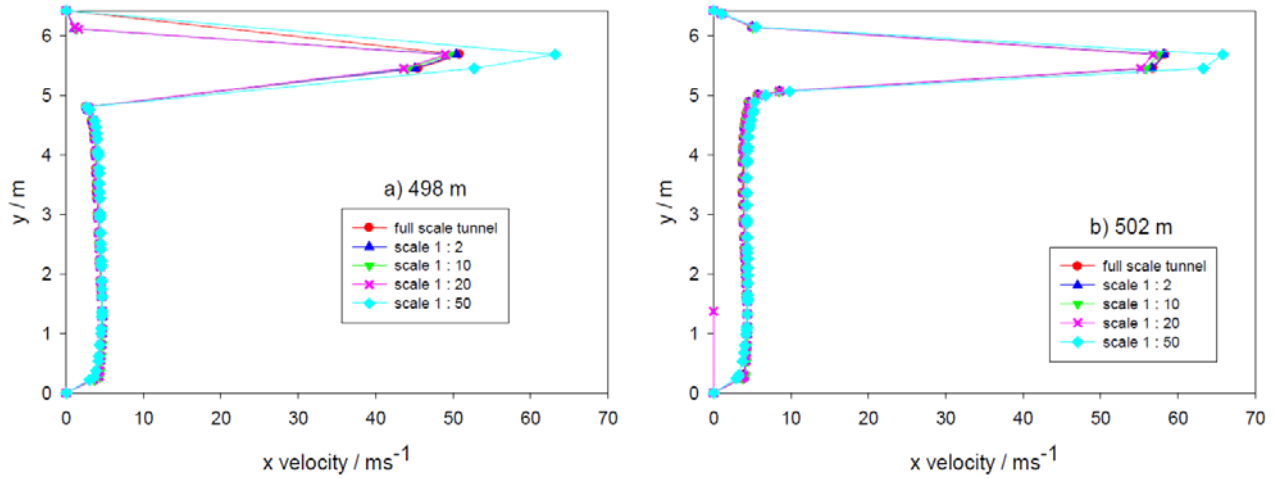

Figure 117 – Axial velocity on tunnel symmetry plane @ (a) inlet and (b) outlet section of 3rd jet fan: comparison between different scaling factors – traditional jet fan case

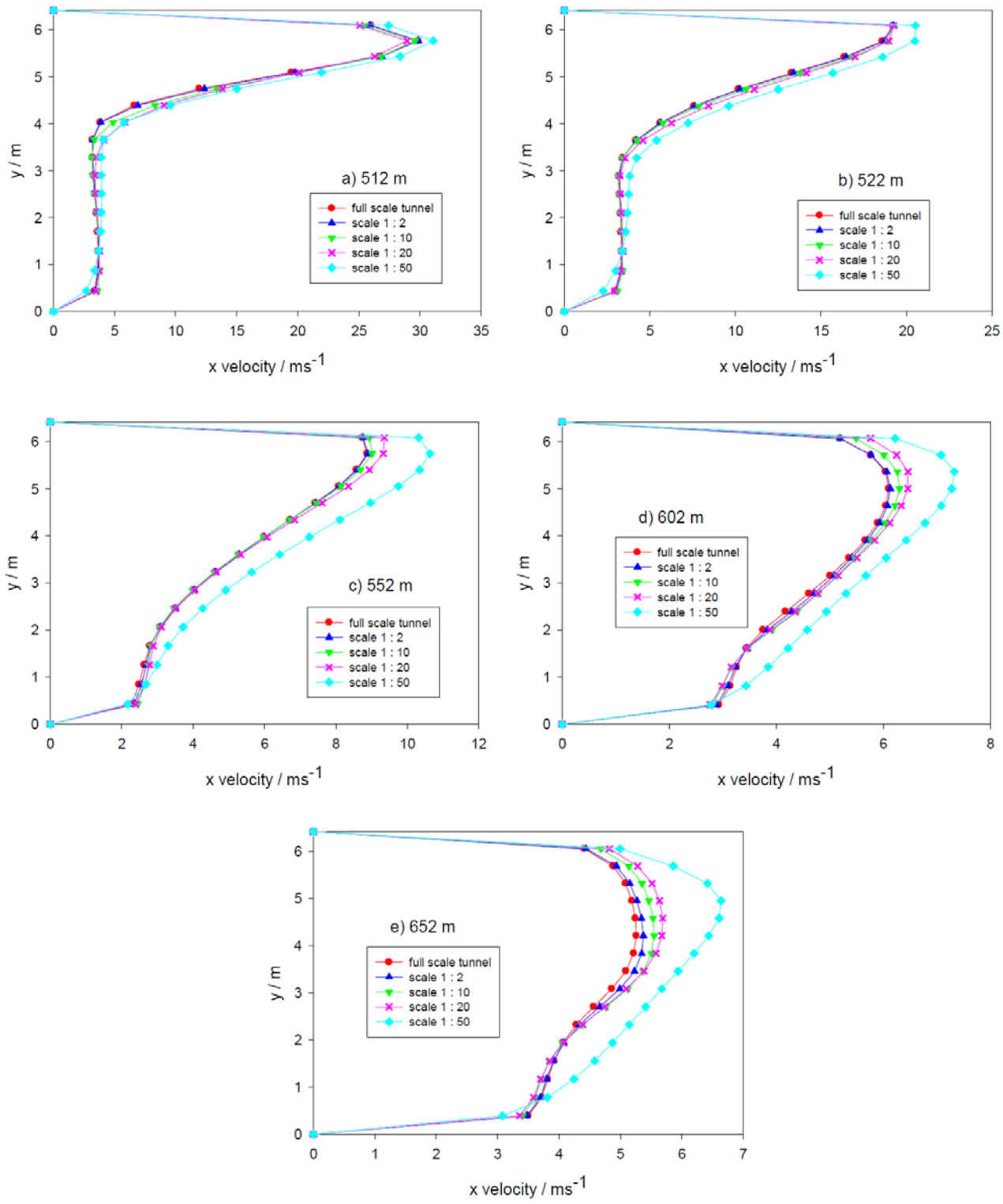

Figure 118 – Axial velocity on tunnel symmetry plane @ (a) 10m, (b) 20 m, (c) 50 m, (d) 100m, (e) 150 m after the HGV: comparison between different scaling factors – traditional jet fan case

Reducing the sale factor, the differences between full and scale models for both velocity and temperature profiles decrease. In order to check the preservation of similitude, x-velocity on tunnel sections (Figure 119 to Figure 129) and temperature fields (Figure 130 to Figure 135) are compared for the full scale with both 1/20 and 1/50 reduced model. Results show a good comparison for the 1/20 model.

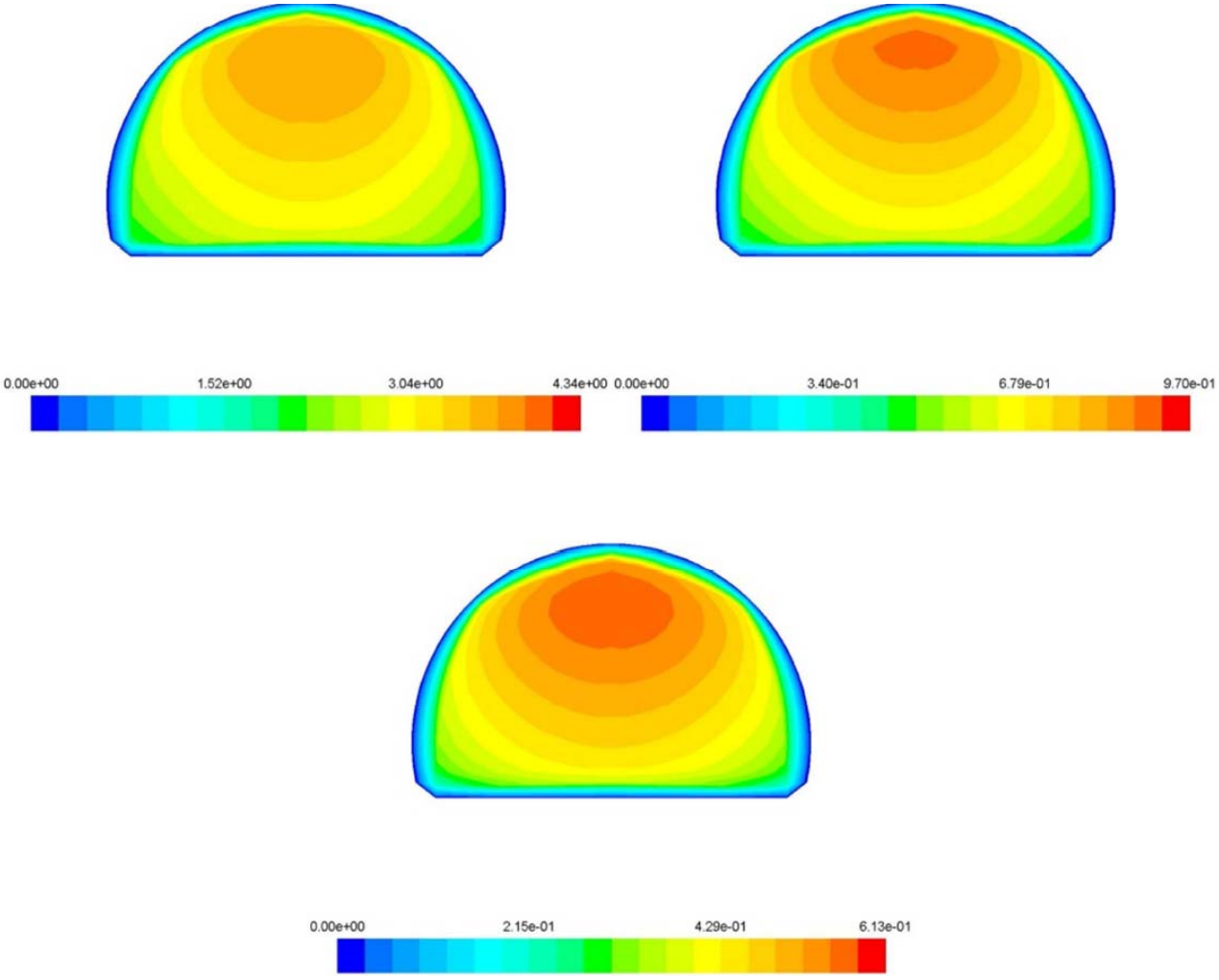

Figure 119 – Axial velocity contour on tunnel section @ 420 m: comparison between full scale (left), 1:20 reduced scale (right), 1:50 reduced scale (bottom) – traditional jet fan case

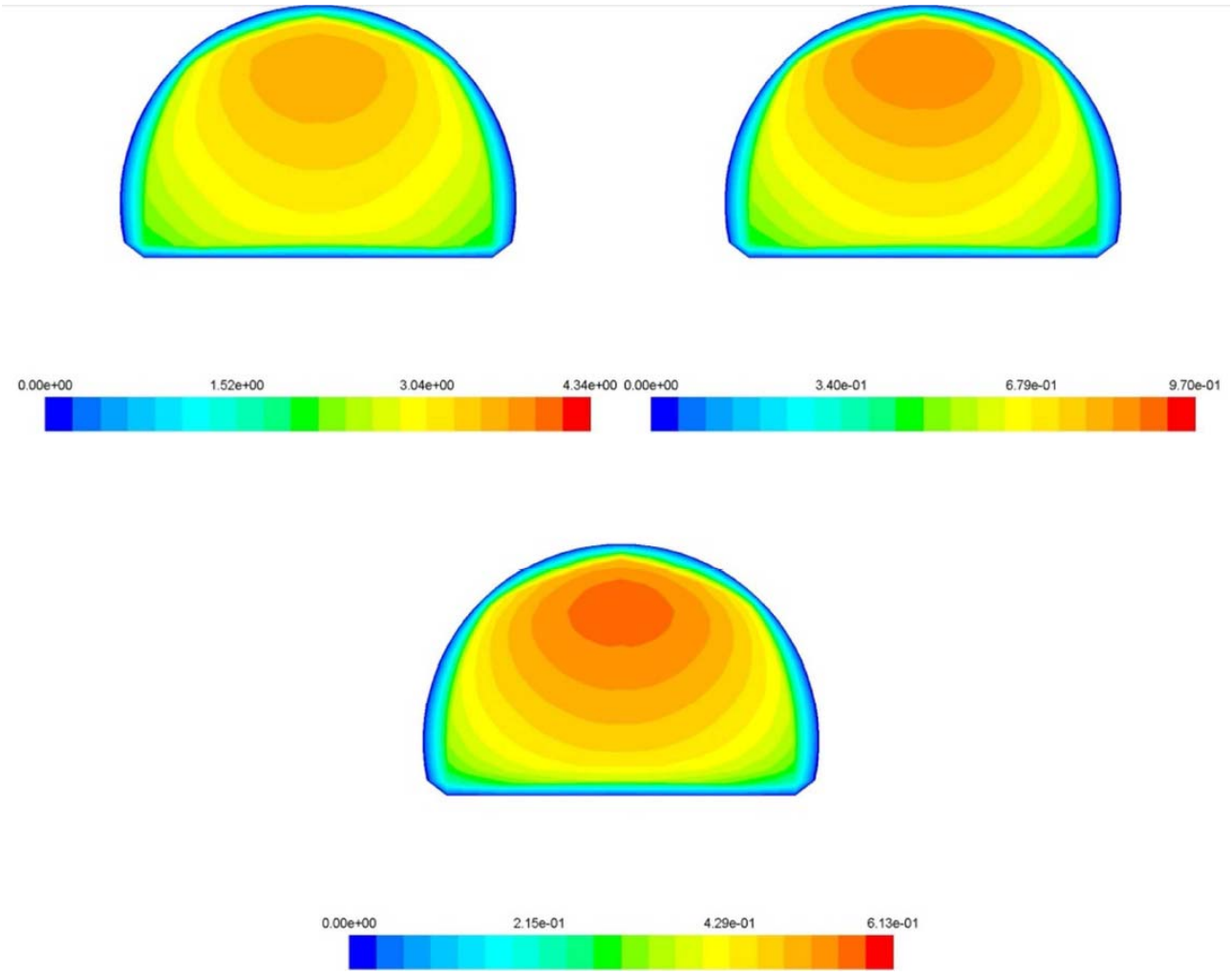

Figure 120 – Axial velocity contour on tunnel section @ 430 m: comparison between full scale (left), 1:20 reduced scale (right), 1:50 reduced scale (bottom) – traditional jet fan case

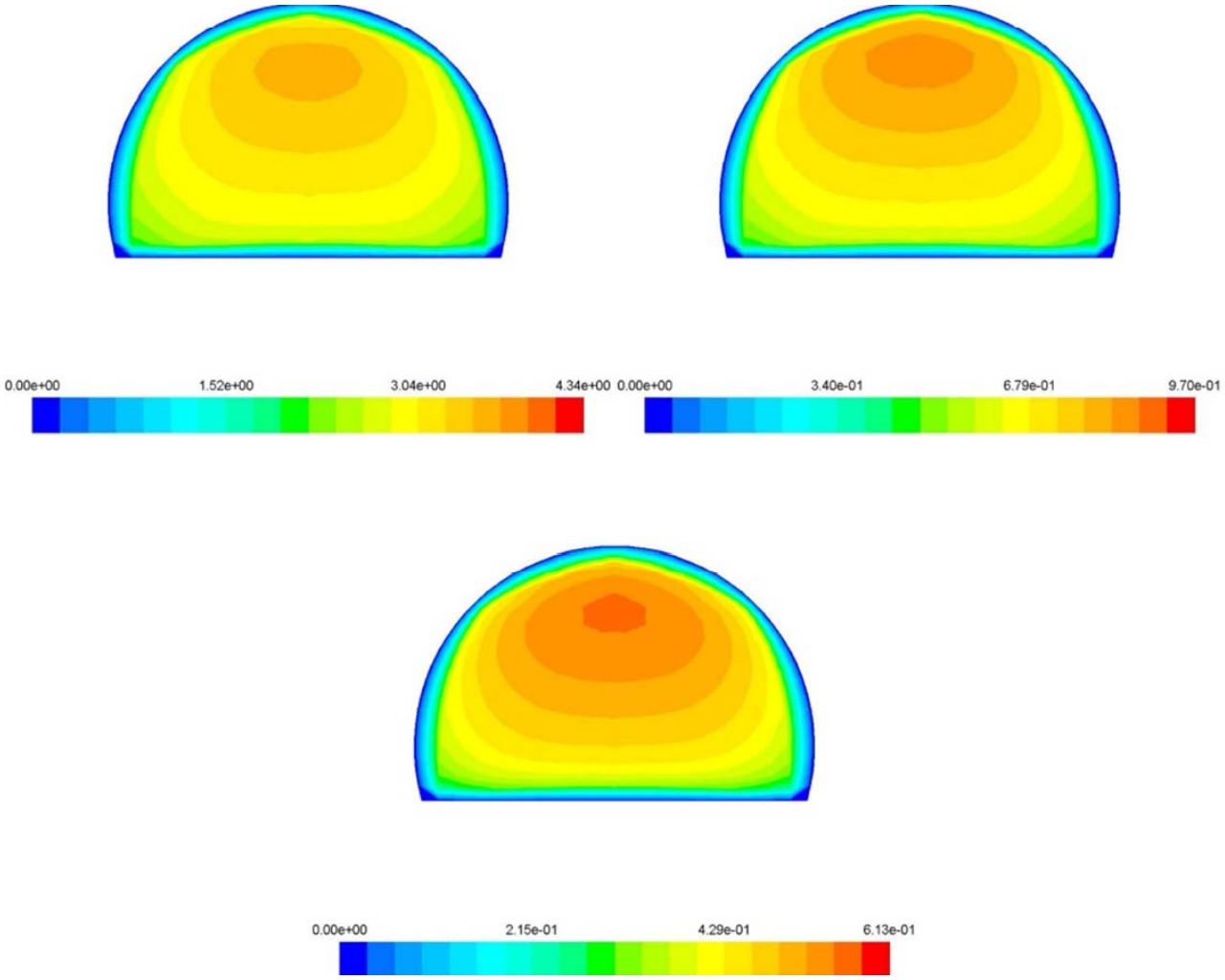

Figure 121 – Axial velocity contour on tunnel section @ 440 m: comparison between full scale (left), 1:20 reduced scale (right), 1:50 reduced scale (bottom) – traditional jet fan case

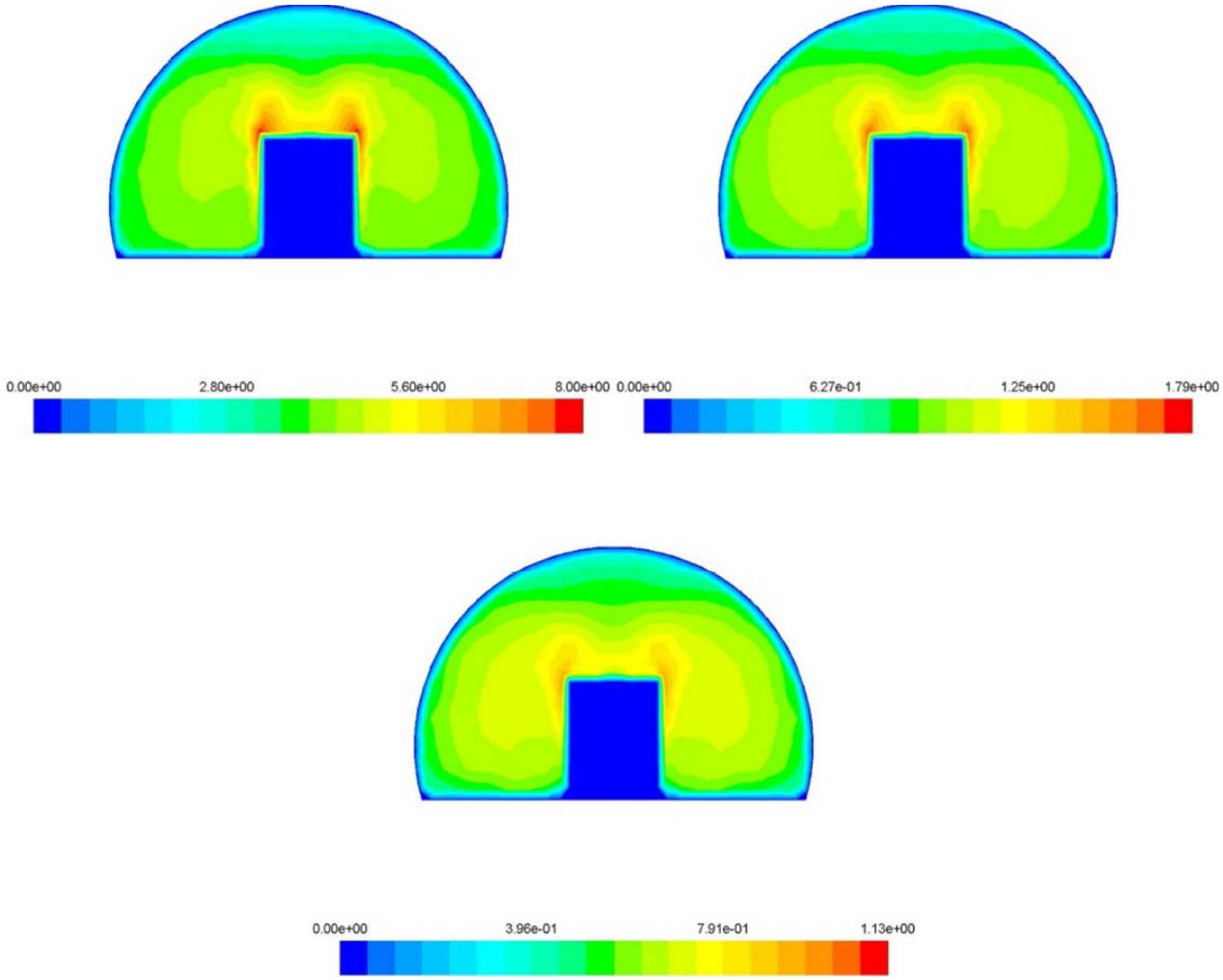

Figure 122 – Axial velocity contour on tunnel section @ 450 m: comparison between full scale (left), 1:20 reduced scale (right), 1:50 reduced scale (bottom) – traditional jet fan case

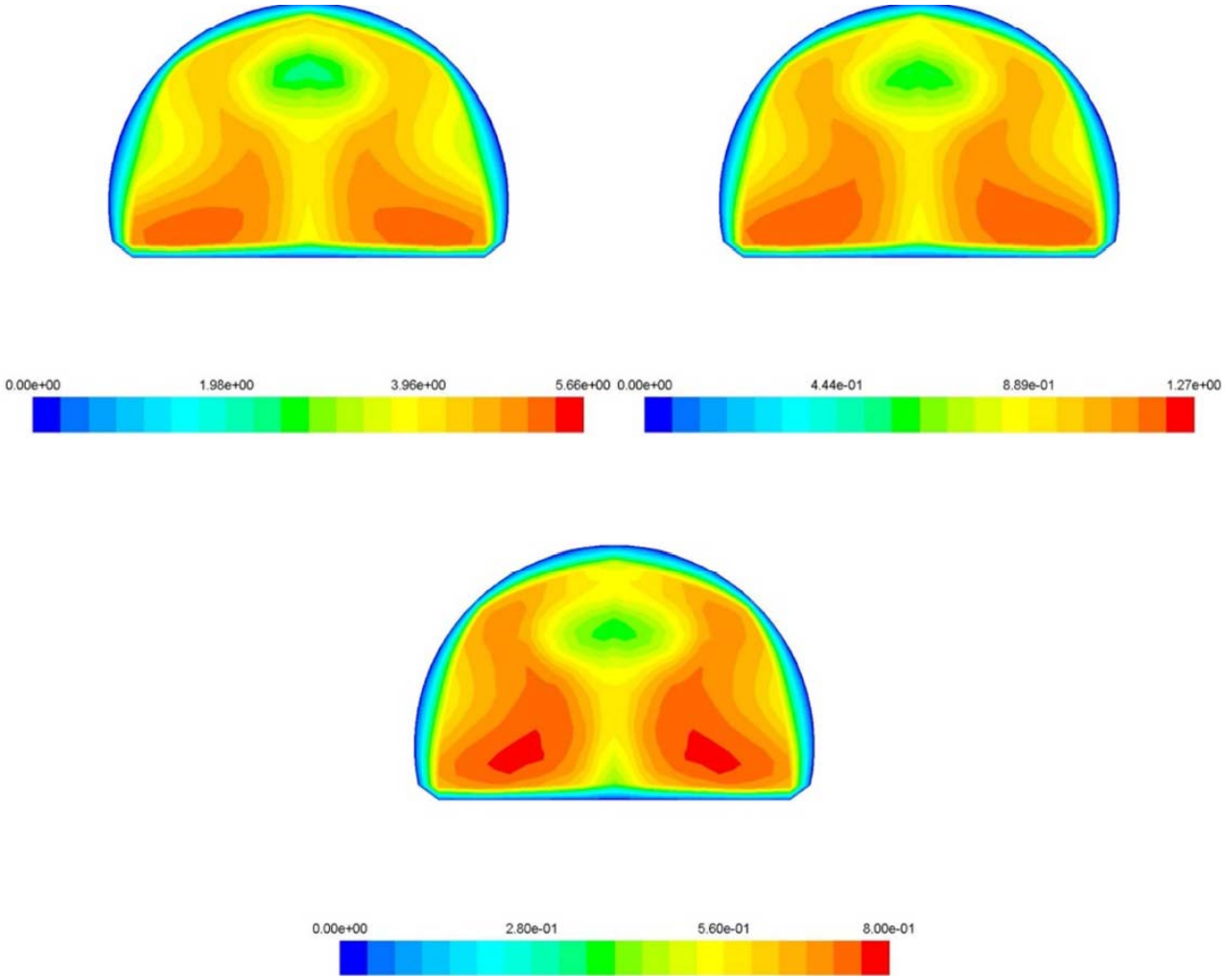

Figure 123 – Axial velocity contour on tunnel section @ 460 m: comparison between full scale (left), 1:20 reduced scale (right), 1:50 reduced scale (bottom) – traditional jet fan case

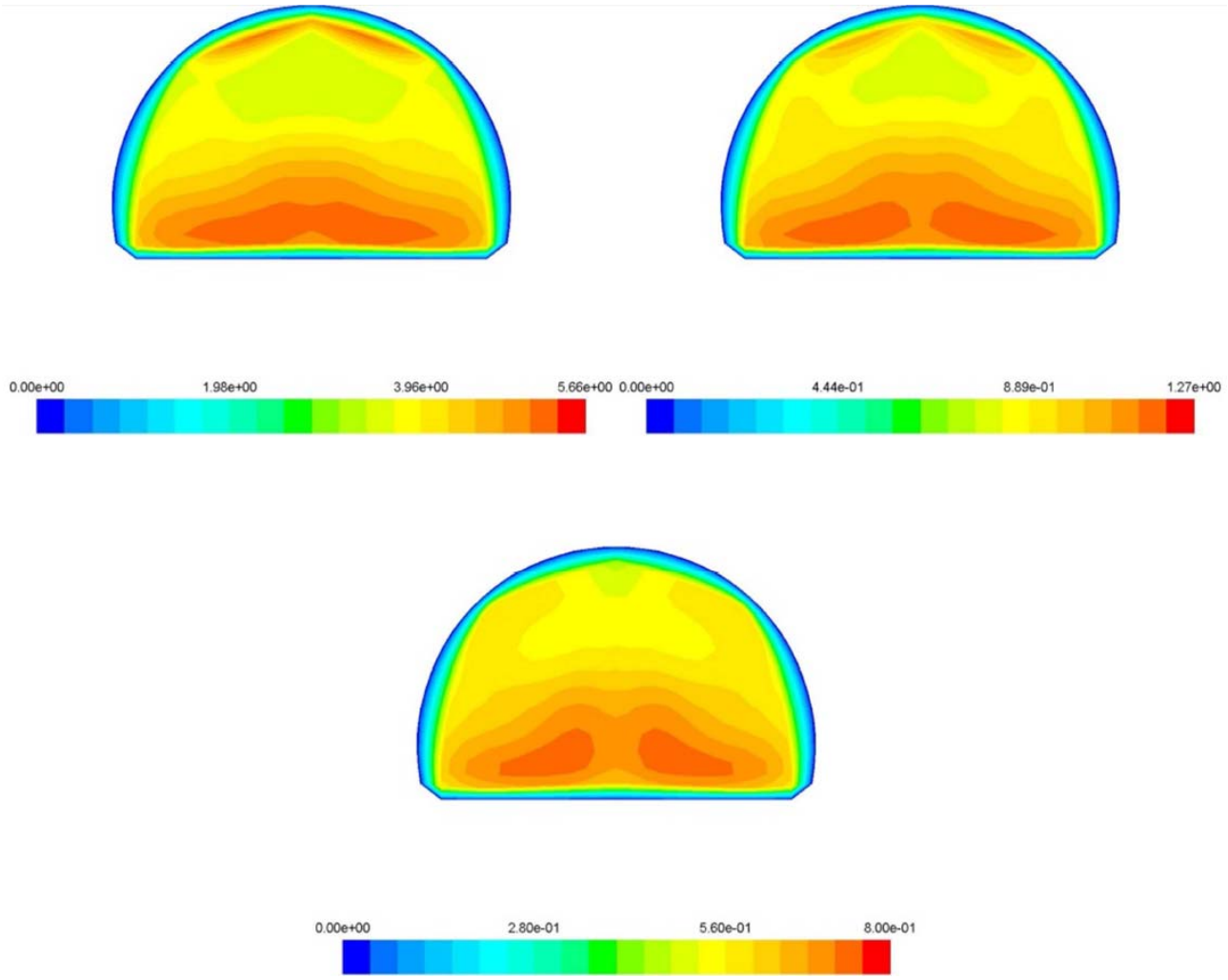

Figure 124 – Axial velocity contour on tunnel section @ 470 m: comparison between full scale (left), 1:20 reduced scale (right), 1:50 reduced scale (bottom) – traditional jet fan case

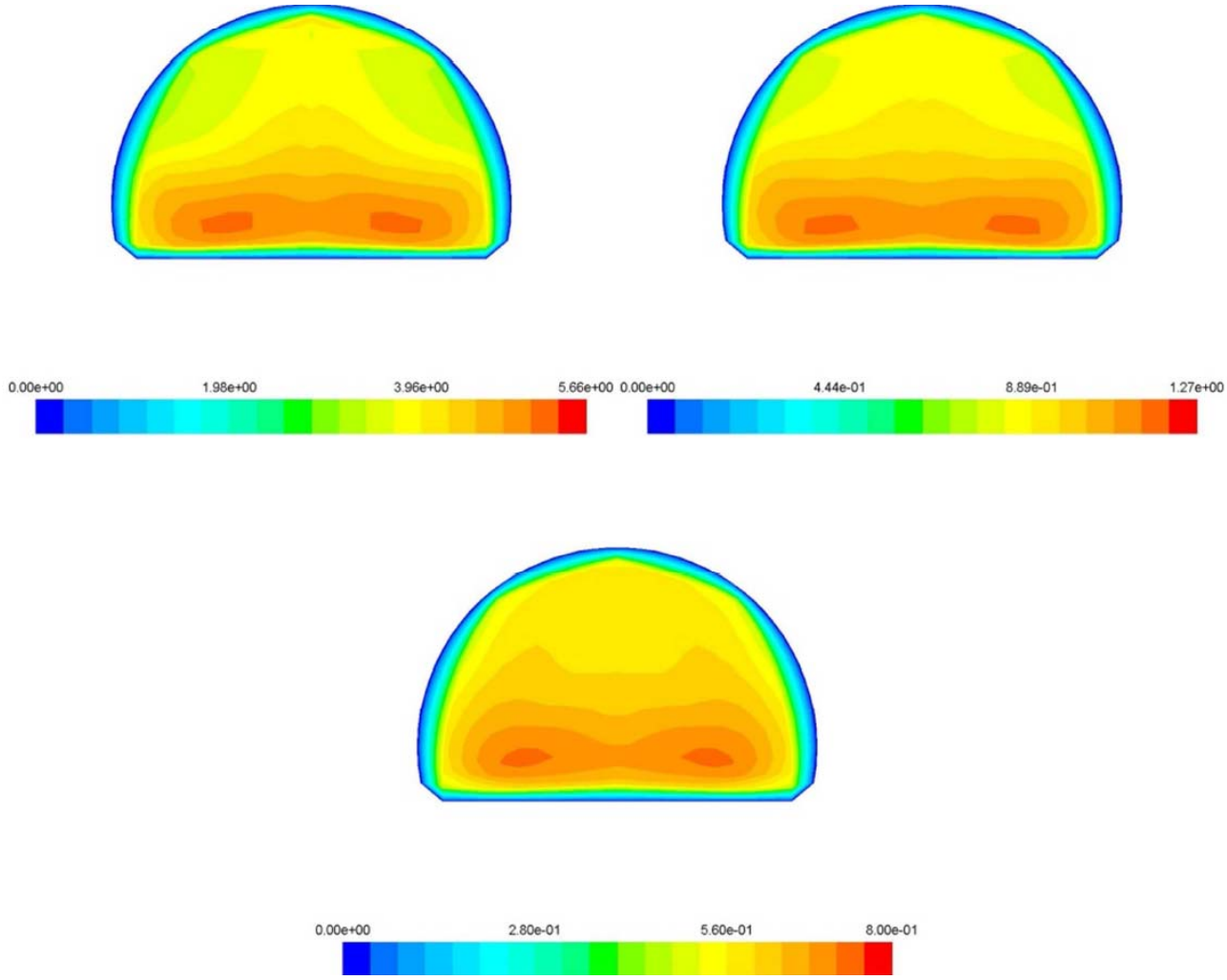

Figure 125 – Axial velocity contour on tunnel section @ 490 m: comparison between full scale (left), 1:20 reduced scale (right), 1:50 reduced scale (bottom) – traditional jet fan case

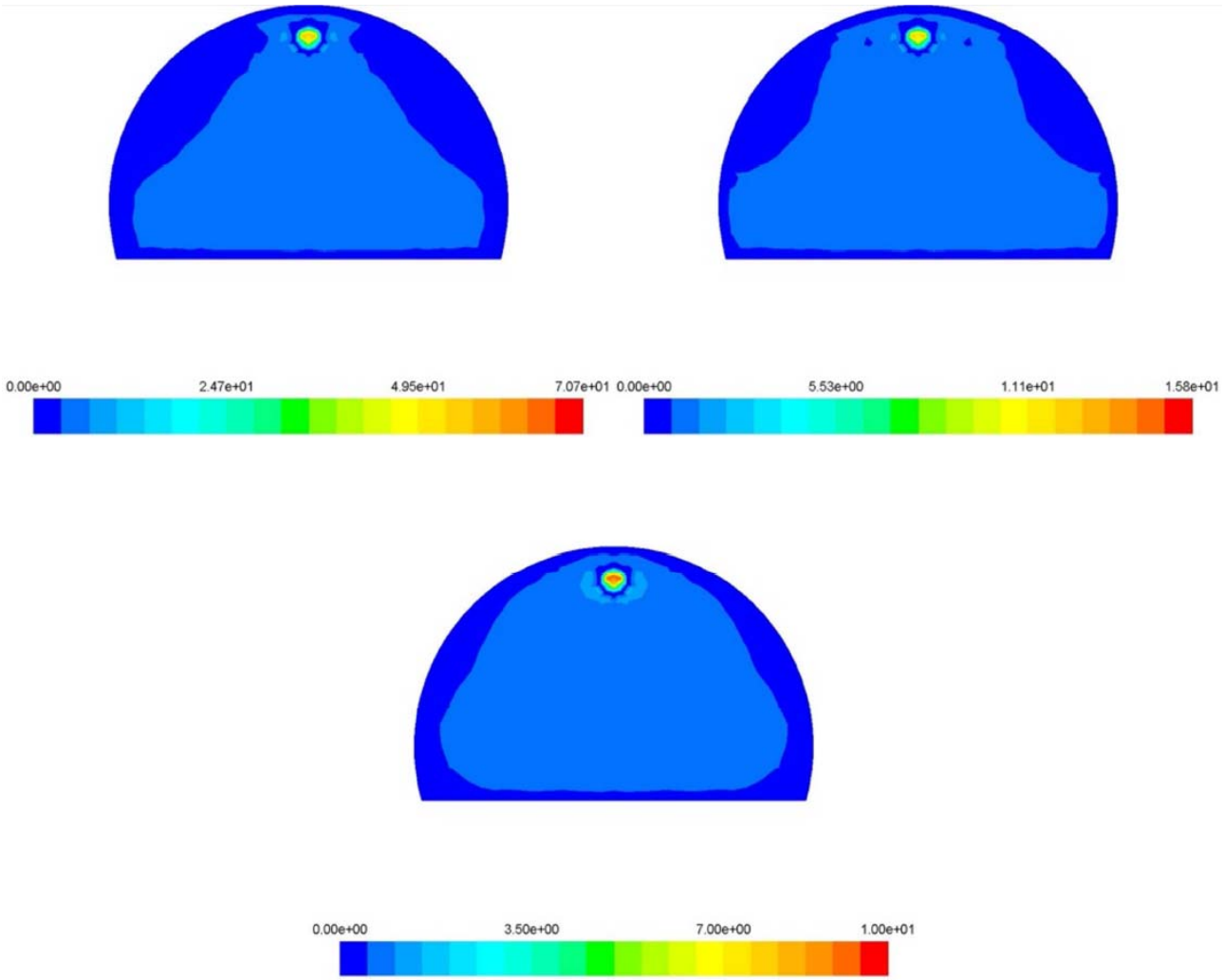

Figure 126 – Axial velocity contour on tunnel section @ 492 m: comparison between full scale (left), 1:20 reduced scale (right), 1:50 reduced scale (bottom) – traditional jet fan case

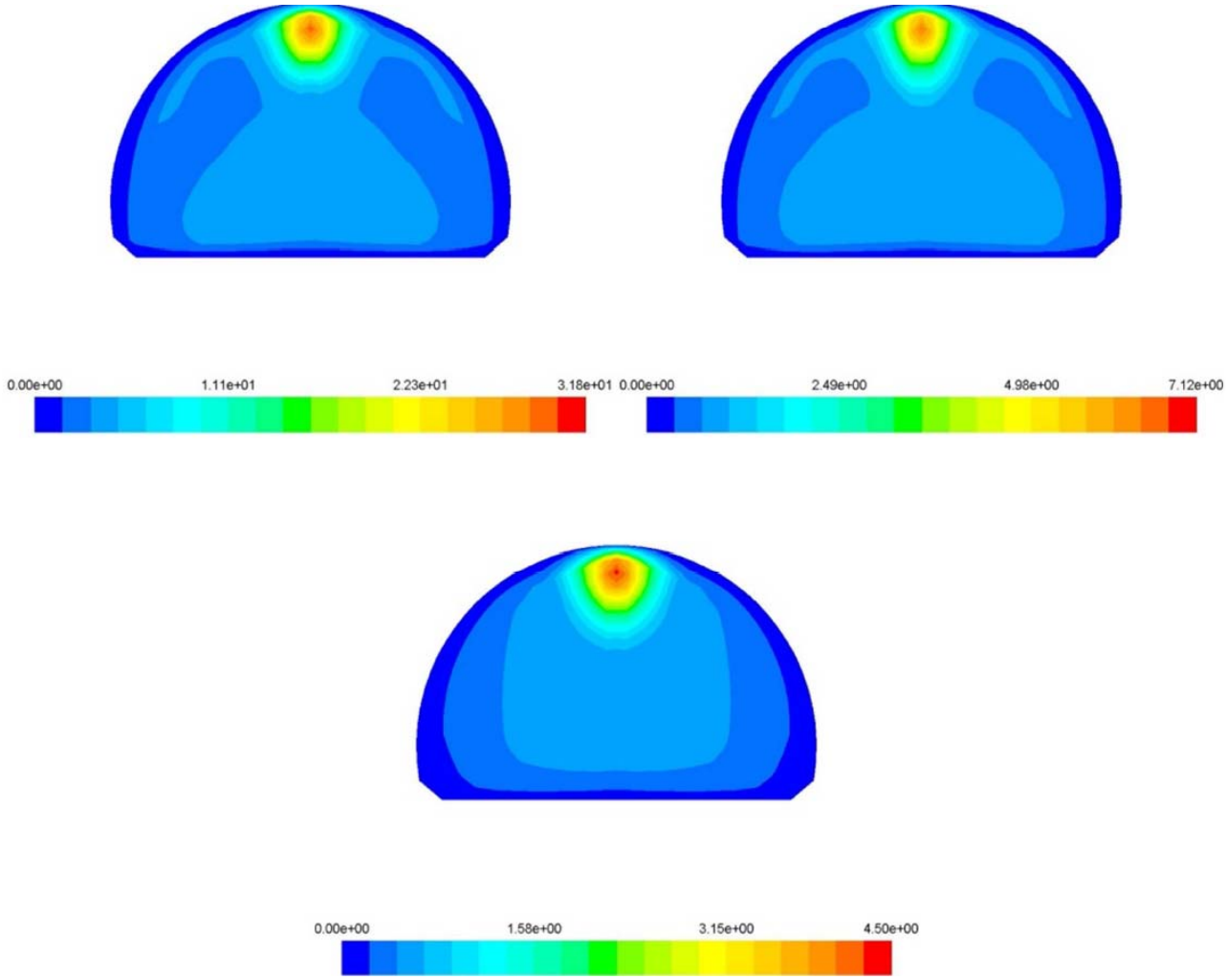

Figure 127 – Axial velocity contour on tunnel section @ 512 m: comparison between full scale (left), 1:20 reduced scale (right), 1:50 reduced scale (bottom) – traditional jet fan case

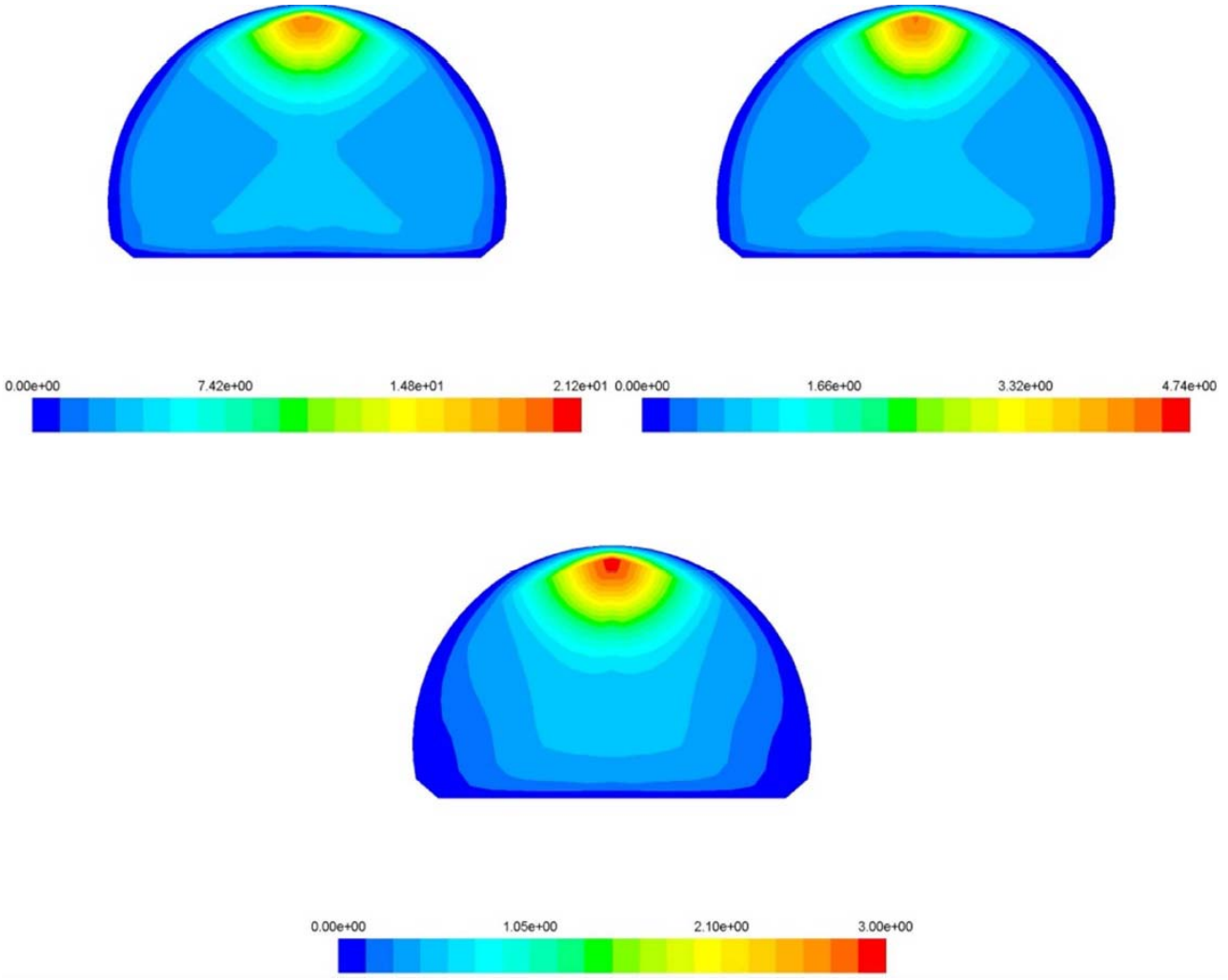

Figure 128 – Axial velocity contour on tunnel section @ 522 m: comparison between full scale (left), 1:20 reduced scale (right), 1:50 reduced scale (bottom) – traditional jet fan case

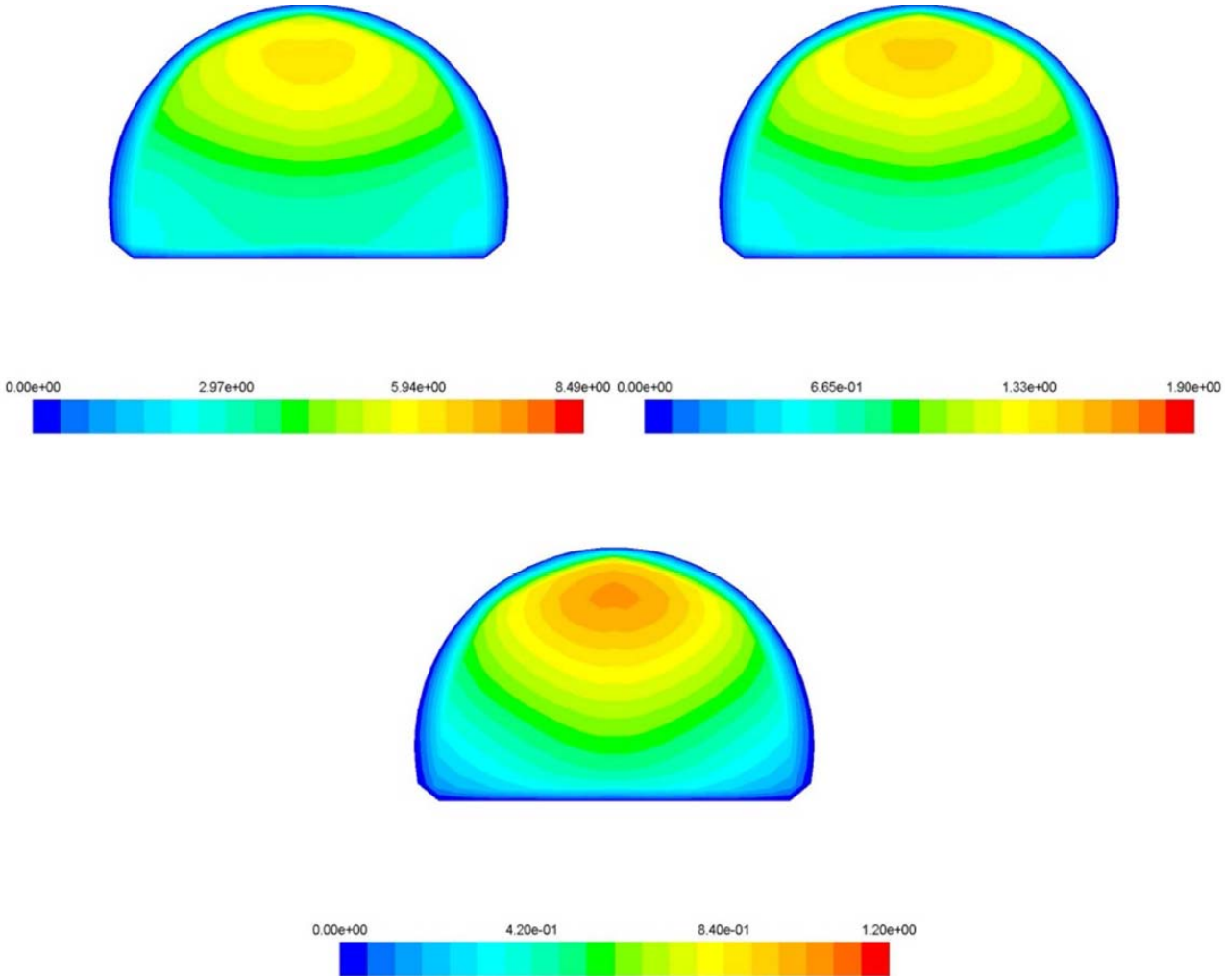

Figure 129 – Axial velocity contour on tunnel section @ 602 m: comparison between full scale (left), 1:20 reduced scale (right), 1:50 reduced scale (bottom) – traditional jet fan case

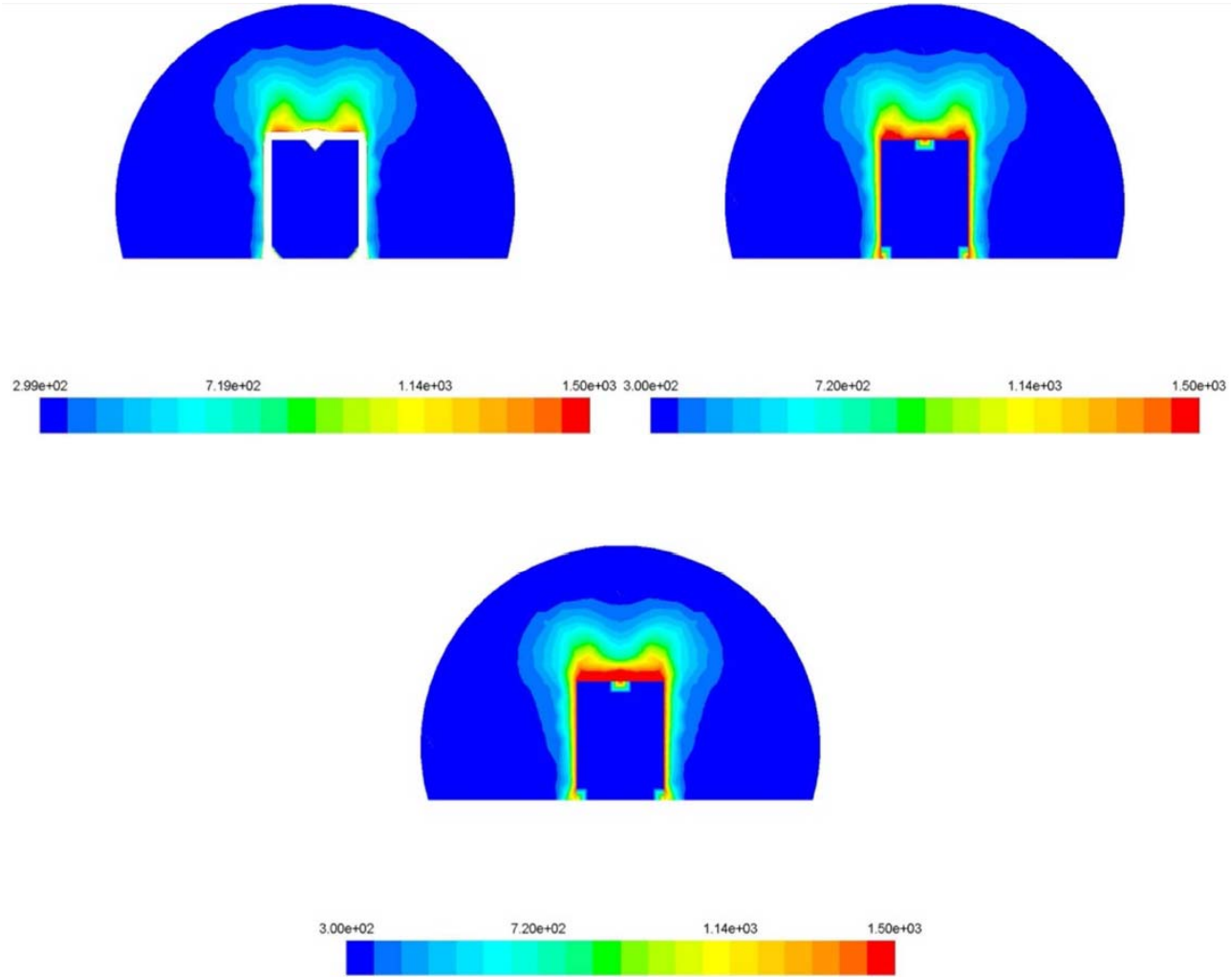

Figure 130 – Temperature contour on tunnel section @ 450 m: comparison between full scale (left), 1:20 reduced scale (right), 1:50 reduced scale (bottom) – traditional jet fan case

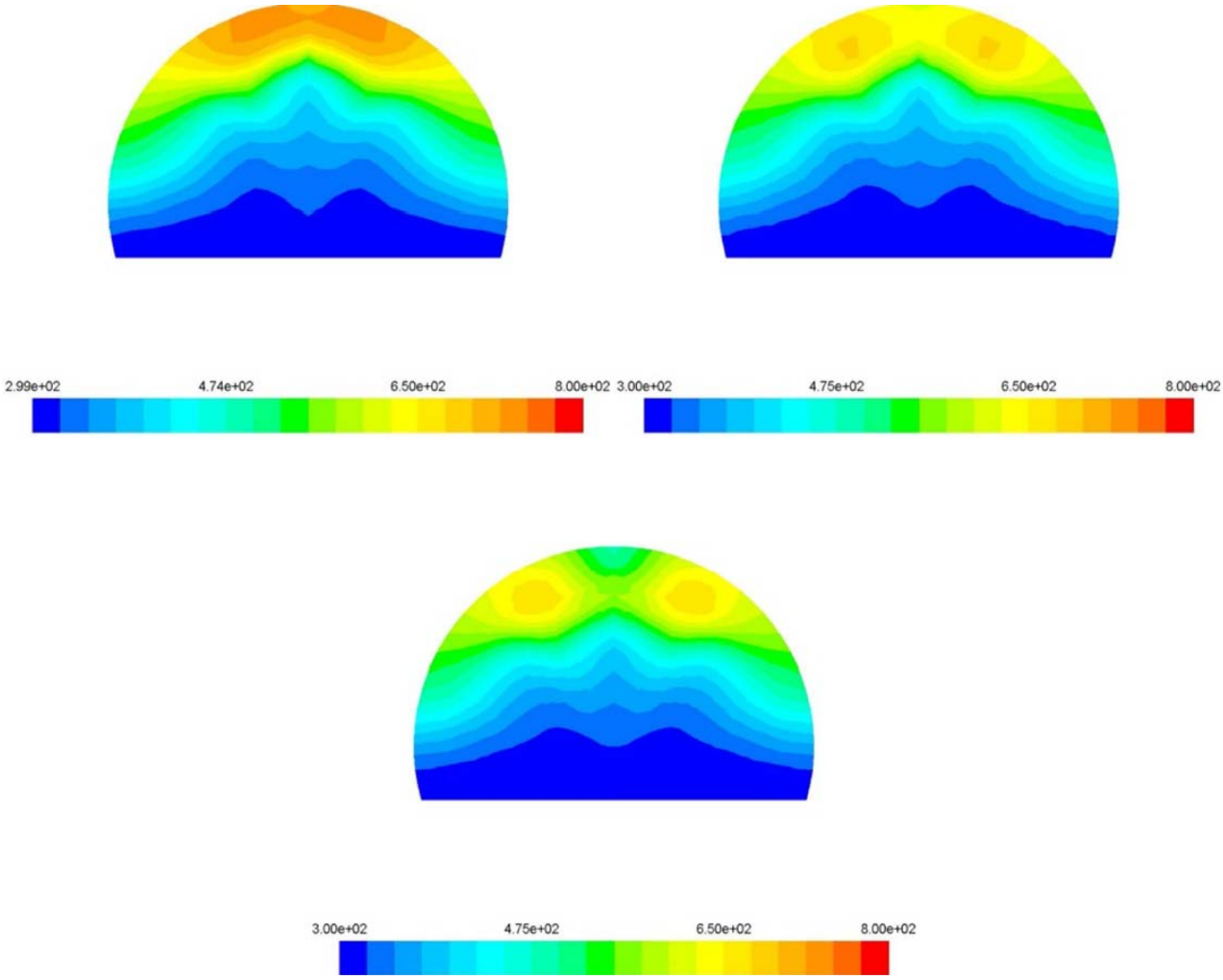

Figure 131 – Temperature contour on tunnel section @ 460 m: comparison between full scale (left), 1:20 reduced scale (right), 1:50 reduced scale (bottom) – traditional jet fan case

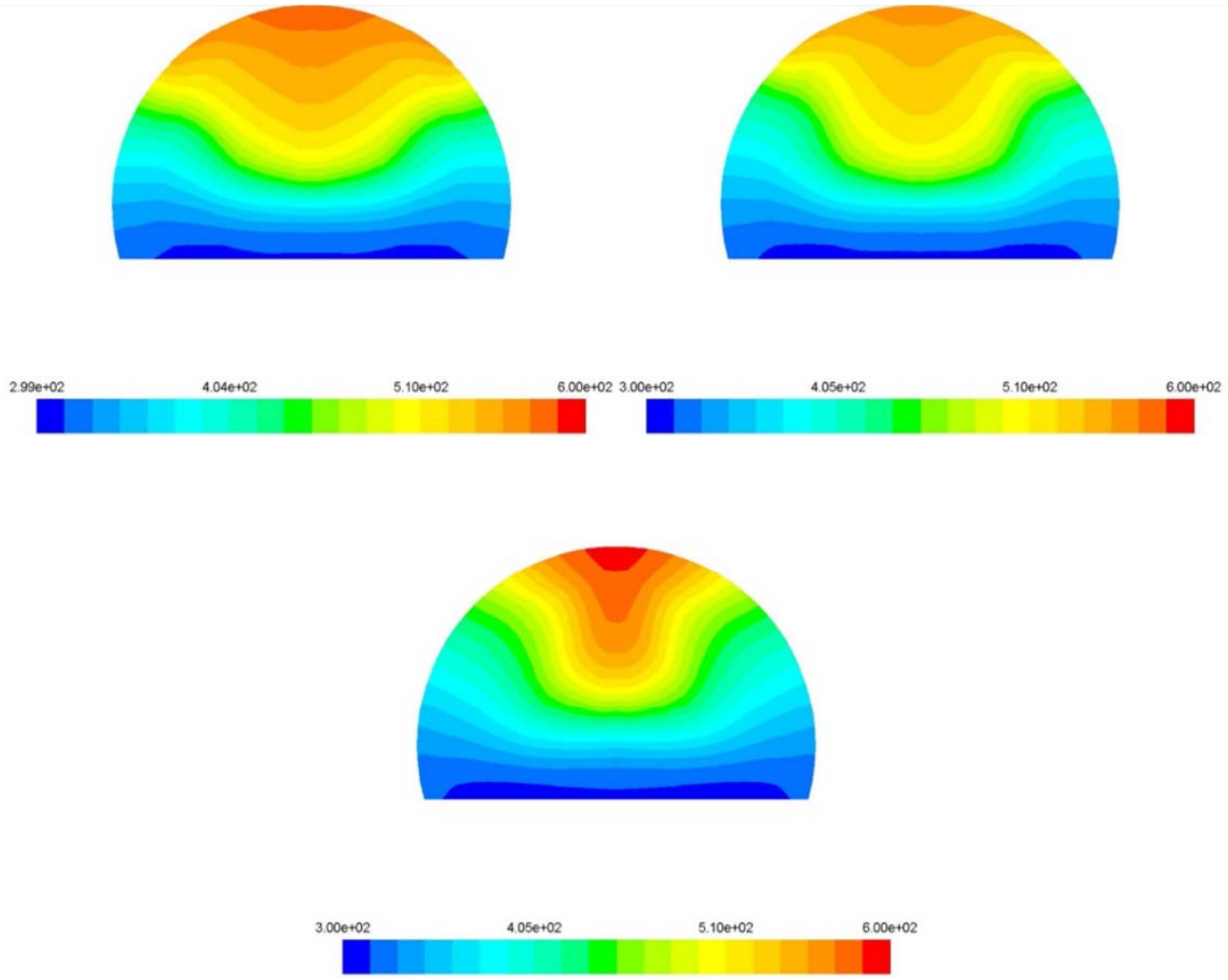

Figure 132 – Temperature contour on tunnel section @ 480 m: comparison between full scale (left), 1:20 reduced scale (right), 1:50 reduced scale (bottom) – traditional jet fan case

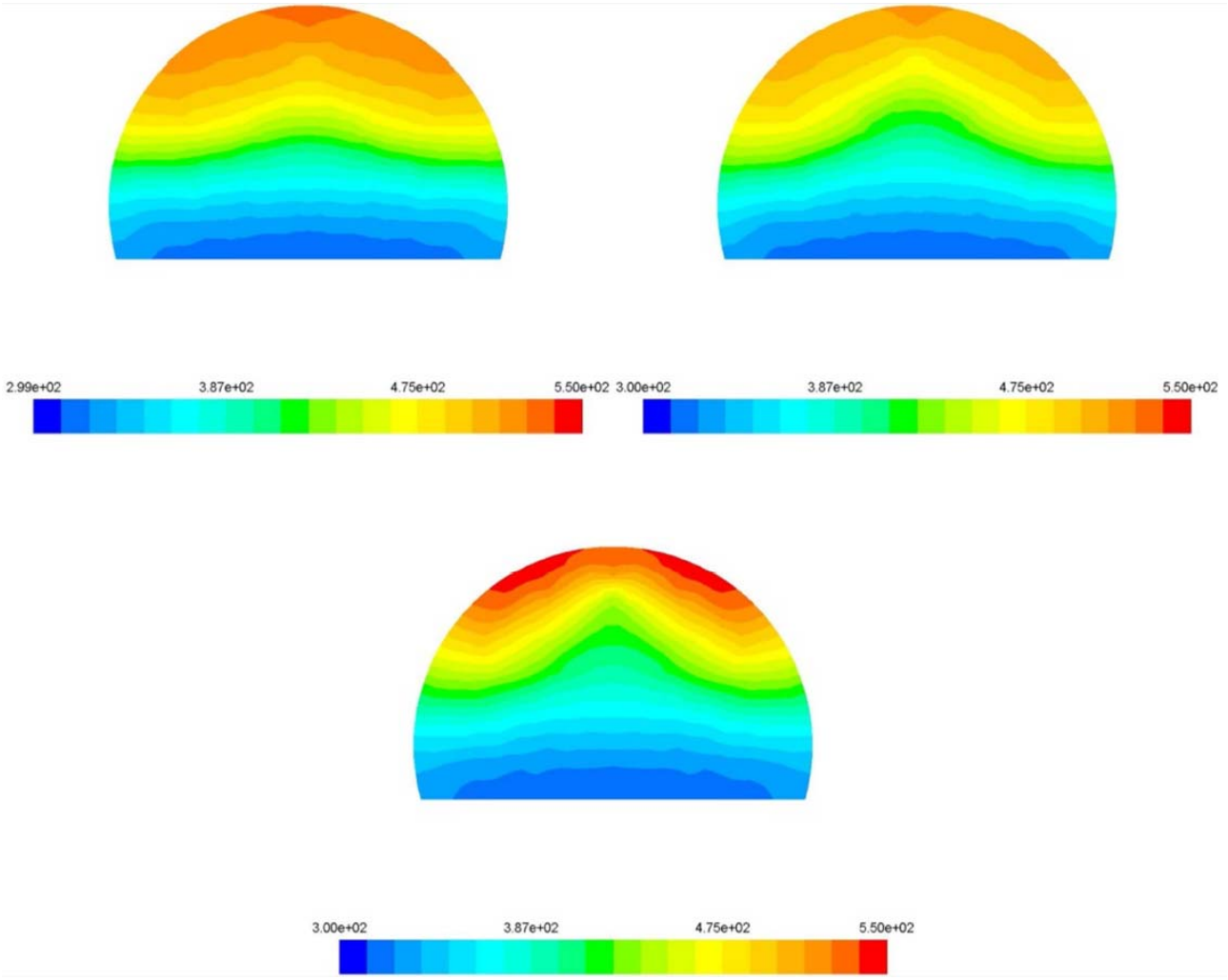

Figure 133 – Temperature contour on tunnel section @ 498 m: comparison between full scale (left), 1:20 reduced scale (right), 1:50 reduced scale (bottom) – traditional jet fan case

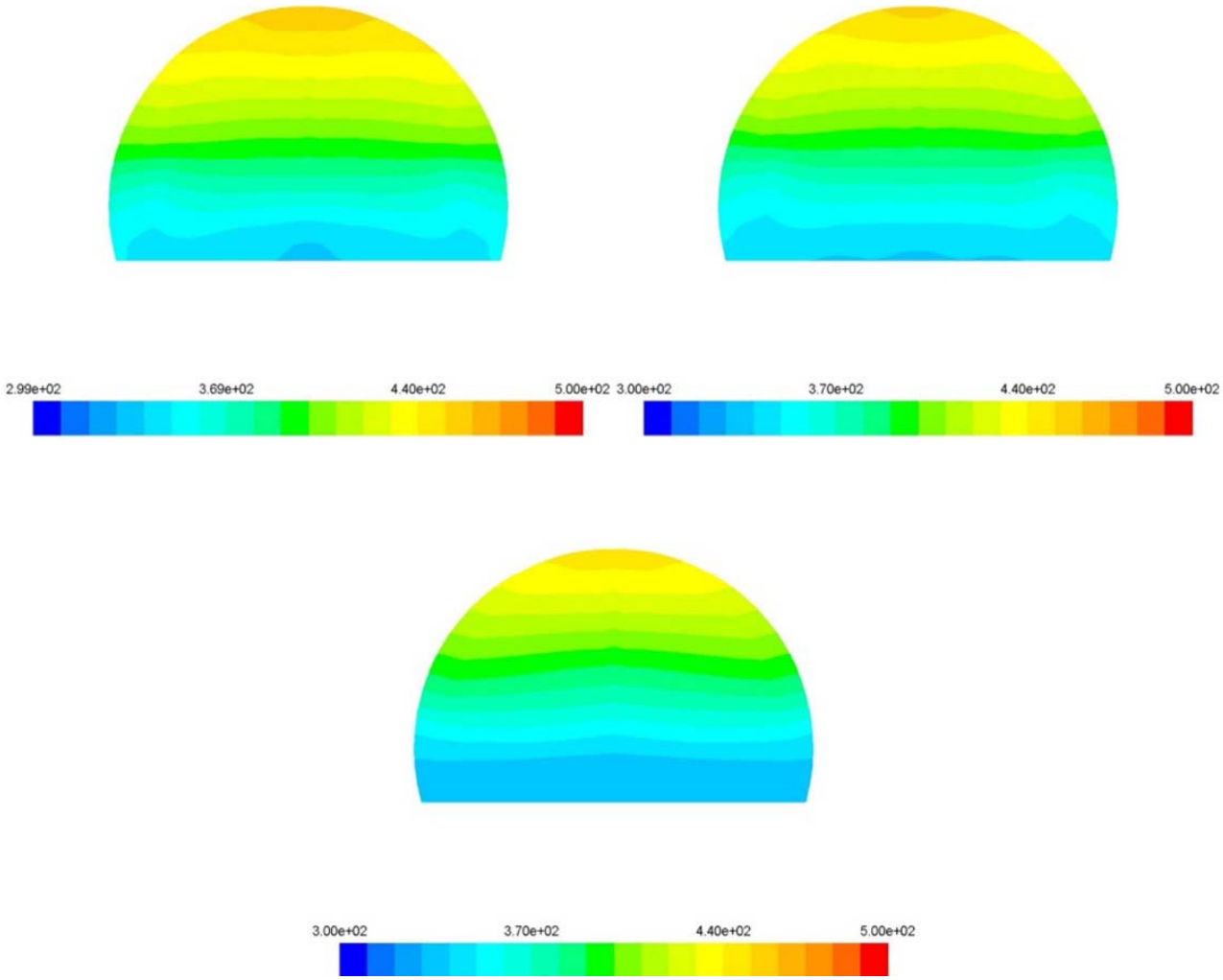

Figure 134 – Temperature contour on tunnel section @ 552 m: comparison between full scale (left), 1:20 reduced scale (right), 1:50 reduced scale (bottom) – traditional jet fan case

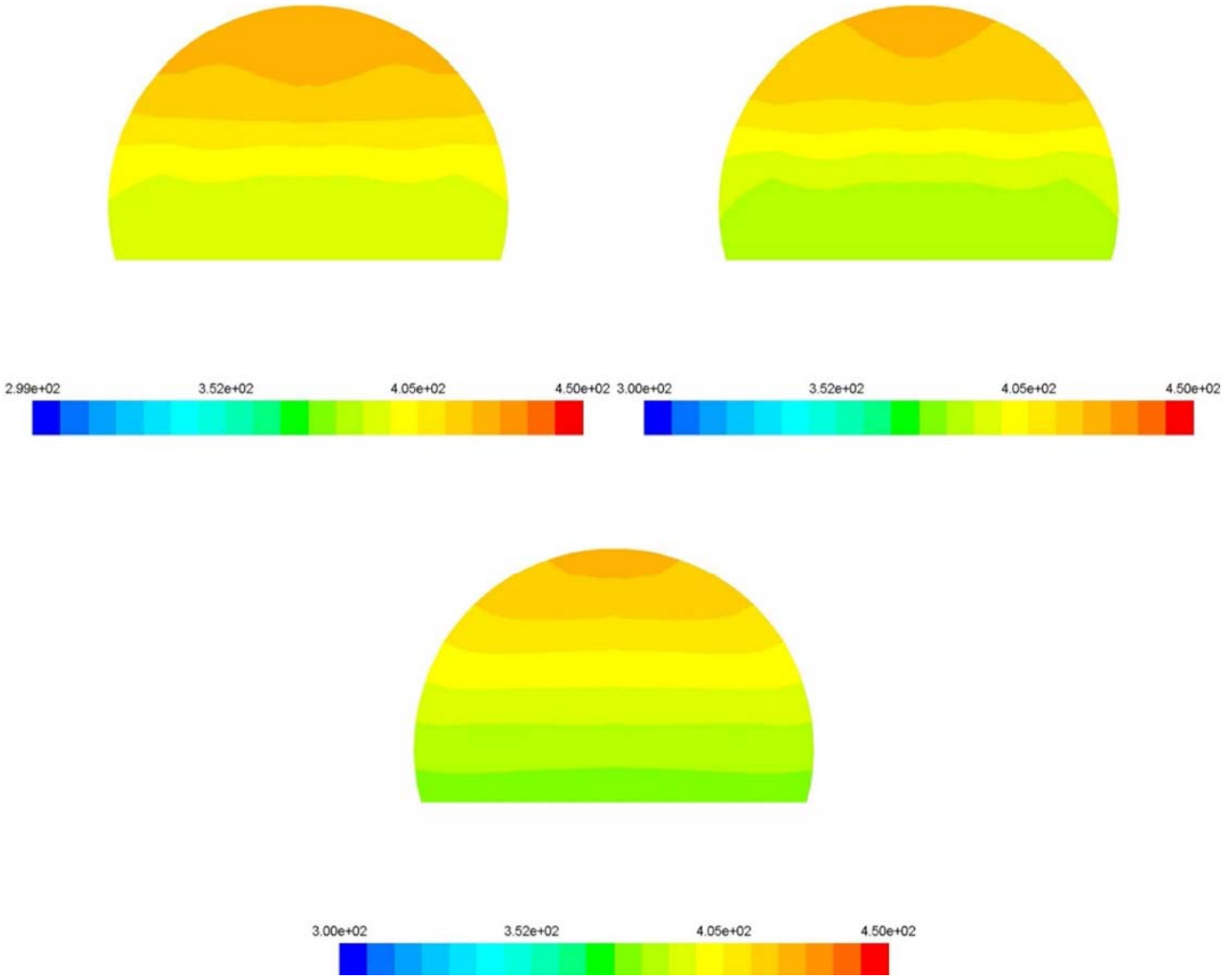

Figure 135 – Temperature contour on tunnel section @ 652 m: comparison between full scale (left), 1:20 reduced scale (right), 1:50 reduced scale (bottom) – traditional jet fan case

As results, the model used to the fire scenario gives not realistic results since temperature values reaches locally not real values. Moreover, results show that temperature peaks decrease with a lower scale factor. Simulation with banana jet fan are carried out considering the combustion model only.

7.1.7. Case 2 – Mesh and boundary conditions

As shown in par. 7.1.4, the combustion model is introduced in the analysis. The same mesh considered in "Case 1" analysis, is now considered. The Discrete Phase Model and the species transport model are adopted in order to simulate the liquid fuel particle vaporization and combustion; the liquid n-heptane species are chosen as fuel in the combustion process.

The fire is modelled as liquid diffusive combustion process due to an instantaneous temperature increase. A simplified model is chosen considering only two substances: oxidant and liquid fuel is introduced in the domain trough the injection of a dispersed liquid second phase constituted by smaller particles, from the HGV up surface.

Model boundary conditions are shown in following Table 18 and Table 19.

Table 18 – Boundary conditions – Traditional jet fan case

	Full scale	Reduced scale (λ=20)
Solver	Pressure based	Pressure based
Fluid's material	Air	Air
Pressure drop	2300 Pa	64 Pa
Fluid temperature	300 K	300 K
Gauge pressure at Inlet and outlet tunnel section	0 Pa	0 Pa
Floor roughness,	0.01 m	0.0015 m
Roof roughness	0.03 m	0.0005 m
Fuel	n-heptane	n-heptane
Fuel mass flow rate	0.2 kg/s	0.000112 kg/s
Fuel injecting velocity	0 m/s	0 m/s

Table 19 – Boundary conditions – Alternative jet fan case

	Full scale	Reduced scale (λ=20)
Solver	Pressure based	Pressure based
Fluid's material	Air	Air
Pressure drop	1800 Pa	90 Pa
Fluid temperature	300 K	300 K
Gauge pressure at Inlet and outlet tunnel section	0 Pa	0 Pa
Floor roughness,	0.01 m	0.0015 m
Roof roughness	0.03 m	0.0005 m
Fuel	n-heptane	n-heptane
Fuel mass flow rate	0.2 kg/s	0.000112 kg/s
Fuel injecting velocity	0 m/s	0 m/s

Finally, the EDC model is chosen to model the turbulence-chemistry interaction.

7.1.8. Case 2 – Results

In following figures, results for both traditional and alternative jet fans are presented. A good performance for both temperature and velocity fields is reached; in particular, the considered combustion model leads to maximum temperature values of 2000÷2400 K in line with realistic previsions.

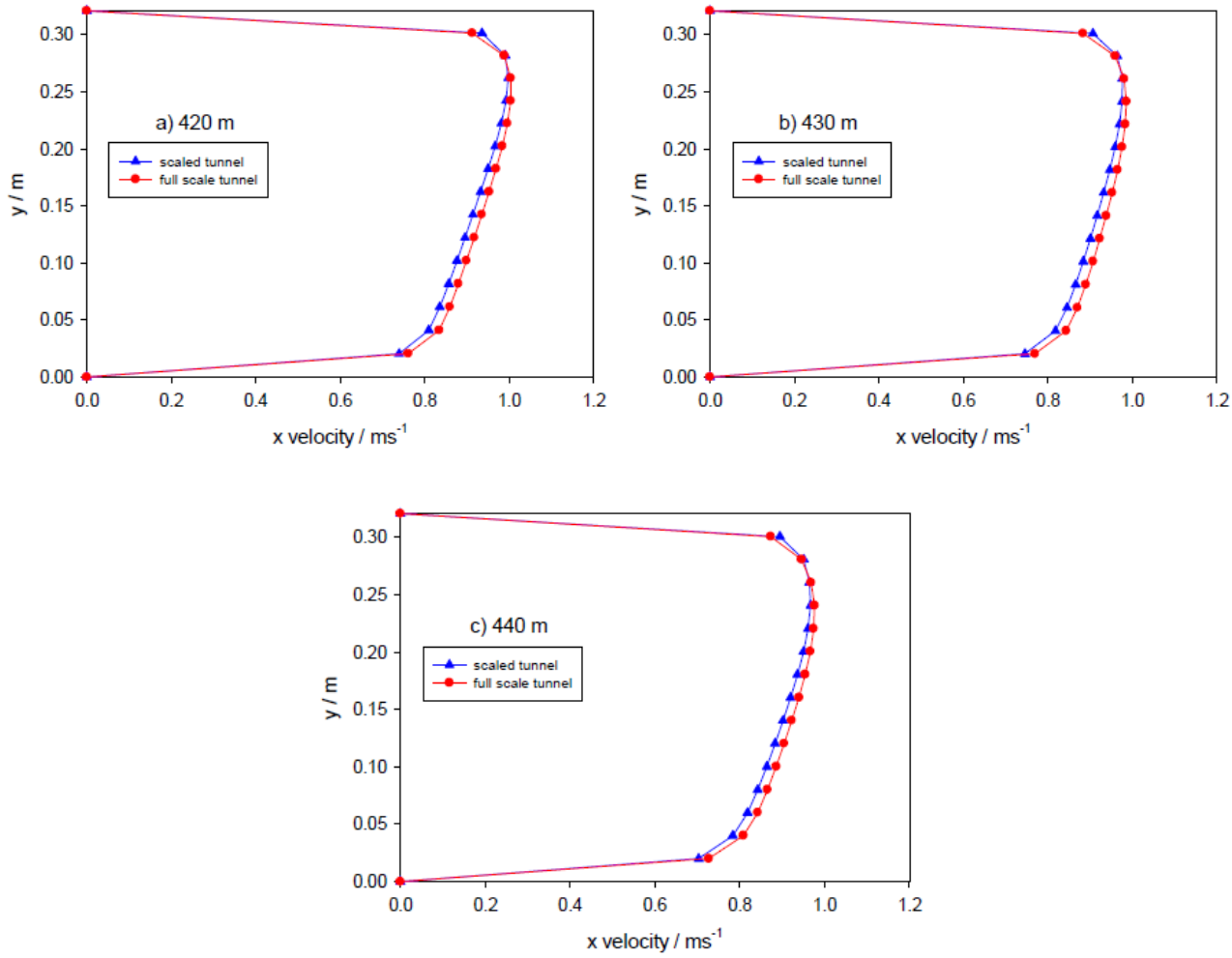

Figure 136 – Axial velocity profile on tunnel symmetry plane at (a) 10 m, (b) 20 m, (c) 30 m before the HGV: comparison between full and reduced (1:20) model – traditional jet fan case

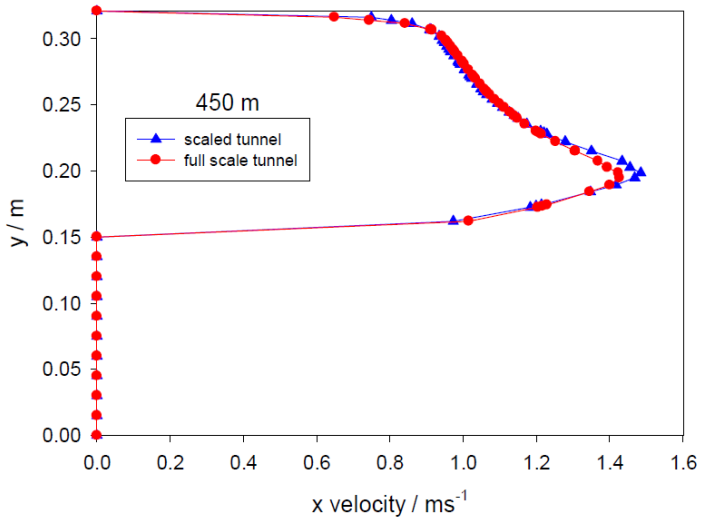

Figure 137 – Axial velocity profile on tunnel symmetry plane in correspondence of the HGV: comparison between full and reduced (1:20) model – traditional jet fan case

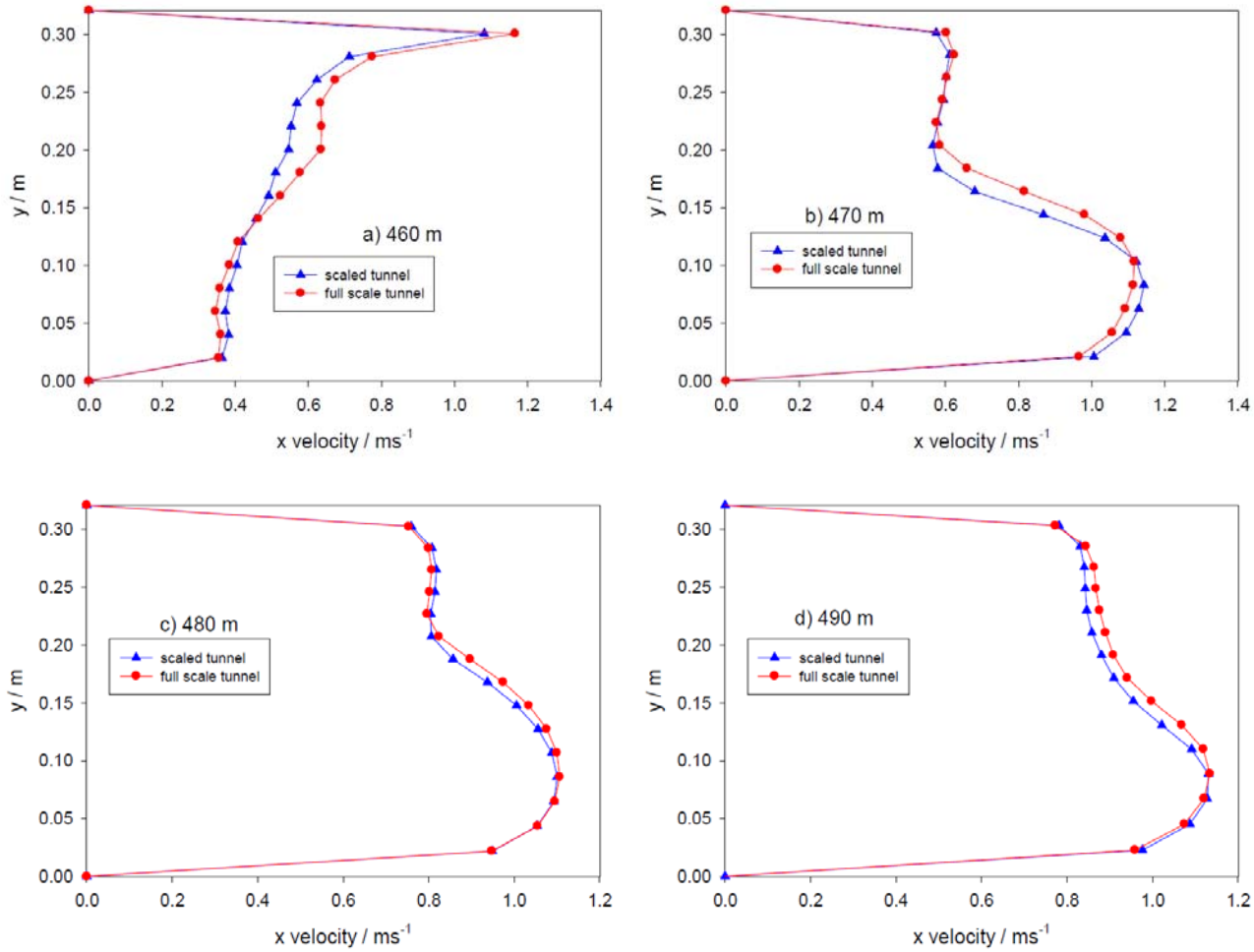

Figure 138 – Axial velocity profile on tunnel symmetry plane at (a) 10 m, (b) 20 m, (c) 30 m, (d) 40 m after the HGV: comparison between full and reduced (1:20) model – traditional jet fan case

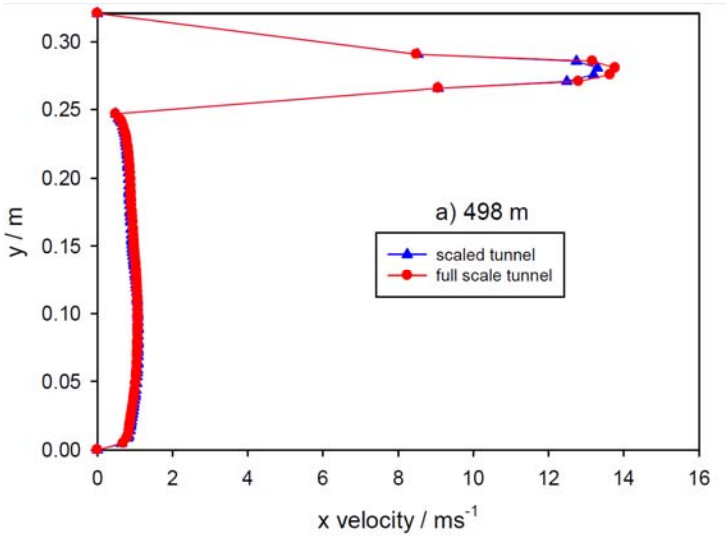

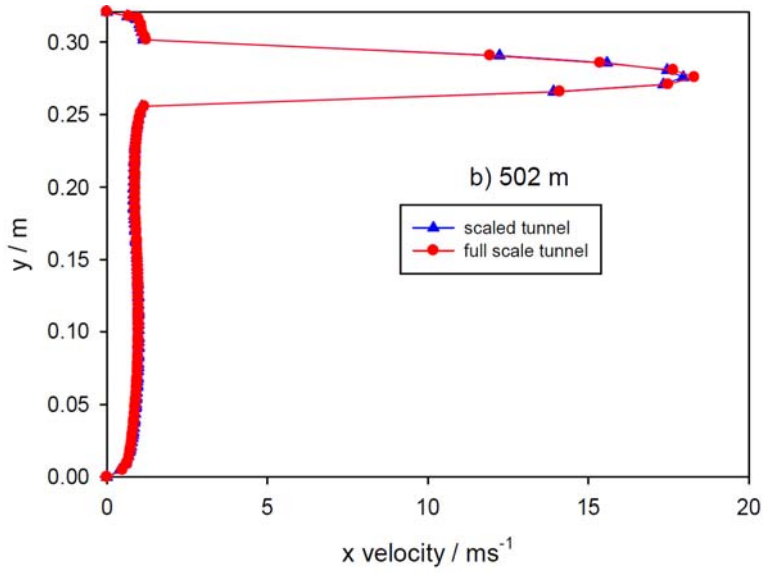

Figure 139 – Axial velocity profile on tunnel symmetry plane at (a) inlet and (b) outlet section of 3rd jet fan: comparison between full and reduced (1:20) model – traditional jet fan case

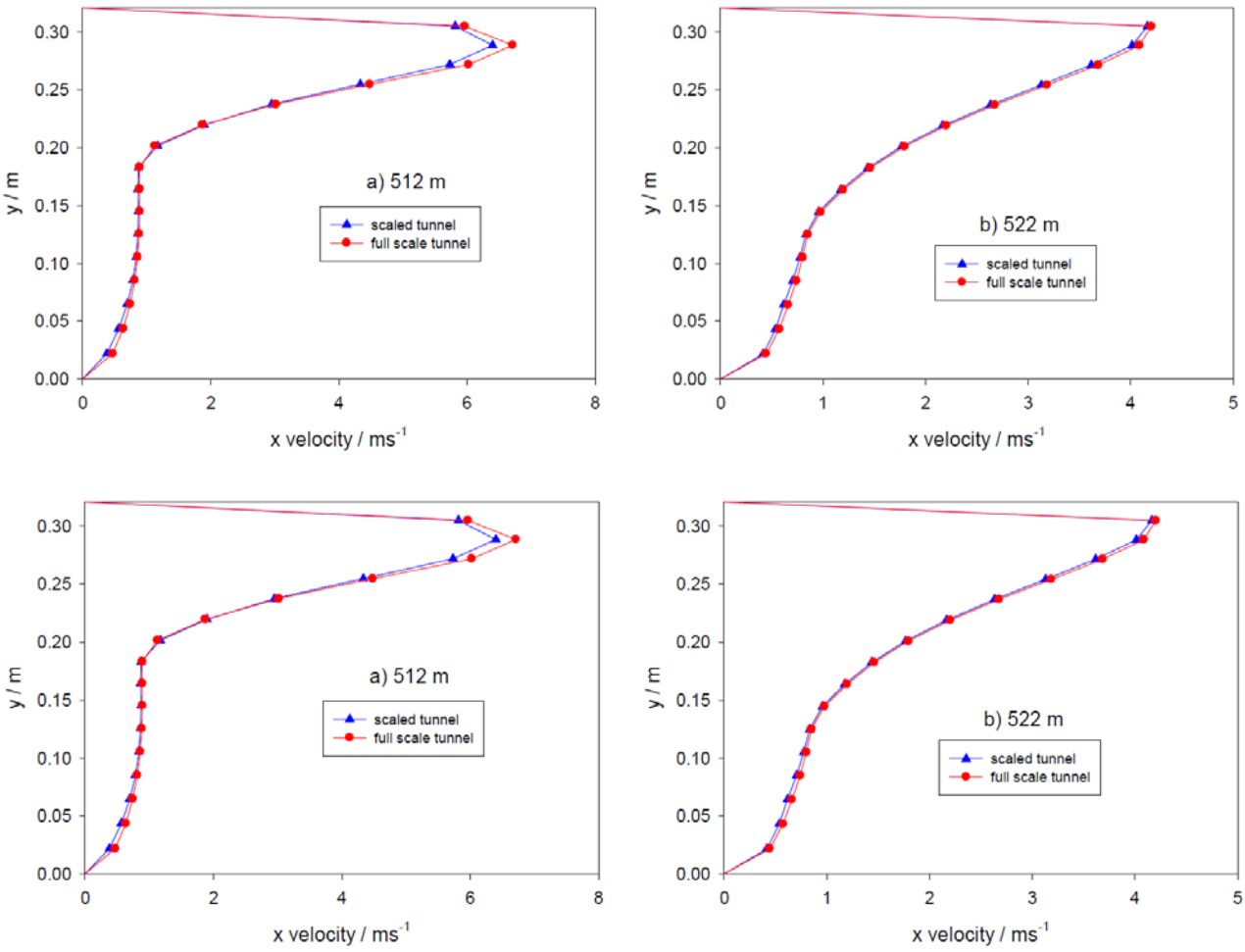

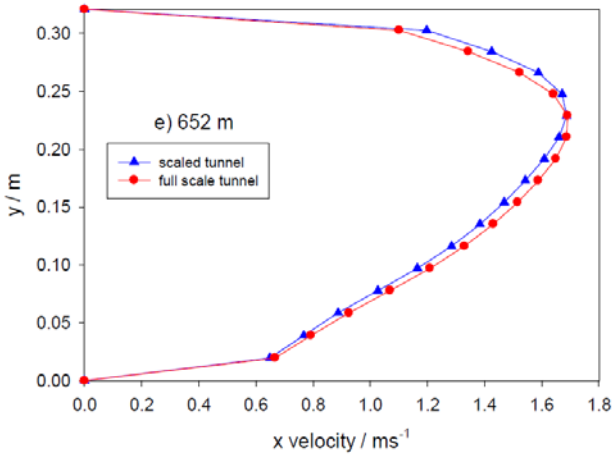

Figure 140 – Axial velocity profile on tunnel symmetry plane at (a) 10 m, (b) 20 m, (c) 50 m, (d) 100 m, (e) 150 m after the HGV: comparison between full and reduced (1:20) model – traditional jet fan case

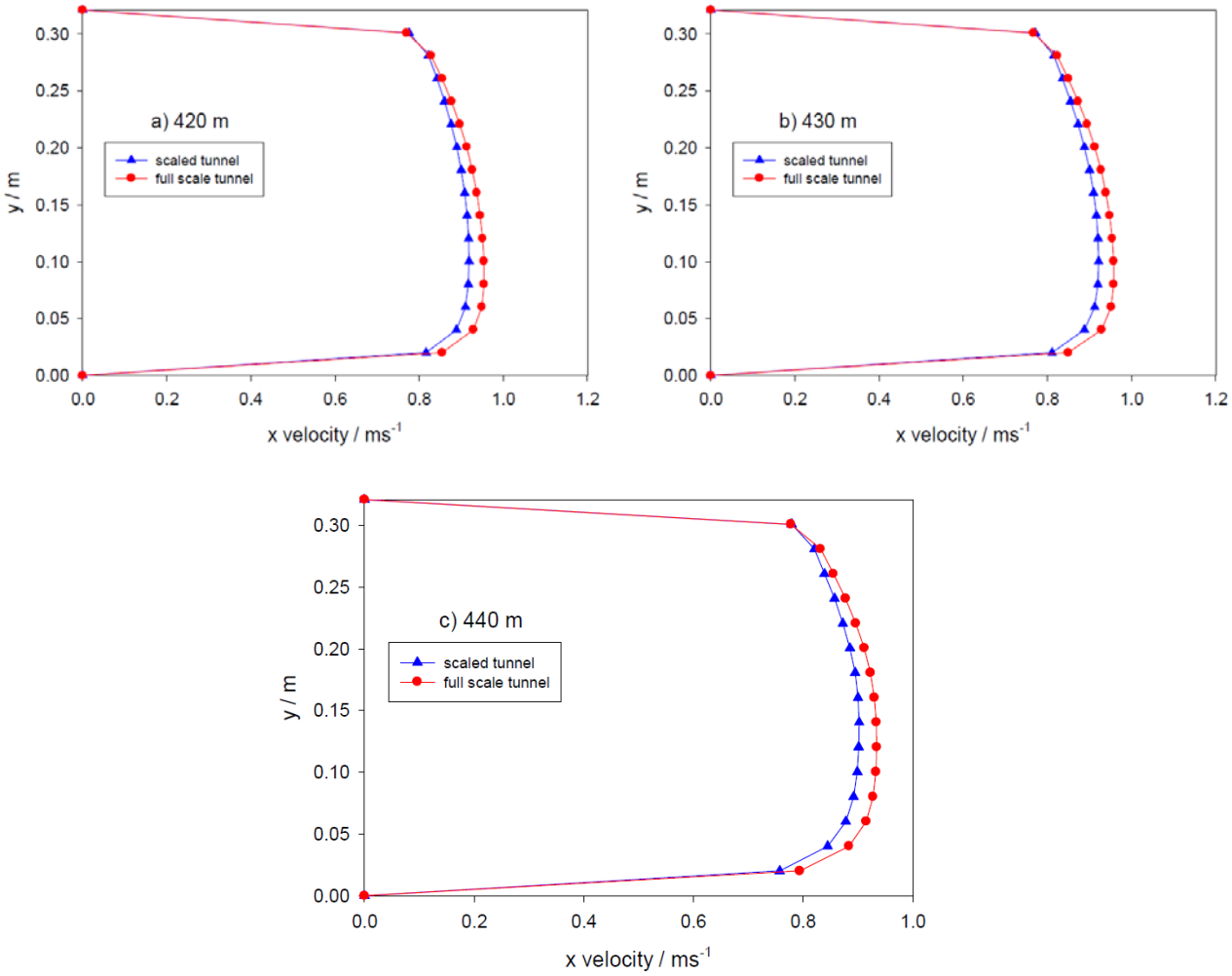

Figure 141 – Axial velocity profile on tunnel symmetry plane at (a) 10 m, (b) 20 m, (c) 30 m before the HGV: comparison between full and reduced (1:20) model – alternative jet fan case

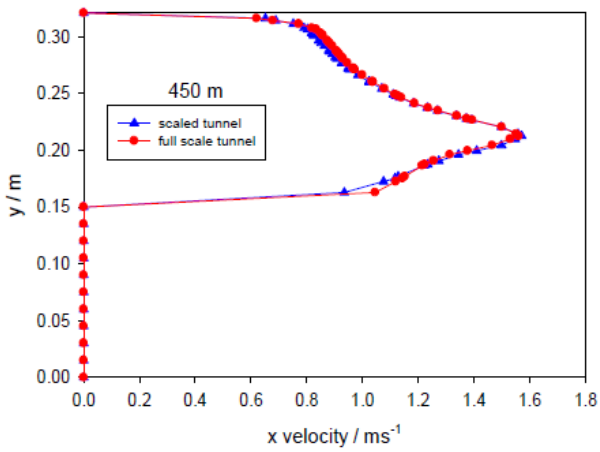

Figure 142 – Axial velocity profile on tunnel symmetry plane in correspondence of the HGV: comparison between full and reduced (1:20) model – alternative jet fan case

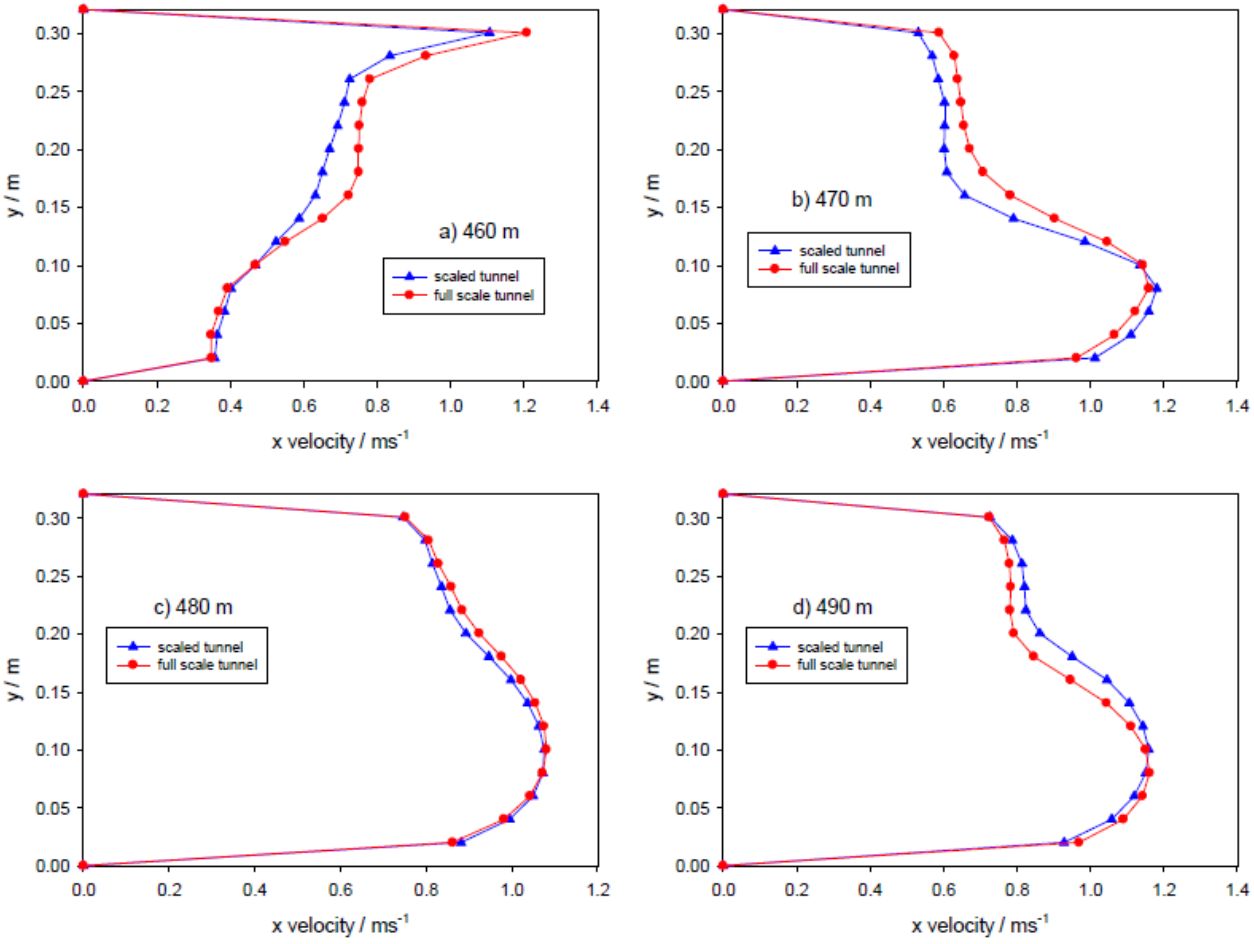

Figure 143 – Axial velocity profile on tunnel symmetry plane at (a) 10 m, (b) 20 m, (c) 30 m, (d) 40 m after the HGV: comparison between full and reduced (1:20) model – alternative jet fan case

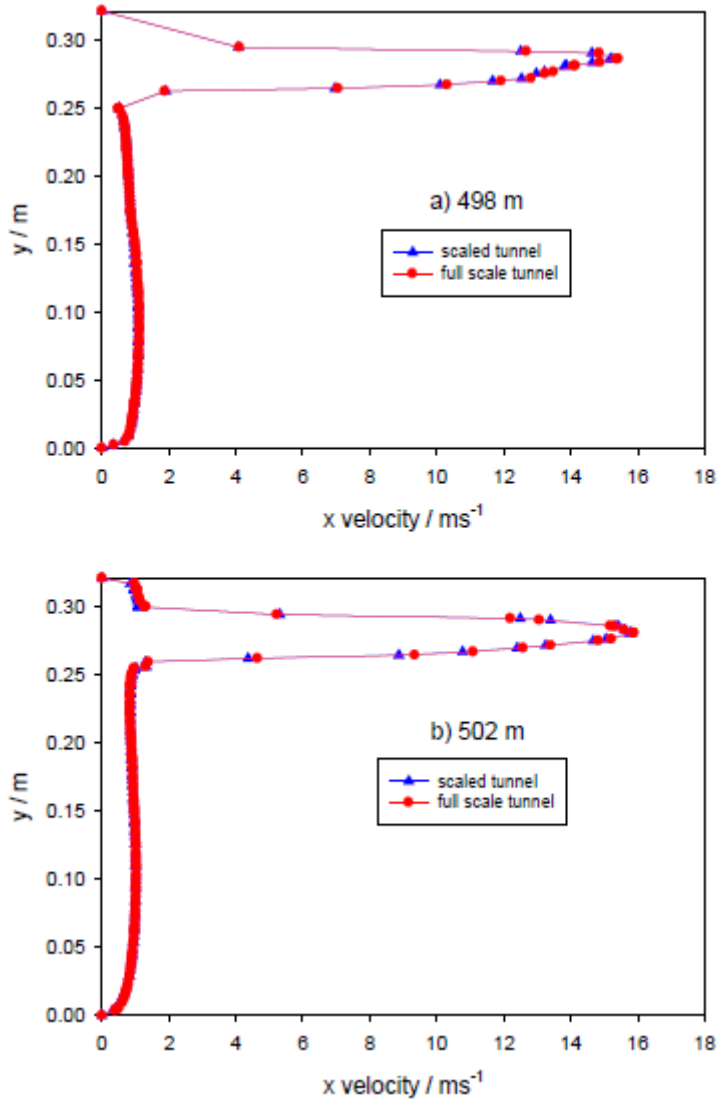

Figure 144 – Axial velocity profile on tunnel symmetry plane at (a) inlet and (b) outlet section of the 3rd jet fan: comparison between full and reduced (1:20) model – alternative jet fan case

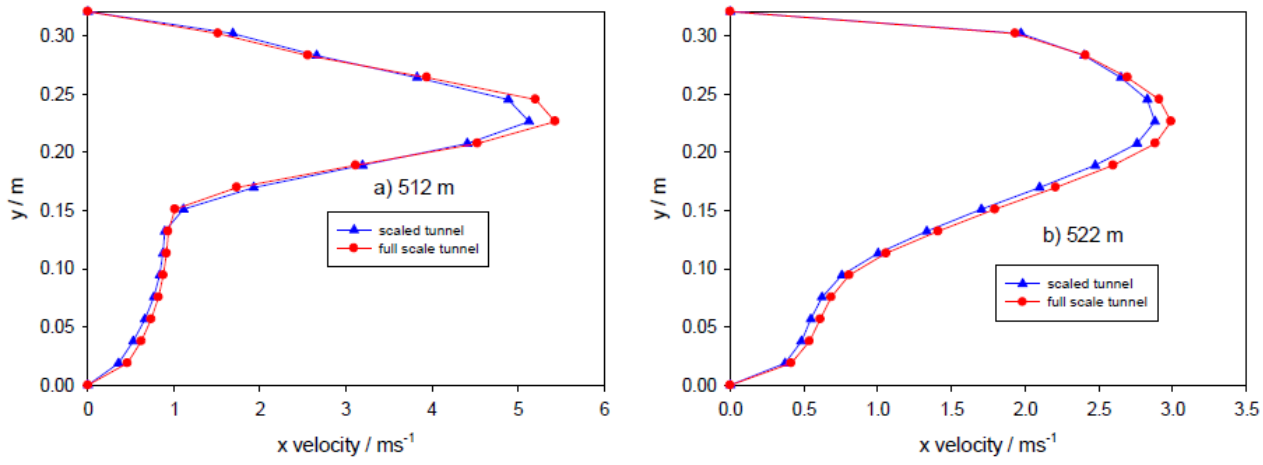

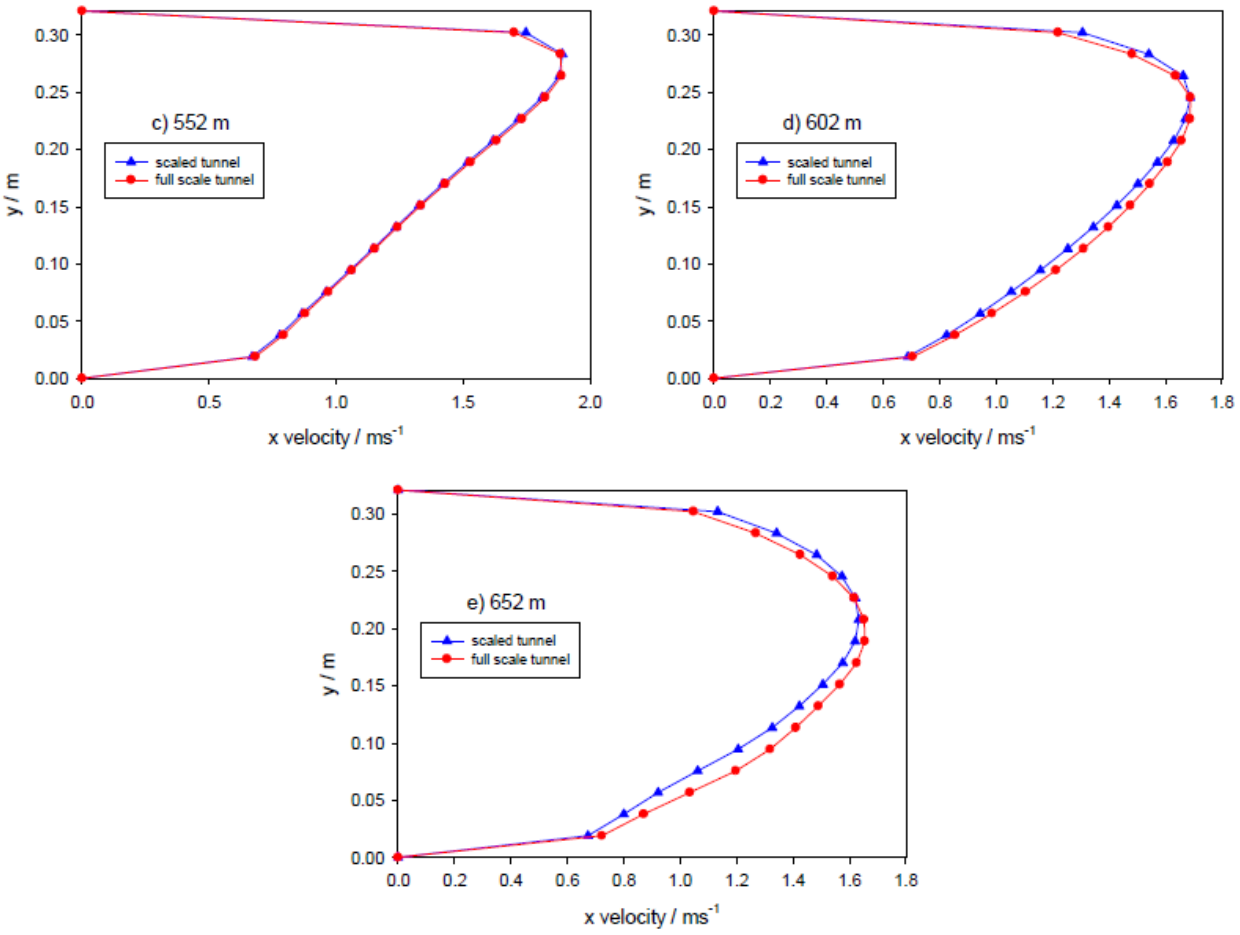

Figure 145 – Axial velocity profile on tunnel symmetry plane at (a) 10 m, (b) 20 m, (c) 50 m, (d) 100 m, (e) 150 m after the HGV: comparison between full and reduced (1:20) model – alternative jet fan case

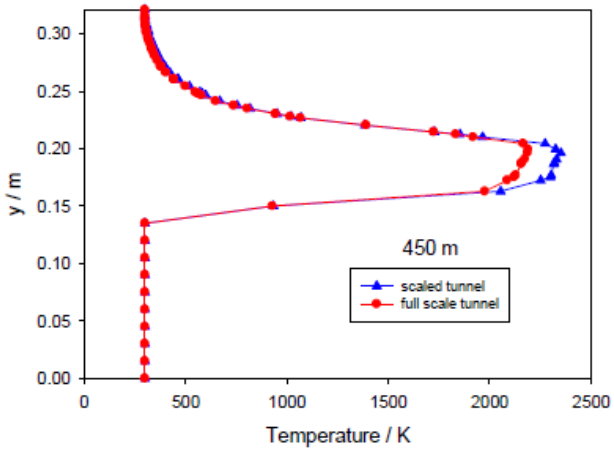

Figure 146 – Axial velocity profile on tunnel symmetry plane in correspondence of the HGV: comparison between full and reduced (1:20) model – alternative jet fan case

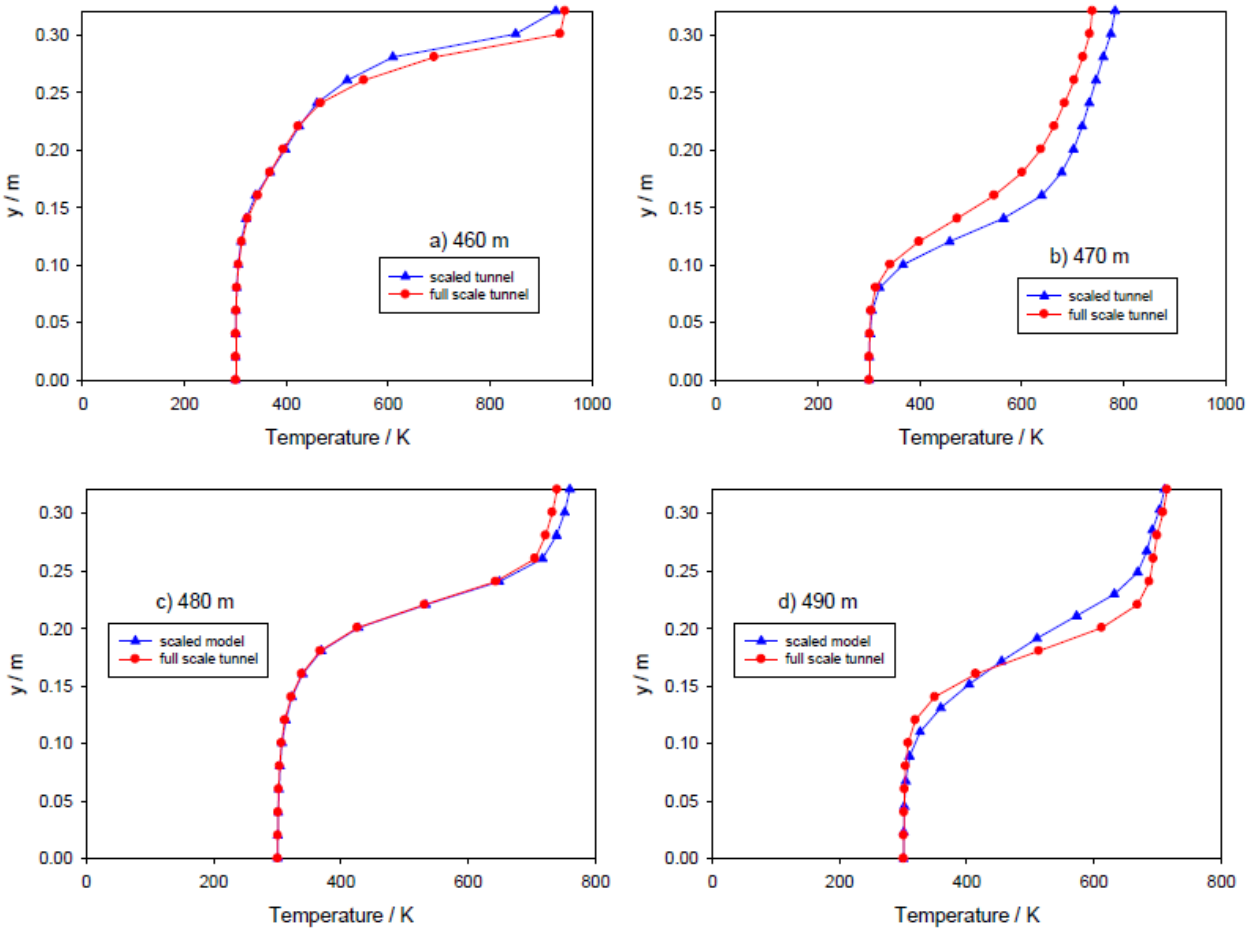

Figure 147 – Axial velocity profile on tunnel symmetry plane at (a) 10 m, (b) 20 m, (c) 30 m, (d) 40 m after the HGV: comparison between full and reduced (1:20) model – alternative jet fan case

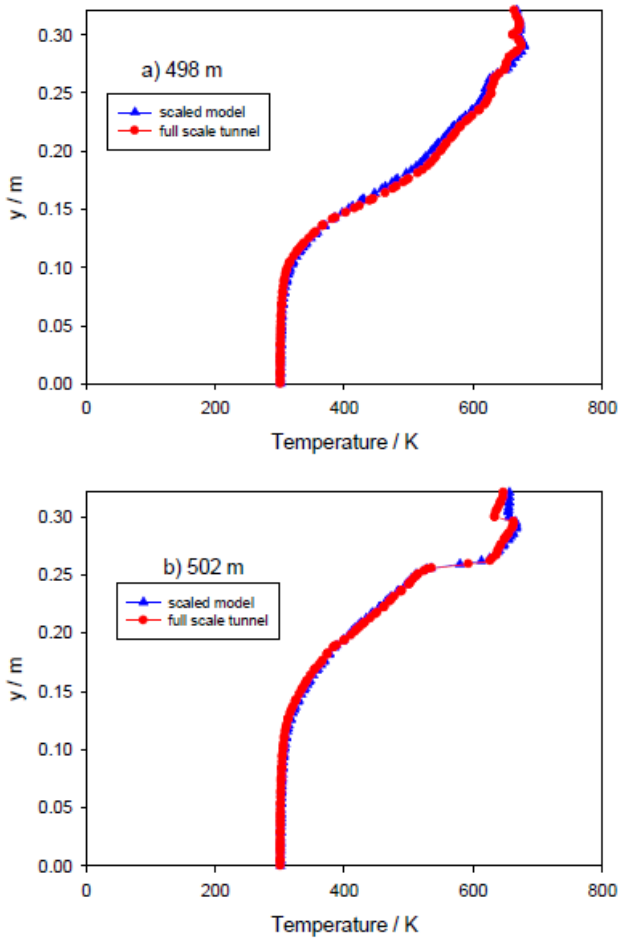

Figure 148 – Axial velocity profile on tunnel symmetry plane at (a) inlet and (b) outlet section of 3rd jet fan: comparison between full and reduced (1:20) model – alternative jet fan case

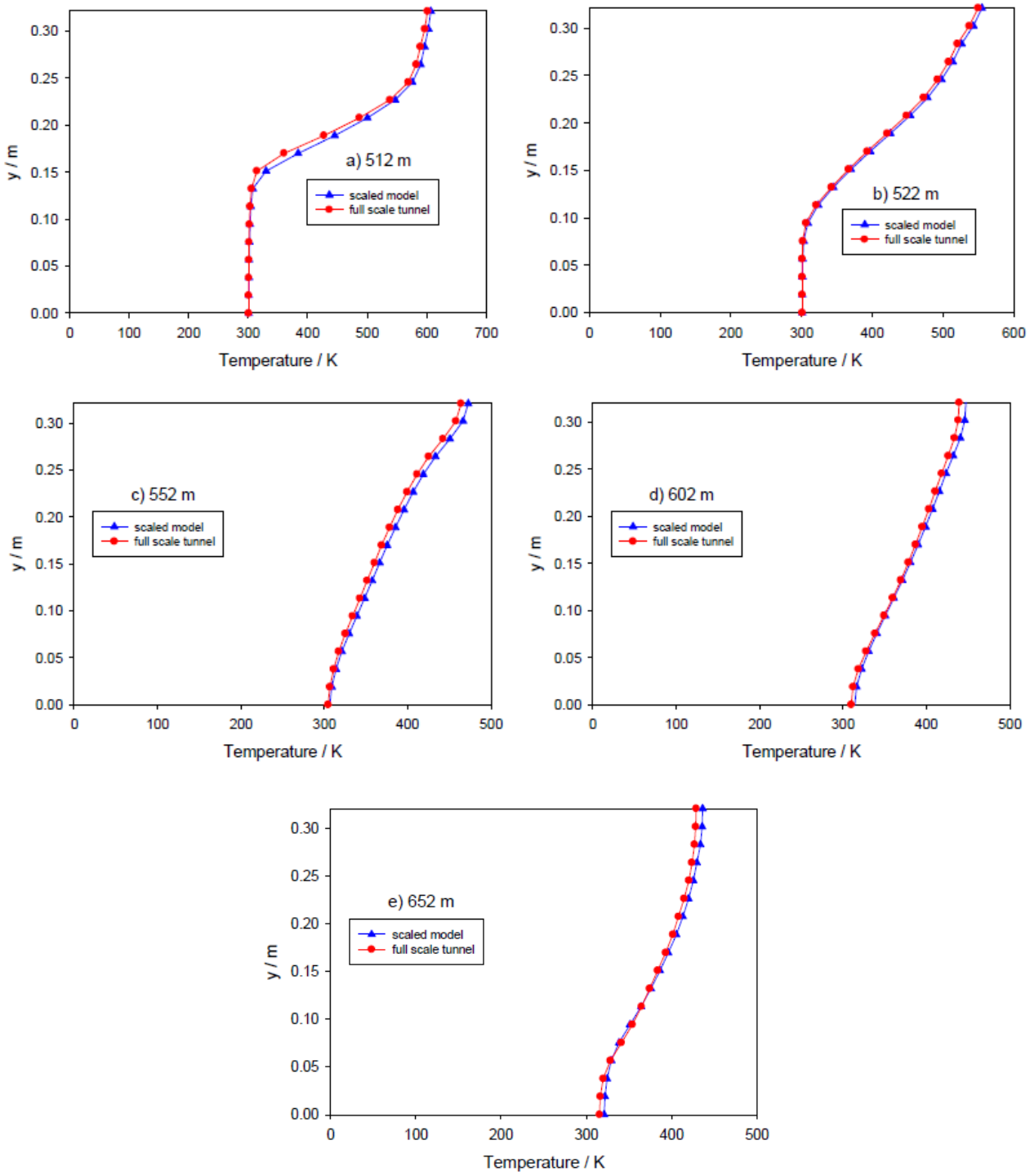

Figure 149 – Axial velocity profile on tunnel symmetry plane at (a) 10 m, (b) 20 m, (c) 50 m, (d) 100 m, (e) 150 m after the HGV: comparison between full and reduced (1:20) model – alternative jet fan case

As results, although previous figures show a good fitting between full and reduced model, main divergences occur for alternative jet fan case. Anyway, the 1:20 ratio for the reduced scale model lets to reach good results with the use of the simplified combustion model. In

following Table 20 and Table 21 errors for velocity and temperature respectively are shown.

Table 20 – Average axial velocity error for traditional and alternative ventilation systems – Combustion model case

Axial distance (m)	Average axial vekocity error (%)	
	Traditional ventilation system	Alternative ventilation system
420	1.8	2.5
430	1.8	2.6
440	1.8	2.6
450	1.7	2.0
460	6.5	6.2
470	4.1	6.8
480	1.4	1.5
490	2.2	4.1
498	3.4	2.1
502	2.8	3.4
512	4.2	6.9
522	2.6	4.8
552	1.0	0.9
602	2.6	2.9
652	3.1	4.8

Table 21 – Average temperature error for traditional and alternative ventilation systems – Combustion model case

Axial distance (m)	Average temperature difference (K)	
	Traditional ventilation system	Alternative ventilation system
450	65	17
460	10	14
470	17	41
480	5	5
490	10	17
498	5	6
502	14	4
512	4	7
522	4	3
552	4	6
602	4	4
652	4	4

Analyzing the difference temperature trend for both systems, results show that the highest value occurs near the HGV, in the fire zone. Since temperature filed and turbulence influence each other, because of different Reynolds number, two different maximum temperature values are reached. The 1:20 scaled tunnel consider a lower Reynold number causing an higher temperature value in the tunnel. Vice versa for full scale tunnel.

Despite this, far from the HGV not significant temperature differences occur.

7.2. Results

The evaluation of the optimal scale factor to the set up a reduced scale experimental apparatus is made by two different analyses carried out by means of CFD simulations: alternative and traditional jet fan systems are analyzed for both ordinary and emergency case (fire in tunnel). Temperature and (axial) velocity fields are analyzed in deep.

First simulations consider a 1:50 reduced model: both scenarios with and without fire are considered. Results show that good results can be reached only in the ordinary case (without fire) when Froude method is applied and appropriate roughness values is considered. However, main differences between velocity profiles occur in regions with high gradients (obstruction or momentum source). In the fire case, instead, differences for both temperature and velocity fields became not acceptable since kinematic similitude is not respected.

Starting from these results, different scale ratios are considered for the purpose: decreasing the scale factor, results show a lower divergence between temperature (trend and maximum values) and velocity fields. The optimal scale factor is evaluated as 1:20 by considering both numerical results and constructive aspects for the experimental apparatus such as tunnel section geometry, wall roughness (i.e. material choice), instrumentation and facilities to be installed.

7.3. 1:20 reduced scale model

As result of the full scale tunnel geometrical reduction, according to 1:20 ratio evaluated in previous paragraphs, the reduced scale model considers a total length of 40 m. Since these dimensions are very extended for a laboratory apparatus, a smallest tunnel is analyzed by means of numerical analysis and comparison with a full scale model similar to the previous one (same cross section, 60 m length, one jet fan at 15 m from the inlet – Figure 150). The reduced model considered in this chapter consists 3 m tunnel length, hydraulic diameter equal to 0.365 m, 35 mm fan diameter.

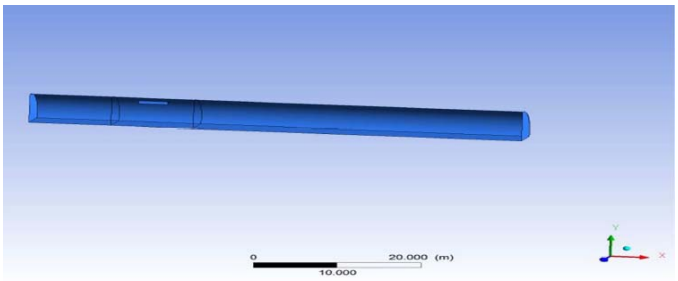

Figure 150 – Full scale model (60 m)

Traditional jet fans					
	Δp (Pa)	**v (m/s)**	**Roof roughness (m)**	**Floor roughness (m)**	**Re**
Full scale	2300	2.85	0.03	0.01	1.4E+6
Reduced scale	115	0.57	1.5E-6	5E-7	1.4E+6
Alternative jet fans					
	Δp (Pa)	**v (m/s)**	**Roof roughness (m)**	**Floor roughness (m)**	**Re**
Full scale	1800	3.60	0.03	0.01	1.7E+6
Reduced scale	115	0.77	1.5E-6	5E-7	1.9E+5

Axial velocity profiles on tunnel symmetry plane are shown in following figures.

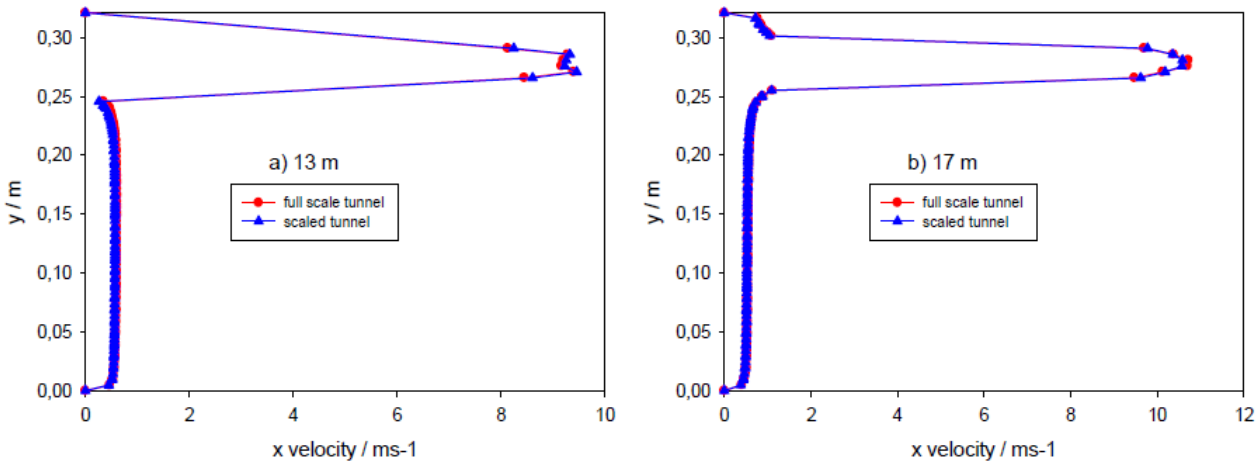

Figure 151 – Axial velocity profile on tunnel symmetry plane, comparison between full and reduced model at (a) inlet and (b) outlet section of 3rd jet fan – traditional jet fan case

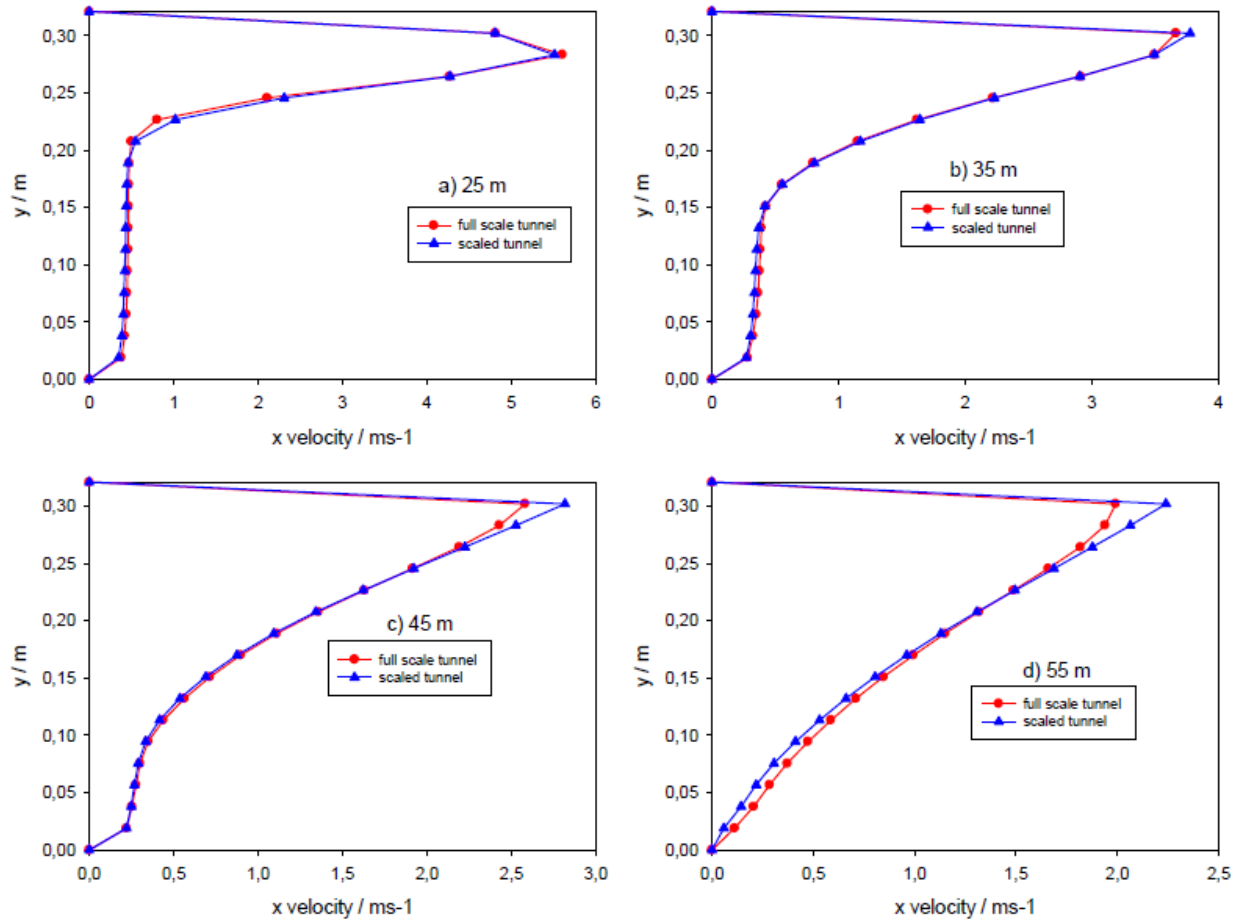

Figure 152 – Axial velocity profile on tunnel symmetry plane, comparison between full and reduced model at (a) 10 m, (b) 20 m, (c) 30 m, (d) 40 m – traditional jet fan case

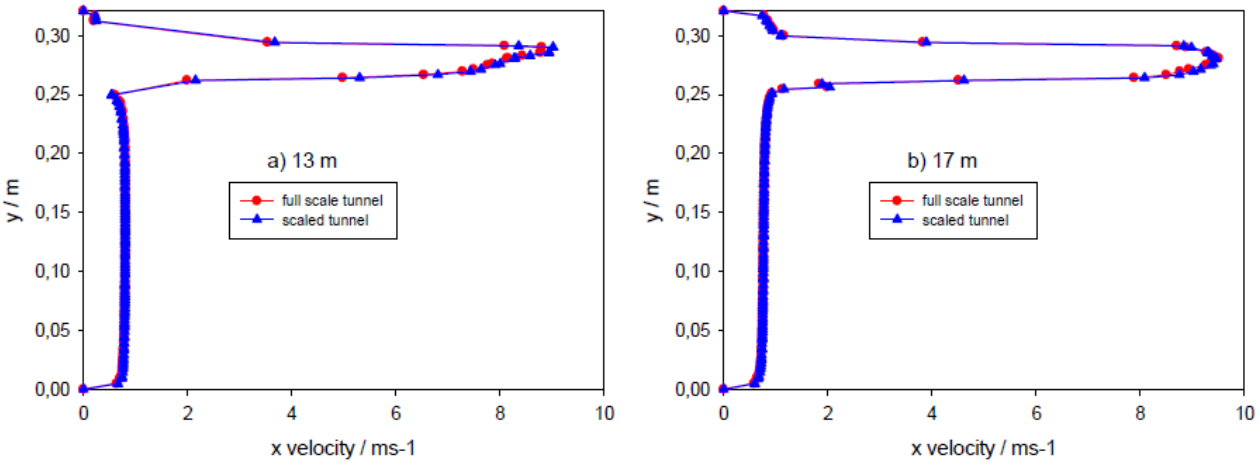

Figure 153 – Axial velocity profile on tunnel symmetry plane, comparison between full and reduced model at (a) inlet and (b) outlet section of 3rd jet fan – alternative jet fan case

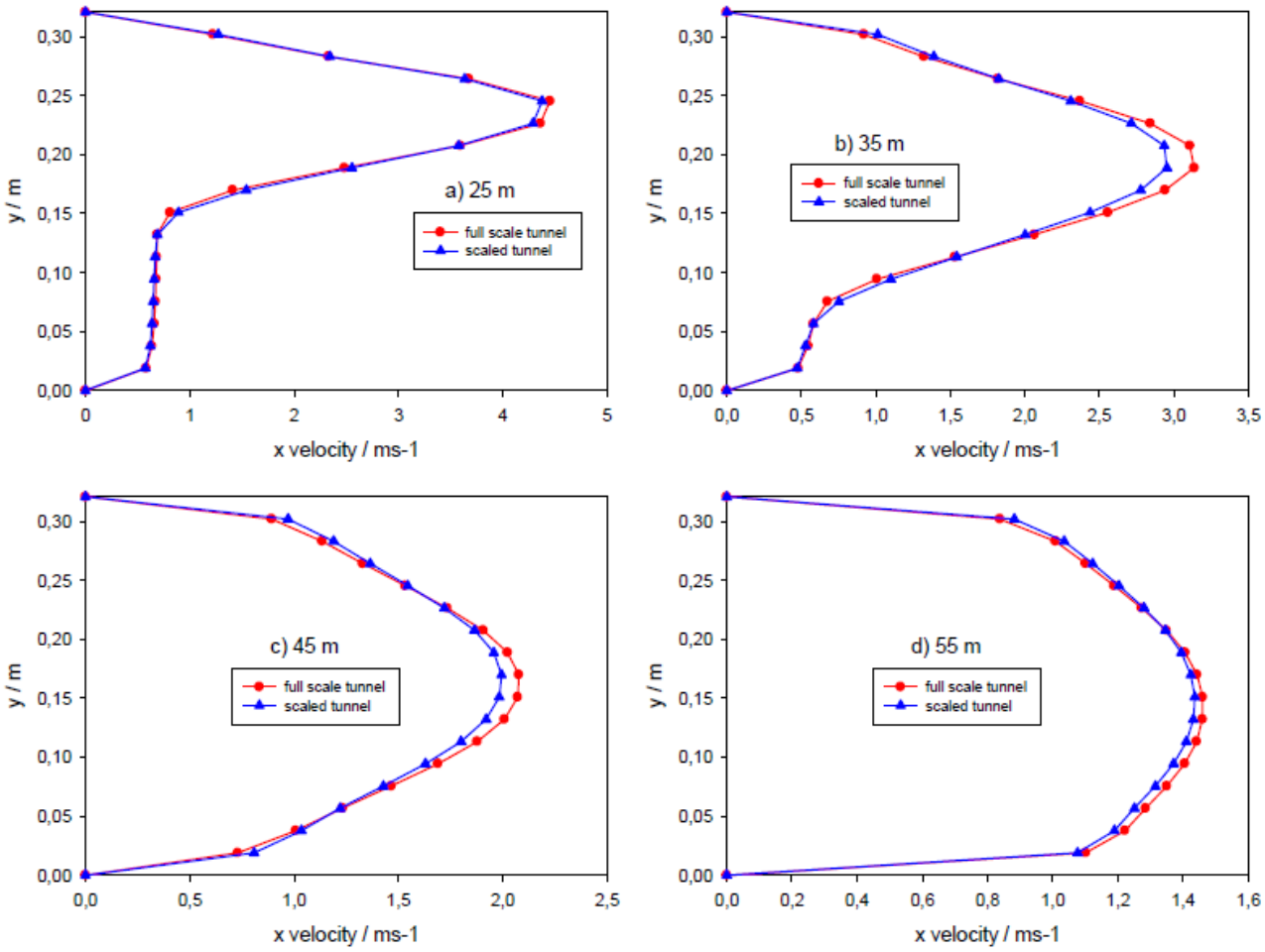

Figure 154 – Axial velocity profile on tunnel symmetry plane, comparison between full and reduced model at (a) 10 m, (b) 20 m, (c) 30 m, (d) 40 m – alternative jet fan case

In following Table 22, errors between full and reduced scale model configurations are shown for both traditional and alternative jet fans. By means of numerical simulations, pressure drop for both ventilation systems are evaluated: 115 Pa and 90 Pa for traditional and alternative systems respectively. Related to this, thrusts are evaluated.

Table 22

	Axial velocity error between full and reduced scale model	
Axial distance (m)	**Traditional**	**Alternative**
13	5.8	2.3
17	3.7	0.9
25	6.4	2.6
35	3.1	4.0
45	2.6	3.4
55	10.1	1.8

Table 23

	Ventilation system	
	Alternative	**Traditional**
Pressure drop (Pa)	90	115
Fan area (m^2)	0.001256	0.001256
Static thrust (g)	15	12

8. Numerical analyses and comparison with experimental data of laboratory reduced scale model

8.1. Validation of experimental apparatus as tunnel subsystem

In previous chapters, several results of numerical analyses are presented as support to the design and construction activities for a scaled model tunnel set-up at Metrology Lab of the University "Federico II" of Naples. Hence, according to these results, the reduced scale model is built with reference to an optimized scale factor, suitable to consider both similitude and constructive aspects. A 1:25 scale factor is considered for the realization of the experimental apparatus which, with its 4 m length, represents a subsystem (100 m length) of the longitudinal tunnel (800 m). Close to the physical realization of the laboratory model (tunnel, roof, etc.), several evaluations are also carried out in order to define auxiliary facilities for the model: instrumentation for main physical variable measurements (e.g. velocity, temperature), control systems to manage main components such as jet fan (CPU).

Aim of this chapter is to provide CFD analyses in order to made available numerical results to be compared with the experimental ones obtained from the laboratory reduced-scale model. In particular, results mainly consist in velocity profiles for different configurations in ordinary conditions (no fire occur).

8.1.1. Models description

8.1.1.1. Full scale tunnel

The full scale model refers to the same one shown previously in this work, with the only difference of a 12.1 m x 6.3 m rectangular cross section and 800 m length. No slopes are considered in the analysis.

About materials, tunnel walls are in concrete (roughness 0.012 m) and walls in asphalts (roughness 0.016 m).

8.1.1.2. Reduced scale tunnel

By applying a 1:25 scale factor, the reduced model (plexiglass, 0.001 m roughness) became 0.484 m x 0.252 m x 32 m. The subsystem made from this 1:25 reduced scale tunnel, consists in a tunnel portion of 4 m length. In order to validate that results provided by this subsystem can be extended to the whole tunnel, the following procedure is considered [82].

At first, a CFD analysis is performed on the 800 m tunnel in order to extract the boundary conditions to be applied on the subsystem; results for both models are compared. Then, the velocity field of the reduced scale model is compared with those of the full scale subsystem. At least, experimental measurements are carried out on the reduced scale in terms of velocity profiles and compared with CFD results.

In Figure 155, results show a good comparison between full scale tunnel (800 m) and full scale subsystem (100 m) in terms of axial velocity values on symmetry plane. The percentage error e(%), as defined in previous paragraph 7.1.1.1, is less than 5.5%.

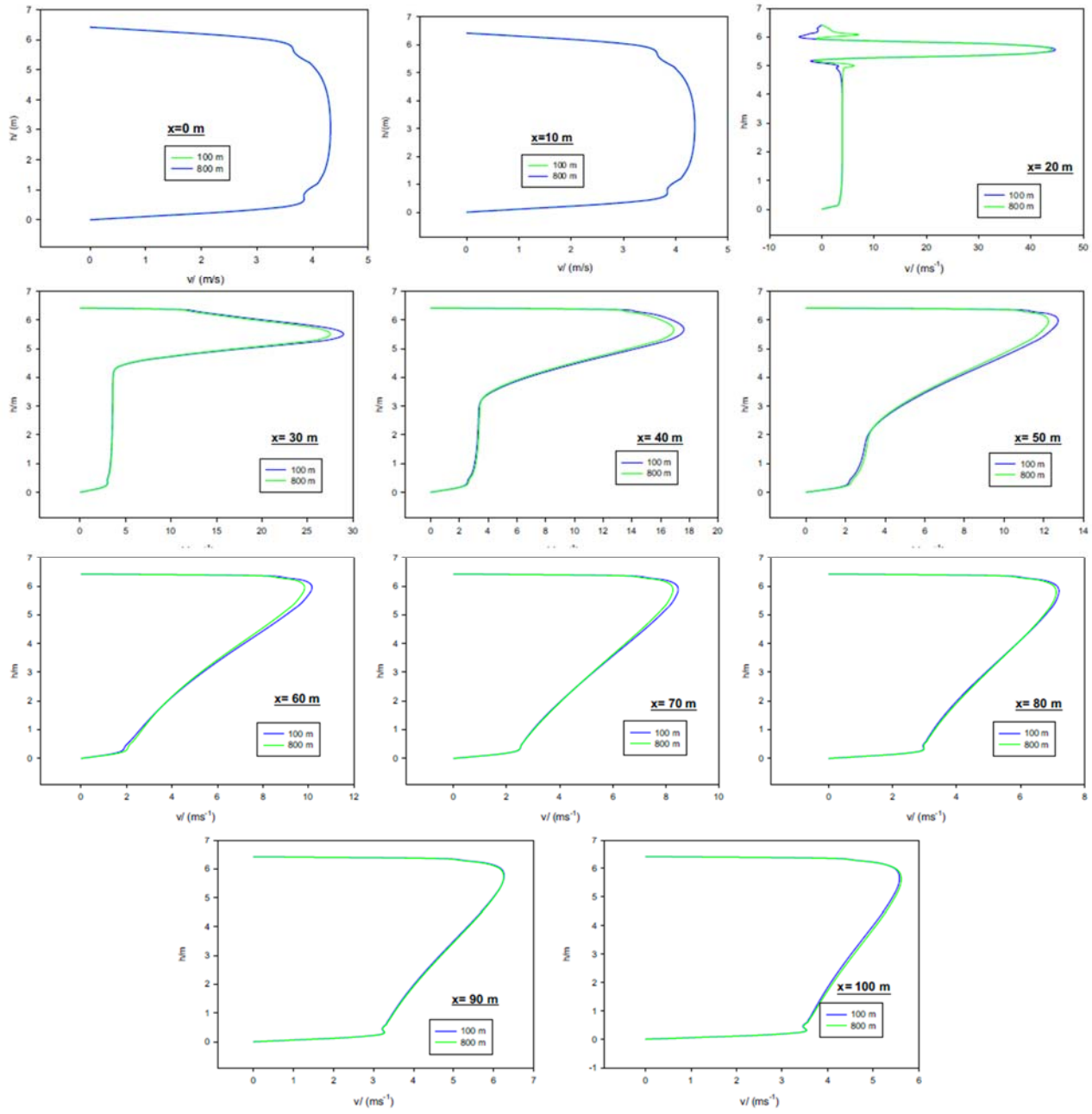

Figure 155 – Axial velocity on tunnel symmetry plane: comparison between full scale tunnel (800 m) and full scale subsystem (100 m) [82]

In order to verify the quality of scale reduction, the comparison between the full scale subsystem (100 m) and 1:25 reduced scale model (subsystem is carried out according to the scaling procedure shown in previous paragraph 7; results are always in terms of axial velocity. In Figure 156, velocity profiles are rescaled according to the proper scale ratio and compared: results shows a good agreement between the two models with a percentage error e(%) less than 6.0%.

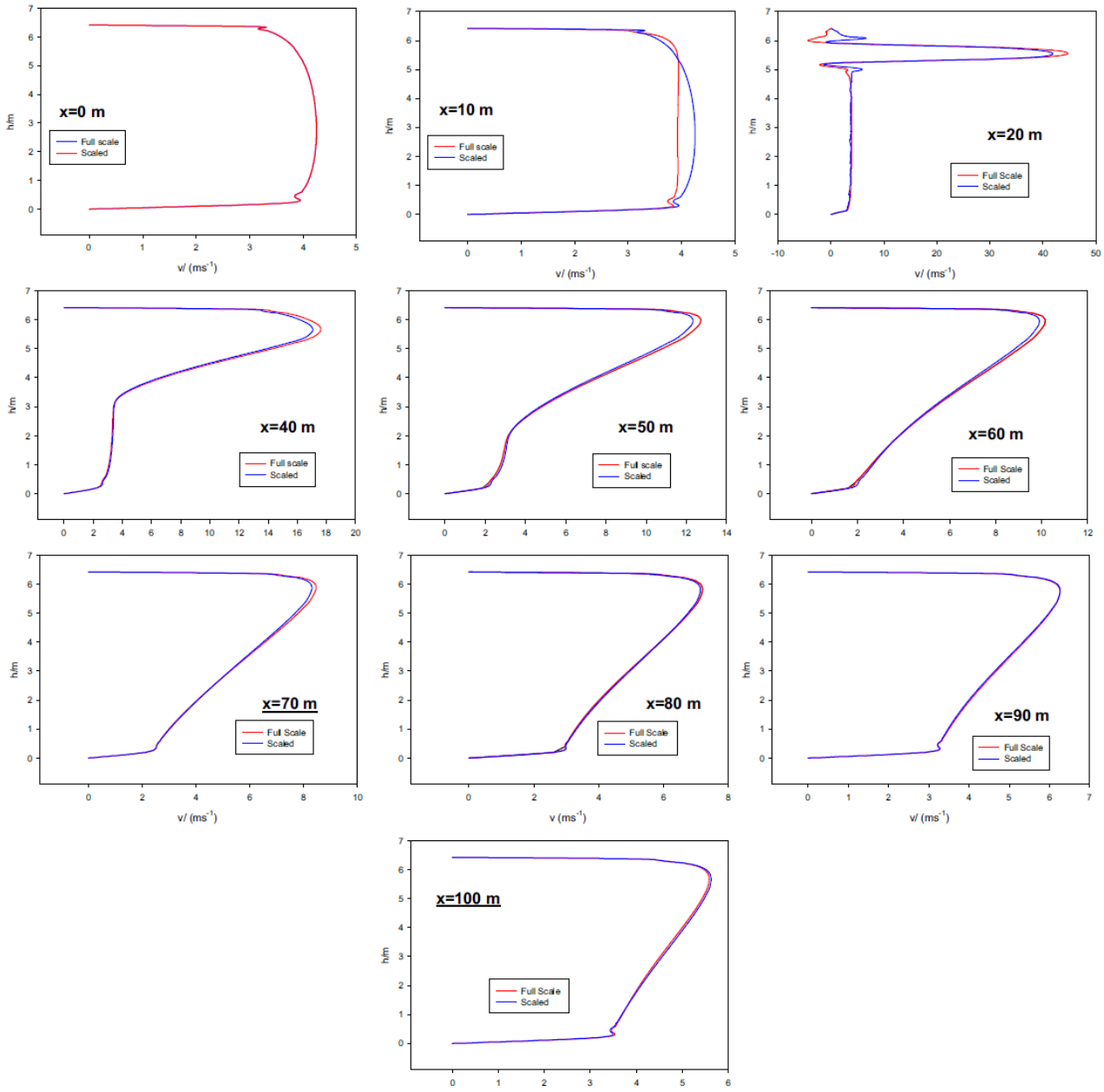

Figure 156 – Axial velocity on tunnel symmetry plane: comparison between full scale subsystem (100 m) and 1:25 reduced scale model [82]

The third step for the subsystem validation procedure involves the experimental apparatus for the evaluation of axial velocities to be compared with numerical results. The fan installed in the tunnel (Figure 157 and Figure 158), deriving from the nautical modeling (0.028 m inner diameter), has warped blade (0.009 m height) fixed to the shaft with a 60° angle. The rotation speed (19000 rpm) is guaranteed by a 3÷6 V DC brushed motor governed by a square wave voltage performed by ARDUINO UNO logic board.

Figure 157 – Experimental apparatus in Metrology Lab @ "Federico II" university

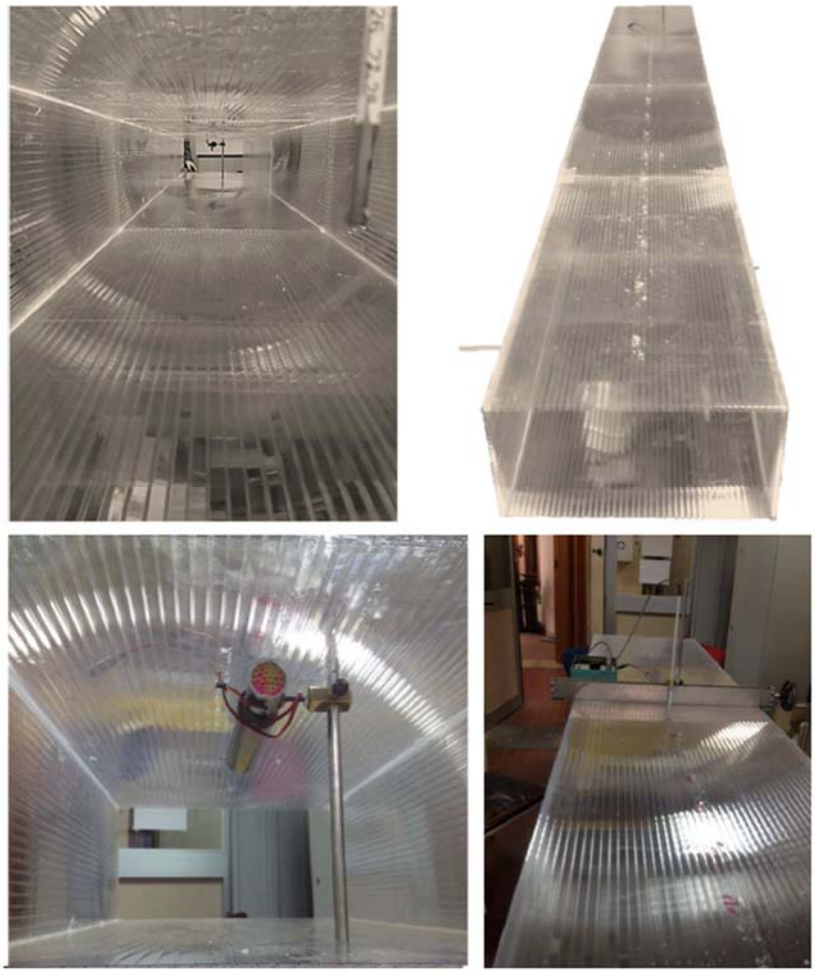

Figure 158 – Experimental apparatus in Metrology Lab @ "Federico II" university

Differently from several experimental studies in scientific literature, where the ventilation is realized by means of external fans, here a jet fan is installed inside the tunnel in order to consider directly its influence on flow field. The fan is also installed on a rigid structured in order to maintain its axis parallel to the tunnel one and it is connected with a dynamometer to evaluate the relationship between voltage vs thrust and thrust vs outflow velocity (Figure 159).

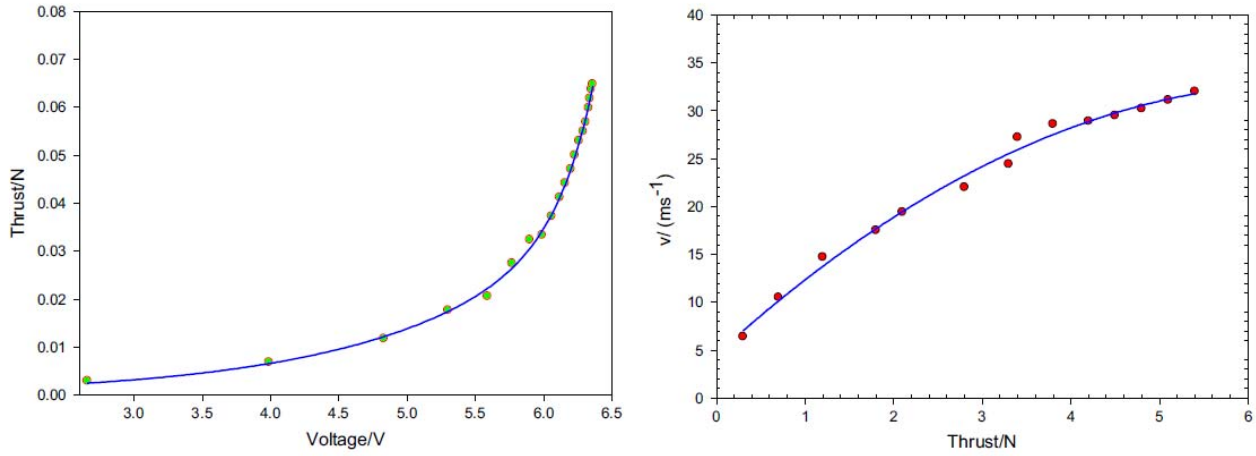

Figure 159 – Correlation curves for 1:25 model jet fan [82]

In order to ensure the repeatability of measurements, the tunnel surface is equipped with several intakes (50 x 1 cm^2; 10 cm pitch) in which the probe (hot wire anemometer) can be moved (Figure 160). A graduated scale is provided in order to ensure the measurement identification. The measurement points are equally spaced from the jet fan outflow (from 0 m to 4 m, with a step equal to 0.40 m), to detect the average axial and radial velocity for different elevations from floor for each considered fan thrust value.

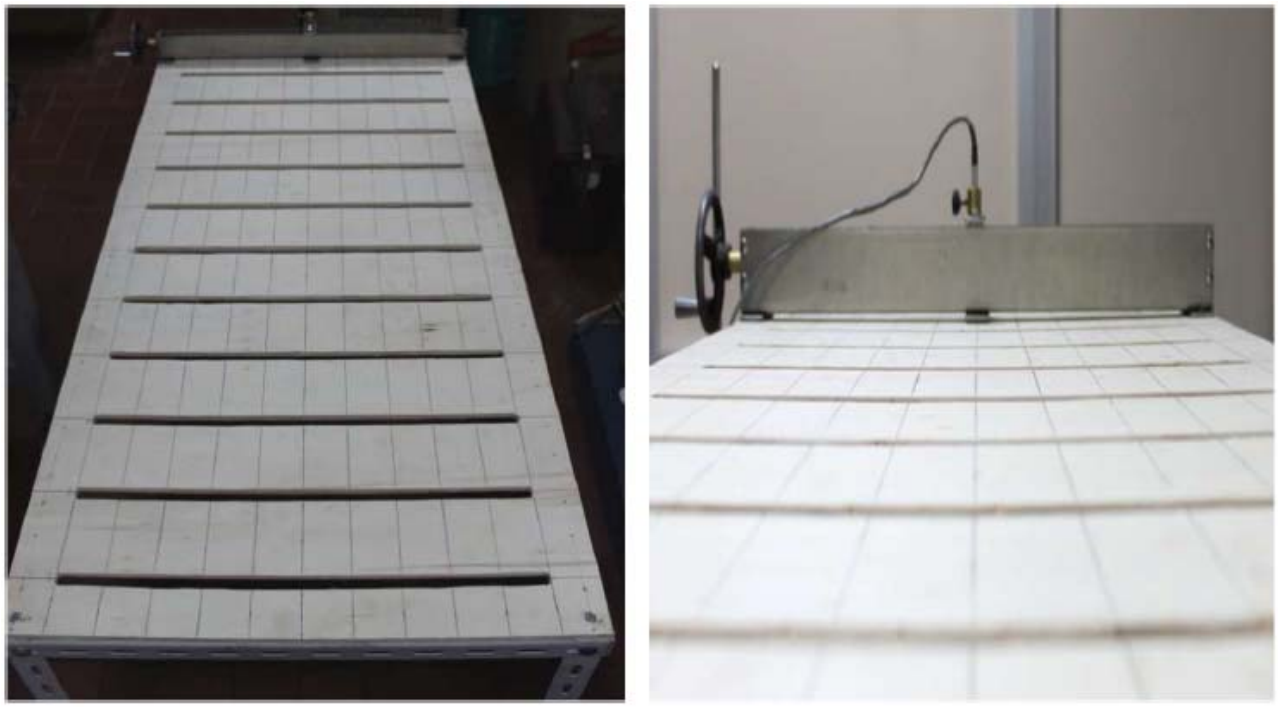

Figure 160 – Tunnel intakes for probe movement

The experimental data are then made available by the laboratory staff to let a comparison with numerical data provided in this work. In Figure 161, axial velocities on tunnel symmetry plane are compared for both laboratory and CFD scaled tunnel.

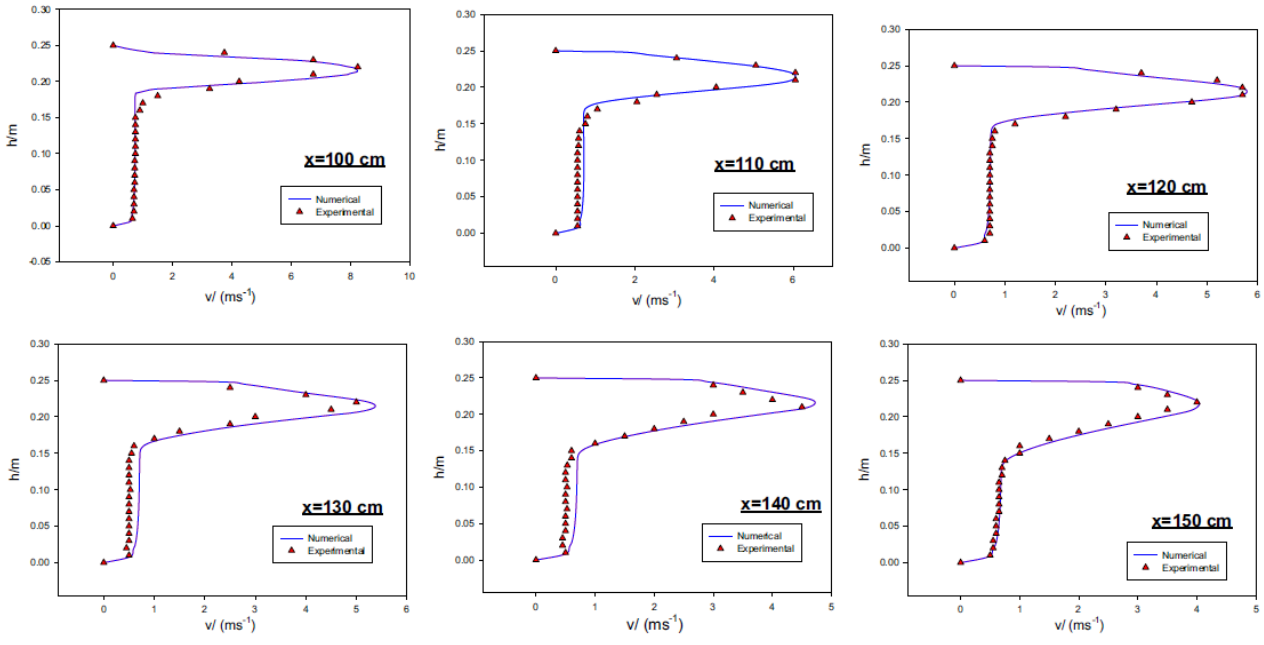

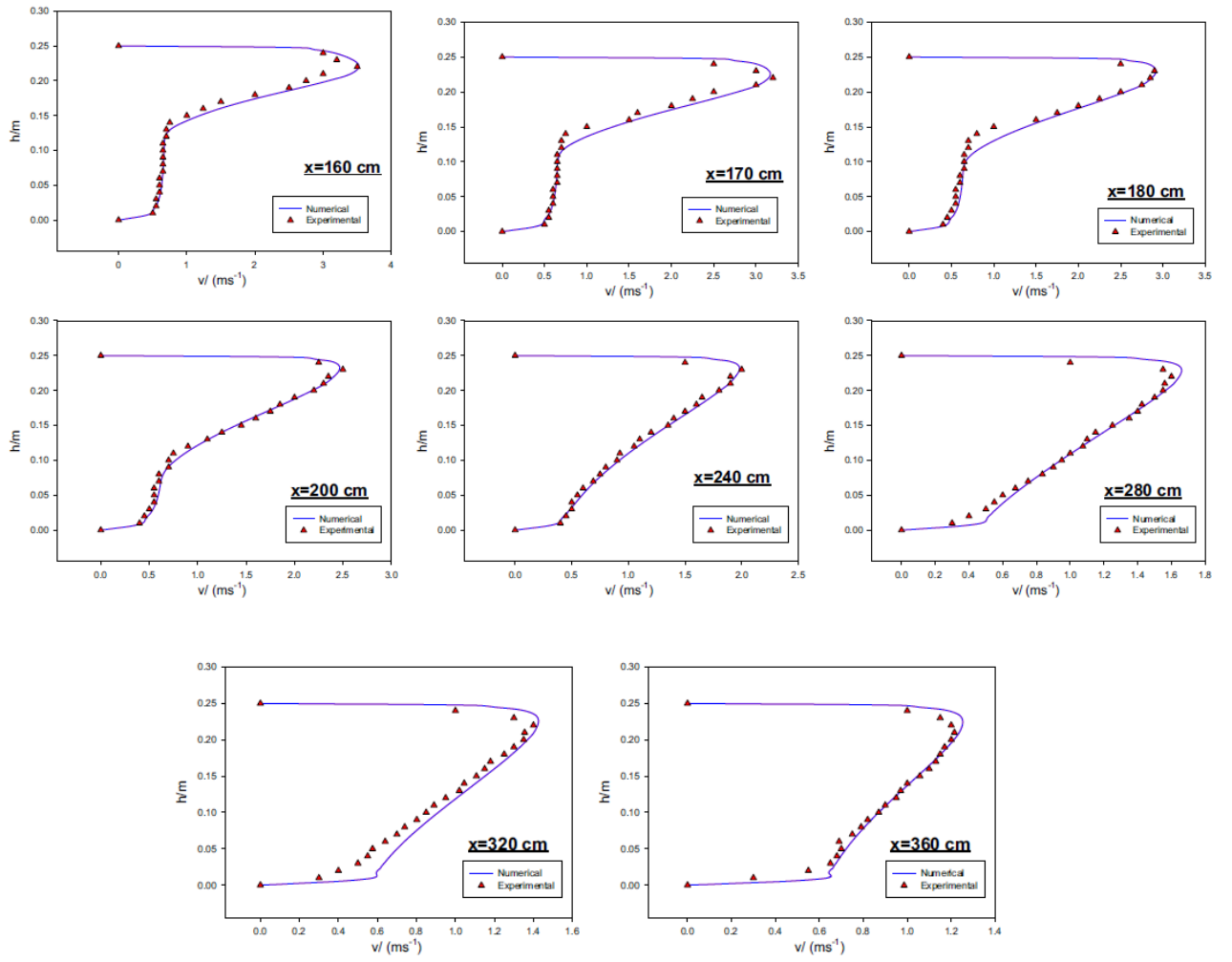

Figure 161 – Axial velocity on 1:25 tunnel symmetry plane: comparison between numerical (1:25 reduced scale model) and experimental data (1:25 reduced scale apparatus) [82]

For the first 100 m, the comparison consider a 10 m pitch while a 40 m one refers to the rest of tunnel. As results, Figure 161 shows a good comparison between these two models: the 4 m laboratory tunnel can be used as sub-model of the main 1:25 tunnel (100 m).

8.2. Numerical analysis for different traffic conditions and comparison with experimental data

In this paragraph, numerical simulations on a reduced scale tunnel are carried out to investigate the effects of vehicle presence in the tunnel on the ventilation system performance. CFD results from simulation are made available to be compared with laboratory measurements.

8.2.1. Boundary conditions

Since the laboratory is located at sea level, corresponding environmental conditions are considered:

- operative pressure: 101325 Pa;
- maximum wind intensity: 7 m/s;
- operative wind intensity: 0 m/s;
- operative temperature: 298.15 K;
- air density: 1.225 kg/m3.

According to actual availability of instrumentation for the experimental apparatus, the operative condition only is considered for the analysis.

8.2.2. Pressure drop evaluation

Starting from the tunnel geometry and boundary conditions (e.g. altitude), by means of graph shown in Chapter 1 it is possible to evaluate corresponding flowrate for both visibility and CO concentration limits (0.009 m^{-1} and 250 ppm respectively).

Since Figure 2 and Figure 3 refer to 1 km length and 1 line traffic, the following scaling factor should be used:

- 0.8 for 800 m total length;
- 2 for 2 vehicle line traffic.

Thus, Q_{CO} = 60 x 2 x 0.8 = 96 m^3/h while $Q_{visibility}$ = 40 x 2 x 0.8 = 64 m^3/h. Although the maximum values between Q_{CO} and $Q_{visibility}$ represent the design flowrate, as a conservative assumption, the summation of both values is considered (160 m^3/h). The corresponding mean velocity reads:

$$Q = 160\,\frac{m^3}{h} \rightarrow v = \frac{Q}{A_{tunnel}} = 2.1\,m/s$$

Since the total pressure drop consists in 4 different terms (friction, vehicles, wind and temperature), the following evaluations are carried out.

The contribute of the tunnel walls and air friction ($\Delta p_{friction}$) is calculated considering the mean velocity and hydraulic dimensions at ambient contidion:

$$\Delta p_{friction} = \frac{1}{2} \cdot \rho \cdot v^2 \cdot \frac{\beta \cdot L}{\overline{H}} = 6.5\ Pa$$

The pressure loss due to vehicles ($\Delta p_{vehicle}$) is considered in the congested traffic condition which represents the worst case since moving vehicles can introduce fresh air in tunnel (see piston effect) reducing *de facto* the ventilation system work.

$$\Delta p_{vehicle} = \frac{1}{2} \cdot \rho \cdot (v_{vehicle} - v)^2 \cdot \frac{A_{vehicle} \cdot C_R}{L_{vehicle}} = 2.2\ Pa$$

where $A_{vehicle}$ represents the vehicle's front surface (5 m^2), C_R the drag coefficient (0.8) and $L_{vehicle}$ the distance between two adjacent vehicles (5 m) evaluated by the graph in Figure 162 (courtesy of Woods Inc. – www.flaktwoods.it).

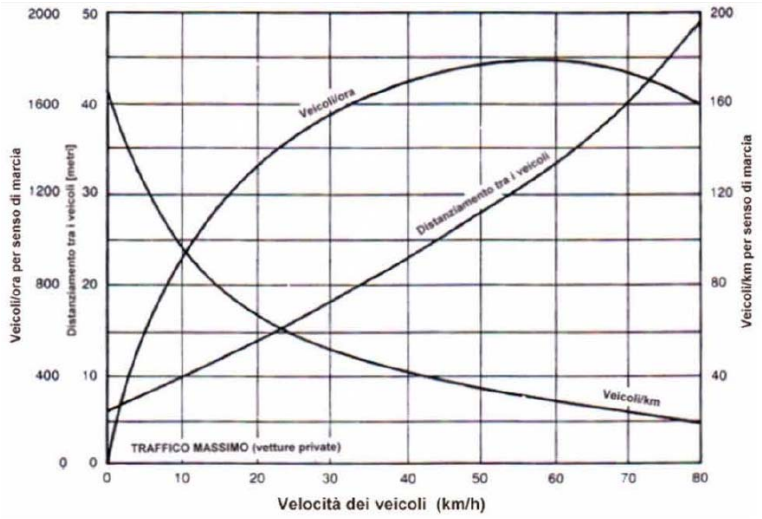

Figure 162 – Woods abacus for vehicle distance

Considering the worst case where the lack of wind does not introduce fresh air in the tunnel, the pressure drop due to this term became equal to zero: $\Delta p_{wind} = \frac{1}{2} \cdot \rho \cdot {v_{wind}}^2 = 0$ against 30 Pa for 7 m/s.

Similarly, the contribute of temperature on air density, of course relevant for sloped tunnels, is neglected:

$$\Delta p_{temp} = slope \cdot \gamma_{air} \cdot \frac{T - T_{external}}{T_{external}} = 0\ Pa$$

As result, by cumulating the 4 mentioned terms, the total thrust reads 39 Pa which corresponds a total thrust of $\Delta p_{tot} \cdot A_{tunnel} = 39\ Pa\ \cdot 76\ m^2 = 2949$ N.

The total thrust can be dived for the total number of jet fan in order to evaluate the jet fan specific thrust by means of the following expression:

$$Total\ Thrust = N_{fan} \cdot K_1 \cdot K_2 \cdot \rho \cdot Q_{fan} \cdot v_{fan,mean}$$

Both the coefficients K_1 and K_2 are applied to evaluate the operating thrust from the nominal one: the first one considers the effects of exhaust airflow while second one the distance Z of each jet fan from the roof (Figure 163 and Figure 164).

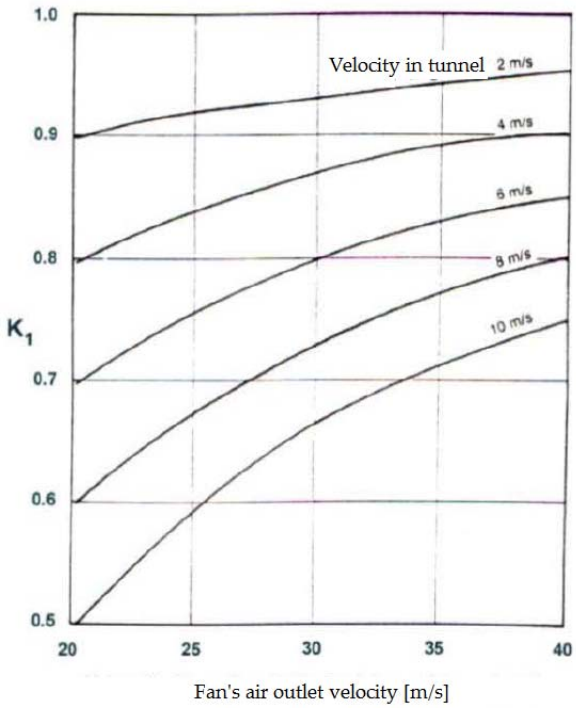

Figure 163 – K_1 coefficient against outlet air velocity

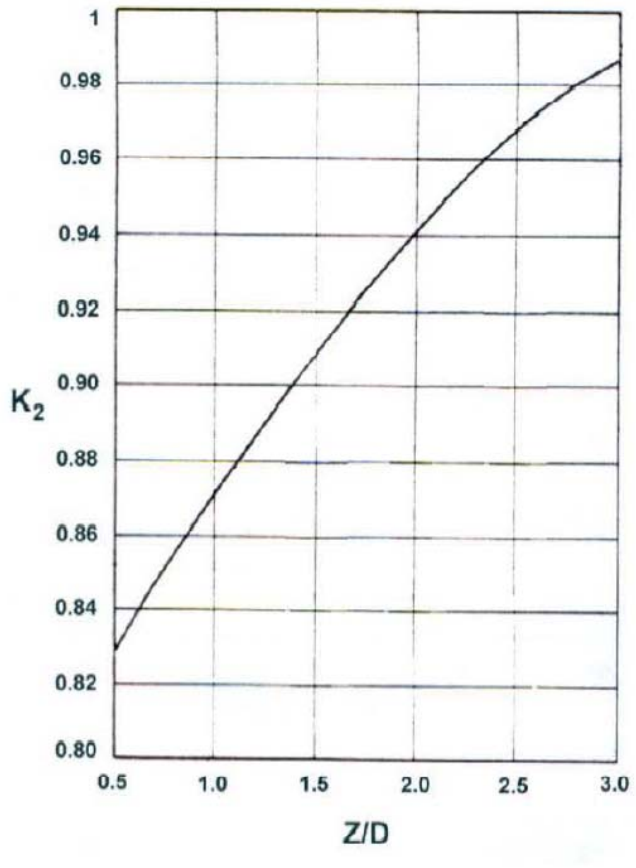

Figure 164 – K_2 coefficient against dimensionless distance of jet fan from roof

Similarly to previous CFD simulations, four jet fans are considered (200 m distance each) in the tunnel. From Figure 163 and Figure 164, K_1 reads 0.65 while K_2 0.87.

$$Fan\ tot\ thrust = 1300\ N\ \rightarrow Fan\ Operative\ thrust = 737\ N$$

In order to compare the operative thrust (737 N) with the normal one, K_1 is considered equal to 1 while $\Delta p_{wind} = 0\ Pa$ by neglecting the effect of the wind.

Thus, starting from the total pressure drop $\Delta p_{tot} = 8.7\ Pa$, the total thrust reads 661 N (166 N nominal for each fan). Finally, applying K_1 x K_2 factors the thrust became 144 N.

8.2.3. Reduced scale parameters

Similar to previous paragraph, the same procedure is applied to the reduced scale model. The scaling procedure is considered starting from the tunnel airflow ratio with a scaling factor equal to 25:

$$\frac{Q_{SM}}{Q_{FS}} = \left(\frac{1}{SF}\right)^{5/2} \rightarrow Q_{tot} = Q_{CO} + Q_{visibility} = 0.0512\ m^3/s$$

where Q_{CO} = 0.0192 x 2 x 0.8 = 0.0307 m^3/s and $Q_{visibility}$ = 0.0128 x 2 x 0.8 = 0.0205 m^3/s. Since the reduced tunnel cross section area is 0.122 m^2, the air average velocity reads 0.420 m/s.[3]

Starting from this velocity (0.420 m/s), the pressure drops (friction, vehicles, wind, temperature) are calculated:

$$\Delta p_{friction} = 0.0104\ Pa$$

$$\Delta p_{vehicle} = 0.00346\ Pa$$

$$\Delta p_{wind} = 1.2005\ Pa$$

$$\Delta p_{temperature} = 0\ Pa$$

Thus, $\Delta p_{tot} = 1.214\ Pa$ which correspond a total thrust of 0.148 N by multiplying pressure drop per tunnel cross section area. The thrust of a single fan reads:

$$\frac{0.148}{4} \cdot K_1 \cdot K_2 = 0.0209\ N$$

The same procedure for normal operating condition lead (for K_1=1) to 0.00036 N for each fan.

In order to measure air velocity in the tunnel and the fan thrust at each rotation speed, an air velocity meter instrument is installed. With a ±2% accuracy for each full scale range and ±0.25% reproducibility of full scale over the temperature range -20°C/+55°C, the measurements are referred to standard condition of pressure and temperature. Thus, the actual ones have to be obtained by a scaling formula: $v_{actual} = v_{std} \cdot \rho_{std}/\rho_{actual}$ where ρ is the air density at standard and actual conditions and v_{std} is the measured air velocity.

Varying the fan rotation speed, air velocity value and mass flow rate can be evaluated (Figure 165).

[3] The same result can be obtained applying the kinematic similarity: $V_{SM}/V_{FS} = (1/SF)^{1/2}$.

Duty Cycle		Air velocity [m/s]			Airflow mass [m^3/s]
	%	Min	Max	Average	
255	100.00%	0.999	1.092	1.0455	0.001162808
230	90.20%	0.957	1.02	0.9885	0.001099412
205	80.39%	0.739	0.888	0.8135	0.000904777
180	70.59%	0.656	0.713	0.6845	0.000761303
155	60.78%	0.599	0.619	0.609	0.000677331
130	50.98%	0.433	0.468	0.4505	0.000501047
105	41.18%	0.293	0.322	0.3075	0.000342002
80	31.37%	0.116	0.131	0.1235	0.000137357
55	21.57%	0.001	0.001	0.001	1.1122E-06
30	11.76%	0	0	0	0
5	1.96%	0	0	0	0
0	0%	0	0	0	0

Figure 165 – Airflow and velocity measurements at several fan rotation speeds

In order to set the logic board to the correct air velocity, the following calculation procedure is considered.

From the total fan thrust in normal operation for the scaled model (0.000422 N), the pressure gauge between sections reads 0.47 Pa (fan area 9E-4 m^2), so the average air velocity can be evaluated applying the Bernoulli formula: $(2*\Delta p/\varrho)^{0.5}$ = 0.875 m/s which correspond to a specific duty cycle.

8.2.4. The influence of vehicles

In order to evaluate the effect of vehicle for the ventilation system, 3 different scenarios are set-up:

- 4 vehicles @ tunnel end;
- 4 vehicles @ tunnel end + 4 vehicles @ tunnel beginning;
- 16 vehicles equally-spaced in the tunnel.

Since the scaled model represents the first part of the whole tunnel, the comparison between numerical and experimental data needs to consider a CFD geometry identical to the experimental one. In following table, main dimensions for both full and scaled model are presented.

Item	Scaled Model [m]	Full scale Model [m]
J-F distance from inlet	0.6	15
Vehicle height	0.06	1.5
Vehicle width	0.08	2
Vehicle length	0.16	4
Vehicle distance from walls	0.06	1.6
4 vehicle configuration		
Vehicle 1 from inlet	3	75
Vehicle 2 from inlet	3	75
Vehicle 3 from inlet	3.62	90.5
Vehicle 4 from inlet	3.62	90.5
8 vehicle configuration		
Vehicle 1 from inlet	3	75
Vehicle 2 from inlet	3	75
Vehicle 3 from inlet	3.62	90.5
Vehicle 4 from inlet	3.62	90.5
Vehicle 5 from inlet	1	25
Vehicle 6 from inlet	1	25
Vehicle 7 from inlet	0.38	9.5
Vehicle 8 from inlet	0.38	9.5
16 vehicle configuration		
Vehicle 1 from inlet	3.16	79
Vehicle 2 from inlet	3.16	79
Vehicle 3 from inlet	3.78	94.5
Vehicle 4 from inlet	3.78	94.5
Vehicle 5 from inlet	2.84	71
Vehicle 6 from inlet	2.84	71
Vehicle 7 from inlet	3.46	86.5
Vehicle 8 from inlet	3.46	86.5
Vehicle 9 from inlet	0.84	21
Vehicle 10 from inlet	0.84	21
Vehicle 11 from inlet	0.22	5.5
Vehicle 12 from inlet	0.22	5.5
Vehicle 13 from inlet	1.16	29
Vehicle 14 from inlet	1.16	29
Vehicle 15 from inlet	0.54	13.5
Vehicle 16 from inlet	0.54	13.5

As reference for each case, the geometry considered in CFD software for 16 vehicles case is shown in Figure 166.

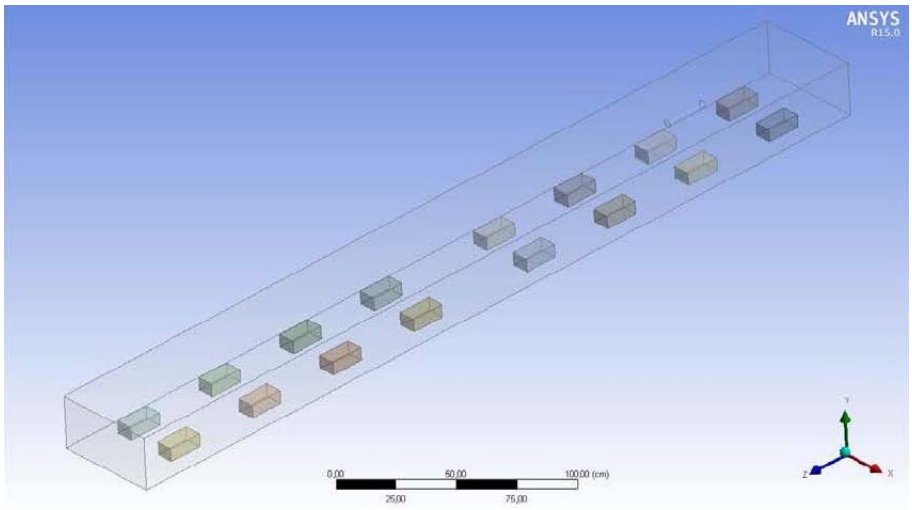

Figure 166 – CFD model, 16 vehicles case

8.2.5. CFD parameters

An unstructured mesh is considered for the numerical analysis (tetra/hexa grid) with minimum element size set at 0.1 mm. RANS equations are applied with the Eddy Viscous Models.

As boundary conditions, static pressure for both inlet and outlet section is 0 Pa, pressure drop on fan sections is 0.47 Pa, standard working pressure is 101 kPa and temperature is 298.15 K. Convergence limit is set at 1E-3.

8.2.6. Results

Thanks to support of laboratory team which have made available experimental results, several measurements are carried out for different positions: the scaled tunnel is made by 14 equally spaced holes on the roof to let the insertion of the probe and move it at several vertical position to evaluate airflow, temperature and total pressure. Starting from the middle position (considered as 0), ten different depths are considered for measurements:

Different elevations for probe position (m)										
0.1	0.08	0.06	0.04	0.02	0	-0.02	-0.04	-0.06	-0.08	-0.1

Considering the air turbulence in tunnel, 4 different measurements are carried out with 40 s period; the average one is plotted in following figures with blue points and compared with numerical results (red line).

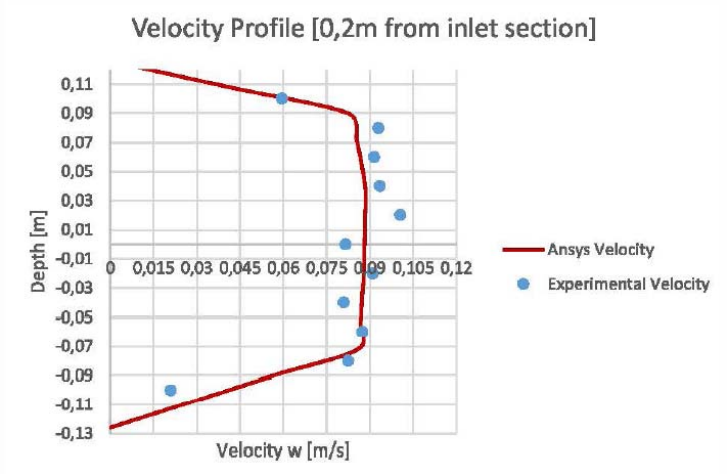

Figure 167 – Velocity profile @ 0.2 m from inlet section – 4 vehicles case

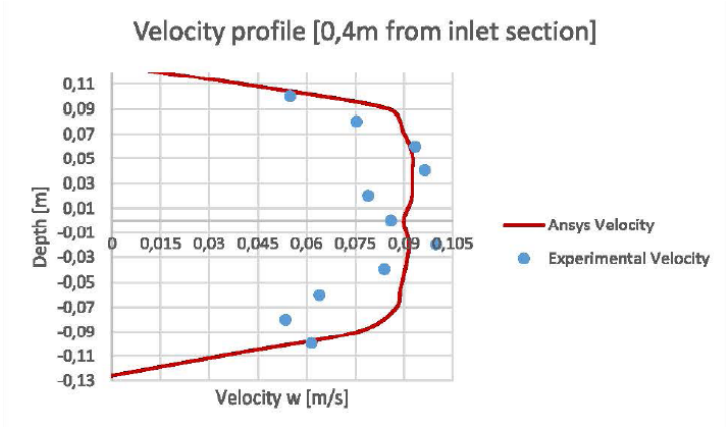

Figure 168 – Velocity profile @ 0.4 m from inlet section – 4 vehicles case

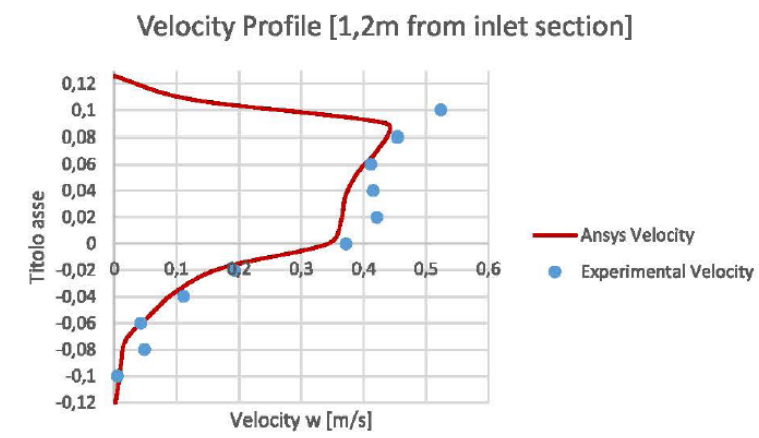

Figure 169 – Velocity profile @ 1.2 m from inlet section – 4 vehicles case

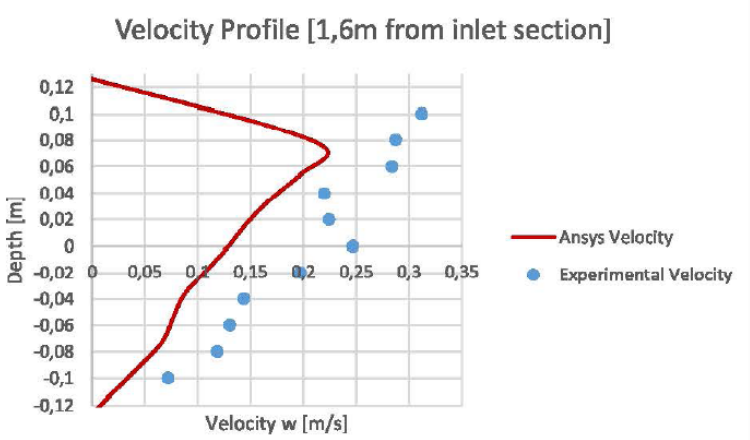

Figure 170 – Velocity profile @ 1.6 m from inlet section – 4 vehicles case

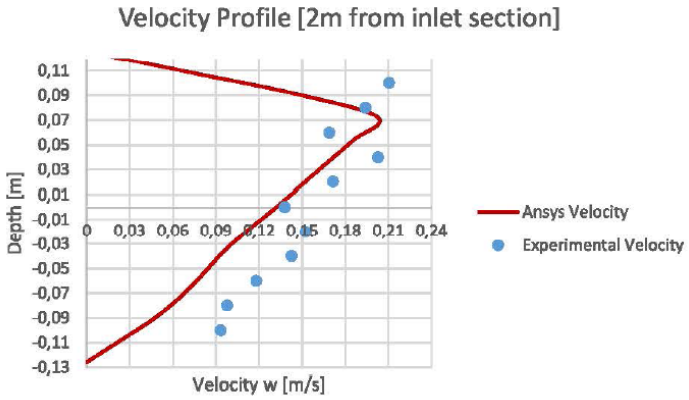

Figure 171 – Velocity profile @ 2 m from inlet section – 4 vehicles case

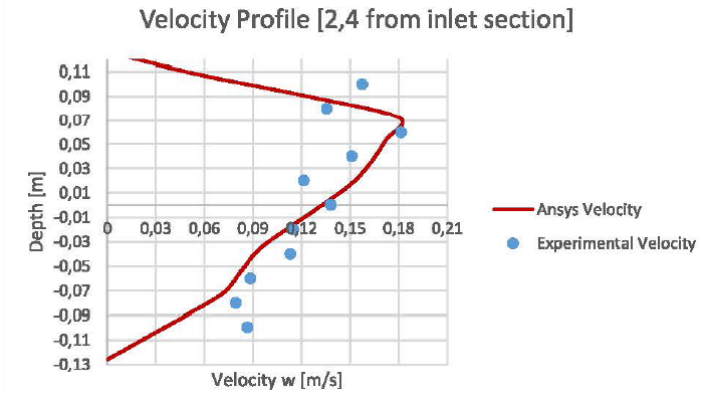

Figure 172 – Velocity profile @ 2.4 m from inlet section – 4 vehicles case

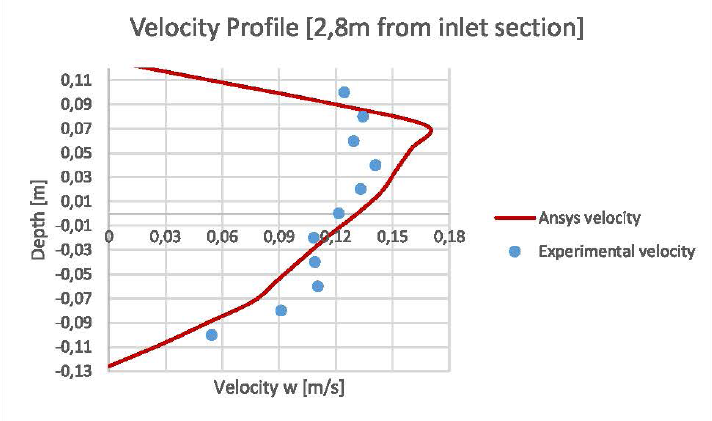

Figure 173 – Velocity profile @ 2.8 m from inlet section – 4 vehicles case

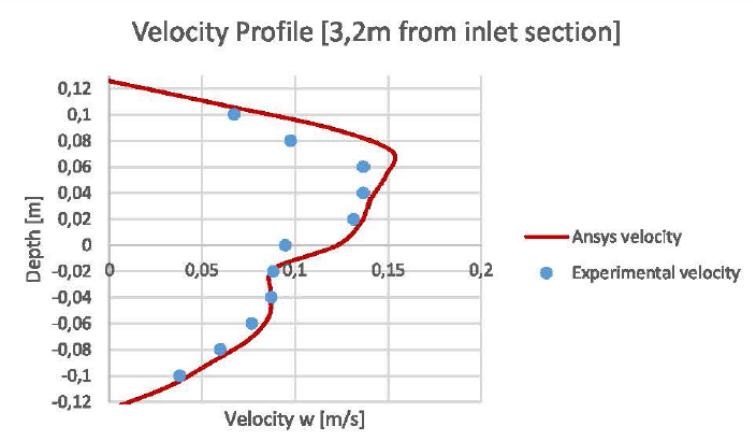

Figure 174 – Velocity profile @ 3.2 m from inlet section – 4 vehicles case

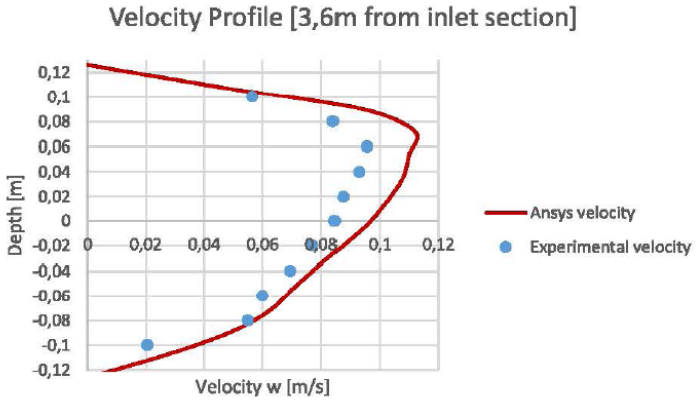

Figure 175 – Velocity profile @ 3.6 m from inlet section – 4 vehicles case

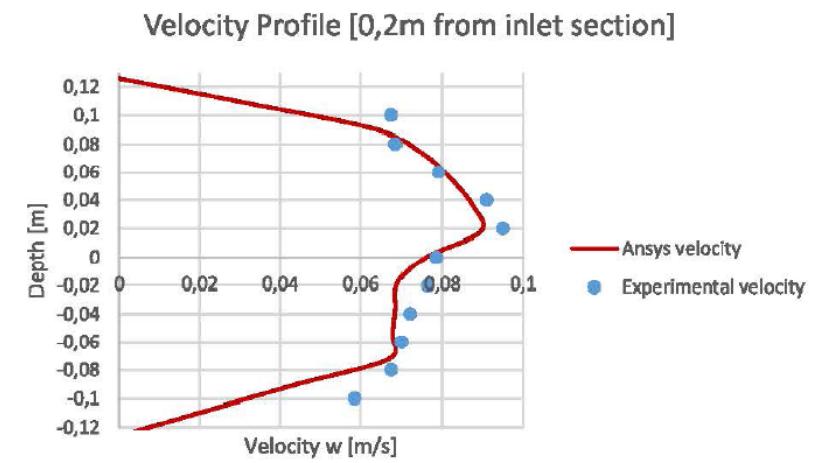

Figure 176 – Velocity profile @ 0.2 m from inlet section – 16 vehicles case

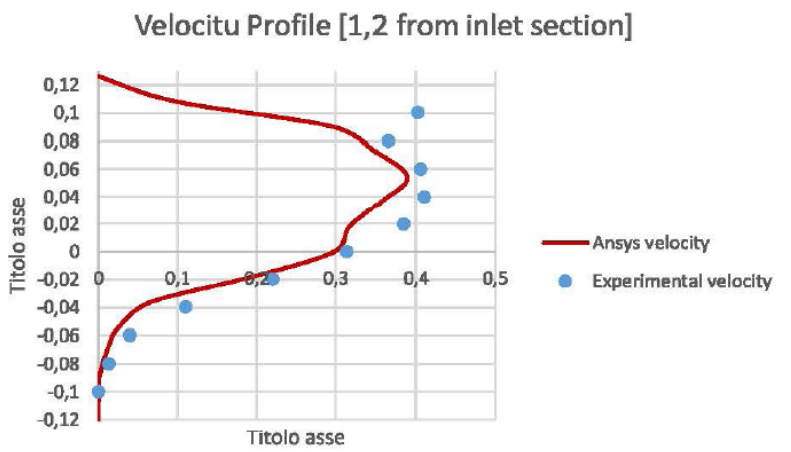

Figure 177 – Velocity profile @ 1.2 m from inlet section – 16 vehicles case

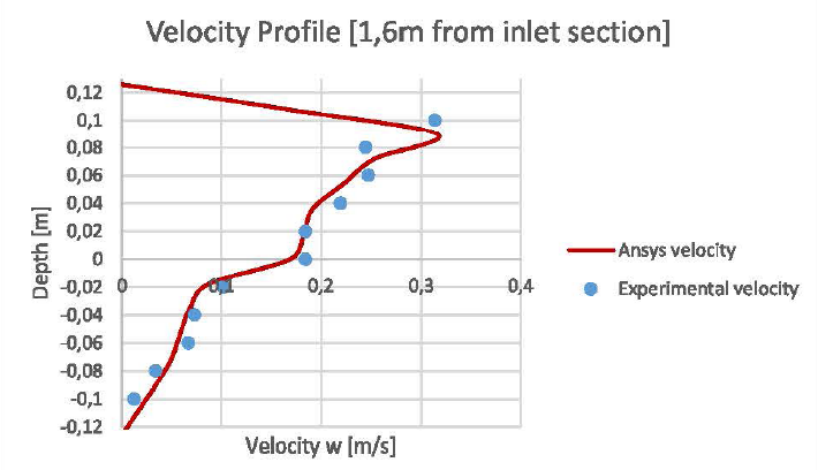

Figure 178 – Velocity profile @ 1.6 m from inlet section – 16 vehicles case

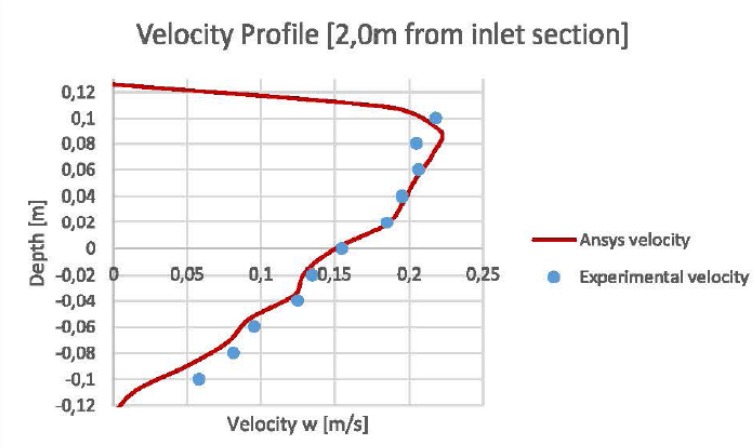

Figure 179 – Velocity profile @ 2.0 m from inlet section – 16 vehicles case

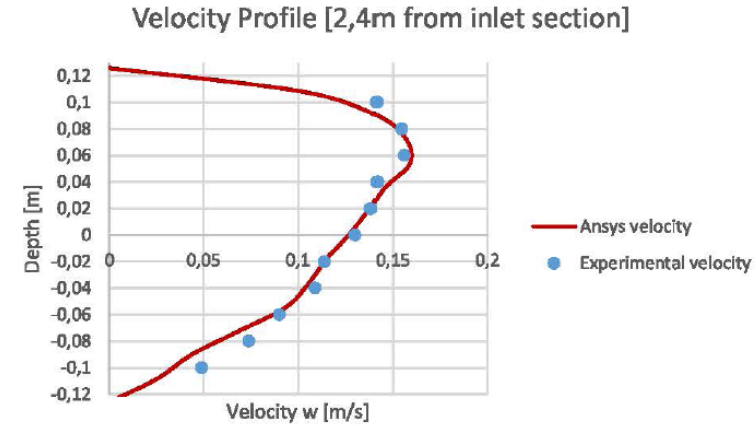

Figure 180 – Velocity profile @ 2.4 m from inlet section – 16 vehicles case

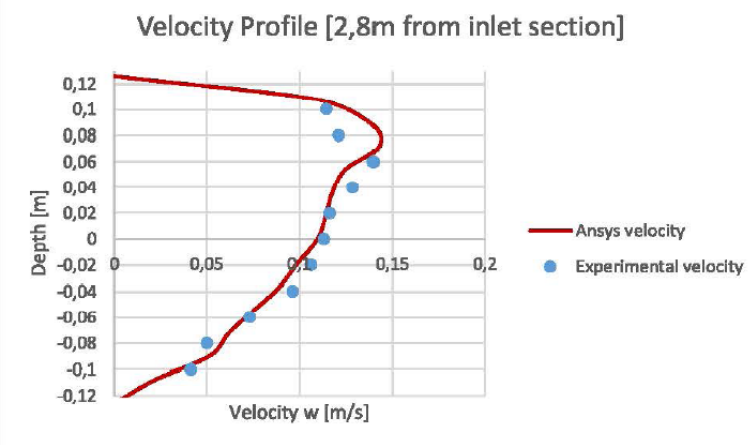

Figure 181 – Velocity profile @ 2.8 m from inlet section – 16 vehicles case

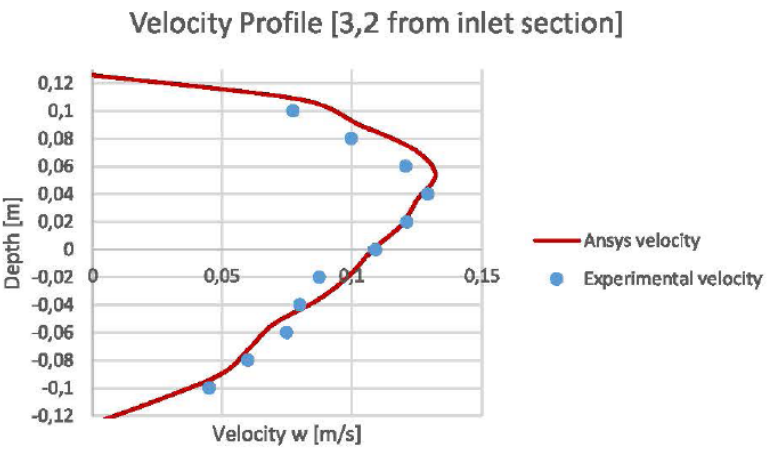

Figure 182 – Velocity profile @ 3.2 m from inlet section – 16 vehicles case

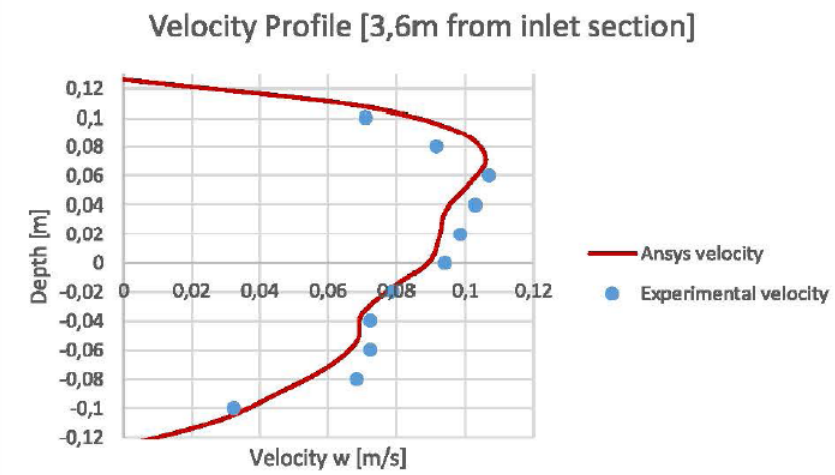

Figure 183 – Velocity profile @ 3.6 m from inlet section – 16 vehicles case

As result, the scale model fit the numerical data of the full scale one. In particular, the presence of vehicles causes the air flow reduction in the roof region vice versa there is an acceleration in the upper part.

Conclusions

In recent years, the theme of improvement of safety and efficiency conditions in road tunnels has involved several subjects from legislator to scientific community. In European Union, minimum safety requirements for road tunnel are defined by means of EU Directive 2004/54. Together with the legislative path, research activity received a significant impulse to investigate several aspects that contribute to ventilation systems design. These shall provide a suitable level of air quality during operating conditions pushing-out the exhaust gases while, when a fire accident occurs, they shall avoid the back-layering phenomenon by confining fire gases and allow a fast and safety tunnel evacuation.

In this scenario, the present work investigate an alternative technology with the aim of increase general performances for both operating and emergency conditions, by means of a new generation of jet fans with an innovative and optimized geometry which consists in adjustable suction and exhaust nozzles, able to optimize the flow field in tunnel.

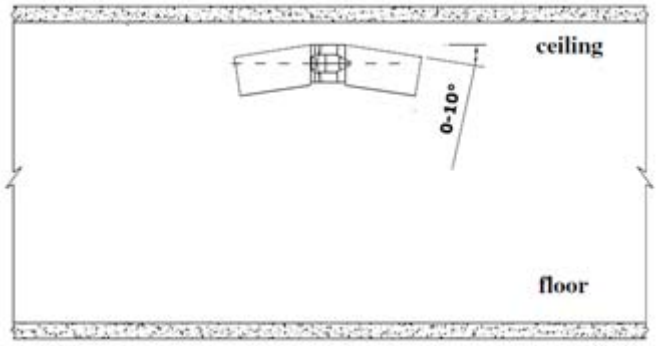

As shown in scientific literature, several parameters are involved in the design of these kind of systems, such as tunnel geometry (section, length, slope), traffic jam condition, fire case, etc. Thus, the use of computational fluid dynamics simulations (CFD) represented a suitable and good solution to carry out the comparison between traditional jet fan and alternative ones in terms of safety and performance. Low capex costs and a great flexibility of numerical tools allowed this comparison for several cases: in following table, the optimal pitch angle of alternative jet fans is shown for different conditions. The numerical analyses carried out for the study consider the same tunnel geometry and boundary conditions (both numerical and physical).

Case		Optimal pitch angle
No fire	Free tunnel	6°
	Traffic jam	2°÷4°
Fire case	-	2°

Moreover, since the tunnel slope has a direct impact on pressure profile in tunnel and thus on the thrust needed for each jet fan, a specific analysis is carried out to compare both alternative and traditional jet fans performance for emergency conditions (vehicle on fire in tunnel). Considering a fixed pitch angle equal to 6° for the alternative one, the comparison is carried out in terms of jet fan thrust. As shown in following table, the alternative configuration guarantee less thrust for each tunnel slope (0% to 10%).

	Slope (%)			
	0.0	**2.5**	**5.0**	**10.0**
Δp (Pa) - traditional	1800	3900	5775	9175
Δp (Pa) - alternative	1400	3000	4450	7063
Thrust (N) - traditional	648	1404	2079	3303
Thrust (N) - alternative	504	1080	1602	2543
Thrust reduction for alternative jet fan with respect to traditional one (%)	**22**	**23**	**23**	**23**

Numerical results show how the alternative jet fan guarantees best performances with respect to traditional ones for several cases. Hence, the interest to set up an experimental apparatus (following figure) in order to validate CFD analyses. Considering main technical and economical aspects, several numerical analysis are carried out to define main features of the laboratory model.

First simulations consider a 1:50 reduced model where good results can be reached only in the ordinary case (without fire) when Froude method is applied and appropriate roughness values is considered. However, main differences between velocity profiles occur in regions with high gradients (obstruction or momentum source). In the fire case, instead, differences for both temperature and velocity fields became not acceptable since kinematic similitude is not respected. Starting from these results, different scale ratios are considered for the purpose: decreasing the scale factor, results show a lower divergence between temperature (trend and maximum values) and velocity fields. The optimal scale factor is evaluated as 1:25 by considering both numerical results and constructive aspects

for the experimental apparatus such as tunnel section geometry, wall roughness (i.e. material choice), instrumentation and facilities to be installed.

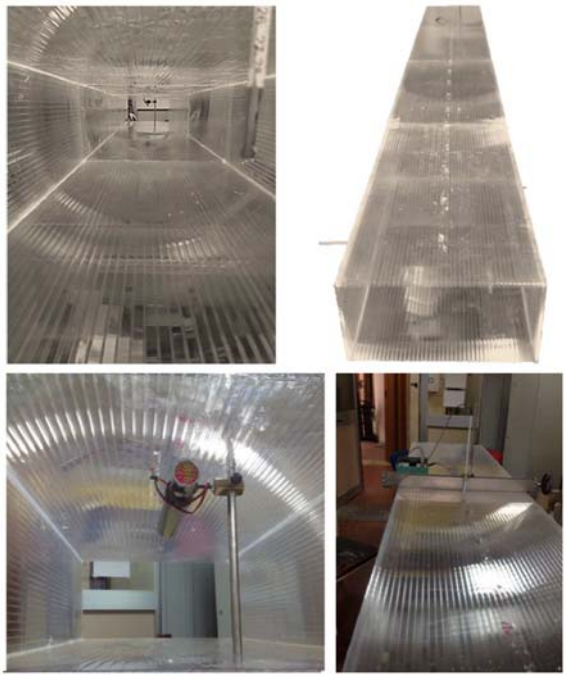

Starting from results, the experimental apparatus consists in a plexiglass tunnel (0.484 m (w) x 0.252 m (h) x 4 m (l)) with a nautical fan is installed (0.028 m inner diameter) where each warped blade (0.009 m height) is fixed to the shaft with a 60° angle. The rotation speed is guaranteed by a 3÷6 V DC brushed motor governed by a square wave voltage performed by ARDUINO UNO logic board. The scaled tunnel is made by 14 equally spaced holes on the roof to let the insertion of the probe and move it at several vertical position to evaluate airflow, temperature and total pressure.

Several CFD simulations are carried out in order to made available numerical results to be compared with the experimental ones obtained for the reduced-scale model. In particular, results mainly consist in velocity profiles for different configurations in ordinary conditions (no fire occur). The first comparative analyses, aim to validate the laboratory scaled tunnel (4 m) as a submodel suitable to extend results to the whole full scale system (800 m). Then, another set of numerical simulations are made available to investigate the effects of different traffic condition on ventilation system performance comparing numerical results and experimental ones considering traditional jet fan for each case: 4, 8, 16 vehicles. For both the comparative analysis, results show a good agreement between both numerical and experimental values: the laboratory apparatus is able to give results

extendible to a full scale road tunnel; these ones validate fluid-dynamic values for the investigated scenarios.

As future purpose, the apparatus should be equipped in order to simulate emergency conditions: materials shall be updated by means of refractory ones considering all impacts of roughness on internal tunnel fluid dynamic.

Appendix

Appendix 1 – Fire Accidents in the world's road tunnels

Year	TUNNEL length	Location	Most possible cause of fire	Duration of fire	Consequences people
1949	Holland 2 550 m	New York USA	Load falling off lorry explosion	4 h	66 injured smoke inhalation
1974	Mont Blanc 11 600 m	France-Italy	Motor	15 min	1 injured
1976	Crossing BP - A6 430 m	Paris France	High speed	1 h	12 light injuries (smoke)
1978	Velsen 770 m	Velsen Nederland	Front-rear-collision	1h 20	5 dead 5 injured
1979	Nihonzaka 2 045 m	Shitzuoka Japan	Front-rear-collision	159 h	7 dead 1 injured
1980	Kajiwara 740 m	Japan	Collision with side wall and overturning		1 dead
1982	Caldecott 1 028 m	Oakland USA	Front-rear-collision	2h 40	7 dead 2 injured
1982 3. Nov.	Salang 2 700 m	Mazar-e-Sharif - Kabul Afghanistan	Front collission Destroyed tank		> 400 dead
1983	Pecorila Galleria 662 m	Gênes Savone Italy	Front-rear-collision		9 dead 22 injured
1986	L'Arme 1 105 m	Nice France	Braking after high speed		3 dead 5 injured
1987	Gumefens 343 m	Berne Switzerland	Front-rear-collision	2 h	2 dead
1990	Røldal 4 656 m	Røldal Norway		50 min	1 injured
1990	Mont Blanc 11 600 m	France-Italy	Motor		2 injured
1993	Serra	Bologne-	Collision	2h 30	4 dead

	Ripoli 442 m	Florence Italy			4 injured
1993	Hovden 1 290m	Høyanger Norway	Front-rear-collision	1h	5 injured in the collision.
1994	Huguenot 3 914 m	South-Afrika	Electrical fault	1h	1 dead 28 injured
1995 **10. April**	Pfander 6 719 m	Austria	Collision	1h	3 dead in the collision 4 injured
1996 **18. March**	Isoladelle Femmine 148 m	Palermo Italy	Front-rear-collision		5 dead 20 injured
1999 **24. March**	Mont Blanc 11 600 m	France-Italy	Oil leakage Motor		39 dead
1999 **29. May**	Tauern 6 401 m	A10 Salzburg-Spittal Austria	Front-rear-collision 4 cars and 2 lorries		12 dead 49 injured
2000 **14. July**	Seljestad 1 272 m	E 134 Drammen - Haugesund Norway	Front-rear-collision A trailer-truck pushed a car into 4 cars that had stopped behind another truck.	45 min	6 injured
2001 **28. May**	Prapontin 4 409 m	A 32 Torino - Bardonecchia Italy	Mechanical problem		19 injured by smoke
2001 **6. Aug.**	Gleinalm 8 320 m	A 9 near Graz Austria	Front collission lorry - car		5 dead 4 injured
2001 **24. Oct.**	St. Gotthard 16 918 m	A 2 Switzerland	Front collission 2 lorries	2 days	11 dead
2003 **14 April**	Baregg 1 390 m	A 1 Switzerland	Fron-rear collission A lorry drove into the last car in a pile-up		1 dead 5 injured
2005 **4. June**	Fréjus 12 895 m	T 2 France - Italy	Diesel leakage in lorry loaded with tyres. Spread to 3 other lorries.	6 hours. Fire extinguished before it reached glue	2 dead. 21 treated for smoke inhalation

				load in 4th lorry	
2005 25 Dec		B 31 Germany	Front collission		5 dead
2006 16. sept.	Viamala 742 m	A 13 Switzerland	Front collission		6 dead 6 injured
2007 23 Mar.	Burnley 3400 m	Australia	Rear-end collission		3 dead
2007 10 Sep.	San Martino 4 800 m	SS 36 Italy	A lorry crashed into the wall and caught fire		2 dead 10 injured
2007 12 Oct.		I 5 USA	2 lorries collided. Another 13 lorries crashed into the accident site and caugt fire		10 injured

References

[1] A.D. Martegani, G. Pavesi, Uno studio sperimentale sulla ventilazione longitudinale nelle gallerie, Ventilia 37 (1994);

[2] Armstrong, J., Bennett, E.C., and Matthews, R., D., 1994, "Three-dimensional flows in a circular section tunnel due to jet fans," Proceedings of BHR Group Ltd, 8th International Symposium on Aerodynamics and Ventilation of Vehicle Tunnels, ed., I.J. Cockram, Mechanical Engineering Publications Ltd., London, UK, pp. 743-756.

[3] Camby M.K. Se, Eric W.M. Lee, Alvin C.K. Lai, Impact of location of jet fan on airflow structure in tunnel fire, Tunneling and Underground Space Technology 27 (2012) 30-40;

[4] Jojo S.M. Li, W.K. Chow, Numerical studies on performance evaluation of tunnel ventilation safety systems, Tunneling and Underground Space Technology 18 (2003) 435-452;

[5] V. Betta, F. Cascetta, M. Musto, G. Rotondo, Fluid dynamic performances of traditional and alternative jet fans in tunnel longitudinal ventilation systems, Tunneling and Underground Space Technology 25 (2010) 415-422;

[6] V. Betta, F. Cascetta, M. Musto, G. Rotondo, Numerical study of the optimization of the pitch angle of an alternative jet fan in a longitudinal tunnel ventilation system, Tunneling and Underground Space Technology 24 (2009) 164-172;

[7] T.Y. Chen, Y.T. Lee, C.C. Hsu, Investigations of piston-effect and jet-fan-effect in model vehicle tunnels, Journal of wind Engineering and Industrial Aerodynamics 73 (1998) 99-110;

[8] H.Y. Wang, Numerical and theoretical evaluations of the propagation of smoke and fire in a full-tunnel, Fire Safety Journal 49 (2012) 10-21;

[9] H. Ingason, A. Lönnermark, Heat release rates from heavy goods vehicle trailer fires in tunnels, Fire Safety Journal 40 (2005) 646-668;

[10] J. Modic, Fire simulation in road tunnels, Tunneling and Underground Space Technology 18 (2003) 525-530;

[11] O. Vauquelin, Experimental simulations of fire-induced smoke control in tunnels using an "air-helium reduced scale model": Principle, limitations, results and future, Tunneling and Underground Space Technology 23 (2008) 171-178;

[12] W.K. Chow, K.Y. Wong, W.Y. Chung, Longitudinal ventilation for smoke control in a tilted tunnel by scale modeling, Tunneling and Underground Space Technology 25 (2010) 122-128;

[13] LI Junmei, LIU Shanshan, LI Yanfeng, CHEN Chao, LIU Xuan, YIN Chenchen, Experimental study of smoke spread in tilted urban traffic tunnels fires, 2012

International Symposium on Safety and Technology, Procedia Engineering 45 (2012) 690-694;

[14] V.B. Apte, Effect of scale and fuel type on the characteristics pool fires for fire fighting training, Fire Safety Journal 31 (1998) 283-298;

[15] L.H. Hu, F. Tang, D. Yang, S. Liu, R.Huo, Longitudinal distribution of CO concentration and difference with temperature field in a tunnel fire smoke flow, International Journal of Heat Transfer 53 (2010) 2844-2855;

[16] L.H. Hu, N.K. Fong, L.Z. Yang, W.K. Chow, Y.Z. Li, R. Huo, Modeling fire-induced smoke spread and carbon monoxide transportation in a long channel: Fire Dynamics Simulator comparison with measured data, Journal of Hazardous Materials 140 (2007) 293-298;

[17] L.H. Hu, N.K. Fong, L.Z. Yang, W.K. Chow, Y.Z. Li, R. Huo, Corrigendum to "Modeling fire-induced smoke spread and carbon monoxide transportation in a long channel: Fire Dynamics Simulator comparison with measured data" [J. Hazard. Mater. 140 (1/2)(2007) 293-298], Journal of Hazardous Materials 148 (2007) 780;

[18] L.H. Hu, J.W. Zhou, R. Huo, W. Peng, H.B. Wang, Confinement of fire-induced smoke and carbon monoxide transportation by air curtain in channels, Journal of Hazardous Materials 156 (2008) 327-334;

[19] O. Vauquelin, D. Telle, Definition and experimental evaluation of the smoke "confinement velocity" in tunnel fires, Fire Safety Journal 40 (2005) 320-330;

[20] R. Deutrieue, E. Jacques, Pressure loss caused by fire in a tunnel, BHR Group 2006 AVVT 12 77-84;

[21] L. Li, S. Li, X. Wang, H. Zhang, Fire-induced flow temperature along tunnels with longitudinal ventilation, Tunneling and Underground Space Technology 32 (2012) 44-51;

[22] Y.Z. Li, H. Ingason, The maximum ceiling gas temperature in a large tunnel fire, Fire Safety Journal 48 (2012) 38-48;

[23] H. Nyman, H. Ingason, Temperature stratification in tunnels, Fire Safety Journal 48 (2012) 30-37;

[24] L.H. Hu, R. Huo, H.B. Wang, Y.Z. Li, R.X. Yang, Experimental studies on fire-induced buoyant smoke temperature distribution along tunnel ceiling, Building and Environment 42 (2007) 3905-3915;

[25] J.P. Kunsch, Simple model for control of fire gases in a ventilated tunnel, Fire Safety Journal 37 (2002) 67-81;

[26] D. Yang, L.H. Hu, R. Hou, Y.Q. Jiang, S. Liu, F. Tang, Experimental study on buoyant flow stratification induced by a fire in a horizontal channel, Applied thermal Engineering 30 (2010) 872-878;

[27] H. Kurioka, T. Oka, H. Satoh, O. Sugawa, Fire properties in near field of square fire source with longitudinal ventilation in tunnels, Fire Safety Journal 38 (2003) 319-340;

[28] R.O. Carvel, A.N. Beard, P.W. Jowitt, The influence of longitudinal ventilation systems on fires in tunnels, Tunneling and Underground Space Technology 16 (2001) 3-21;

[29] R.O. Carvel, A.N. Beard, P.W. Jowitt, D.D. Drysdale, Variation of heat release rate with forced longitudinal ventilation for vehicle fires in tunnels, Fire Safety Journal 36 (2001) 569-596;

[30] F. Colella, G. Rein, R. Carvel, P. Reszka, J.L. Torero, Analysis of the ventilation system in the Dartford tunnels using a multi-scale modeling approach, Tunneling and Underground Space Technology 25 (2010) 423-432;

[31] L. Li, P. Mei, S. Li, H. Zhang, Effect of longitudinal ventilation on heat release rate of tunnel fire, Tunneling and Underground Space Technology 30 (2012) 230-232;

[32] J.S. Roh, S.S. Yang, H.S. Ryou, M. O Yoon, Y.T. Jeong, An experimental study on the effect of ventilation velocity on burning rate in tunnel fires – heptanes pool fire case, Building and Environment 43 (2008) 1225-1231;

[33] H. Ingason, Y.Z. Li, Model scale tunnel fire tests with longitudinal ventilation, Fire Safety Journal 45 (2010) 371-384;

[34] L. Hu, S. Liu, Y. Xu, D. Li, A wind tunnel experimental study on burning rate enhancement behavior of gasoline pool fire by cross air flow, Combustion and flame 158 (2011) 586-591;

[35] S. Jain, S. Kumar, S. Kumar, T.P. Sharma, Numerical simulation of fire in a tunnel: Comparative study of CFAST and CFX prediction, Tunneling and Underground Space Technology 23 (2008) 160-170;

[36] M.G. Vega, K.M.A. Diaz, J.M.F. Oro, R.B. Tajadura, C.S. Morros, Numerical 3D simulation of a longitudinal ventilation system: Memorial Tunnel case, Tunneling and Underground Space Technology 23 (2008) 539-551;

[37] E. Migoya, A. Crespo, J. Garcia, J. Hernandez, A simplified model of fires in road tunnels. Comparison with three-dimensional models and full-scale measurements, Tunneling and Underground Space Technology 24 (2009) 37-52;

[38] G. Yang, Y. An, L. Peng, J. Zhang, Simulation of smoke flow and longitudinal ventilation in tunnel fire, Transactions of Nonferrous Metals of China 16 (2006) 741-746;

[39] H. Jang, F. Chen, On the determination of the aerodynamic coefficients of highway tunnels, Journal of Wind Engineering and Industrial Aerodynamics 90 (2002) 869-896;

[40] K.V. Maele, B. Merci, Application of RANS and LES field simulations to predict the critical ventilation velocity in longitudinally ventilated horizontal tunnels, Fire Safety Journal 43 (2008) 598-609;

[41] P.Z. Gao, S.L. Liu, W.K. Chow, N.K. Fong, Large eddy simulations for studying tunnel smoke ventilation, Tunneling and Underground Space technology 19 (2004) 577-586;

[42] F. Colella, G. Rein, R. Borchiellini, R. Carvel, J.L. Torero, V. Verda, Calculation and desgin of tunnel ventilation systems using a two-scale modelling apprach, Building and Environment 44 (2009) 2357-2367;

[43] P.H. Thomas, The movement of smoke in horizontal passage against an air flow, Fire Research Station Note No. 723, Fire Research Station (1968);

[44] P.H. Thomas, The movement of buoyant fluid against a stream and the venting of underground fires, Fire Research Note No. 351, Fire Research Station, Watford, UK 1958;

[45] C.K. Lee, R.F. Chaiken, J.M. Singer, Interaction between duct fires and ventilation flow: an experimental study, Combustion Science and Technology 20 (1979) 59-72;

[46] P.L. Hinkley, The flow of hot gases along an enclosed shopping mall. A tentative theory. Fire Research Note No.807, March 1970;

[47] A.J.M. Heselden, Studies of fire and smoke behavior relevant to tunnels, Proceedings of the Second International Symposium of Aerodynamics and Ventilation of Vehicle Tunnels, Paper J1, 1976;

[48] N.H. Danziger, W.D. Kennedy, Longitudinal ventilation analysis for the Glenwood Canyon tunnels, 4th International Symposium on Aerodynamics and Ventilation of Vehicle Tunnels, BHR Group (1982) 169-186;

[49] Y. Oka, G. T. Atkinson, Control of Smoke Flow in Tunnel Fires, Fire Safety Journal 25 (1995) 305-322;

[50] G.T. Atkinson, Y. Wu, Smoke control in sloping tunnels, Fire Safety Journal 27 (1997) 335-341;

[51] O. Vauquelin, Parametrical study of the back flow occurrence in case of buoyant release into a rectangular channel, Experimental Thermal and Fluid Science 29 (2005) 725-731;

[52] O. Vauquelin, Y. Wu, Influence of tunnel width on longitudinal smoke control, Fire Safety Journal 41 (2006) 420-426;

[53] Y. Wu, M.Z.A. Bakar, Control of smoke flow in tunnel fires using longitudinal ventilation system – a study of the critical velocity, Fire Safety Journal 35 (2000) 363-390;

[54] K. Kang, Characteristic length scale of critical ventilation velocity in tunnel smoke control, Tunneling and Underground Space Technology 25 (2010) 205-211;

[55] D. Tetzner, R. Pollak, W. Foit, M. Sippel, Critical velocity – comparative assessment of test results and CFD simulation, Proceedings of the International Conference on Tunnel Fire and Escape from Tunnels, Lyon, France (1999);

[56] L.H. Hu, R. Huo, Y.Z. Li, H.B. Wang, W.K. Chow, Full-scale burning tests on studying smoke temperature and velocity along the corridor, Tunneling and Underground Space Technology 20 (2005) 223-229;

[57] L.H. Hu, R. Huo, W.K. Chow, Studies on buoyancy-driven back-layering flow in tunnel fires, Experimental Thermal and Fluid Science 32 (2008) 1468-1483;

[58] C.C. Hwang, J.C. Edwards, The critical ventilation velocity in tunnel fires – a computer simulation, Fire Safety Journal 40 (2005) 213-244;

[59] E. Palazzi, F. Currò, B. Fabiano, A study on road tunnel fires using hazmat, with emphasis on critical ventilation velocity, Process Safety and Environment Protection, 83(B5) (2005) 443-451;

[60] J.S. Roh, H. S. Ryou, D.H. Kim, W.S. Jung, Y. J. Jun, Critical velocity and burning rate pool fire during longitudinal ventilation, Tunneling and Underground Space Technology 22 (2007) 262-271;

[61] Y. Hui, J. Li, Y. Lixin, Numerical analysis of tunnel thermal plume control using longitudinal ventilation, Fire Safety Journal 44 (2009) 1067-1077;

[62] K. Tsai, Y. Lee, S. Lee, Critical ventilation velocity for tunnel fires occurring near tunnel exits, Fire Safety Journal 46 (2011) 556-557;

[63] Y.Z. Li, B. Lei, H. Ingason, Study of critical velocity and backlayering length in longitudinally ventilated tunnel fires, Fire Safety Journal 45 (2010) 361-370;

[64] J. Mao, Y.H. Xi, G. Bai, H.M. Fan, H.Z. Ji, A model experimental study on backdraught in tunnel fires, Fire Safety Journal 46 (2011) 164-177;

[65] Q. Zhang, X. Guo, E. Trussoni, G. Astore, S. Xu, P. Grasso, Theoretical analysis on plane fire plume in a longitudinally ventilated tunnel, Tunneling and Underground Space Technology 30 (2012) 124-131;

[66] X. Guo, Q. Zhang, E. Simone, G. Astore, S. Xu, P. Grasso, The critical condition of longitudinal emergency tunnel ventilation – Comparison of theoretical prediction with experimental data, Tunneling and Underground Technology 32 (2012) 78-86;

[67] Fluent User's Guide (2005);

[68] B.E. Launder and D.B. Spalding, The numerical computation of turbulent flows, Comput. Methods Appl. Mech. Eng. 3 (1974) 269-289;

[69] K.C.Witt, J. Schutze, Bend it like a Banana, Proceedings BHR Group, 12th International Symposium on Aerodynamics and Ventilation of vehicle tunnels (2006);

[70] M. Musto, G. Rotondo, Numerical comparison of performance between traditional and alternative jet fans in tiled tunnel in emergency ventilation, Tunnelling and Underground Space Technology 42 (2014) 52–58;

[71] Regenscheit B. 1959. Die Luftbewegung in Klimatisierten Raumen, Kaltetechnik vol. 11(1): p. 3-11;

[72] Regenscheit B. 1970. Die Archimedes-Zahl, Gesundheids-Ingenieur, vol. 91 (7): p. 172-177;

[73] Regenscheit B.1971. Die Die Berechnung von radial stromenden Frei- und Wandstrahlen, sowie von Recheckstralen, Gesundheids-Ingenieur, vol. 91(7): p. 172-177;

[74] Regenscheit B.1984. Strahlen in begrenzten Räumen, Journal of Wind Engineerind and Industrial Aerodynamic, vol.16: p.133-153;

[75] Awbi H.B. 1991. Ventilation of Buildings, first edition, E & FN Spon; Chapman & Hall, London;

[76] K. R. Mutama and A. E. Hall. "The experimental investigation of jet fan aerodynamics sing wind tunnel modelling." Journal of Fluids Engineering. vol. 118. no. 2. pp. 322–327. 1996;

[77] Jojo Li SM. Chow WK.. "Numerical studies on performance evaluation of tunnel ventilation safety systems". Tunnelling and Underground Space Technology 2003; vol. 18. p. 435-452;

[78] Matjaˇz Eberlinc, Braneˇ Sirok, Marko Hoˇcevar, Matevˇz, "Numerical and experimental investigation of axial fan with trailing edge self-induced blowing"; Dular Forsch Ingenieurwes (2009) 73: 129–138;

[79] Karaaslan, S, Hepkaya, E, Yucel N, Cfd simulation of longitudinal ventilation systems in a scaled short tunnel. Journal of thermal science and technology 2013; 33.1: 63-77.

[80] Cascetta, Musto, Rotondo, Barbato, The influence of filling percentage traffic on required ventilation thrust in road tunnel, Internationa Journal of Heat and Technology, Vol. 34 – special issue 2, October 2016;

[81] Costantino, Musto, Rotondo, Zullo, Numerical analysis for reduced-scale road tunnel model equipped with axial jet fan ventilation system, Energy Procedia 45 (2014) 1146-1154;

[82] Cascetta, Musto, Rotondo, Innovative experimental reduced scale model of road tunnel equipped with realistic longitudinal ventilation system, Tunnelling and Underground Space Technology 52 (2016) 85-98;